

Network Communities and the Foreign Exchange Market



Daniel Fenn
St. Anne's College
University of Oxford

A thesis submitted for the degree of
Doctor of Philosophy
Trinity 2010

To my parents

Acknowledgements

I would like to thank HSBC bank and the EPSRC for funding this work. I am grateful to Mark McDonald and Stacy Williams for helping me to understand the intricacies of the financial data and for many useful (and occasionally enjoyable) discussions. I would particularly like to thank Nick Jones and Mason Porter for guiding this research and for the countless suggestions and insights that have helped to shape the ideas that I present. I would also like to thank them for comments on various manuscripts, which encouraged me to make my explanations clearer and my arguments more precise. I am also grateful to Sam Howison for helpful conversations and guidance and to J.-P. Onnela for many fruitful discussions and suggestions. Finally, I would like to thank Neil Johnson and Peter Mucha for valuable input at various stages of this work.

Abstract

Many systems studied in the biological, physical, and social sciences are composed of multiple interacting components. Often the number of components and interactions is so large that attaining an understanding of the system necessitates some form of simplification. A common representation that captures the key connection patterns is a network in which the nodes correspond to system components and the edges represent interactions. In this thesis we use network techniques and more traditional clustering methods to coarse-grain systems composed of many interacting components and to identify the most important interactions.

This thesis focuses on two main themes: the analysis of financial systems and the study of network communities, an important mesoscopic feature of many networks. In the first part of the thesis, we discuss some of the issues associated with the analysis of financial data and investigate the potential for risk-free profit in the foreign exchange market. We then use principal component analysis (PCA) to identify common features in the correlation structure of different financial markets. In the second part of the thesis, we focus on network communities. We investigate the evolving structure of foreign exchange (FX) market correlations by representing the correlations as time-dependent networks and investigating the evolution of network communities. We employ a node-centric approach that allows us to track the effects of the community evolution on the functional roles of individual nodes and uncovers major trading changes that occurred in the market. Finally, we consider the community structure of networks from a wide variety of different disciplines. We introduce a framework for comparing network communities and use this technique to identify networks with similar mesoscopic structures. Based on this similarity, we create taxonomies of a large set of networks from different fields and individual families of networks from the same field.

Publications

Much of the work in this thesis has been published or a manuscript has been submitted and is under review. Details of these publications are given below.

- [P1] D. J. FENN, M. A. PORTER, M. McDONALD, S. WILLIAMS, N. F. JOHNSON, AND N. S. JONES, *Dynamic Communities in Multichannel Data: An Application to the Foreign Exchange Market During the 2007-2008 Credit Crisis*, *Chaos*, 19 (2009), 033119.
- [P2] D. J. FENN, S. D. HOWISON, M. McDONALD, S. WILLIAMS, AND N. F. JOHNSON, *The Mirage of Triangular Arbitrage in the Spot Foreign Exchange Market*, *International Journal of Theoretical and Applied Finance*, 12 (2009) pp. 1–19.
- [P3] D. J. FENN, M. A. PORTER, P. J. MUCHA, M. McDONALD, S. WILLIAMS, N. F. JOHNSON, AND N. S. JONES, *Dynamical Clustering of Exchange Rates*, arXiv:0905.4912, submitted (2010).
- [P4] J.-P. ONNELA*, D. J. FENN*, S. REID, M. A. PORTER, P. J. MUCHA, M. D. FRICKER, AND N. S. JONES, *A Taxonomy of Networks*, arXiv:1006.5731, submitted (2010).
- [P5] D. J. FENN, M. A. PORTER, M. McDONALD, S. WILLIAMS, N. F. JOHNSON, AND N. S. JONES, *Temporal Evolution of Financial Market Correlations*, arXiv:1011.3225, submitted (2010).

*These authors are listed as joint first authors on these papers. I performed all of the analysis that we describe in publication [P4] and that I present in this thesis.

I have undertaken additional research during my D. Phil. that I do not include in this thesis due to its disparate nature. For completeness, I list the publications resulting from this work below.

- [P7] Z. ZHAO, J.-P. CALDERON, C. XU, G. ZHAO, D. J. FENN, D. SORNETTE, R. CRANE, P.-M. HUI, AND N. F. JOHNSON, *Common group dynamic drives modern epidemics across social, financial and biological domains*, Physical Review E, 81 (2010), 056107. [Selected to appear in Volume 19, Issue 11 (2010) of the Virtual Journal of Biological Physics Research.]
- [P8] D. J. FENN, Z. ZHAO, P.-M. HUI, AND N. F. JOHNSON, *Competitive carbon emission yields the possibility of global self-control*, Journal of Computational Science, 1 (2010) pp. 63–74.
- [P9] Z. ZHAO, D. J. FENN, P.-M. HUI, AND N. F. JOHNSON, *Self-organized global control of carbon emissions*, Physica A, 389 (2010) pp. 3546–3551.

Statement of Originality

The research in this thesis is a result of collaboration between myself and my coauthors on the listed publications. My collaborators have helped develop the ideas described in this thesis, but I have performed all of the analysis leading to the results that I present.

Contents

1	Introduction	1
1.1	Networks	1
1.1.1	Topology and weighted networks	3
1.1.2	Community structure	4
1.1.3	Dynamics of and on networks	4
1.2	Financial systems	5
1.3	Outline	6
2	Triangular Arbitrage in the FX Market	9
2.1	Introduction	9
2.1.1	The foreign exchange market	10
2.1.2	Indicative versus executable prices	11
2.1.3	Prior studies	13
2.2	Triangular arbitrage	14
2.3	Data	14
2.4	Arbitrage properties	16
2.4.1	Rate products	16
2.4.2	Durations	17
2.4.3	Magnitudes	19
2.4.4	Seasonal variations	21
2.4.5	Annual variations	23
2.5	Profitability	24
2.6	Fill probabilities	26
2.7	Summary	30
3	Financial Market PCA	33
3.1	Introduction	33
3.1.1	Components and factors	34

Contents

3.1.1.1	Factor models	34
3.1.1.2	Principal component and factor analysis	35
3.1.2	Random matrix theory	37
3.2	Data	38
3.2.1	Description	38
3.2.2	Returns	40
3.2.3	Correlations	42
3.2.3.1	Correlations for all assets	42
3.2.3.2	Intra-asset-class correlations	43
3.3	Principal component analysis	44
3.3.1	Eigenvalues	45
3.3.2	Eigenvectors	46
3.4	Temporal evolution	48
3.4.1	Proportion of variance	50
3.4.2	Significant principal component coefficients	51
3.4.3	Number of significant components	53
3.5	Asset-component correlations	55
3.6	Summary	58
4	Community Structure in Networks	61
4.1	Introduction	61
4.2	Notation	62
4.3	Community detection methods	62
4.3.1	k -clique percolation	63
4.3.2	Modularity maximization	64
4.3.3	Potts method	65
4.4	Edge communities	67
4.5	Clustering networks	67
4.6	Community dynamics	68
4.6.1	Early studies	69
4.6.2	Comparing and mapping communities	71
4.6.3	Dynamics of known partitions	72
4.6.4	Dynamic subgraphs and cliques	74
4.6.5	Dynamic clique percolation	76
4.6.6	Edge betweenness methods	77
4.6.7	Density methods	79

4.6.8	Random walkers	80
4.6.9	Graph colouring	83
4.6.10	Graph segmentation and change points	83
4.6.11	Node-centric methods	85
4.6.12	Evolutionary clustering	88
4.6.13	Summary	90
5	Dynamic Communities in the FX Market	93
5.1	Introduction	93
5.2	Data	94
5.2.1	Returns	95
5.2.2	Adjacency matrix	96
5.3	Detecting communities	98
5.4	Robust community partitions	99
5.5	Community detection in dynamic networks	102
5.5.1	Choosing a resolution	102
5.5.2	Testing community significance	103
5.5.3	Community properties	105
5.6	Minimum spanning trees	107
5.7	Exchange rate centralities and community persistence	113
5.7.1	Centrality measures	113
5.7.2	Community tracking	114
5.7.3	Exchange rate roles	115
5.8	Major community changes	117
5.8.1	Mexican peso crisis	121
5.8.2	Asian currency crisis	121
5.8.3	Credit crisis	121
5.9	Visualizing changes in exchange rate roles	124
5.9.1	Average roles	124
5.9.2	Annual roles	125
5.9.3	Quarterly roles	127
5.10	Robustness of results	129
5.11	Summary	130

6	A Taxonomy of Networks	131
6.1	Introduction	131
6.2	Multi-resolution community detection	133
6.2.1	Resolution matrix	133
6.2.2	Problems with comparing networks using resolution	134
6.2.3	Effective fraction of antiferromagnetic links	135
6.2.3.1	Properties	136
6.3	Mesoscopic response functions	137
6.3.1	Example MRFs	139
6.3.2	MRFs for Erdős-Rényi networks	142
6.3.2.1	Varying the fraction of possible edges	142
6.3.2.2	Varying the number of nodes	143
6.3.3	Synthetic MRFs	145
6.4	Distance measures	148
6.4.1	PCA distance	149
6.4.2	Distance matrices	150
6.5	Clustering networks	151
6.5.1	Network categories	153
6.5.2	Selecting a subset of networks	153
6.5.3	Choosing a linkage clustering algorithm	155
6.5.4	Comparison of clusterings for different distances	156
6.5.4.1	Visual comparison	156
6.5.4.2	Metric comparison	158
6.6	Network taxonomies	161
6.6.1	Taxonomy of all networks	161
6.6.2	Taxonomy of a sub-set of networks	161
6.6.3	Taxonomy of network categories	164
6.6.4	Comparison with prior clusterings	166
6.6.5	Synthetic networks	167
6.7	Clustering networks using other properties	168
6.7.1	Simple network statistics	168
6.7.2	Strength distribution	170
6.8	Robustness of MRFs for different heuristics	171
6.9	Case studies	172
6.9.1	U.S. Congressional roll-call voting	172
6.9.1.1	Party polarization	173

6.9.1.2	Using MRFs to identify periods of polarization . . .	174
6.9.1.3	Effect of polarization on the MRFs	178
6.9.2	United Nations General Assembly voting	178
6.9.3	Facebook	181
6.9.4	New York Stock Exchange	183
6.9.4.1	NYSE composite index	184
6.9.5	Foreign exchange market	187
6.9.6	Case studies summary	189
6.10	Summary	189
7	Conclusions	191
7.1	Outlook	193
A	Details of Financial Assets	199
B	Robustness of FX Communities	203
B.1	Comparison of partition energies	203
B.2	Temporal changes in communities	203
B.3	Example community comparison	205
B.4	Node role comparison	207
C	Network Details	209
D	Hamiltonian and Network Details	233
D.1	Potts Hamiltonian summation	233
D.2	Removing self-edges	233
E	Robustness of MRFs: Network Perturbations	235
E.1	Rewiring mechanisms	235
E.1.1	Partial rewiring	236
E.1.2	Complete rewiring	236
F	Robustness of MRFs: Alternative Heuristics	241
F.1	Robustness of MRFs	241
F.2	Robustness of taxonomies	243
F.2.1	Dendrogram correlations	243
F.2.2	Dendrogram randomizations	244
	References	247

List of Figures

2.1	Example exchange rate time series	15
2.2	Example rate product evolution	16
2.3	Rate product distributions	17
2.4	Arbitrage durations distributions	18
2.5	Daily arbitrage statistics	21
2.6	Hourly arbitrage statistics	22
2.7	Annual arbitrage statistics	24
2.8	Mean arbitrage profit/loss	26
2.9	Total arbitrage profit/loss	27
2.10	Break-even fill probabilities	29
3.1	Return distribution examples	41
3.2	Autocorrelation functions	41
3.3	Correlation coefficients distribution	43
3.4	Intra-assets-class correlations	44
3.5	Eigenvalue distribution	47
3.6	Principal component coefficients distribution	49
3.7	Fraction of the variance explained by each component	51
3.8	Participation ratio	54
3.9	Number of significant components	56
3.10	Assets-principal component correlations	59
5.1	Effect of window length on edge weights	97
5.2	Effect of window shift on edge weights	98
5.3	Network statistics as a function of resolution and time	101
5.4	Main plateau properties	104
5.5	Community size and scaled energy distribution	105
5.6	Example FX minimum spanning tree	110
5.7	Example FX dendrograms	112

List of Figures

5.8	Community centrality statistics	116
5.9	Community evolution: major market events	119
5.10	Major community changes schematic	120
5.11	Carry trade unwinding	123
5.12	Average node roles	126
5.13	Annual node roles	127
5.14	Quarterly node roles: 1995–1998	128
5.15	Quarterly node roles: 2005–2008	129
6.1	Problems with using resolution parameter	135
6.2	Cumulative resolution distribution	137
6.3	Zachary karate club fragmentation	140
6.4	Example MRFs	141
6.5	MRFs for Erdős-Rényi networks	143
6.6	Distribution of Λ_{ij} for Erdős-Rényi networks	144
6.7	Synthetic MRFs	147
6.8	Example of the distance between mesoscopic response functions	149
6.9	Distance measure correlations	150
6.10	Distributions of distances	151
6.11	Block-diagonalized distance matrices	152
6.12	Energy dendrogram	157
6.13	Entropy dendrogram	157
6.14	Number of communities dendrogram	158
6.15	PCA distance dendrogram	159
6.16	Metric comparison of distance measures	160
6.17	All-network dendrogram	162
6.18	Network category MRFs	165
6.19	Network category taxonomy	166
6.20	Dendrogram showing the positions of the synthetic networks	168
6.21	Dendrogram showing basic network statistics	169
6.22	Strength distribution dendrogram	171
6.23	Metric comparison of the PCA and strength distribution distances	172
6.24	U.S. Congress taxonomies	175
6.25	U.S. Congress polarization	177
6.26	U.S. Congress MRFs	179
6.27	Comparison of Congresses with different polarizations	180

6.28 U.N. General Assembly dendrogram	181
6.29 Facebook dendrogram	182
6.30 Facebook mesoscopic response functions	183
6.31 New York Stock Exchange dendrogram	184
6.32 New York Stock Exchange composite index	186
6.33 New York Stock Exchange volatility	186
6.34 Foreign exchange market dendrogram	188
B.1 Distribution of energies for different heuristics	204
B.2 Comparison of greedy and simulated annealing partitions	205
B.3 Heuristic comparison: community change schematic	206
B.4 Heuristic comparison: quarterly node roles	208
D.1 The problem with summing over all i, j in the Potts Hamiltonian . . .	234
E.1 Distance matrices for partially rewired networks	237
E.2 Distribution of the number of edge rewirings	239
E.3 Distance matrices for completely rewired networks	240
F.1 MRF comparison for different heuristics	242
F.2 Dendrogram comparison for different heuristics	243
F.3 Ultrametric correlation coefficient distributions	246

List of Tables

2.1	Arbitrage duration statistics	19
2.2	Arbitrage magnitude statistics	20
2.3	Hours of market liquidity	22
2.4	Annual arbitrage statistics	23
5.1	Examples of frequently observed communities	108
5.2	Exchange rates with high centralities	118
6.1	Network categories	154
A.1	Details of financial assets	199
C.1	Network details	212

Chapter 1

Introduction

1.1 Networks

A variety of systems studied across a range of academic disciplines are composed of multiple components that interact with each other in some way. Often these systems are described as *complex* [47]. Although there is no precise definition of a *complex system*, roughly speaking, a system is considered complex if it possesses many parts, whose behaviours are highly variable and strongly dependent on the behaviours of the other parts [270,274]. Many authors also agree that for a system to be considered complex, it should possess *emergent* properties that arise through the interactions of the components in the absence of any central controller [13]. However, the concept of emergence is also slippery and there is currently no standard definition [25, 51, 172]. Irrespective of the precise definitions of complex systems and emergence, for systems composed of interacting components, the pattern of connections between the components are often crucial to the behaviour of the system. The system cannot be understood by studying the parts in isolation; it is essential to consider the interactions.

When studying systems that possess many components and interactions, to make the analysis tractable it is often necessary to simplify the analysis by focusing on a subset of key interactions. A common way of studying the pattern of interactions in a given system is to construct a *network* (or *graph*) in which the components are represented as nodes and the connections are represented as edges [9, 60, 217, 223].¹ A network is therefore a simplified representation that reduces a system to a structure that captures only the key connection patterns; however, information is lost in the simplification process, so for any analysis to be meaningful it is important to

¹Nodes are sometimes referred to as vertices and edges as links. In this thesis, we use these terms interchangeably.

ensure that the discarded details are not critical to the properties of the system being investigated. Networks can take different forms: they can be embedded in Euclidean space, such as airline networks and neural networks; or they can be defined in an abstract space, such as social networks² and language networks [46].

Traditionally, the study of networks lay within the domain of graph theory [49], which is usually considered to date back to 1736 when Euler published a solution to the Königsberg bridge problem. Initially graph theory focused on regular graphs, but since the 1950s graph theorists have also investigated random graphs [50]. This shift was stimulated by the work of Rapoport [249,250,277] and Erdős and Rényi [86–88] on a simple random graph model. In the model, one begins with N nodes and connects them uniformly at random with probability p , creating a graph which on average has $\frac{1}{2}pN(N - 1)$ edges distributed at random.

In addition to the developments in mathematical graph theory, beginning in the 1920s, social scientists started to use networks to study the relationships between social entities, e.g., [76, 98, 111, 213, 249, 251, 258, 304]. Because of the difficulty in collecting and analyzing large data sets, most of the early studies of social networks were very small and the networks usually only included tens of nodes. In many of these studies, the social scientists were often interested in answering questions relating to the meaning of edges in the networks, such as whether they arose through friendship, obligation, strategic alliance, or something else [127].

In the late 1990s, a surge of interest in network research across a wide range of disciplines [225] was sparked by the publication of seminal papers by Watts and Strogatz [305] and Barabási and Albert (BA) [26]. These and subsequent developments in network science were made possible by two key factors: (1) the computerization of data acquisition, which meant that it was significantly easier to collect data for large networks, and (2) the increase in computational resources, which enabled researchers to analyze these data sets. An important observation from the new data was that, in contrast to ER random graphs, real-world networks often possess significant inhomogeneities.³ For example, many networks display the “small-world” phenomenon – despite the fact that networks contain a large number of nodes, there is often a relatively short path between two nodes (i.e., a small average path length) – studied by Milgram [209], whose work spawned the phrase the six degrees of separation. Watts and Strogatz observed that networks that possess the small-world property often also

²Social networks can sometimes contain implicit geographical information.

³An example of a homogeneous property of ER random graphs is the degree (number of neighbours) of each vertex. Because there is an equal probability of all edges existing, most nodes in ER networks have similar degrees.

show high levels of clustering – two nodes with a common neighbour are more likely to be connected [305]. Another important observation was that the degree distribution of many real-world networks significantly deviates from the Poisson distribution expected for random graphs, with some nodes having significantly more edges than expected. This led Barabási and Albert (BA) [26] to propose a preferential attachment model for network growth (in which there is a higher probability for new edges to attach to nodes with high degree) which produces network with a power-law degree distribution.⁴

1.1.1 Topology and weighted networks

Much of the early work on networks focused on topological properties and the characterization of unweighted networks. In unweighted networks, two nodes are either connected or they are not; all edges in the network have the same weight. Many features of a network depend on its topology. For example, topology is crucial to the robustness of a network to external perturbations such as random failures or targeted attacks on nodes [10, 46, 56, 62, 70, 151]. Topology also plays an important role in the behaviour of different spreading processes operating on the network, such as the spread of diseases, information, or rumours [46, 191, 213, 236, 316]. In many networks there are also heterogeneities in the capacity or intensity of the edges [232]. The heterogeneities in the interaction strengths between components has important effects on the function and behaviours of many systems, which has led to the study of networks in which a weight (usually a real number) is associated with each edge. For example, a consideration of weighted networks [232] has provided insights into Granovetter’s *weak ties hypothesis* [135], which states that the relative overlap of the friendship circles of two individuals increases with the strength of the links connecting them. Another network in which connection weights play an important role is the internet. The internet is a network for transmitting data; in its simplest network representation, the nodes correspond to computers and other devices and the edges represent physical connections between them, such as optical fibre lines [223]. These connections have different bandwidths and different amounts of data flowing down them at any point in time. Because of these heterogeneities, it is necessary to consider link weight in order to determine optimal paths for routing data around the internet.

⁴In fact, this type of “rich get richer” growth mechanism dates back to the works of Yule [314], Simon [273], and Price [246].

1.1.2 Community structure

A further inhomogeneity in the structure of real-world networks is in the local distribution of edges. In many networks, there are high concentrations of edges between particular groups of vertices, with relatively fewer edges between different groups. This feature of networks is termed *community structure* [105, 244]. Although there is no rigorous definition, a “community” is usually considered to be a group of nodes that are relatively densely connected to each other but sparsely connected to other dense groups in the network. Network communities can represent functionally-important sub-networks [2, 75, 105, 107, 121, 139, 243, 244, 295] and their identification can have useful applications. For example, identifying groups of customers with similar interests in networks representing the relationships between customers and products that they purchase can lead to the development of improved product recommendation systems for on-line retailers [253]. The algorithmic detection of communities and the development of tools to analyze them is currently one of the most active areas of research in networks [105, 244]. We return to communities in Chapter 4 in which we present a more detailed discussion of the different community detection methods.

1.1.3 Dynamics of and on networks

Another active area of research is the study of the dynamical behaviour of networks, both in terms of the structural dynamics of the networks themselves, e.g., [23, 185, 233] and the dynamics of processes taking place on the network, e.g., [10, 46, 56, 62, 70, 123, 151]. Most early studies of networks involved the analysis of a network at a fixed point in time or the analysis in a single network of all of the cumulative interactions up to a point in time, e.g., [127]. An example of the latter is the construction of coauthorship networks that represent all collaborations between researchers during a time period [216]. Many different approaches have been adopted for constructing and analyzing the structural dynamics of networks. For example, networks have been constructed in which the interactions accumulate over time and the network dynamics investigated by comparing the structure of the aggregate network with its structure at earlier points in time, e.g., [152]. A related approach is to construct cumulative networks, but to add an additional decay parameter that reduces the weight of edges based on the time that had elapsed since the interaction took place and to remove edges whose weight falls below a threshold. The network dynamics can then be investigated by observing changes taking place in the network, e.g., [233]. A

third possibility is the comparison of networks for interactions aggregated over non-overlapping time windows, e.g., [92].

The spreading processes on network (such as the spread of diseases, information, or rumours) mentioned earlier in this section in the context of network topology are particular examples of the more general concept of dynamical systems on networks [223]. A dynamical system is any system whose state, as represented by some set of variables, changes over time according to a set of rules or equations [281]. Typically, dynamical systems on networks consist of independent dynamical variables associated with each node that are only coupled together along the edges of the network. Many real-world processes can be represented as dynamical systems operating on a network. For example, the flow of traffic on roads, electricity over power grids, or the changing concentrations of metabolites in cells [223]. One particular area of focus is the study of the synchronization of coupled oscillators on networks, which represents an important feature of many real-world systems [15,46]. For example, evidence suggests that there is a pathological synchronization of neural populations during epileptic attacks [46].

In this thesis, we investigate the properties of networks possessing each of the characteristics described in the previous three sections. In Chapter 5, we analyze the evolving community structure of a dynamic, weighted network, and in Chapter 6 we compare the community structures of a wide variety of weighted and unweighted networks.

1.2 Financial systems

In Chapters 2, 3, and 5, we focus on financial markets, which are often considered to be evolving complex systems [14, 18, 19, 45]. Markets are composed of a myriad of financial agents, such as banks, consumers, investors, and companies, that continually adjust their buying and selling decisions, prices and forecasts based on the state of the market, which is itself determined by these decisions [18]. The state of the market emerges through this system of interactions and feedback and cannot be determined by considering the individual components in isolation. Because of the wealth of components and the complex pattern of connections between them, to gain any insights into financial systems it is necessary to focus on particular subsets of components and interactions. For example, insights into the global economy can be attained by studying the flow of imports and exports between different countries [275]. However, even focusing on a particular aspect of the financial system, the number of interactions is often so large that further simplification is required.

Several studies have attempted to tackle this problem using networks. For example, networks have been used to analyze the trade relationships between nations [275] and liabilities in the inter-bank lending market [52]. Perhaps the most common application of networks to financial market is in the study of the relationships between the price time series of financial assets, e.g., [197, 198, 229]. In this approach, each node in the network represents an asset and each weighted edge represents a time-dependent correlation between the asset price time series.

In Chapter 5, we study FX market networks in which each node represents an exchange rate and the edges represent the correlations between rates. An argument made to justify the study of networks constructed from asset price time series is as follows [228]. In markets, traders repeatedly compete for a limited resource, as they buy and sell assets, with the exact timing of these trading decisions often driven by exogenous events, such as news announcements, scheduled economic data releases, and other events. Although the exact nature of the interactions between market participants is often not known, the asset prices should reflect the complex pattern of actions, feedback, and adaptation of traders, so the price time series can be considered as the manifestation of these interactions. Under these assumptions, instead of the nodes representing the interacting components (i.e., the traders), they represent the resource that the components are competing for (i.e., the assets) and instead of the edges representing the interactions between the components (i.e., buying and selling actions) they represent correlations in a signal that results from this process (i.e., the asset price).

Irrespective of the exact relationship between the network and the underlying financial system, it is insightful to investigate networks based on the correlations between different assets. In fact, this example demonstrates the power of the network framework. Because we work with networks in an abstract form, the tools of network analysis can in theory be applied to any system that can be represented as a network [223]. In essence, networks methods are simply a set of techniques for studying and identifying patterns in data generated by interacting systems. Of course, the insights that can be gained using a network approach depend on the suitability of the technique to the problem and for some systems other methods will be more appropriate.

1.3 Outline

This thesis is organized into six additional chapters. In each chapter in which we present new research we provide an overview of the relevant literature and a motiva-

tion for the work. The chapters are more or less distinct and can be read in isolation. However, a continuous thread runs through the thesis as we move from an analysis of financial systems to an investigation of communities in financial systems to a study of communities in systems from a wide variety of different disciplines.

In Chapter 2, we discuss some of the problems associated with analyzing financial data and present a study in which the type of data used is critical to the output of the analysis. We also describe the FX market, which is the focus of Chapters 2 and 5. The results of Chapter 2 answer a question of particular interest to market practitioners regarding the possibility of making risk-free profit in the FX market. In Chapter 5, we continue to investigate financial markets, but we extend the analysis to include assets from a variety of different markets. We study the correlation structure across these different markets by using principal component analysis to coarse-grain the data and identify common features. We then study the way in which these relationships evolve through time and discuss how the features are affected by different market events.

In the remainder of the thesis, we focus on communities in networks. In Chapter 4 we describe some of the most widely used techniques for detecting communities in networks and present a relatively comprehensive review of the literature on communities in dynamic networks. In Chapter 5, we study the structure of the FX market by representing the correlations between currency exchange rates as time-dependent networks and investigating the evolution of network communities. We propose a method for tracking communities in dynamical networks and use this approach to identify significant changes in the structure of the FX market. In Chapter 6, we investigate the community structure of networks from a range of different disciplines, including biology, sociology, politics, and finance, and introduce a framework for comparing network communities. We use this technique to identify networks with similar mesoscopic structures. Based on this similarity, we create taxonomies of a large set of networks from different fields and individual families of networks from the same field. Finally, in Chapter 7, we offer some conclusions and suggest some possible directions for future research.

Chapter 2

The Mirage of Triangular Arbitrage in the Foreign Exchange Market

The work described in this chapter has been published in reference [P2]. We highlight that this is an empirical chapter and the analysis we present is not technical. However, this simplicity serves to emphasize one of the main purposes of this chapter which is to demonstrate that one needs to exercise caution when analyzing financial data. If one uses data that is inappropriate for a particular analysis, it is easy to reach false conclusions. We show how even for the simplest financial questions, seemingly similar data can produce very different results. In demonstrating this, we answer a question of interest to financial market practitioners.

2.1 Introduction

The advance in computing power during the last two decades has facilitated the storage and analysis of increasingly large data sets. The increased storage capacity is particularly useful in financial markets because, as well as enabling market participants to record details of executed transactions, institutions are now able to record additional market information even if a trade is not executed (such as the best available price and the volume available at this price). The increased computing power has also enabled exchanges to publish prices at increasingly higher frequencies, with some exchanges in the FX market now publishing price updates every 250 milliseconds.

The availability of these enormous, accurate, high-frequency data sets has provided economists and financial mathematicians with unprecedented resources to test their models and has resulted in many researchers from other disciplines studying fi-

financial problems. However, the widespread availability of this data is a double-edged sword: while it is undoubtedly positive that more financial data is widely accessible, this has also led to work in which data is used that is not appropriate for the study.

Asset prices provide a good example of where confusion can arise because single assets can have several prices associated with them. For example, assets can have an indicative price (a quote providing an indication of the level at which an asset is currently trading), an executable price (the price at which a trade can actually be executed in the market at a particular time, although the party posting the price can remove it before an opposite trade is matched against it), or a traded price (the price at which a trade is actually executed). The most appropriate price for a study depends on the question being posed. Financial time series can also have specific peculiarities associated with them. For example, many currencies are pegged to the U.S. dollar, which results in their exchange rates tracking the U.S. dollar exchange rate. If one does not use the correct type of data, or fails to deal properly with asset-specific artifacts, then the wrong conclusions can easily be reached.

In this chapter, we investigate triangular arbitrage within the spot FX market¹ using high-frequency executable prices [73]. Arbitrage is the practice of taking advantage of mis-pricings in financial markets to realize risk-free profits; triangular arbitrage is the simplest arbitrage in the FX market. As an example of triangular arbitrage, consider the situation where one initially holds x_i euros. If one sells these euros and buys dollars, converts these dollars into Swiss francs, and then converts these francs into x_f euros, if $x_f > x_i$ a profit is realized. This is a triangular arbitrage.

Prior studies of triangular arbitrage indicate the existence of large arbitrage opportunities that remain in the market for long periods of time, e.g., [7, 169]; however, such profit opportunities would come as something of a surprise to most FX traders. We demonstrate that the incorrect identification of triangular arbitrage opportunities in these prior studies results from the use of the wrong type of data. Although the original objective of this study was to determine whether or not triangular arbitrage opportunities exist, the study serves as a good example of the care that one needs to take when analyzing financial data.

2.1.1 The foreign exchange market

The FX market is the world's largest financial market with an average daily trade volume of approximately 3.2 trillion U.S. dollars [147]. Prices in the FX market

¹In the spot FX market, currencies are bought and sold for immediate delivery (actually two business days after the trade day), rather than for delivery in the future.

are quoted as exchange rates of the form XXX/YYY, which indicate the amount of currency YYY that one would receive in exchange for one unit of currency XXX. In this thesis, we refer to currencies with the standard three letter abbreviations (tickers) used to identify them in the FX market. The codes for the currencies we study are USD - U.S. dollar, CHF - Swiss franc, JPY - Japanese yen, EUR - euro, DEM - German mark, AUD - Australian dollar, CAD - Canadian dollar, XAU- gold², GBP - pounds sterling, NZD - New Zealand dollar, NOK - Norwegian krone, and SEK - Swedish krona. In contrast to most other markets, the FX market is liquid 24 hours a day.³ There are two prices quoted for an exchange rate: a bid and an ask price. These give the different prices at which one can buy and sell currency, respectively, with the ask price tending to be larger than the bid price. The exchange rate between EUR and USD may, for example, be quoted as 1.4085/1.4086. A trader then looking to convert USD into EUR might have to pay 1.4086 USD for each EUR, while a trader looking to convert EUR to USD may receive only 1.4085 USD per EUR. The difference between the bid and ask prices is the *bid-ask spread*.

2.1.2 Indicative versus executable prices

Although prior studies of triangular arbitrage exist, e.g., [7, 169], there is no robust study that provides a definitive answer to the question of whether triangular arbitrage can be profitable. The main reason for this is that, until recently, the available data has not been sufficiently accurate or of a sufficiently high frequency.

As a result of the size and liquidity of the FX market, price updates occur at extremely high frequencies. For example, the EUR/USD rate has in excess of 100 price updates a minute during the most liquid periods. Therefore one requires an equally high-frequency data set to test for triangular arbitrage opportunities. In addition, it is necessary to know that the prices are ones at which a trade could indeed be executed as opposed to simply being *indicative* price quotes. An indicative bid/ask price is a quote that gives an approximate price at which a trade can be executed; at a given time one may be able to trade at exactly this price or, as is often the case, the real price at which one executes the trade, the *executable* price, differs from the indicative price

²We include gold in the study because it has many similarities with a currency [204].

³There are many different definitions of liquidity [263]. We consider the market to have high liquidity if there is a large depth of resting orders and this depth is refreshed quickly when orders are filled. A resting order is an order to buy at a price below or sell at a price above the prevailing market price. Such orders are not filled immediately, but instead rest on the order book until they are matched. High liquidity implies that one can usually find a counterparty to a trade.

by a few basis points⁴. The main purpose of an indicative price is to supply clients of banks with a gauge of where the price is. A large body of academic research into the FX market has been performed using indicative quotes often under the assumption that, due to reputational considerations, “serious financial institutions” are likely to trade at exactly the quoted price, especially if they are hit a short time after the quote is posted [73, 74, 138]. The efficiency of using indicative quote data for certain analyses has, however, been drawn into question, e.g., [193, 200]. In Ref. [193], Lyons highlights some of the key problems with indicative prices: indicative prices are not transactable; the indicative bid-ask spread, despite usually “bracketing” the actual tradeable spread, is usually two to three times as large (i.e., the tradeable bid and ask prices usually lie between the indicative bid and ask prices); during periods of high trading intensity market makers are too busy to update their indicative quotes; and market makers themselves are unlikely to garner much of their high-frequency information from indicative prices. In the FX market today indicative prices are typically updated by automated systems, nevertheless the quoted price is still not necessarily a price at which one could actually execute a trade.

Goodhart *et al.* [131] performed a comparison of indicative bid-ask quotes from the Reuters FXXF page and executable prices from the Reuters D2000–2 electronic broking system over a 7 hour period and found that the behaviour of the bid-ask spread and the frequency at which quotes arrived were quite different for the two types of quote. In particular, the spread from the D2000–2 system showed greater temporal variation, with the variation dependent upon the trading frequency. In contrast, the indicative price spread tended to cluster at round numbers, a likely artifact of the use of indicative prices as a market gauge. This discrepancy between indicative and executable prices is likely to be less important if one is performing a low frequency study, arguably down to time scales of 10–15 minutes [138]. If, however, one is considering very high-frequency data, this difference becomes highly significant. For example, in Ref. [130] Goodhart and Figliuoli find a negative first-order auto-correlation in price changes at minute-by-minute frequencies using indicative data. In Ref. [131], however, Goodhart finds no such negative auto-correlation when real transaction data is used. Indicative data seem particularly unsuitable to many market analyses today because banks are now able to provide their clients with automated

⁴A basis point is equal to 1/100th of a percentage point. In this paper we will also discuss points, where a point is the smallest price increment for an exchange rate. For example, for the EUR/JPY exchange rate, which takes prices of the order of 139.60 over the studied period, 1 point corresponds to 0.01. In contrast, for the EUR/USD rate with typical values around 1.2065, 1 point corresponds to 0.0001.

executable prices through an electronic trading platform so there is even less incentive for them to make their indicative quotes accurate.

2.1.3 Prior studies

Some analyses of triangular arbitrage have been undertaken using indicative data. In Ref. [7], Aiba *et al.* investigated triangular arbitrage using indicative quote data provided by information companies for the set of exchange rates $\{\text{EUR/USD}, \text{USD/JPY}, \text{EUR/JPY}\}$ over a roughly eight week period in 1999. They found that, over the studied period, arbitrage opportunities appeared to exist about 6.4% of the time, or around 90 minutes each day, with individual arbitrages lasting for up to approximately 1,000 seconds. In Ref. [169], Kollias and Metaxas investigated 24 triangular arbitrage relationships, using quote data for seven major currencies over a one month period in 1998, and found that single arbitrages existed for some currency groups for over two hours, with a median duration of 14 and 12 seconds for the two transactions formed from $\{\text{USD/DEM}, \text{USD/JPY}, \text{DEM/JPY}\}$.

When considering whether triangular arbitrage transactions can be profitable it is important to consider how long the opportunities persist. The time delay between identifying an opportunity and the arbitrage transaction being completed is instrumental in determining whether a transaction results in a profit because the price may move during this time interval. Kollias and Metaxas [169] tested the profitability of triangular arbitrage transactions by considering execution delays of between 0 and 120 seconds and, in a similar manner, Aiba *et al.* accounted for delays by assuming that it took an arbitrageur between 0 and 9 seconds to recognize and execute an arbitrage transaction. Kollias and Metaxas found that for some transactions triangular arbitrage continued to be profitable for delays of 120 seconds and Aiba *et al.* for execution delays of up to 4 seconds. These durations differ markedly from the beliefs of market participants; we suggest that this discrepancy results from the invalid use of indicative data in these studies.

In contrast to prior studies, in this chapter we use high-frequency, *executable* price data to investigate triangular arbitrage. This means that, for each arbitrage opportunity that we identify, one could potentially have executed a trade at the arbitrage price. Furthermore, and importantly, we consider the issue of not completing an arbitrage transaction. In the FX market today, where electronic trading systems are widely used, it is possible to undertake the three constituent trades of an arbitrage transaction in a small number of milliseconds; but, despite this execution speed, one

is not guaranteed to complete a triangular arbitrage transaction. We discuss the reasons for this in Section 2.4.2.

2.2 Triangular arbitrage

In a market as liquid as the FX market, one would expect triangular arbitrage opportunities to be limited and, if they do occur, for the potential profits to be small. This means that when identifying arbitrage opportunities on a second-by-second time scale the possible discrepancy between an indicative and an executable price becomes extremely important. It is, in fact, essential to use executable data if one is to draw reliable conclusions on whether triangular arbitrage opportunities exist.

Triangular arbitrage opportunities can be identified through the rate product

$$\gamma(t) = \prod_{i=1}^3 p_i(t), \quad (2.1)$$

where $p_i(t)$ denotes an exchange rate at time t [7]. An arbitrage is theoretically possible if $\gamma > 1$, but a profit will only be realized if the transaction is completed at an arbitrage price.

For each group of exchange rates there are two unique rate products that can be calculated. For example, consider the set of rates {EUR/USD, USD/CHF, EUR/CHF}. If one initially holds euros, one possible arbitrage transaction is EUR→USD→CHF→EUR with a rate product given by

$$\gamma_1(t) = \left[\text{EUR/USD}_{\text{bid}}(t) \right] \times \left[\text{USD/CHF}_{\text{bid}}(t) \right] \times \left[\frac{1}{\text{EUR/CHF}_{\text{ask}}(t)} \right]; \quad (2.2)$$

the second possible arbitrage transaction is EUR→CHF→USD→EUR with a rate product

$$\gamma_2(t) = \left[\frac{1}{\text{EUR/USD}_{\text{ask}}(t)} \right] \times \left[\frac{1}{\text{USD/CHF}_{\text{ask}}(t)} \right] \times \left[\text{EUR/CHF}_{\text{bid}}(t) \right]. \quad (2.3)$$

These two rate products define all possible arbitrage transactions using this set of exchange rates.

2.3 Data

The data we use for the analysis consists of second-by-second executable prices for {EUR/USD, USD/CHF, EUR/CHF, EUR/JPY, USD/JPY}. We investigate triangular arbitrage opportunities for the transactions involving {EUR/USD, USD/CHF,

EUR/CHF} and {EUR/USD, USD/JPY, EUR/JPY} for all week days over the period 02/10/2005–27/10/2005 and we compare the results with those for two earlier periods: 27/10/2003–31/10/2003 and 01/10/2004–05/10/2004.⁵ The full data set consists of approximately 2.6 million data points for each of the rate products γ_1 and γ_2 , 5.2 million data points for each of the currency groups, and 10.4 million data points in total. A rate product, indicating whether or not a triangular arbitrage opportunity existed, was found for each of these points. We show a sample of one of the sets of exchange rates and the corresponding time series of bid-ask spreads in Fig. 2.1.

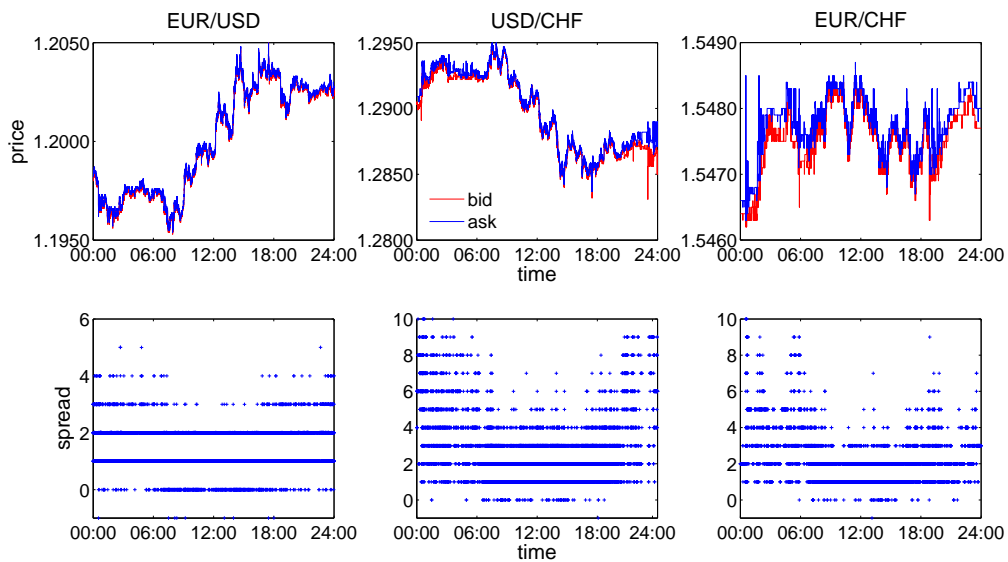


Figure 2.1: Exchange rate time series for EUR/USD, USD/CHF and EUR/CHF on 12/10/2005. Upper: bid and ask prices. Lower: bid-ask spread. Each marker represents the spread at a single time step. The vertical axes have been truncated to make the detail around the typical values clearer.

⁵All times in this paper are given in GMT. The full day 28/10/2005 is excluded from the analysis for the JPY group of exchange rates due to an error with the data feed on this day. During periods of lower liquidity it is possible that there were times at which no party was offering a bid and/or ask price. At these times it would not have been possible to complete a triangular transaction involving the missing exchange rate so we set the associated rate product to zero.

2.4 Arbitrage properties

2.4.1 Rate products

Figure 2.2 shows an example of the temporal evolution of the rate product γ over one of the weeks analyzed. If it were possible to buy and sell a currency at exactly the same price then one would expect the rate product to always equal one. However, the prices at which currencies can be bought and sold differ, with the ask price exceeding the bid price, and as a result the rate product is typically expected to be slightly less than one. Rate products with a value just below one can be considered to fall in a region of “triangular parity”.⁶

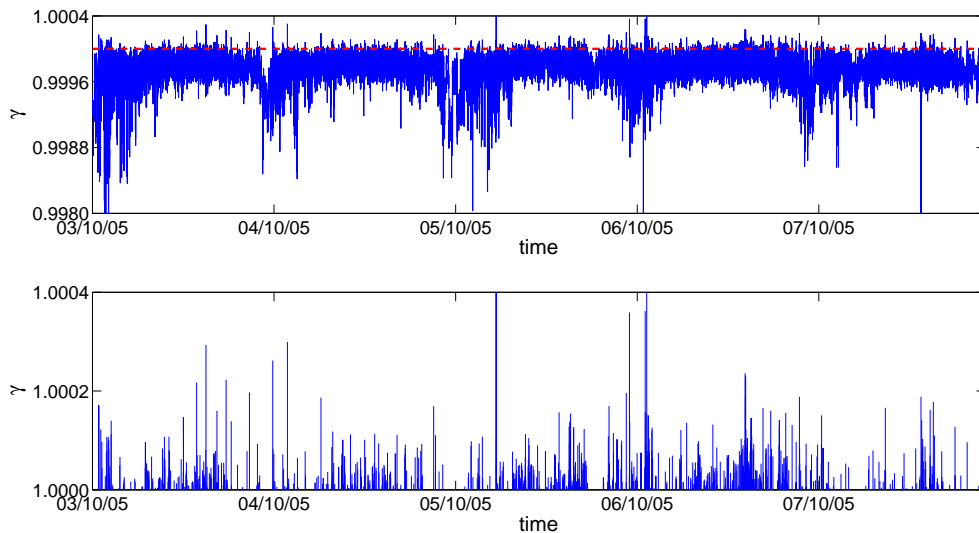


Figure 2.2: Rate product evolution for the period 03/10/2005–07/10/2005 for the transaction EUR→USD→JPY→EUR. Upper: all rate products, with a few extreme values removed so that the structure around the typical values is clearer. All points above the red line correspond to potential triangular arbitrages. Lower: the same plot truncated vertically at $\gamma = 1$ so that each spike represents an arbitrage opportunity.

The distributions in Fig. 2.3 show that, as expected, the rate product tends to be slightly less than one and typically $\gamma \in [0.9999, 1]$. The log-linear plots also highlight that the distributions possess long tails extending to smaller values of the rate product and that there are some times when $\gamma > 1$. This means that for the majority of

⁶Triangular parity implies that the direct exchange rate is equal to the exchange rate generated through the cross-rates. For example, $\text{EUR}/\text{USD} = (\text{EUR}/\text{JPY})/(\text{USD}/\text{JPY})$, where one needs to use the correct bid and ask price to construct the synthetic exchange rate.

deviations from triangular parity the individual exchange rates are shifted in such a direction that triangular arbitrage is not possible, but that occasionally potential profit opportunities do occur. Over the four week period analyzed there are 10,018 triangular arbitrage opportunities for the two CHF-based transactions given by Eqs. (2.2) and (2.3) and 11,367 for the equivalent JPY transactions.

We now establish both the duration and magnitude of these potential arbitrages and attempt to determine whether or not they represent genuine, executable profit opportunities.

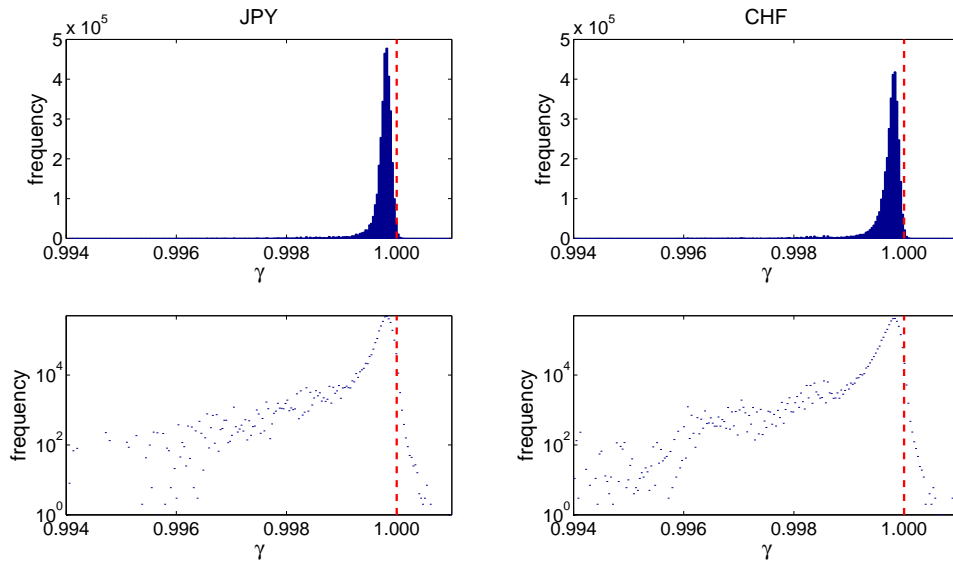


Figure 2.3: Occurrence frequency for rate products of different magnitudes for the period 02/10/2005–27/10/2005. Upper: aggregated results for both JPY transactions and CHF transactions. Any parts of the histograms to the right of the line at $\gamma = 1$ correspond to potential triangular arbitrages. The JPY panels show all data points within this period and the CHF panels all points except a few at very small and very large γ . Lower: the same distributions on a log-linear scale.

2.4.2 Durations

Firstly, we consider the length of periods for which $\gamma > 1$ and thus over which triangular arbitrage opportunities exist. We define an X second arbitrage as one for which $\gamma > 1$ for more than $X - 1$ seconds, but less than X consecutive seconds. In Fig. 2.4, we show the distributions of the observed durations of arbitrage opportunities and we provide summary statistics for these distributions in Table 2.1. The vast majority of arbitrage opportunities are very short in duration; although some opportunities

appear to exist for in excess of 100s, for both currency groups 95% last for 5 seconds or less and 60% for 1 second or less.

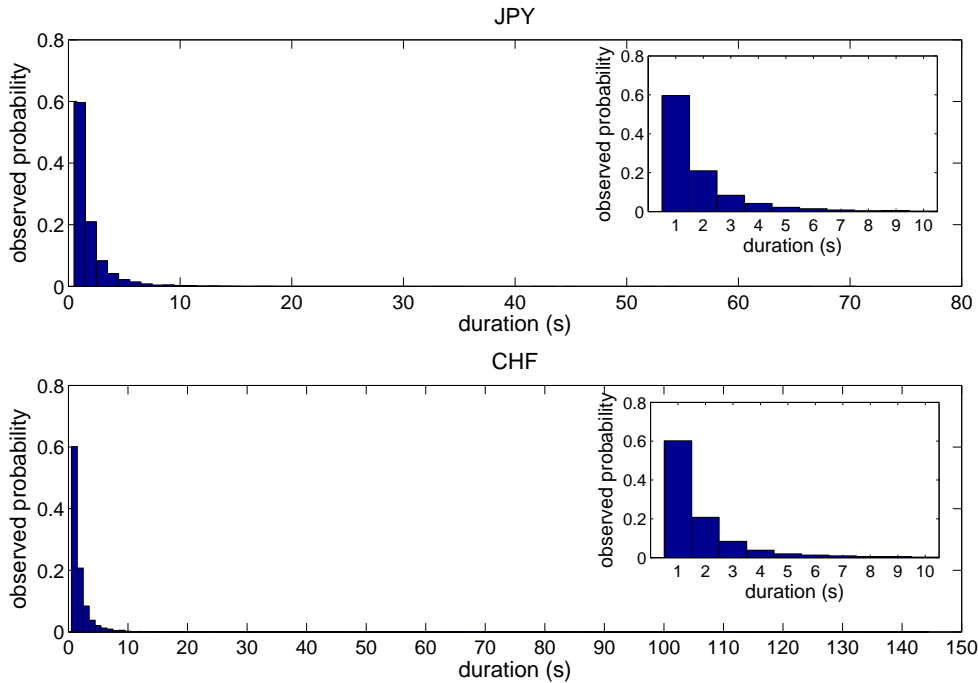


Figure 2.4: Distributions showing the durations of arbitrage opportunities for the period 02/10/2005–27/10/2005 for JPY (upper) and CHF (lower) transactions. The insets show the region of the distributions for arbitrage opportunities with durations of between 1 and 10 seconds.

The three constituent trades of a triangular arbitrage transaction can be submitted extremely fast using an electronic trading system, but there is still a delay from the time that the opportunity is identified, and the trades initiated, to the time that the trades arrive at the price source. Although this delay is typically only of the order of milliseconds, it is nonetheless significant. If the trader places each trade as a limit order that will only be filled at the arbitrage price then if one of the prices moves, due to trading activity or the removal of a price by the party posting it, the transaction will not be completed. For example, consider the transaction $EUR \rightarrow USD \rightarrow CHF \rightarrow EUR$ and assume that a trader completes the $EUR \rightarrow USD$ and $CHF \rightarrow EUR$ transactions at arbitrage prices. If the $USD \rightarrow CHF$ transaction is not completed because the USD/CHF has moved to an arbitrage-free price the trader will be left with a long

Transaction	Duration (s)				Percentage of opportunities					
	mean	median	min.	max.	1s	2s	3s	4s	5s	> 5s
JPY	2.01	1	1	70	60	21	8	4	2	5
CHF	2.09	1	1	144	60	21	8	4	2	5

Table 2.1: Summary statistics for the duration of arbitrage opportunities for the two JPY and two CHF transactions for the period 02/10/2005–27/10/2005. An opportunity labelled as X s lasted for more than $X - 1$ but less than X seconds.

position in USD and a short position in CHF.⁷ The trader may choose to unwind⁸ this position immediately by converting USD into CHF and this transaction will cost the amount by which the price has moved from the arbitrage price. Over a short time-scale, this is likely to be 1–2 points (approximately 1.5–2 basis points). Incomplete arbitrage transactions therefore typically cost a small number of basis points.

The extremely short time scales involved in these trades means that the physical distance between the traders and the location where their trades are filled is important in determining which trade arrives first and is completed at the arbitrage price. This explains why a number of exchanges have begun to offer the possibility of locating trading systems on their premises. A trader has a higher chance of completing an arbitrage transaction for opportunities with longer durations because the arbitrage prices remain active in the market for longer. When an arbitrage signal is received, however, there is no way of knowing in advance how long the arbitrage will exist. Over half of all arbitrage opportunities last for less than 1 second, so there is a high probability that any signal that is traded on is generated by an opportunity of less than a second. This includes many opportunities that last for only a few milliseconds. For these opportunities there is a smaller chance of the transaction being completed at an arbitrage price. For each attempted arbitrage, one cannot eliminate the risk that one of the prices will move to an arbitrage-free price before the transaction is completed.

2.4.3 Magnitudes

Given these risks, one possible criterion that could be used to decide whether or not to trade is the magnitude of the apparent opportunity. If the value of the rate product

⁷In market parlance, a trader buying an asset is opening a long position and a trader selling an asset is opening a short position.

⁸This is the closure of an investment position by executing the opposite transaction. For example, if a trader has bought an asset A, they can unwind their position in A by selling the asset.

is large, and thus it appears that a significant profit could potentially be gained, one may decide that the potential reward outweighs the associated risks and execute the arbitrage transactions. In this section we consider the magnitudes of the arbitrage opportunities.

	Basis point threshold	0	0.5	1	2	3	4	5	6	7	8	9	10
JPY	No. of arbitrages	17,314	5,657	1,930	220	50	21	7	3	1	1	1	0
	Mean duration (s)	3.3	3.0	2.6	1.5	1.6	1.4	1.6	1.0	1.0	1.0	1.0	0
CHF	No. of arbitrages	10,018	2,376	649	119	37	20	15	7	6	6	6	5
	Mean duration (s)	2.1	1.5	1.5	1.9	1.9	1.8	2.0	2.6	2.8	2.8	2.3	2.2

Table 2.2: The number and mean duration of arbitrage opportunities exceeding different thresholds for the two JPY transactions and two CHF transactions for the period 02/10/2005–27/10/2005. A one basis point threshold corresponds to a rate product of $\gamma \geq 1.0001$.

Table 2.2 demonstrates that most arbitrage opportunities have small magnitudes, with 94% less than 1 basis point for both the JPY and CHF. An arbitrage opportunity of 1 basis point corresponds to a potential profit of 100 USD on a 1 million USD trade. A single very large trade (or a large number of smaller trades) would thus be required in order to realize a significant profit on such an opportunity. Large volume trades are, however, often not possible at the arbitrage price. For example, consider the transaction $\text{EUR} \rightarrow \text{USD} \rightarrow \text{JPY} \rightarrow \text{EUR}$ at a time when $\text{EUR}/\text{USD}_{\text{bid}} = 1.2065$, $\text{USD}/\text{JPY}_{\text{bid}} = 115.72$ and $\text{EUR}/\text{JPY}_{\text{ask}} = 139.60$, resulting in $\gamma = 1.000115903$. If there are only 10 million EUR available on the first leg of the trade at an arbitrage price then the potential profit is limited to 1,159 EUR. In practice, the amount available at the arbitrage price may be substantially less than 10 million USD and consequently the potential profit correspondingly smaller.

This calculation also assumes that it is possible to convert the full volume of currency at an arbitrage price for each of the other legs of the transaction. In practice, however, the volumes available on these legs will also be limited. For example, again consider the case where there are 10 million EUR available at an arbitrage price on the first leg of the above transaction. If the full 10 million are converted into USD, the trader will hold 12.065 million USD. There may, however, only be 10 million USD available at an arbitrage price on the next leg of the trade. In order for the full volume to be traded at an arbitrage price, the trader should therefore limit the initial EUR trade to $10/1.2065 = 8.29$ million EUR. The volume available on the final leg of the trade would also need to be considered in order to determine the total volume that

can be traded at an arbitrage price. This volume and the total potential profit are therefore determined by the leg with the smallest available volume.

Occasionally, larger magnitude arbitrage opportunities can occur. Table 2.2 shows that, over the studied period, there are potential arbitrages of more than 9 basis points for both currency groups, with a mean duration⁹ of in excess of 2 seconds for the large CHF opportunities. This duration suggests that one would have stood a good chance of completing an arbitrage transaction for one of these opportunities. However, this mean was calculated using only six opportunities and so does not represent a reliable estimate of the expected duration. The fact that these large opportunities occur so infrequently (with only around 20 potential arbitrages in excess of 4 basis points occurring for each transaction over the four week period analyzed) means that trading strategies that only trade on these larger opportunities would need to make large volume trades in order to realize significant profits. As we have already discussed though, there is only ever a limited volume available at the arbitrage price.

2.4.4 Seasonal variations

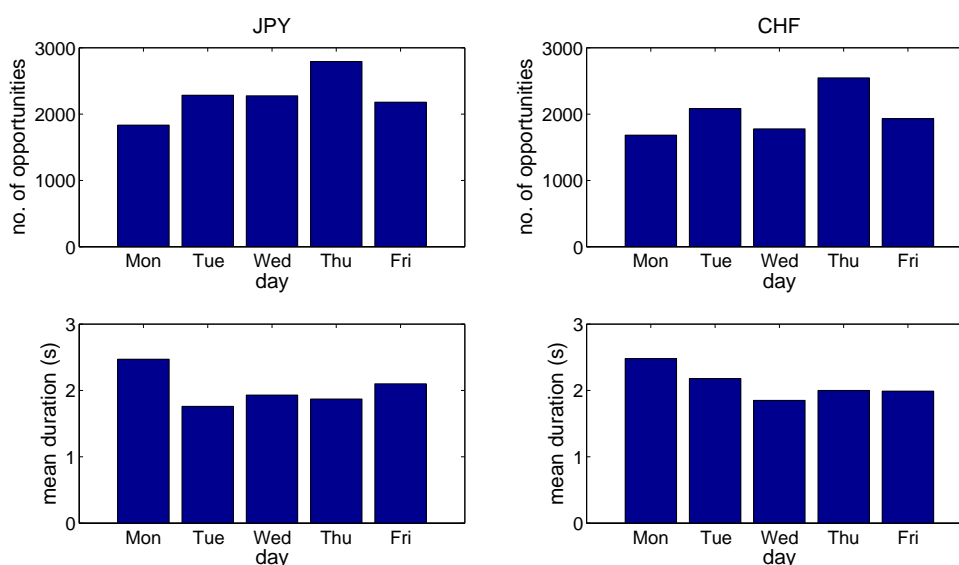


Figure 2.5: Daily arbitrage statistics for the period 02/10/2005–27/10/2005. Upper: the number of arbitrage opportunities. Lower: mean duration of arbitrage opportunities.

⁹Each mean duration represents an upper bound. This is because each opportunity labelled as X s may have existed for anywhere between $X - 1$ and X seconds, but in calculating the mean duration we assume that it lasted for exactly X seconds.

We now consider whether there is any seasonality in the number and duration of arbitrage opportunities by investigating daily and hourly statistics. Figure 2.5 shows that the number of arbitrage opportunities per day and their mean duration is reasonably uniform across days. However, Fig. 2.6 demonstrates that there is a large amount of variation in these quantities for different hours of the day. Both the JPY and CHF transactions show a particularly small number of opportunities, with a large mean duration, between approximately 22:00 and 01:00, and a large number of opportunities, with a short duration, between 13:00 and 16:00. In general, the hours with larger numbers of arbitrage opportunities correspond to those with shorter mean durations and vice versa.

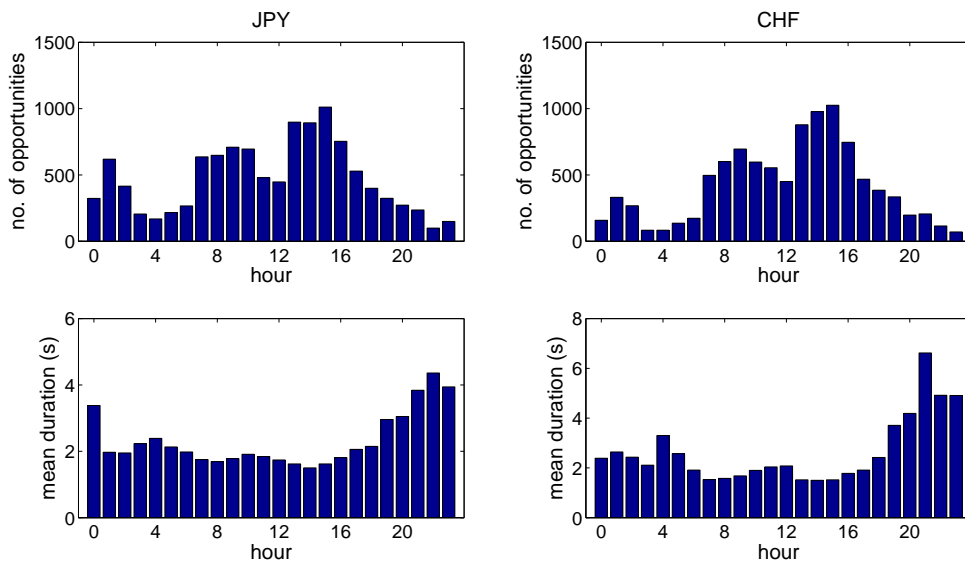


Figure 2.6: Hourly arbitrage statistics for the period 02/10/2005–27/10/2005. Upper: the number of arbitrage opportunities. Lower: mean duration of arbitrage opportunities.

	0	1	2	3	4	5	6	7	8	9	10	11	12	13	14	15	16	17	18	19	20	21	22	23	
Asia																									
Europe																									
Americas																									

Table 2.3: Grey blocks indicate the hours corresponding to high liquidity for the Asian, European and American markets.

These differences can be explained by the variation in liquidity throughout the trading day. Table 2.3 shows the periods during which the Asian, European and

American FX markets are at their most liquid. The period of highest liquidity is from 08:00–16:00; over almost all of this period two of the markets are highly liquid at similar time. The period of least liquidity is from around 22:00–01:00. The hours with the largest number of arbitrage opportunities and the shortest mean durations in Fig. 2.6 thus correspond to the periods of highest liquidity. This observation of more arbitrage opportunities during the periods of highest liquidity seems counter-intuitive but can be explained as follows. During liquid periods the bid-ask spread is narrower (see Fig. 2.1) and prices move around at a higher frequency due to the large volume of trading. This results in more price mis-alignments and consequently more potential arbitrages. The high trade frequency, however, also ensures that the mis-pricings are quickly traded away or removed and that any arbitrage opportunities are short-lived. In contrast, during less liquid periods the spread is wider and the trading volume lower which leads to fewer arbitrage opportunities. The smaller number of traders available to correct any mis-pricings during less liquid times also results in the arbitrages having longer durations.

2.4.5 Annual variations

The analysis so far has focused on a four week period in October 2005. We now consider how the number and distribution of triangular arbitrage opportunities has changed over the years by comparing results for the weeks 27/10/2003–31/10/2003, 01/11/2004–05/11/2004 and 17/10/2005–21/10/2005. These three weeks all fall at the same time of year, so any seasonal factors are eliminated.

Transaction	Year	No. arbitrages	Percentage of opportunities						Rate product statistics	
			1s	2s	3s	4s	5s	> 5s	mean	stand. dev.
JPY	2003	4,220	40	30	14	6	3	7	0.999625	4.32×10^{-4}
	2004	3,662	49	28	12	5	3	3	0.999723	2.25×10^{-4}
	2005	2,963	62	21	7	4	3	3	0.999758	2.17×10^{-4}
CHF	2003	3,590	41	29	13	6	4	7	0.999549	6.02×10^{-4}
	2004	3,441	49	27	11	5	3	5	0.999663	3.54×10^{-4}
	2005	2,672	64	20	8	3	1	4	0.999725	3.10×10^{-4}

Table 2.4: Comparison of the number and percentage of arbitrage opportunities of selected durations and the mean and standard deviation of the rate product for the periods 27/10/2003–31/10/2003, 01/11/2004–05/11/2004 and 17/10/2005–21/10/2005. An opportunity labelled as X s lasted for more than $X - 1$ but less than X seconds.

Table 2.4 shows that the number of arbitrage opportunities decreased from 2003–2005 for the JPY and CHF transactions. This can be explained by the increasingly wider use of electronic trading platforms and trading algorithms over this period.

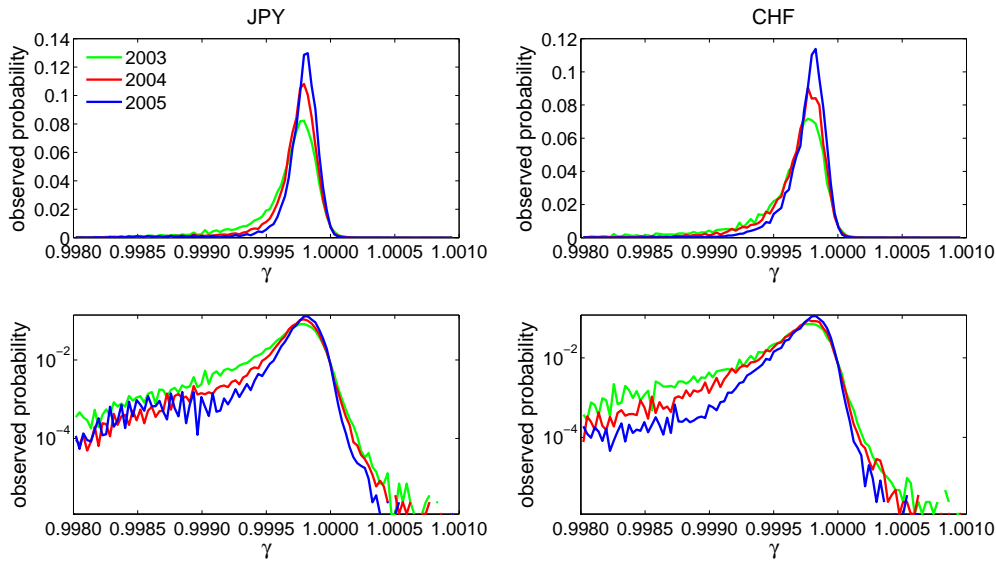


Figure 2.7: Comparison of the rate product distributions for the periods 27/10/2003–31/10/2003, 01/11/2004–05/11/2004 and 17/10/2005–21/10/2005. Lower: distributions on a log-linear scale.

These systems enabled traders to execute trades faster and to react more quickly to price changes, which in turn gave rise to increased trading efficiency, fewer mispricings and fewer triangular arbitrage opportunities. Table 2.4 also demonstrates the significant effect that this increased execution speed had on the duration of arbitrage opportunities. From 2003–2005, the proportion of opportunities lasting less than 1 second increased from 40% to 62% for the JPY transactions and from 41% to 64% for the CHF transactions; and the proportion of opportunities lasting in excess of 5 seconds halved for both sets of transactions.

The distributions in Fig. 2.7 and the distribution statistics in Table 2.4 provide further evidence of the increased pricing efficiency of the FX market from 2003 to 2005. Over this period the distribution of rate products became concentrated in a sharper peak, with a smaller standard deviation and mean closer to one, which demonstrates that triangular parity held a larger proportion of the time.

2.5 Profitability

We provide further insights into the profitability of trading on triangular arbitrage signals by running simulations to determine the profit or loss that could potentially be achieved using different trading strategies. For the full time series of JPY and CHF

rate products (over the period 02/10/2005–27/10/2005) we execute a simulated trade each time γ exceeds some threshold amount γ_t . We consider the cases $\gamma_t = 1$, i.e., all arbitrage signals are traded on irrespective of their magnitude, and $\gamma_t = 1.00005$ and 1.0001 , corresponding to thresholds of half and one basis points respectively. We consider the following two scenarios for determining whether an arbitrage is filled:

- (1) Each traded arbitrage is filled with a fixed probability P_1 .
- (2) All arbitrages with a duration $l \geq 1$ second are definitely filled. All opportunities traded on with a length $l < 1$ second are filled with probability P_2 .

We consider that, for each completed arbitrage transaction, a profit determined by the rate product at the corresponding time step is received and for each unfilled transaction a fixed loss, L , is incurred.¹⁰ We assume that each arbitrage opportunity with a duration $l \geq 1$ second can only be traded on once, at its initial value, because if the simulated trader is left unfilled a competing trader must have been filled, resulting in the opportunity being removed. It is further assumed that, for each filled transaction, there is sufficient liquidity on each leg of the trade for it to be fully completed at the arbitrage price.

Figure 2.8 shows the mean profit per trade for scenario (1), as a function of P_1 and L , for the JPY transactions. For a typical fixed loss per unfilled arbitrage of $L = 1.5$ (see Section 2.4.2), an 80% fill probability is required to just break-even. Even for $P_1 = 1$ the maximum potential profit is less than half a basis point per transaction (about 50 USD on a 1 million USD trade).

We consider the total potential profit for the JPY transactions over the four week period 02/10/2005–27/10/2005 by simulating a trade of 1 million EUR, each time $\gamma > \gamma_t$, and we assume a loss of $L = 1.5$ basis points for each incomplete arbitrage transaction. Figure 2.9 shows that for a 100% fill probability, and a trade threshold of $\gamma_t = 1$, a total profit of just under 400,000 EUR appears possible for both scenarios (1) and (2). For higher values of γ_t , and a 100% fill probability, the potential profit over the same period is smaller. The profit is smaller for higher γ_t because there are fewer opportunities exceeding the thresholds, so fewer profit opportunities. The larger mean profit possible for each opportunity exceeding γ_t is not sufficient to compensate for their reduced frequency. For a fill probability of zero, the lower trade frequency at higher thresholds limits the total possible loss relative to lower thresholds.

¹⁰A fixed loss for each unfilled transaction is unrealistic and means that it is not possible to reliably estimate the volatility of the returns. It is, however, a reasonable first approximation.

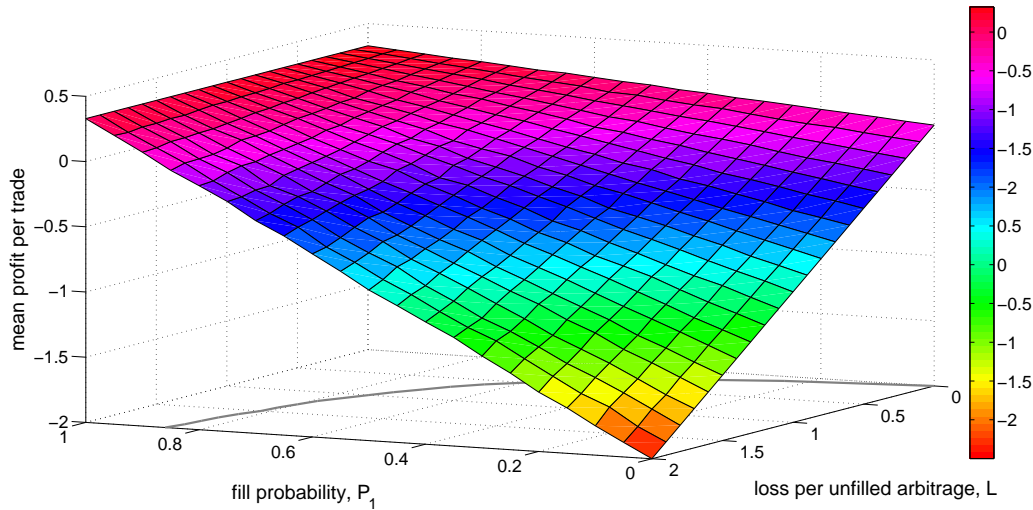


Figure 2.8: Mean profit/loss per trade (in basis points) as a function of the probability of a transaction being filled at an arbitrage price and the loss incurred on missed arbitrages for JPY transactions over the period 10/02/2005–10/27/2005. We assume a trade threshold $\gamma = 1$ and scenario (1). The grey curve shows the break-even fill probabilities. The probabilities are averaged over 100 simulations.

In order to achieve the 400,000 EUR profit, it would have been necessary to stake 1 million EUR more than 17,000 times. If we estimate transaction fees and settlement costs at 2 EUR per trade, then each arbitrage transaction costs 6 EUR. The total cost of 17,000 transactions is then 102,000 EUR, which is a significant proportion of the potential profits. This profit is also likely to be a significant over-estimate. In the simulations, we assumed that each arbitrage transactions is completed for the full 1 million EUR initially staked. As discussed in Section 2.4.3, however, the amount available at the arbitrage price is limited and may be less than this amount. More importantly, a 100% fill probability is extremely unrealistic and in practice the achievable fill probability will be significantly smaller. At a still unrealistic fill probability of $P_2 = 0.8$, for scenario (2), the potential profit is reduced to around 100,000 EUR. This potential profit is already less than the estimated transaction costs and there are additional infrastructure costs that also need to be considered.

2.6 Fill probabilities

Finally, we investigate the fill probabilities in more detail to provide more insight into the chances of completing an arbitrage transaction. For scenario (1), consider a

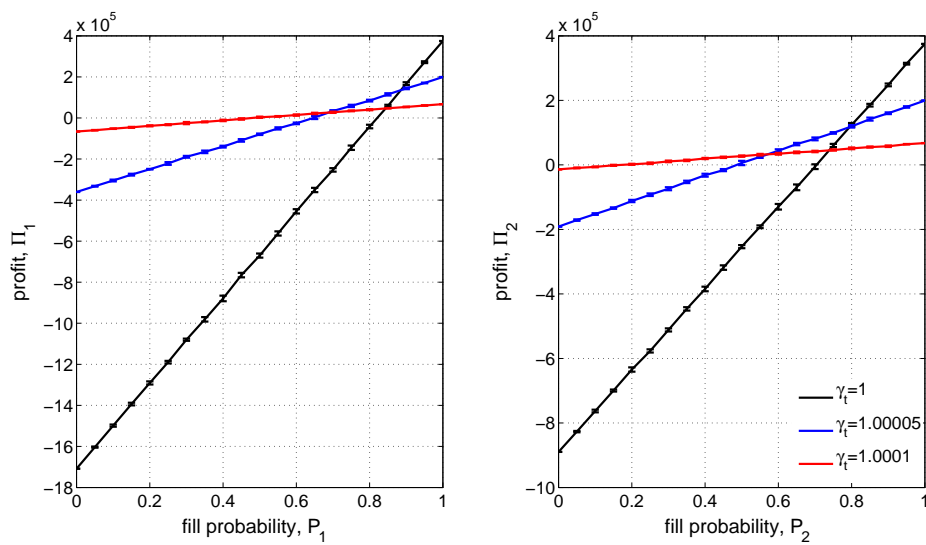


Figure 2.9: Total profit (in EUR) for JPY transactions over the period 02/10/2005–27/10/2005. Each arbitrage transaction is traded with an initial currency outlay of 1 million EUR and each completed transaction is filled for the full traded volume. We assume a fixed loss $L = 1.5$ basis points for each incomplete arbitrage transaction. Left: scenario (1). Right: scenario (2). Error bars indicate the standard deviation in the profit over 100 simulations. The standard deviations in the profit for $P_1 = 0$, $P_1 = 1$, $P_2 = 0$, and $P_2 = 1$ are zero because the same arbitrage opportunities are filled for each simulation.

trading strategy in which a volume V is traded on each of N_a arbitrage opportunities exceeding a threshold γ_t over some time interval W . The total potential profit Π_1 over this interval is then given by

$$\Pi_1 = N_a V [P_1 \langle \gamma - 1 | \gamma > \gamma_t \rangle - (1 - P_1)L], \quad (2.4)$$

where $\langle \gamma - 1 | \gamma > \gamma_t \rangle$ denotes the average value of $\gamma - 1$ over the interval W given that $\gamma > \gamma_t$, and the break-even fill probability P_1^b (found when $\Pi_1 = 0$) is given by

$$P_1^b = \left[1 + \frac{\langle \gamma - 1 | \gamma > \gamma_t \rangle}{L} \right]^{-1}. \quad (2.5)$$

The break-even fill probability P_1^b is therefore independent of the number of arbitrage opportunities and decreases with increasing $\langle \gamma - 1 | \gamma > \gamma_t \rangle$. This can be seen in Fig. 2.10 where the break-even fill probabilities are smaller for larger γ_t . For scenario (2), we take $N_a = n_g + n$, where n_g is the number of opportunities over W that last for $l \geq 1$ second, and n the number with $l < 1$ second. The total profit Π_2 is then given by

$$\Pi_2 = n_g V \langle \gamma - 1 | \gamma > \gamma_t, l \geq 1 \rangle + n V [P_2 \langle \gamma - 1 | \gamma > \gamma_t, l < 1 \rangle - (1 - P_2)L], \quad (2.6)$$

and the break-even fill probability by

$$P_2^b = \left[1 - \frac{n_g \langle \gamma - 1 | \gamma > \gamma_t, l \geq 1 \rangle}{nL} \right] \left[1 + \frac{\langle \gamma - 1 | \gamma > \gamma_t, l < 1 \rangle}{L} \right]^{-1}. \quad (2.7)$$

For this scenario, the break-even fill probability P_2^b therefore depends on the proportion of arbitrage opportunities with length $l \geq 1$, the mean value of the rate product for opportunities with length $l \geq 1$, and the mean rate product for opportunities with $l < 1$.

Figure 2.10 shows break-even fill probabilities generated by trading simulations and highlights the fact that P_2^b is lower than P_1^b , for the corresponding loss, and that the break-even fill probabilities tend to be slightly lower for the CHF than for the JPY transactions. This difference is most marked for scenario (2), with $\gamma_t = 1.0001$. In this case, if a fixed loss of 2 basis points per unfilled arbitrage is assumed, a fill probability of only 17% is needed to break-even.

Although this fill probability seems low, it would nevertheless be difficult to achieve. Consider a strategy where a similar fill probability of 20% is required to break-even. This implies that one would need to be filled on 1 in 5 of the arbitrage opportunities traded on. If there are 5 market participants trading on each opportunity, each able to transact at the same speed, then this fill frequency is feasible.

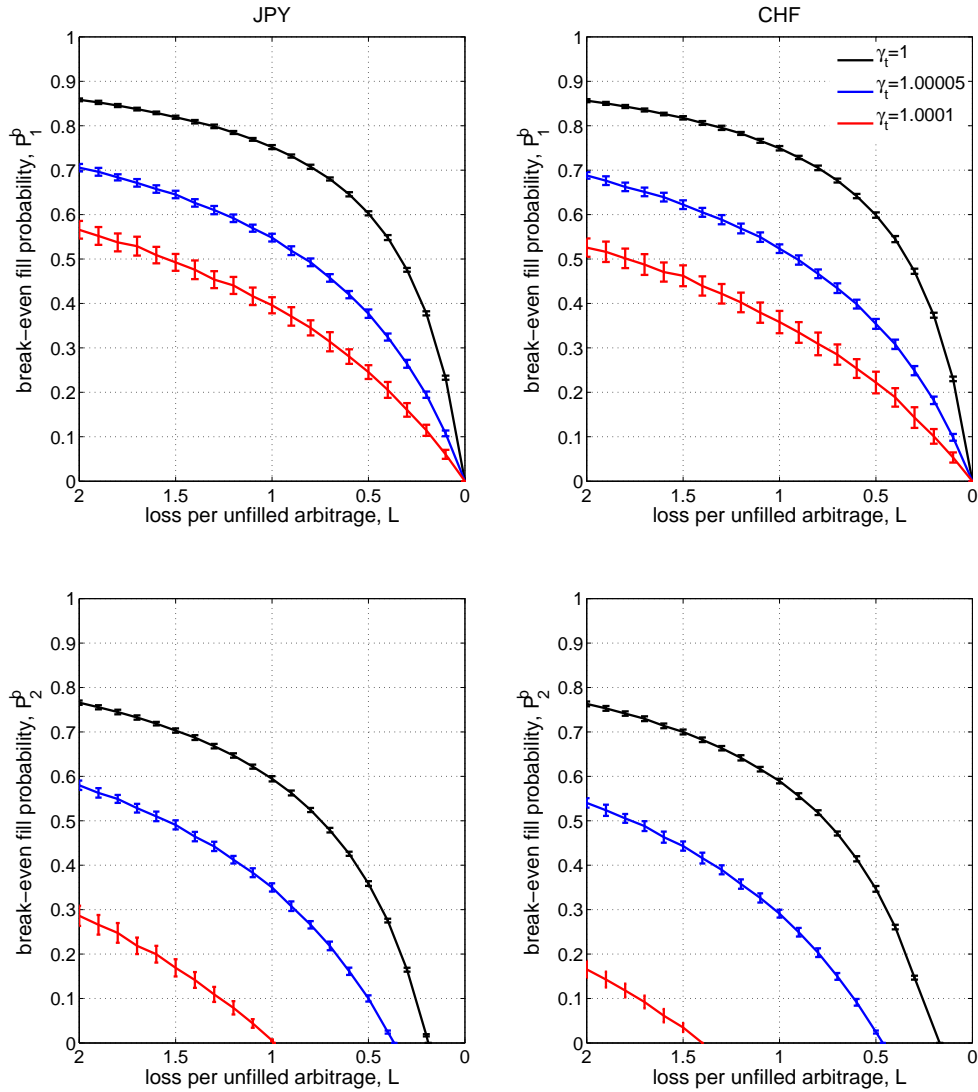


Figure 2.10: The fill probability required to break-even as a function of the loss incurred per incomplete arbitrage transaction. Upper: scenario (1). Lower: scenario (2). Error bars indicate the standard deviation in the fill probability over 100 simulations.

However, in the FX market there are many more market participants than this competing for each arbitrage opportunity, so to achieve this fill probability one would need to identify and execute each arbitrage opportunity faster than most of these competitors. These competitors are also likely to be continually striving to increase their execution speeds in the electronic trading “arms race”. Given the costs associated with staying ahead in this race, it would be extremely costly to maintain the fastest execution speeds and to regularly beat the majority of other competitors to the arbitrage prices over a prolonged period of time. The fill probabilities required to realize the profits indicated in Fig. 2.9 are therefore very difficult to achieve and, as a consequence, the profit levels are also extremely unrealistic.

The calculated fill probabilities also represent lower bounds of acceptability because to justify trading on an opportunity a trader would expect a reasonably high expected profit and not simply to break-even. When one factors in costs such as brokerage, the internet connections required to access the market, and the cost of developing and supporting a sophisticated electronic trading system, the actual fill probabilities necessary to achieve an acceptable level of profit would be substantially higher than those calculated. It therefore appears that, although mis-pricings do appear in the FX market, an unfeasibly large fill probability would need to be achieved over a prolonged period of time to realize any significant profits from them.

2.7 Summary

We have shown that triangular arbitrage opportunities exist in the FX market, but the vast majority of these opportunities are less than 1 second in duration and 1 basis point in magnitude. The longer, larger opportunities that do occur appear with a significantly lower frequency. We showed that, somewhat counter-intuitively, more arbitrage opportunities occur during periods of higher liquidity, but these opportunities tend to be removed from the market very rapidly. The increased number of opportunities during liquid periods was attributed to the higher trading frequency, which resulted in more mis-pricings, but also ensured that they were quickly corrected. We have also shown that from 2003 to 2005 the market became increasingly efficient at eliminating mis-pricings and explained this by the increased use of electronic trading platforms, which enabled traders to react faster to price changes.

Finally, we used trading simulations to investigate the profitability of trading on triangular arbitrage signals. Considering the strong competition for each arbitrage, the costs of trading, and the costs required to maintain a technological advantage, it

seems that a trader would need to beat other market participants to an unfeasibly large proportion of arbitrage opportunities for triangular arbitrage to remain profitable in the long-term. We therefore conclude that the FX market appears internally self-consistent and these results provide a limited verification of FX market efficiency.

This chapter has also demonstrated the critical importance of using the correct type of data to study financial markets. If one uses data that is inappropriate for a particular analysis, it is easy to conclude that data artifacts represent meaningful structure. For example, when indicative FX price data is used to investigate triangular arbitrage, arbitrage opportunities appear to remain active in the market longer, and to be more profitable, than when executable data is used.

Chapter 3

A Principal Component Analysis of Financial Market Correlations

In this chapter, we continue to investigate financial markets, but extend the analysis to include assets from other major markets in addition to the FX market. We have submitted a paper based on this work for publication [P5]. We return to the FX market in Chapter 5.

3.1 Introduction

The global financial system is composed of a multitude of markets spread across a range of geographic locations with a wide variety of assets traded in each market. There is strong coupling between different financial markets such that the price changes of particular assets can be driven not only by the price changes of assets traded in the same market, but also by price changes of assets traded in other markets. Because of the close relationships between different assets and markets, a primary concern of market practitioners is estimating the correlations between the changes in asset price time series. There are many reasons for wanting to understand correlations in price movements; perhaps the most common motivation is for risk management purposes. For a portfolio of assets, the likelihood of large losses can be significantly higher when the assets held in the portfolio are correlated [176]; an understanding of the correlation between different financial instruments can therefore help in managing the risk associated with a portfolio. The standard approach for representing the correlations of a group of financial assets is to calculate the linear correlation coefficient between pairs of assets. However, for N assets, this results in $\frac{1}{2}N(N-1)$ correlation coefficients, so simultaneous investigation of these interactions

is difficult for even moderate N . Attaining an understanding of the market system therefore necessitates some form of simplification.

In this chapter, we simplify the analysis of financial market correlations by extracting common features using PCA. We first coarse-grain the correlation matrix by identifying the principal components (PCs) that account for a large proportion of the variability of the system. We then characterize the evolving relationships between the different assets by analyzing the correlations between the asset price times series and PCs. By focusing on correlations between the price time series and PCs, we significantly reduce the number of correlations that we need to consider to attain an understanding of the system. Using this approach, we uncover notable changes that occurred in financial markets and we identify the assets that were significantly affected by these changes.

3.1.1 Components and factors

It has been widely observed that price time series for different financial assets display similar characteristics and, because the prices often depend on the same economic data and market signals, it is often hypothesized that financial time series can be decomposed into common drivers or *factors* [296]. The aim of factor modelling in finance is to try to identify these factors. Several approaches to factor modelling are closely related to PCA and some use PCA as a tool for identifying factors [63]. Because of the close ties between the two techniques, we provide an overview of factor modelling in this section. We highlight, however, that there is an important difference between what we are trying to achieve using PCA and the objective of factor modelling. In factor modelling, the aim is to identify a number of “fundamental” market factors that drive asset prices; these factors can be unobservable and often factor models incorporate random errors that represent the variability in the system not explained by the factors. In contrast, we use PCA to produce a parsimonious representation of market correlations and we make no assumptions about whether the components that we identify correspond to fundamental market variables. In fact, it is likely that the PCs are themselves a combination of several underlying factors.

3.1.1.1 Factor models

Factor models can be separated into two classes: confirmatory and exploratory. Although this classification is slightly fuzzy, it helps to illustrate the different techniques. Many of these models assume that the observed price series can be written as linear combinations of common factors. In confirmatory factor modelling, a number

of indicator variables are selected that are posited to drive the observed price time series and a factor model is constructed to test this prediction. There are two main types of confirmatory factor models in finance [296]: macroeconomic and fundamental models. Macroeconomic factor models attempt to explain the behaviour of asset returns using macroeconomic variables, such as interest rates and GDP growth rates. The relationship between these indicator variables and the observed assets is usually determined using linear regression. Fundamental factor models try to explain price movements using fundamental properties of the assets; for example, using properties such as market capitalization and industrial sector to explain equity price movements. Again, the relationships between the indicator variables and the observed assets are usually determined using linear regression [63, 296].

3.1.1.2 Principal component and factor analysis

The second class of factor models are exploratory methods. In contrast to confirmatory models, exploratory methods make no assumptions about which variables correspond to the underlying factors; instead, the factors are estimated directly from the asset return time series. Two widely used exploratory techniques are factor analysis¹ (FA) and PCA [63, 301]. The two names are often used interchangeably in the literature and the two approaches share the common goal of reducing a set of N observed variables to a set of $m < N$ new variables [301]. However, there are clear distinctions between the two techniques.

In FA the aim is first to identify factors that are common to two or more variables and these factors can either be correlated or uncorrelated. In addition to the common factors, a set of unique factors are also identified that are specific to each variable and orthogonal to each other and to all of the common factors [103]. In PCA the PCs are identified on the basis of variance. The first component accounts for as much of the variance in the system as possible, the second as much of the remaining variance as possible, and so on. In PCA the components are chosen such that they are mutually orthogonal and account for all of the variability in the system; there are no unique components specific to particular variables.

The differences between PCA and FA can be better understood by considering the decomposition of the covariance matrix of the observed variables in the two cases. If we let \mathbf{Z} represent an $N \times T$ matrix of T observations of the return time series of

¹Note the distinction between factor modelling and factor analysis – factor analysis is a type of factor modelling.

N assets, for FA the covariance matrix $\Sigma_{\mathbf{Z}}$ of \mathbf{Z} can be written as

$$\Sigma_{\mathbf{Z}} = \mathbf{\Omega}_F \Sigma_F \mathbf{\Omega}_F^T - \varepsilon^2, \quad (3.1)$$

where $\mathbf{\Omega}_F$ is a matrix of common factor weights, Σ_F is the covariance matrix of the common factors, ε^2 is a diagonal matrix of unique factor variances, and T indicates a matrix transpose. Using PCA the covariance matrix $\Sigma_{\mathbf{Z}}$ can be written as

$$\Sigma_{\mathbf{Z}} = \mathbf{\Omega} \Sigma_{\mathbf{Y}} \mathbf{\Omega}^T, \quad (3.2)$$

where $\mathbf{\Omega}$ is the matrix of PC coefficients and $\Sigma_{\mathbf{Y}}$ is the covariance matrix of the principal components.² Equations 3.1 and 3.2 highlight the key differences between the two models. The additional term ε^2 in the FA equation allows for specific factors that are unique to particular observed variables [297]. In contrast, PCA does not explicitly allow for unique factors, instead the components represent both unique and common variance. The components identified using PCA therefore account for all of the variability of the system, whereas the common factors in FA often do not.

There is some debate on the relative merits of FA and PCA for factor modelling and on whether the outputs of the two methods are equivalent [297,301,307]. Because it is not our objective to use PCA to derive a factor model in this chapter, it is not necessary to perform a comprehensive comparison of the two techniques. Nevertheless, it is instructive to highlight some of the main performance differences. It is often argued that one of the major advantages of PCA over FA is the relative simplicity of the process of fitting the model [160,297] and, in fact, some FA techniques use PCA as just a first step in the process of identifying the factors [103]. Another argument used in support of PCA is that it is able to identify the elements in the matrix $\mathbf{\Omega}$ (to within a sign), whereas the entries in $\mathbf{\Omega}_F$ cannot be determined exactly [297]. Despite these differences, it has been noted that the two methods produce very similar results if the error terms in the factor model all have the same variance [66,72]. In fact, it can be seen from Eqs. 3.1 and 3.2 that when the unique variances are zero, the two models are equivalent.

In this chapter, we use PCA in the same way that it is employed in factor modelling: to decompose the correlation matrix of multiple assets into a few explanatory variables. However, in contrast to factor modelling, we use PCA simply to characterize the changing correlation structures within markets and do not assume that the components that we identify are fundamental market factors. To emphasize this, we refer to components rather than factors.

²We discuss this equation in more detail in Section 3.3.

PCA is a well established tool in data analysis for generating lower-dimensional representations of multivariate data [159] and has provided useful insights in a diverse range of fields, including chemistry, e.g., [89], genetics, e.g., [245], psychology, e.g., [252], and astrophysics, e.g., [149]. In finance, PCA has been used to identify common factors in international bond returns, e.g., [81, 237] and in equity returns, e.g., [159, 296], and has been applied to other problems, such as arbitrage pricing theory, e.g., [66, 72], portfolio theory, e.g., [298], and to produce market indices, e.g., [101].

3.1.2 Random matrix theory

PCA is closely linked to random matrix theory (RMT), which was originally developed by Wigner to deal with the statistics of the energy levels of many-body quantum systems [308]. Wigner replaced the Hamiltonian of the system under investigation by an ensemble of random Hamiltonians (given by real symmetric matrices with independent random elements), which were considered to describe the generic properties of the system [137]. Using this method he successfully described the spectra of atomic nuclei and complex atoms. Subsequently, RMT has become an important tool in a wide range of other areas, including quantum field theory and two-dimensional gravity [137, 206], and recently in finance, e.g., [176, 239].

The standard financial approach is to compare the eigenvalues and eigenvectors of an empirical correlation matrix of asset returns with correlation matrices generated using time series of randomly distributed returns and with analytic distributions from RMT. The bulk of the eigenvalues of empirical correlation matrices are found to fall within the range predicted by RMT, which is usually taken as an indication that to a large extent the correlation matrix is random and dominated by noise. Further, it has been found that the smallest eigenvalues of the empirical correlation matrix are most sensitive to noise and, because the eigenvectors corresponding to the smallest eigenvalues are used to determine the least risky portfolios in Markowitz portfolio theory [199], this has implications for risk management [166, 176, 238, 239]. For example, if one holds a portfolio of two assets with highly correlated price movements, a decrease in the value of one of the assets is likely to be accompanied by a decrease in value of the other asset. If the assets in a portfolio are highly correlated, there is therefore a higher risk of a significant decrease in the portfolio value. This risk would be lower if there were a small correlation between the asset values. An understanding of correlations in asset price movements is therefore an important part of successful risk management and optimal portfolio selection [166, 176, 199, 238, 239]. The degree

to which it is possible to diversify risk is intrinsically linked to the number of common factors. If there are only a few significant factors driving markets, one would expect asset prices to be highly correlated and for it to be more difficult for market practitioners to hold diversified portfolios and consequently to lower their investment risk.

Prior studies of financial market price data using RMT and PCA have focused on specific markets. For example, there is a large body of work analyzing equity markets, e.g., [166, 176, 238, 239], and there have also been investigations of emerging market equities, e.g., [64, 235, 309], the FX market, e.g., [82], and bond markets, e.g., [81, 237]. Most prior studies only analyze a single correlation matrix and do not investigate the temporal evolution of correlations. However, changes in correlations are of critical importance in many financial applications; for example, changes in the extent to which assets held in a portfolio are correlated can have a significant impact on the risk associated with the portfolio. The work in this chapter differs from prior studies by investigating a diverse range of asset classes and by studying the evolution of the correlations between these assets. By studying the time dynamics of the correlations, we uncover periods during which there were major changes in the correlation structure of markets and identify the assets affected by these changes.

3.2 Data

3.2.1 Description

We study correlations for a wide variety of markets, but several factors limit the assets that we can include. For example, for some time series there are a large number of missing data points. One solution to this problem is to fill-in the missing data by interpolating between the data points that we do have, but this approach is inappropriate when there are several consecutive missing data points. A second reason for excluding time series is that they begin too recently. In this study, we use time series beginning in January 1999 because this time interval contains periods of very different market behaviour that we can compare. However, data is only available for some instruments for a few years. For example, although some emerging market corporate bond indices are now published, they have only been published since 2005 and consequently we do not include them. Other time series are complete and cover the full time period, but are excluded because of the nature of the data. For example,

we exclude any exchange rate that has been pegged³ for any of the studied period. The peg implies that the value of the pegged exchange rate can be determined using the rate (or rates) to which it is pegged, so the pegged rate is redundant.

Taking all of these factors into account, we include time series for 98 financial products from all of the major markets. This includes 25 developed market equity indices, 3 emerging market equity indices, 4 corporate bond indices, 20 government bond indices, 15 exchange rates, 9 metals, 4 fuel commodities, and 18 other commodities. (See Table A.1 in Appendix A for a description of all of the assets that we include.) For many markets, we study indices rather than specific assets so that we have an aggregate view of the market.⁴ For all of the commodities, we use futures⁵ contracts because commodities are most widely traded in the futures market. However, for single futures contracts, the price time series will have a discontinuity at the contract expiry date. To minimize this discontinuity, we use the “Generic 1st futures” contract for each commodity, which is the price of the nearest dated futures contract (i.e., the contract with the closest expiry date).

We include assets from a range of geographical regions, so many are traded during different hours of the day. For example, stocks included in the Nikkei 225 are traded on the Tokyo Stock Exchange, which operates between midnight and 6 AM GMT, whereas stocks included in the FTSE 100 index are traded on the London Stock Exchange, which operates between 8 AM and 4:30 PM GMT. To minimize any effects resulting from the non-synchronicity of the price time series for markets from different time zones, we use weekly price data. We take the weekly price of an asset to be the last price posted each week. In this study, we investigate the period from 08/01/1999–01/01/2010 and we have 575 prices for each asset.

³A pegged exchange rate is an exchange rate regime wherein a currency’s value is matched to the value of a single currency or a basket of currencies.

⁴By using indices the data is also representative of a larger set of assets than if we included time series for individual assets. For example, if we studied individual equities, we would need to include several stocks from each industrial sector to obtain a representative cross-section of the market; however, we can only include a limited number of assets in the analysis. We discuss the reasons for this in Section 3.2.3.

⁵A future is a standardized contract to buy or sell an asset at a specified future date at a price agreed on the day that the contract is entered in to.

3.2.2 Returns

We denote the price of asset i at discrete time t as $p_i(t)$, $i = 1, \dots, N$, and define a logarithmic return $z_i(t)$ for asset i between consecutive time steps as⁶

$$z_i(t) = \ln \left[\frac{p_i(t)}{p_i(t-1)} \right]. \quad (3.3)$$

In Fig. 3.1, we show that there are large differences between the return distributions for assets from different classes. For example, returns for U.S. government bonds are concentrated in a sharp peak around zero, whereas the distribution for oil has much more weight in the tails as a result of regular large moves in the oil price.

In calculating a correlation coefficient for a pair of time series, it is important to ensure that the time series are stationary [134]. We study returns rather than prices because, in general, return time series are close to stationary whereas price time series are not [73]. This can be demonstrated by considering the autocorrelation function (acf) of the two types of time series. The autocorrelation α_i of a time series z_i is given by

$$\alpha_i(\tau) = \frac{\sum_{t=1}^{T-\tau} [z_i(t) - \langle z_i \rangle] [z_i(t+\tau) - \langle z_i \rangle]}{\sum_{t=1}^T [z_i(t) - \langle z_i \rangle]^2}, \quad (3.4)$$

where $\langle \dots \rangle$ indicates a time average over $T - \tau$ returns and τ is the lag between time steps over which the autocorrelation is calculated. For stationary time series, the acf decays rapidly with increasing lag, but this is usually not the case for non-stationary series [73]. In Fig. 3.2(a), we demonstrate for the EUR/USD exchange rate that the return time series acf decays rapidly, whereas the price time series decays slowly. In Fig. 3.2(b), we show that the return time series for all of the studied assets decay rapidly, with most values falling within the 95% confidence bounds for Gaussian white noise.⁷ The rapid decay of the acfs of the return time series suggests that the return process is stationary, which implies that these time series are suitable for investigating market correlations.

⁶An alternative return is the *arithmetic return* which is defined as $z_i^a(t) = [p_i(t) - p_i(t-1)]/p_i(t-1)$. This is equal to the first term in the Taylor expansion of the logarithmic return, so arithmetic and logarithmic returns are approximately equal for small returns. Logarithmic returns are, however, often used instead of arithmetic returns because logarithmic returns are symmetric [73]. For example, an investment of £100 that yields an arithmetic return of 50% followed by an arithmetic return of -50% results in £75. In contrast, an investment of £100 that yields a logarithmic return of 50% followed by a logarithmic return of -50% results in £100.

⁷We note that there are two spikes in the acf for frozen pork bellies (PB1) at 26 and 52 week lags, which suggests that there is an interesting periodicity in this return time series.

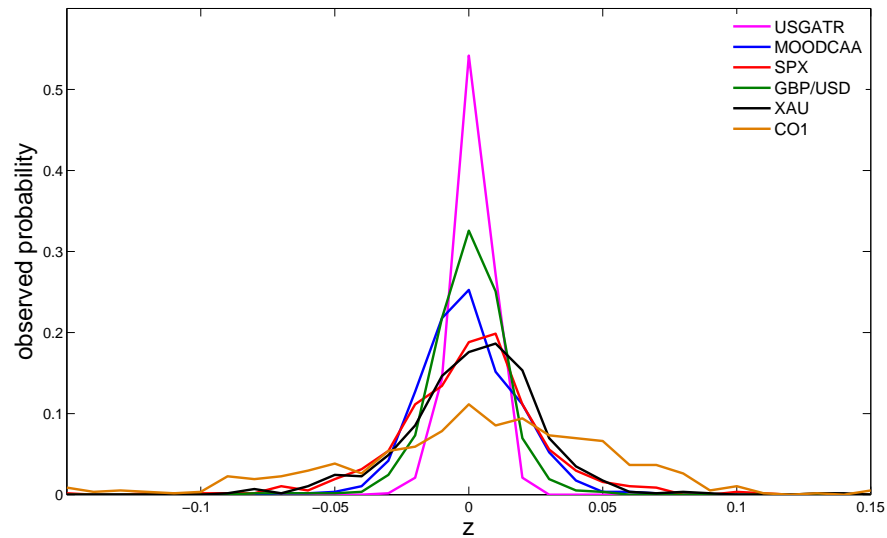


Figure 3.1: Observed return distributions for the period 08/01/1999–24/07/2009. We show the S&P equity index (SPX), a U.S. government bond index (USGATR), a AA-rated corporate bonds index (MOODBAA), the sterling-dollar exchange rate (GBP/USD), gold (XAU), and crude oil futures (CO1).

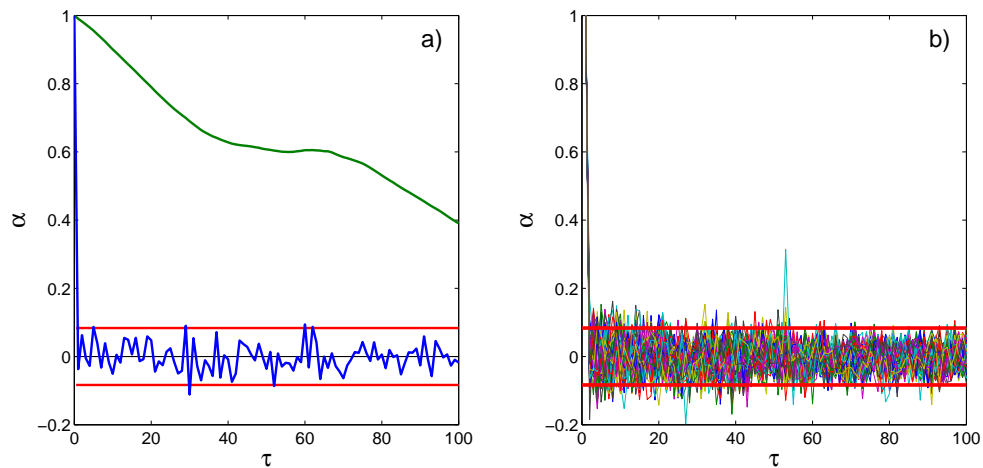


Figure 3.2: a) Comparison of the autocorrelation function for the EUR/USD price (upper green line) and return (lower blue line) time series. The horizontal red lines show the 95% confidence intervals assuming Gaussian white noise. b) Autocorrelation functions for all of the studied return time series. The horizontal red lines show the 95% confidence intervals assuming Gaussian white noise.

3.2.3 Correlations

To simplify the notation for the definition of the empirical correlation matrix, we define a standardized return as

$$\hat{z}_i(t) = \frac{z_i(t) - \langle z_i \rangle}{\sigma(z_i)}, \quad (3.5)$$

where $\sigma(z_i) = \sqrt{\langle z_i^2 \rangle - \langle z_i \rangle^2}$ is the standard deviation of z_i over a time window of T returns and $\langle \dots \rangle$ indicates a time average over T . We represent the standardized returns as an $N \times T$ matrix $\hat{\mathbf{Z}}$, so the empirical correlation matrix \mathbf{R} is given by

$$\mathbf{R} = \frac{1}{T} \hat{\mathbf{Z}} \hat{\mathbf{Z}}^T, \quad (3.6)$$

and has elements $r(i, j)$ that lie in the interval $[-1, 1]$. Note that, because we have standardized the time series, the correlation matrix \mathbf{R} of returns $\hat{\mathbf{Z}}$ is equal to the covariance matrix $\Sigma_{\hat{\mathbf{Z}}}$ of $\hat{\mathbf{Z}}$.

We create an evolving sequence of correlation matrices by rolling the time window of T returns through the full data set. The choice of T is a compromise between overly noisy and overly smoothed correlation coefficients [227, 229], but is usually chosen such that $\Theta = T/N \geq 1$.⁸ In this study, we fix $T = 100$ (each window then contains just under two years of data and $\Theta = 1.02$) and we roll the time window through the data one week at a time. By only shifting the time window by one data point, there is a significant overlap in the data contained in consecutive windows; however, this approach enables us to track the evolution of the market correlations and to identify time steps at which there were significant changes in the correlations. The choice of T results in 452 correlation matrices for the period 1999–2010.

3.2.3.1 Correlations for all assets

In Fig. 3.3, we show the distribution of empirical correlation coefficients aggregated over all time windows. To highlight any interesting features in the correlations, we compare the distribution to corresponding distributions for simulated random returns and randomly shuffled returns. We generate shuffled data by randomly reordering the full return time series for each asset independently. This process destroys the temporal correlations between the return time series, but preserves the distribution of returns for each series. We then produce correlation matrices for the shuffled returns by rolling a time window of T returns through the shuffled data and calculating a

⁸We discuss the compromise between overly noisy and overly smoothed correlations in more detail in Section 5.2.2

correlation matrix for each position of the window. We produce simulated data by independently generating N time series of returns (where each series is the same length as the original data) whose elements are drawn from a Gaussian distribution with mean zero and unit variance. We again roll a time window of length T through the data and calculate a correlation matrix for each window.

Figure 3.3 shows that the distribution of correlation coefficients for the market data is significantly different to the two random distributions, with more large positive and negative correlations for market returns. The differences between the distributions demonstrate that there are temporal correlations between returns for financial assets that are incompatible with the random null models that we consider.

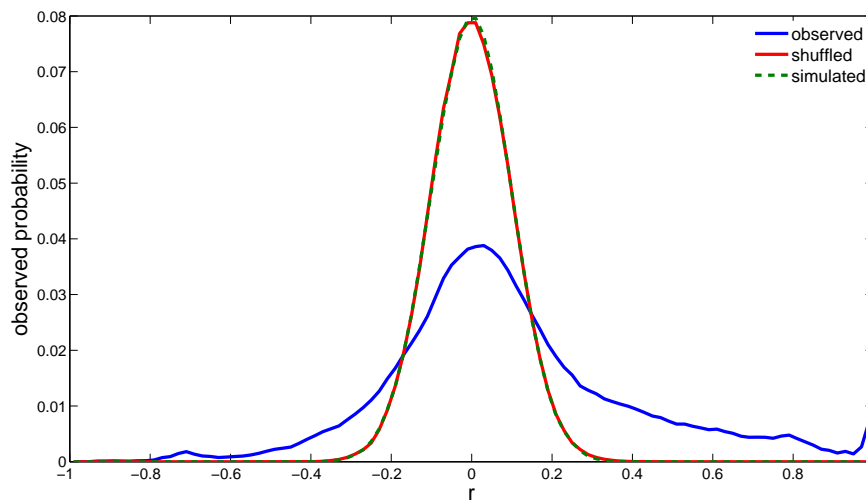


Figure 3.3: Distribution of correlation coefficients $r(i, j)$ aggregated over all time windows for the observed, shuffled and simulated data.

3.2.3.2 Intra-asset-class correlations

Figure 3.3 shows the distribution of correlations between the return time series of all assets, but it is instructive to disaggregate this distribution and to consider only correlations between assets in the same class. In Fig. 3.4 we show that there are clear differences in the intra-class correlations for different assets. For example, corporates bonds and government bonds tend to be highly correlated, whereas many of the assets within the “other commodities” class are uncorrelated (which is unsurprising given the variety of commodities that we include in this class). The distributions of correlation coefficients for all of the asset classes deviate from the distributions

expected for random returns. The deviations from random distributions imply that financial market correlation matrices contain structure that warrants investigation.

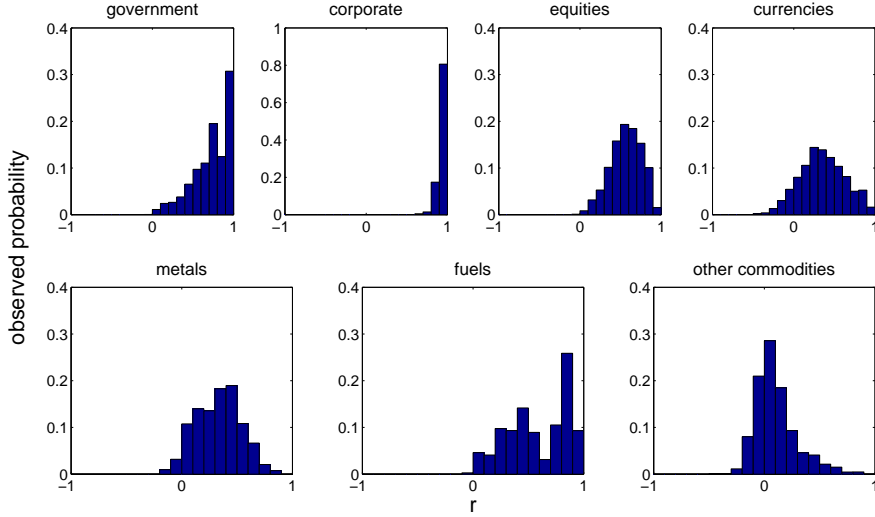


Figure 3.4: The distribution of correlation coefficients $r(i, j)$ between the return time series for assets within each class aggregated over all time windows.

3.3 Principal component analysis

We investigate the structure of the correlation matrices using PCA. The aim of PCA is to find the linear transformation $\mathbf{\Omega}$ that maps a set of observed variables $\hat{\mathbf{Z}}$ into a set of uncorrelated variables \mathbf{Y} [159]. We define the $N \times T$ matrix \mathbf{Y} as

$$\mathbf{Y} = \mathbf{\Omega}\hat{\mathbf{Z}}, \quad (3.7)$$

where each column \mathbf{y}_k ($k = 1, \dots, N$) corresponds to a PC of $\hat{\mathbf{Z}}$ and the transformation matrix $\mathbf{\Omega}$ has elements ω_{ij} . The first row ω_1 of $\mathbf{\Omega}$ (which contains the first PC coefficients) is chosen such that the first PC \mathbf{y}_1 is aligned with the direction of maximal variance in the N -dimensional space defined by $\hat{\mathbf{Z}}$. Each subsequent PC accounts for as much of the remaining variance of $\hat{\mathbf{Z}}$ as possible, subject to the constraint that the ω_k are mutually orthogonal. We further constrain the vectors ω_k such that $\omega_k \omega_k^T = 1$ for all k .

The correlation matrix \mathbf{R} is an $N \times N$ diagonalizable, symmetric matrix that can be written in the form

$$\mathbf{R} = \frac{1}{T} \mathbf{E} \mathbf{D} \mathbf{E}^T, \quad (3.8)$$

where \mathbf{D} is a diagonal matrix of eigenvalues β_k and \mathbf{E} is an orthogonal matrix of its eigenvectors. It can be shown [159] that the eigenvectors of the correlation matrix correspond to the directions of maximal variance such that $\mathbf{\Omega} = \mathbf{E}^T$ and the PCs are easily found through the diagonalization in Eq. 3.8.⁹ We note that the signs of the PCs are arbitrary; if the sign of every coefficient in a component \mathbf{y}_k is reversed, the variance of \mathbf{y}_k and the orthogonality of ω_k with all of the other eigenvectors does not change.

3.3.1 Eigenvalues

In Section 3.1.2, we highlighted the close links between RMT and PCA. A standard financial application of RMT is to compare the eigenvalues of the correlation matrix of market returns with the distribution of eigenvalues for random matrices, e.g., [176, 239]. Any deviations from the predictions of RMT are usually considered to indicate non-random, and potentially insightful, structure in the correlation matrix [176, 239]. The correlation matrix for N mutually uncorrelated time series of length T with elements drawn from a Gaussian distribution is a Wishart matrix [176, 239]. In the limit $N \rightarrow \infty$, $T \rightarrow \infty$, and with the constraint that $\Theta = T/N \geq 1$, the probability density function $\rho(\beta)$ of the eigenvalues β of such correlation matrices is given by [269]

$$\rho(\beta) = \frac{\Theta}{2\pi\sigma^2(\hat{\mathbf{Z}})} \frac{\sqrt{(\beta_+ - \beta)(\beta_- - \beta)}}{\beta}, \quad (3.9)$$

where $\sigma^2(\hat{\mathbf{Z}})$ denotes the variance of the elements of $\hat{\mathbf{Z}}$, and β_+ and β_- are the maximum and minimum eigenvalues and are given by

$$\beta_{\pm} = \sigma^2(\hat{\mathbf{Z}}) \left(1 + \frac{1}{\Theta} \pm 2\sqrt{\frac{1}{\Theta}} \right). \quad (3.10)$$

When $\Theta = 1$, the lower bound of the range of eigenvalues $\beta_- = 0$, the upper bound $\beta_+ = 4\sigma^2(\hat{\mathbf{Z}})$, and as $\beta \rightarrow \beta_- = 0$, the density of eigenvalues $\rho(\beta)$ diverges as $\sim 1/\sqrt{\beta}$. The above results are only valid in the limit $N \rightarrow \infty$; for finite N , the boundaries of the eigenvalue distribution are blurred with a non-zero probability of finding eigenvalues larger than β_+ and smaller than β_- . For the standardized return matrix $\hat{\mathbf{Z}}$ that we investigate, $\sigma^2(\hat{\mathbf{Z}}) = 1$ so $\beta_+ = 4$.

⁹PCA is sometimes performed on the covariance matrix rather than the correlation matrix. However, if there are large differences in the variances of the time series used as inputs in the PCA, the variables with the largest variances will tend to dominate the first few PCs when the covariance matrix is used. Figure 3.1 shows that there are differences in the variances of the returns for different assets, so we use the correlation matrix. Of course, the correlation matrix is simply the covariance matrix for standardized variables.

In Fig. 3.5, we compare the eigenvalue distribution for market data (aggregated over all time windows) with the distributions for shuffled and simulated data. In Fig. 3.5(a), we show that the eigenvalue distribution for market correlations differs from that of random matrices. There are many eigenvalues larger than the upper bound $\beta_+ = 4$ predicted by RMT (with several eigenvalues almost 10 times as large as the upper bound). In prior studies of equity markets, the eigenvector corresponding to the largest eigenvalue has been described as a “market” component, with roughly equal contributions from each of the N equities studied, and the eigenvectors corresponding to the other eigenvalues larger than β_+ have been identified as different market sectors [176, 239]. In Section 3.5, we discuss the interpretation of the observed eigenvectors with eigenvalues $\beta > \beta_+$. For now, we simply note that the deviations of the empirical distribution of eigenvalues from the predictions of RMT again imply that the correlation matrices contain structure that is incompatible with the null models that we consider.

In Figs. 3.5(b) and (c), we illustrate that the distributions for shuffled and simulated data are very similar and that they agree very well with the analytical distribution given by Eq. (3.9) over most of the range of β . In particular, both distributions have an upper bound close to the theoretical maximum $\beta_+ = 4$. However, for $\Theta \approx 1.02$ (the value that corresponds to the selected T and N), the observed distribution of eigenvalues for random data does not fit the distribution in Eq. (3.9) as $\beta \rightarrow 0$. For both the simulated and shuffled data, we observe a much higher probability density near $\beta = 0$ than that predicted by RMT. The high probability density near zero is a result of the fact that $T \approx N$. When we simulate eigenvalue distributions for data with $T \gg N$, we observe a much smaller probability density near zero. In Figs. 3.5(b) and (c), we also show the theoretical distribution for $\Theta = 1$. In this case, $\rho(\beta)$ diverges as $\beta \rightarrow 0$, which fits the randomly generated distributions reasonably well.

3.3.2 Eigenvectors

We now investigate the distribution of the elements ω_{ij} (the PC coefficients) of the eigenvectors of the correlation matrices. We denote the i^{th} element of the k^{th} eigenvector as $\omega_k(i)$ and use the standard approach of normalizing each eigenvector such that $\sum_{i=1}^N \omega_k(i)^2 = N$ [176, 238, 239]. Correlation matrices \mathbf{R} are real symmetric matrices, so we compare the eigenvector properties of the matrices \mathbf{R} with those for real symmetric random matrices. Such random matrices display the universal properties of the canonical ensemble of matrices known as the Gaussian orthogonal ensemble

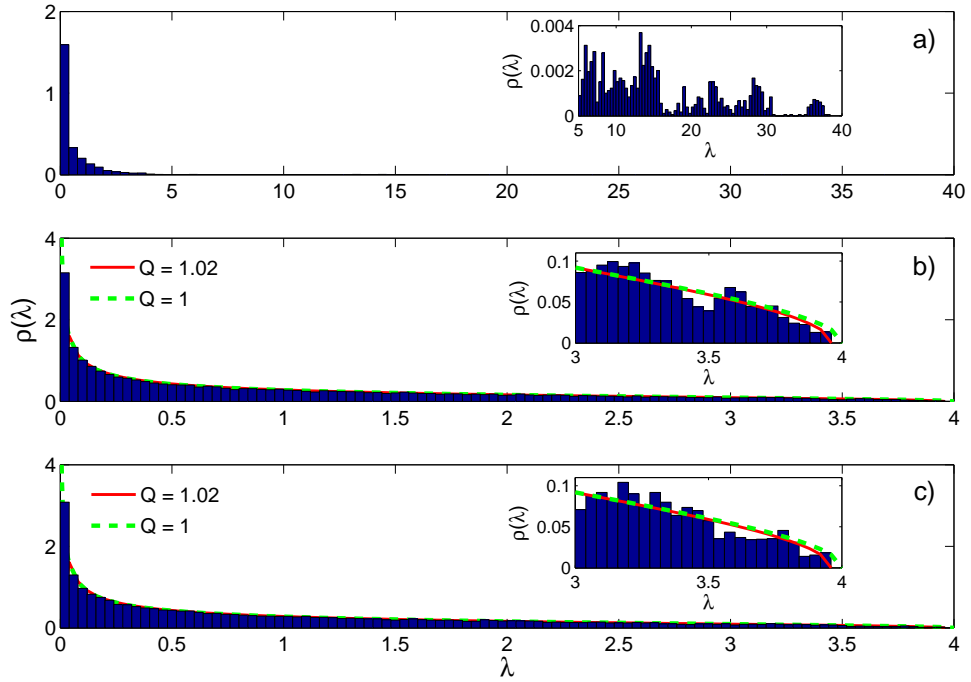


Figure 3.5: The distribution of eigenvalues β of the correlation matrices aggregated over all time windows for (a) market (b) shuffled, and (c) simulated data. In (b) and (c), we show the eigenvalue probability density functions for random matrices given by Eq. 3.9 for $\Theta = 1.02$ (solid red line) and $\Theta = 1$ (dashed green line). The insets show the distributions of the largest eigenvalues. The distributions for shuffled (b) and simulated data (c) both have an upper bound close to the theoretical maximum $\beta_+ = 4$.

(GOE) [238, 239]. For the GOE, the probability density $\rho(\omega_k)$ of the elements of the k^{th} eigenvector is a Gaussian distribution with mean zero and unit variance [137].

In Fig. 3.6, we show the distribution of elements of the eigenvectors $k = \{1, \dots, 6\}$ (the six components with the largest eigenvalues), $k = \{25, 40, 50, 75\}$ (whose eigenvalues lie within the interval $[\beta_-, \beta_+]$ for random matrices), and $k = \{97, 98\}$ (the two components with the smallest eigenvalues). We aggregate the distributions for each eigenvector over all time windows; however, the sign of each eigenvector is arbitrary so, to ensure that the signs of the eigenvectors are consistent through time, we choose the sign of the k^{th} eigenvector ω_k^t at time step t to maximize $\sum_{i=1}^N \text{sgn}[\omega_k^{t-1}(i)] \text{sgn}[\omega_k^t(i)]$, where $\text{sgn}[x]$ is the sign function.¹⁰

Figure 3.6 shows that the RMT distribution closely matches the distributions for shuffled and simulated data, but there are differences between these distributions and the distributions for the market correlation matrices. These differences are most pronounced for the first and second PCs; in particular, there are asymmetries in the distributions for market data that are not present in the random distributions. The eigenvector distributions for eigenvalues within the interval $[\beta_-, \beta_+]$ also deviate from the predictions of RMT, which contrasts with the results of similar studies of equity markets. In Refs. [176, 238], the distributions of elements of the eigenvectors corresponding to eigenvalues falling within the interval $[\beta_-, \beta_+]$ were found to fit a Gaussian distribution, which was taken as an indication that these eigenvectors did not contain any information [176]. However, the eigenvector distributions that we observe for eigenvalues in the interval $[\beta_-, \beta_+]$ have excess kurtosis compared with a Gaussian distribution. A key difference between the analysis that we present and prior studies is that we investigate multiple asset classes, whereas prior studies focused on a single type of asset. The addition of inter-asset-class correlations may explain the differences that we observe in the eigenvector distributions.

3.4 Temporal evolution

In Sections 3.3.1 and 3.3.2, we analyzed aggregate results for all time steps. The results imply that the financial market correlation matrices that we study contain structure that is incompatible with the random null models that we consider. We now investigate the evolution of this structure through time.

¹⁰That is, for each time step we perform the two summations $\sum_{i=1}^N \text{sgn}[\omega_k^{t-1}(i)] \text{sgn}[\omega_k^t(i)]$ and $\sum_{i=1}^N \text{sgn}[\omega_k^{t-1}(i)] \text{sgn}[-\omega_k^t(i)]$ and choose whichever of $-\omega_k^t$ or ω_k^t results in the largest value for the sum.

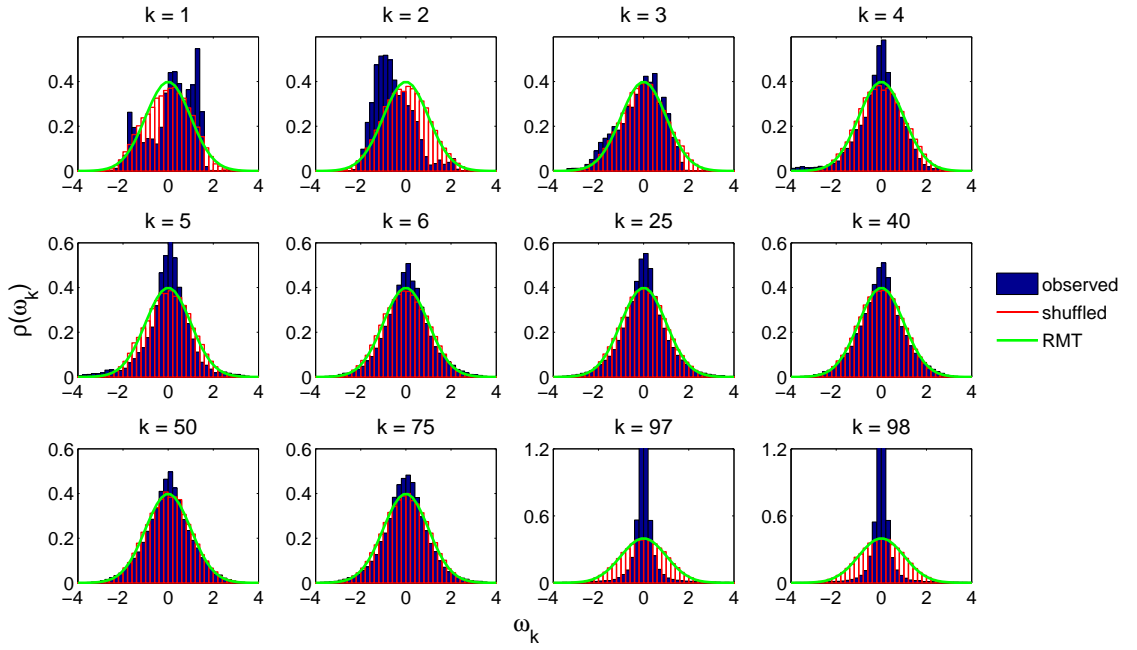


Figure 3.6: The distribution $\rho(\omega_k)$ of the elements $\omega_k(i)$ of the $i = 1, \dots, N$ elements of the k^{th} eigenvector aggregated over all time windows. We show the distributions for $k = 1, \dots, 6$ (the six eigenvectors with the largest eigenvalues), $k = 25, 40, 50, 75$ whose eigenvalues fall within the range $[\beta_-, \beta_+]$ predicted by RMT, and $k = 97, 98$ (which have very small eigenvalues). The red line histograms show the equivalent distributions for shuffled data and the green lines show the distribution predicted by RMT.

3.4.1 Proportion of variance

We begin by investigating the eigenvalues of the correlation matrices. We can write the covariance matrix $\Sigma_{\mathbf{Y}}$ for the PC matrix \mathbf{Y} as

$$\Sigma_{\mathbf{Y}} = \frac{1}{T} \mathbf{Y} \mathbf{Y}^T = \frac{1}{T} \Omega \hat{\mathbf{Z}} \hat{\mathbf{Z}}^T \Omega^T = \mathbf{D}. \quad (3.11)$$

where \mathbf{D} is the diagonal matrix of eigenvalues β . The total variance of the returns $\hat{\mathbf{Z}}$ for the N assets is then given by

$$\sum_{i=1}^N \sigma^2(\hat{\mathbf{z}}_i) = \text{tr}(\Sigma_{\hat{\mathbf{Z}}}) = \sum_{i=1}^N \beta_i = \sum_{i=1}^N \sigma^2(\mathbf{y}_i) = \text{tr}(\mathbf{D}), \quad (3.12)$$

where $\Sigma_{\hat{\mathbf{Z}}}$ is the covariance matrix for $\hat{\mathbf{Z}}$ and $\sigma^2(\hat{\mathbf{z}}_i)$ is the variance of the vector $\hat{\mathbf{z}}_i$ of returns for asset i . The proportion of the total variance in $\hat{\mathbf{Z}}$ explained by the k^{th} PC is then given by

$$\frac{\sigma^2(\mathbf{y}_k)}{\sum_{i=1}^N \sigma^2(\mathbf{z}_i)} = \frac{\beta_k}{\beta_1 + \dots + \beta_N} = \frac{\beta_k}{N}, \quad (3.13)$$

i.e., the ratio of the k^{th} largest eigenvalue β_k of the correlation matrix \mathbf{R} to the number of assets studied N is equal to the the proportion of the variance accounted for by the k^{th} PC.

In Fig. 3.7 we show the fraction of the variance β_k/N accounted for by the first five PCs ($k = 1, \dots, 5$) as a function of time. From 2001–2004 the fraction of the variance explained by the first PC increased; between 2004 and 2006 it decreased before gradually increasing again with a sharp rise as the week including 15th September 2008 entered the rolling time window. This was the day that Lehman Brothers filed for bankruptcy and Merrill Lynch agreed to be taken over by Bank of America. The variance explained by the first PC peaks as the week ending 5th December 2008 enters the rolling window (which was the week during which the National Bureau of Economic Research officially declared that the U.S. was in recession) at which point it accounts for nearly 40% of the variance in $\hat{\mathbf{Z}}$.

The amount of variance in market returns explained by a single component is quite striking and demonstrates that there is a large amount of common variation in financial markets; this highlights the close links between different assets. The increase in the variance accounted by the first PC between 2001 and 2010 also implies that markets have become more closely related in recent years. In particular, the significant rise in the variance of the first PC following the collapse of Lehman Brothers demonstrates that markets became more correlated during the period of crisis following the failure of this major bank.

Although the changes in the variance accounted for by the higher PCs are smaller than the changes for the first PC, the variance explained by the second and third PCs appears to be anti-correlated with the variance explained by the first PC. This is expected because the total variance is constrained to sum to N , so when the first PC accounts for a higher proportion, less remains to be explained by the other components.

It is also instructive to consider the combined variance explained by the first few PCs. In 2001 the first twelve PCs accounted for approximately 65% of the variance of market returns; by 2010 only five PCs explained the same proportion of the variance. The fact that only a few components account for such a large proportion of the variance in market returns highlights the close ties between different markets. The larger amount of common variance also suggests that market correlations can be characterized by fewer than N components.

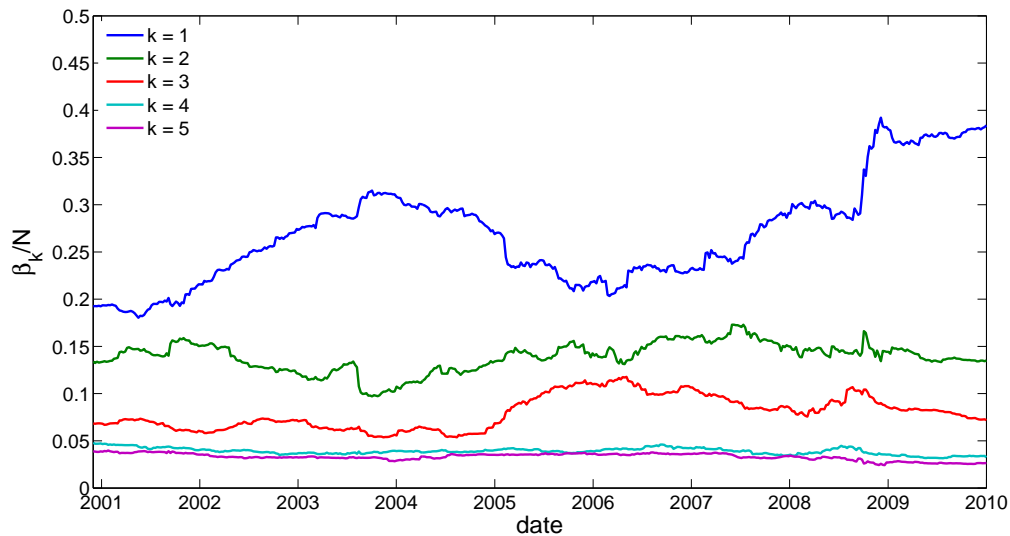


Figure 3.7: Fraction of the variance in $\hat{\mathbf{Z}}$ accounted for by each of the first five PCs as a function of time. The highest line shows the variance accounted for by the first PC, the next highest line the variance accounted for by the second PC, and so on. The date axis shows the date of the last data point lying in each time window.

3.4.2 Significant principal component coefficients

An increase in the variance accounted for by a PC could be the result of increases in the correlations amongst only a few assets (which then have large PC coefficients) or

a market-wide effect in which many assets begin to make significant contributions to the component. This is an important distinction because the two types of changes have very different financial implications. For example, in optimal portfolio selection, when correlations between all assets increase it becomes much more difficult to reduce risk by diversifying across different asset classes. In contrast, increases in correlations within an asset class that are not accompanied by increases in correlations between asset classes have a less significant impact on diversification.

We use the *inverse participation ratio* (IPR) [238] to investigate temporal changes in the number of assets that make significant contributions to each component. The IPR is often applied in localization theory [137, 238] in which it is related to the probability for a quantum particle to remain at a given site for infinite time [115]. In the current context, the IPR I_k of the k^{th} PC ω_k is defined as¹¹

$$I_k = \sum_{i=1}^N [\omega_k(i)]^4. \quad (3.14)$$

The IPR can be better understood by considering two limiting cases: (1) an eigenvector with identical contributions $\omega_k(i) = 1/\sqrt{N}$ from all N assets has $I_k = 1/N$; (2) an eigenvector with a single component $\omega_k(i) = 1$ and remaining components equal to zero has $I_k = 1$. The IPR quantifies the reciprocal of the number of elements that make a significant contribution to each eigenvector. For ease of interpretation, we define a *participation ratio* (PR) as $1/I_k$. A large PR for a PC indicates that many assets are contributing to it.

In Fig. 3.8(a), we show the PR of the first three PCs as a function of time. The PR of the first PC increases from 2001–2010, with sharp increases when the weeks ending 12th May 2006 and 19th September 2008 enter the rolling time window. The second increase is a result of the market turmoil that followed the collapse of Lehman Brothers and occurs at the same time as a significant increase in the variance accounted for by the first PC (see Fig. 3.7). The first increase is largely attributable to surging metal prices. During the week ending 12th May 2006, the price of gold rose to a 25 year high, reaching over \$700 per ounce, and the prices of several other metals also rose to record levels: platinum and copper reached all time highs; aluminium hit an 18-year peak; and silver prices rose to their highest levels since February 1998. In addition, during the same week, corporate bond prices reached a 2 year high and the price of emerging market equities reached record levels. Although these events resulted in a

¹¹We now normalize the eigenvectors such that $\sum_{i=1}^N \omega_k(i)^2 = 1$.

significant increase in the PR of the first PC, this increase was not accompanied by a sharp rise in the variance explained by this component.

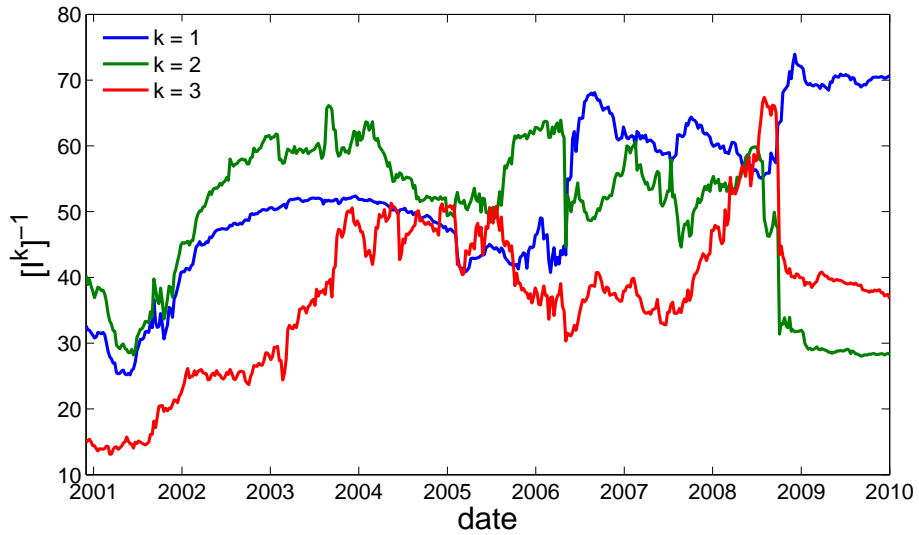
The sharp rise in the PR of the first PC following the collapse of Lehman Brothers implies that many different assets were highly correlated during this period of market turmoil. Based on the value of the PR, over 70% of the assets that we study significantly contribute to the first PC after Lehman’s collapse. To test the significance of the PR of the first PC, in Fig. 3.8(b) we compare it to the corresponding PR for random returns. Figure 3.8(b) shows that between 2006 and 2010 the PR of the observed returns was significantly larger than the PR expected for random returns. This demonstrates the strength of the correlations between a wide range of different assets during this period.

We observe very different behaviours for the evolution of the PRs of the higher components. For example, between 2001 and 2003 the PR of the second PC doubles; it then fluctuates around the same level until the collapse of Lehman Brothers, at which point it decreases sharply. Similarly, the PR of the third PC increases from 2001 until Lehman’s collapse when it also falls sharply. This suggests that following the collapse of Lehman Brothers the first PC influences a large number of assets at the expense of higher components. The dominance of a single component again implies a large amount of common variance in asset returns and further suggests that the key market correlations can be described using only a few PCs.

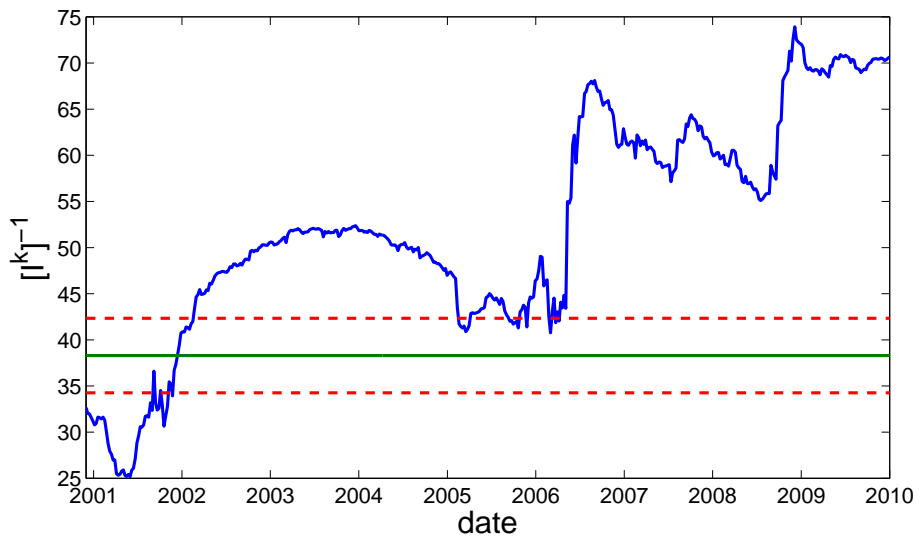
3.4.3 Number of significant components

We now try to determine how many PCs are needed to describe the main market correlations. PCA is widely used to generate lower-dimensional representations of multivariate data in which the first few “significant” components are retained and the remaining components discarded [159]. Many heuristic methods have been proposed for determining the number of significant PCs, but there is no widespread agreement on the optimal approach [153].

We use two alternative methods to determine the number of significant PCs. The first is the Kaiser-Guttman criterion [143], which assumes that a component is significant if its eigenvalue $\beta > 1/N$. Any component that satisfies this criterion accounts for at least a fraction $(1/N)$ of the variance of the system. It is considered significant because it is assumed to summarize more information than any single original variable. In the second method, we compare the observed eigenvalues to the eigenvalues for random data. This method can be understood by considering the scree plot shown in Fig. 3.9(a). A scree plot shows the magnitude of the eigenvalues



(a)



(b)

Figure 3.8: The participation ratio $[I^k]^{-1}$ as a function of time for (a) the three PCs with the largest variance ($k = 1, 2, 3$) (b) the PC with the largest variances ($k = 1$). The horizontal solid line (green) shows the mean IPR for 100,000 simulations of randomized returns with $T = 100$ and $N = 98$ and the dashed horizontal lines (red) show the one standard deviation error bars.

as a function of the eigenvalue index, where the eigenvalues are sorted such that $\beta_1 > \beta_2 > \dots > \beta_N$; the left most data point in a scree plot shows the magnitude of the largest eigenvalue and the right most the smallest eigenvalue. The number of significant PCs is considered to be equal to the number of eigenvalues in the scree plot for which the eigenvalue for the observed data is larger than the corresponding eigenvalue for random data.

In Figs. 3.9(b) and (c), we show the number of significant components as a function of time calculated using the Kaiser-Guttman criterion and the scree plot technique, respectively. There are large differences in the number of significant components identified using the two approaches, but both agree that the number decreased between 2001 and 2010. The discrepancies in the results for the two methods imply that we cannot reliably determine the exact number of significant PCs; however, the similar trends provide evidence that the number of significant components decreased between 2001 and 2010. This again implies that markets have become more closely related in recent years. Both methods also agree that the number of significant components is much lower than the number of assets that we study. Therefore, although we cannot determine the number of significant components using the methods described in this section, the results nonetheless suggest that market correlations can be characterized by fewer than N components.

3.5 Asset-component correlations

We now return to the question that we left open in Section 3.3.1 regarding the interpretation of the eigenvectors with eigenvalues β larger than the upper bound β_+ predicted by RMT. To explain the eigenvectors, we investigate the correlations $R(\hat{\mathbf{z}}_i, \mathbf{y}_j)$ between the asset return time series $\hat{\mathbf{z}}_i$ and the PCs \mathbf{y}_j . These correlations are closely related to the PC coefficients, which represent the weighting of each asset on the PCs; but, because the correlations $R(\hat{\mathbf{z}}_i, \mathbf{y}_j)$ exist over the interval $[-1, 1]$, they are slightly easier to interpret than the PC coefficients. We use these correlations to measure the strength of the asset-PC relationships and to determine which assets contribute to each component. In doing this, we also determine the number of PCs that need to be retained to describe the main features of the correlation matrices.

To derive the relationship between the PC coefficients and the correlation $R(\hat{\mathbf{z}}_i, \mathbf{y}_j)$, we write the covariance matrix of the original variables $\hat{\mathbf{Z}}$ with the PCs \mathbf{Y} as

$$\Sigma_{\mathbf{Y}\hat{\mathbf{Z}}} = \frac{1}{T} \mathbf{Y}\hat{\mathbf{Z}}^T = \frac{1}{T} \mathbf{\Omega}\hat{\mathbf{Z}}\hat{\mathbf{Z}}^T = \mathbf{\Omega}\mathbf{\Omega}^T \mathbf{D}\mathbf{\Omega} = \mathbf{D}\mathbf{\Omega}. \quad (3.15)$$

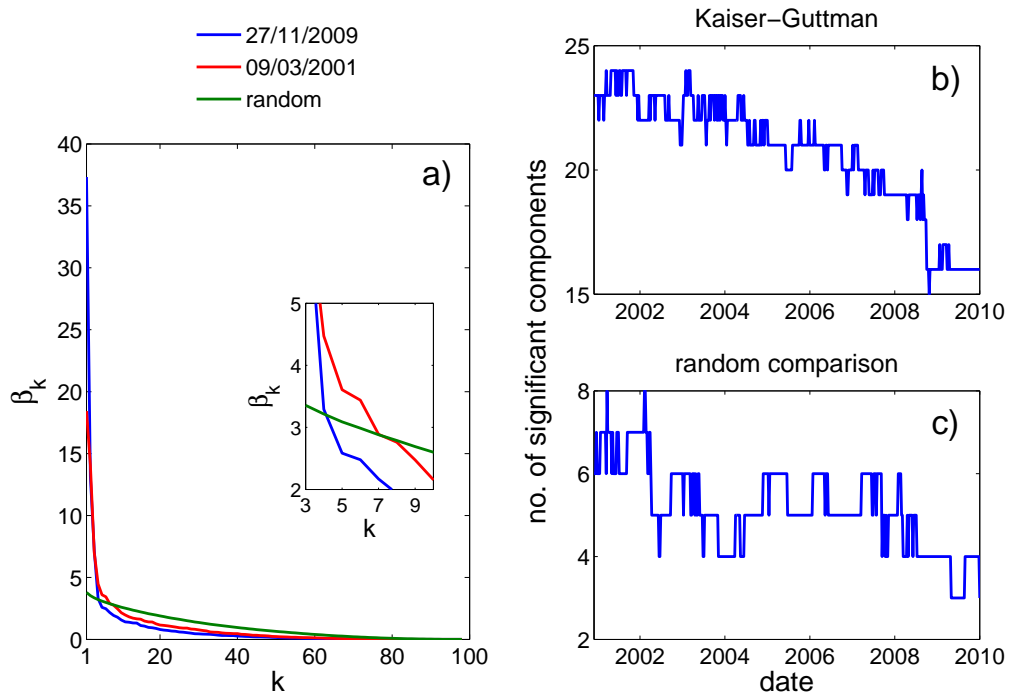


Figure 3.9: (a) Scree plot showing the magnitude of the eigenvalues as a function of the eigenvalue index, where the eigenvalues are sorted such that $\beta_1 > \beta_2 > \dots > \beta_N$. We show curves for correlation matrices for time windows ending on 09/03/2001 and 27/11/2009. We also show the eigenvalues for random correlation matrices, where we have averaged the eigenvalues over 500 realizations of the correlation matrix. The inset zooms in on the region in which the two example curves for observed data cross the curve for random data. The two plots on the right show the number of significant components as a function of time determined using (b) the Kaiser-Guttman criterion (c) by comparing the scree plots of the observed and random data.

This implies that the covariance of the returns of asset i and the j^{th} PC is given by $\Sigma(\hat{\mathbf{z}}_i, \mathbf{y}_j) = \omega_{ij}\beta_j$ and the correlation $R(\hat{\mathbf{z}}_i, \mathbf{y}_j)$ by

$$R(\hat{\mathbf{z}}_i, \mathbf{y}_j) = \frac{\omega_{ij}\beta_j}{\sigma(\hat{\mathbf{z}}_i)\sigma(\mathbf{y}_j)} = \omega_{ij}\sqrt{\beta_j}, \quad (3.16)$$

where $\sigma(\hat{\mathbf{z}}_i) = 1$ is the standard deviation of $\hat{\mathbf{z}}_i$ over T returns and $\sigma(\mathbf{y}_j) = \sqrt{\beta_j}$ is the standard deviation of \mathbf{y}_j . The correlations between the PCs and the original variables are therefore simply equal to the PC coefficients scaled by the appropriate eigenvalue. The signs of the PC coefficients are arbitrary, so the signs of the PCs and the signs of the correlations $R(\hat{\mathbf{z}}_i, \mathbf{y}_j)$ are also arbitrary. To avoid having to choose a sign for each correlation coefficient, we consider the absolute correlations $|R(\hat{\mathbf{z}}_i, \mathbf{y}_k)|$. By considering absolute correlations, we cannot tell if an asset is positively or negatively correlated with a PC; however, we are interested only in determining which assets contribute to each component, so it is reasonable to ignore the signs.

In Fig. 3.10, we show the variation through time of the correlation of every asset with each of the first six PCs. Figure 3.10 highlights that the number of large correlations is significantly lower for the higher components. For the first PC, many of the correlation coefficients are greater than 0.8, but the correlations between the asset returns and the sixth PC very rarely exceed 0.5. As one looks at increasingly higher components the maximum correlation decreases until, for the highest components, all correlations are less than 0.2. The low correlations between the asset return time series and the higher PCs implies that much of the key structure from the correlation matrices is contained within the first few PCs. Based on the correlations shown in Fig. 3.10, it appears that the first five PCs describe the main features of the correlations for the studied assets.

Figure 3.10 also demonstrates the changing correlations between the different asset classes. From 2001–2002, all of the corporate and government bonds (with the exception of Japanese government bonds) are strongly correlated with the first PC. Over the same period, most of the equity indices are strongly correlated with the second PC and most of the currencies with the third PC; six grain commodities (soybean, soybean meal, soybean oil, corn, wheat oats) are strongly correlated with the fourth PC; and fuel commodities are strongly correlated with the fifth PC. Therefore, each of the first five PCs corresponds to a specific market over this period and the separation into components implies low correlations between different assets classes. During 2002, however, these relationships begin to break down as bonds and equities both become strongly correlated with the first PC and both asset-classes have a

correlation of approximately 0.5 with the second PC. The strong correlation of both bonds and equities with the same PCs marks the start of a period during which the coupling between asset classes increased and different markets became more closely related.

There are three major changes in the correlations between the asset return time series and the PCs between 2002 and 2009. These changes are most obvious for the second PC in Fig. 3.10. The first change corresponds to a local peak in corporate bond prices; the second change corresponds to surging metal prices (see Section 3.4.1); and the third, and most striking, change occurs following the collapse of Lehman Brothers. After Lehman's bankruptcy, the first PC becomes strongly correlated with nearly all of the assets, including equities, currencies, metals, fuels, other commodities, and some government bonds. The major exceptions are corporate bonds and, to a lesser extent government bonds, but both sets of bonds are strongly correlated with the second PC. During this period, only a few assets are strongly correlated with the third PC, including EUR/USD, CHF/USD, gold, silver, and platinum; and very few assets are strongly correlated with any of the higher PCs. The strong correlations between the majority of the studied assets and the first PC following Lehman Brothers' collapse further demonstrates the strength of market correlations during this crisis period and highlights the common behaviour of nearly all markets.

Figure 3.10 also shows that for a system in which the first few PCs account for a significant proportion of the variance, a consideration of the correlations between these components and the original variables provides a parsimonious framework to uncover the key relationships within the system. Instead of having to identify the important correlations within a matrix with $\frac{1}{2}N(N - 1)$ elements, one only needs to consider the correlations between the N variables and the first few PCs, which reduces the number of correlations to consider by a factor of N . Figure 3.10 demonstrates that this method uncovers the changing relationships between the different asset classes and highlights assets, such as Japanese government bonds, whose behaviour is unusual. This approach also uncovers notable changes that occurred in markets and the assets that were significantly affected by these changes.

3.6 Summary

We used PCA to investigate the evolving correlation structure of a variety of financial assets and to identify common features across different markets. We found that the percentage of the variance in market returns accounted for by the first PC steadily

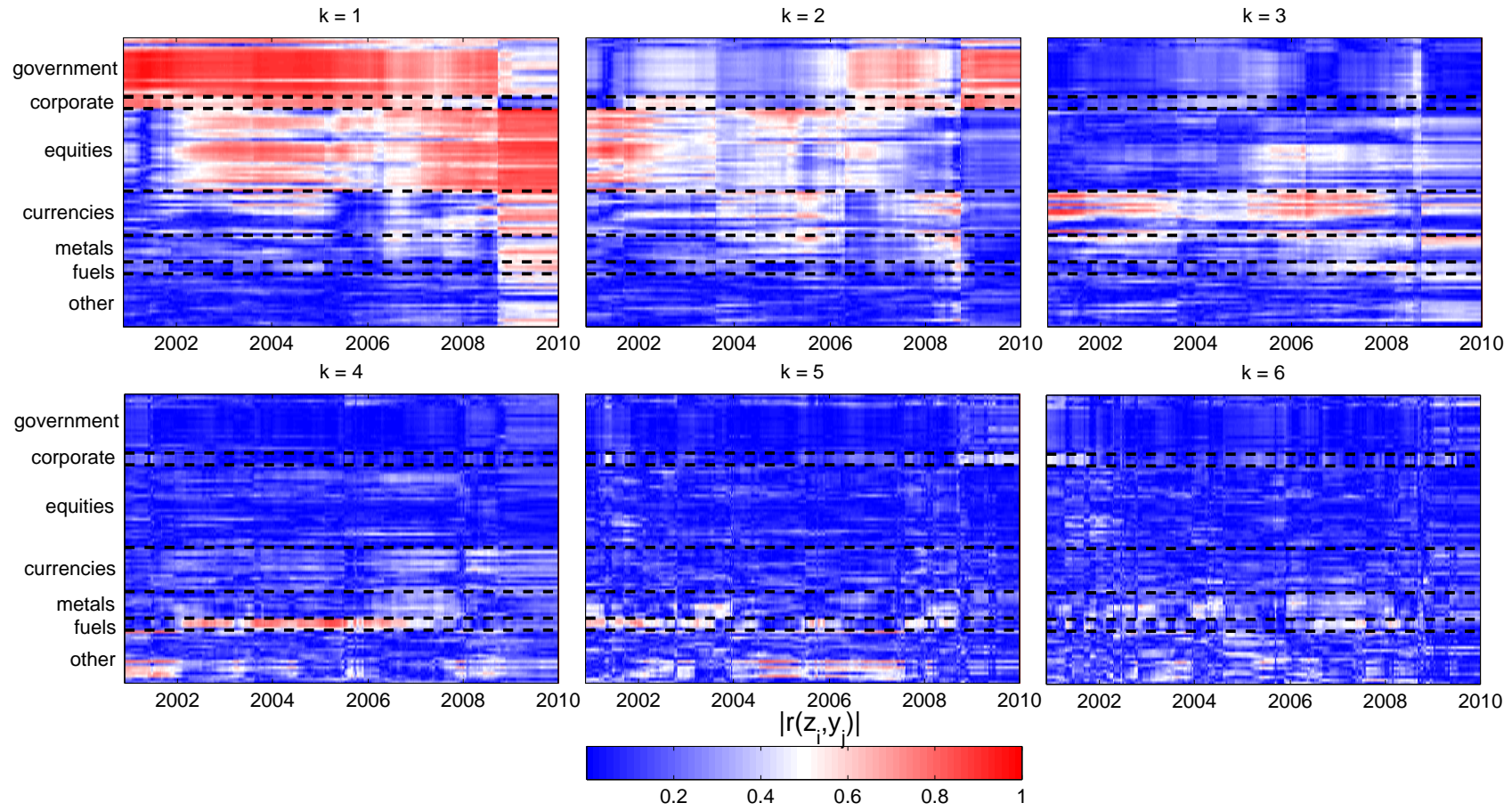


Figure 3.10: The absolute correlation $|R(\hat{z}_i, y_k)|$ between each asset and the first six PCs ($k = 1, \dots, 6$) as a function of time. Each point on the horizontal axis represents a single time window and each position along the vertical axis an asset. Dark red regions indicate strong correlations (positive or negative) between assets and PCs and dark blue regions indicate weak correlations.

increased from 2001–2010, with a sharp rise following the 2008 collapse of Lehman Brothers. We further found that the number of significant components decreased and the number of assets making significant contributions to the first PC increased over this period. We investigated the evolving relationships between the different assets by analyzing the correlations between the asset price times series and the first few PCs. From 2001–2002, each of the first five components corresponded to a specific market; however, after 2002 these relationships broke down and by 2010 nearly all of the studied assets were significantly correlated with the first PC. The major changes in the correlation structure following the collapse of Lehman shows the extent to which market correlations increased during this crisis period.

Chapter 4

Community Structure in Networks

In this chapter, we describe several concepts that we will use in Chapters 5 and 6 in which we study network communities. We define a community, explain some of the most widely used techniques for detecting communities in static networks, discuss attempts to cluster networks using mesoscopic structures, and present a relatively comprehensive review of the literature investigating communities in dynamic networks.

4.1 Introduction

A network community consists of cohesive groups of nodes that are relatively densely connected to each other but sparsely connected to other dense groups in the network. Communities can represent functionally-important subnetworks [2, 75, 105, 107, 121, 139, 243, 244, 295]. For example, a community in a cellular or genetic network might be related to a functional module; a community in a stock market network might correspond to stocks belonging to the same industrial sector; and a community in a social network might correspond to a group of friends or a group of work colleagues. Communities can affect dynamical processes (such as the spread of opinions and diseases) that operate on networks [75, 107, 244], so their identification, and an understanding of their structure, can potentially provide insights into these processes.

In this chapter we review some of the most widely used community detection techniques. Because there is no rigorous definition of a community, different methods often define communities in different ways; the main difference between methods is essentially their precise definition of “relatively densely connected”. A vast amount of research has been published on community detection in recent years, so this review is not exhaustive. More detailed reviews of the community detection literature can be found in Refs. [105, 244]. However, these review articles focus on communities in static

networks (although there is a brief discussion of the dynamic communities literature in Ref. [105]). In Chapter 5, we investigate dynamic communities and propose a method for tracking communities through time; to illustrate how the methods we present relate to other approaches, in Section 4.6 we review the dynamic communities literature.

4.2 Notation

First, we introduce some of the notation that we use in the remainder of the thesis. We consider undirected networks $\mathcal{G} = (\mathcal{V}, \mathcal{E})$ that consist of a set of vertices \mathcal{V} and a set of edges \mathcal{E} . We represent a network as an adjacency matrix \mathbf{A} with elements A_{ij} . For unweighted networks $A_{ij} = 1$ if an edge exists between nodes i and j and is 0 otherwise; in weighted networks A_{ij} can take other values (which are always real numbers for the networks that we consider) that indicate the strength of the tie between i and j .

We consider partitions $\mathcal{P} = \{\mathcal{C}^1, \dots, \mathcal{C}^\eta\}$ of a network \mathcal{G} into η disjoint communities \mathcal{C} such that $\mathcal{C}^k \cap \mathcal{C}^{k'} = \emptyset$ and $\cup_{k=1}^{\eta} \mathcal{C}^k = \mathcal{V}$, where $|\mathcal{V}| = N$ is the number of nodes in the network. We use the letter C to identify a community and the scripted letter \mathcal{C} to represent the set of nodes in that community. We also reference the communities in two different ways: \mathcal{C}^k is the set of nodes in community k ($k = 1, \dots, \eta$), whereas \mathcal{C}_i is the set of nodes in the same community as node i ($i = 1, \dots, N$). We represent the number of nodes in community k as $|\mathcal{C}^k| = n_k$.

4.3 Community detection methods

In statistics and data mining, there are a variety of methods for coarse graining data to extract patterns and identify clusters of similar objects [84, 105]. Partitional clustering techniques such as k -means clustering [84], multidimensional scaling [84], and PCA¹ have been successfully applied to problems from diverse disciplines. For example, multidimensional scaling has been used to analyze voting patterns in the United States Congress and the United Nations General Assembly (see Refs. [203, 241, 302] and Chapter 6) and in Chapter 3 we use PCA to investigate correlations in financial markets. Another widely used set of techniques are hierarchical clustering algorithms, which can be split into two types: agglomerative and divisive. Agglomerative methods, such as linkage clustering, begin with a set of individual objects and iteratively

¹See Chapter 3 for a detailed discussion of PCA

combine them based on their similarity [84].² In contrast, divisive algorithms (which include some spectral methods [221]) begin with all objects in a single cluster and find smaller groups by iteratively splitting clusters.

Data clustering is closely linked to community detection. The widespread interest of statistical physicists and applied mathematicians in community detection was sparked by the 2002 publication of a paper by Girvan and Newman [121] in which they proposed a technique for identifying communities using (geodesic) edge betweenness. Betweenness [110] is widely used in social network analysis to quantify the extent to which edges lie on paths that connect agents³. In the Girvan-Newman method, edges with the largest betweenness are iteratively removed from the network. After each edge removal the betweenness of the remaining edges is recalculated, which is important because it can cause previously low-betweenness edges to have higher betweenness. As the edges are removed the network breaks up into progressively smaller isolated communities.

The main problem with the Girvan-Newman approach is that it tends to be slow for large networks (unless they are very sparse) and typically produces poor results for dense networks [244]. Nevertheless, Ref. [121] was the catalyst that led to the explosion of research on community detection in networks and since its publication many alternative community detection methods have been proposed. We explain three of the more prominent methods below.

4.3.1 k -clique percolation

Communities are detected in k -clique percolation [234] using k -cliques, which are complete subgraphs of k nodes that are connected with all $k(k-1)/2$ possible edges. The clique percolation method (CPM) is based on the idea that intra-community edges are likely to form cliques as a result of their high density, but inter-community edges are not. In Ref. [234], two k -cliques are described as *adjacent* if they share $k-1$ nodes; the union of adjacent k -cliques is called a *k -clique chain*; and two k -cliques are considered to be *connected* if they are part of a k -clique chain. A community is then defined as the union of a k -clique and all k -cliques that are connected to it. By construction k -clique communities can share nodes, so the method allows for the identification of overlapping communities. This is a useful property because

²We discuss linkage clustering in more detail in Chapter 5.

³Note that the Girvan-Newman community detection method uses *edge* betweenness, but the betweenness defined in Ref. [110] is the *node* betweenness [110]. In Chapter 5, we use node betweenness to study the roles of different exchange rates within the FX market.

many empirical networks possess overlapping communities. For example, in social networks people often simultaneously belong to different communities consisting of family, work colleagues, university friends, etc. The CPM has also been extended to weighted networks [99]. The main problem with k -clique percolation is that the community definition is very stringent and the rigid nature of the cliques means that dense groups of nodes that are not quite as well connected as cliques are not identified as communities.

4.3.2 Modularity maximization

Perhaps the most popular approach for detecting communities is a technique that involves the maximization of a quality function known as *modularity* [224]. The identification of communities using graph modularity is based on the idea that random networks are not expected to demonstrate community structure beyond small fluctuations. Modularity therefore identifies communities by finding subsets of nodes that are more strongly connected to each other than one would expect for a random null model. We represent a network by an *adjacency matrix* \mathbf{A} whose elements (edges) A_{ij} indicate how closely nodes i and j are related to each other. In this thesis, we will only consider undirected networks, which implies that \mathbf{A} is symmetric. If we let \mathcal{P} represent a partition of the n nodes in \mathbf{A} into mutually disjoint communities, the modularity Q of partition \mathcal{P} is given by

$$Q(\mathcal{P}) = \frac{1}{2m} \sum_{ij} (A_{ij} - P_{ij}) \delta(C_i, C_j), \quad (4.1)$$

where C_i is the community of node i and the null model P_{ij} denotes the probability that nodes i and j are connected for unweighted networks and the expected weight of the link with which nodes i and j are connected for weighted networks. Modularity is therefore easily extended from unweighted to weighted networks. The quantity m represents the total number of edges in the network for unweighted networks and the total edge weight for weighted networks and is given by $m = \frac{1}{2} \sum_i k_i$, where $k_i = \sum_j A_{ij}$ is known as the *degree* of node i for unweighted networks and the *strength* for weighted networks⁴.

Communities are identified by finding the partition \mathcal{P} that maximizes Q . The choice of null model is not entirely unconstrained because it is axiomatically the case that $Q = 0$ when all of the nodes are placed in a single group.⁵ One is then restricted

⁴For an unweighted network a node's strength is equal to its degree.

⁵When all of the nodes in a network are in a single community, the number of edges within the community and the expected number of such edges are both equal to m .

to null models in which the expected edge weight is equal to the actual edge weight in the original network [220]. The simplest null model satisfying this criterion is a uniform null model in which a fixed average edge weight occurs between nodes [244]. However, the strength distribution produced by this model is significantly different to the distribution observed for many real-world networks. The most popular choice of null model (introduced by Newman and Girvan [224]) is

$$P_{ij} = \frac{k_i k_j}{2m}, \quad (4.2)$$

which preserves the strength distribution of the network and is closely related to the configuration model [212].⁶

An important issue with using modularity as a quality function to identify communities is that it suffers from a resolution limit [106]. Modularity optimization has been shown to fail to find communities smaller than a threshold that depends on the total size of the network and on the degree of interconnectedness between the network communities. Communities smaller than the threshold tend to be merged into larger communities, thereby missing important structures. However, many modularity-maximization techniques can easily be adapted to other quality functions, and several alternatives have been proposed that avoid the resolution limit by uncovering communities at multiple resolutions, e.g., [17, 179, 220, 254].

4.3.3 Potts method

In Ref. [254], Reichardt and Bornholdt proposed a multiresolution method in which the network \mathbf{A} is represented as an infinite-range, N -state Potts spin glass in which each node is a spin, each edge is a pairwise interaction between spins, and each community is a spin state. The Hamiltonian of this system is given by

$$\mathcal{H}(\lambda) = - \sum_{ij} J_{ij} \delta(C_i, C_j), \quad (4.3)$$

where C_i is the state of spin i and J_{ij} is the interaction energy between spins i and j . The coupling strength J_{ij} is given by $J_{ij} = A_{ij} - \lambda P_{ij}$, where P_{ij} again denotes the expected weight of the link with which nodes i and j are connected in a null model and λ is a resolution parameter. If $J_{ij} > 0$ spins i and j interact ferromagnetically

⁶The difference between the two models is that the configuration model is conditioned on the actual degree (strength) distribution, whereas Newman and Girvan's model is conditioned on the expected degree (strength) distribution. In the configuration model, the probability of an edge falling between nodes i and j is also given by Eq. 4.2 in the limit of large network size; however, for smaller networks, there are corrections of order $1/N$ [220].

and seek to align in the same spin-state (join the same community); if $J_{ij} < 0$ i and j interact antiferromagnetically and try to have different orientations (join different communities). One can find communities by assigning each spin to a state and minimizing the interaction energy of these states given by Eq. (4.3). Within this framework, community identification is equivalent to finding the ground state configuration of a spin glass.

Tuning λ allows one to find communities at different resolutions; as λ becomes larger, there is a greater incentive for nodes to belong to smaller communities. The Potts method therefore allows the investigation of communities below the resolution limit of modularity. One can write a scaled energy Q_s in terms of the Hamiltonian in Eq. (4.3) as

$$Q_s = \frac{-\mathcal{H}(\lambda)}{2m}. \quad (4.4)$$

The modularity is then the scaled energy with $\lambda = 1$. Community detection using modularity optimization is therefore a special case of the Potts method.⁷ In this thesis, we use the Potts method to detect communities and we employ the standard model of random link assignment $P_{ij} = k_i k_j / 2m$ as the null model.

The number of possible community partitions grows rapidly with the number of nodes [218], so it is typically computationally impossible to sample the energy space by exhaustively enumerating all partitions [55]. A number of different heuristic procedures have been proposed to balance the quality of the identified optimal partition with computational costs, e.g., [75, 107, 244]. In this thesis, we minimize Eq. (4.3) at each resolution using the greedy algorithm of Ref. [44] which finds good quality partitions and is computationally fast, so can be used to detect communities in large networks. We note that quality functions like Eq. 4.3 have complex energy landscapes and we are optimizing using an optimization heuristic, so care needs to be taken when interpreting results for this method for real networks [128]. With this in mind, we validate the results obtained using the greedy algorithm by reproducing the analysis using spectral [221] and simulated annealing [141] algorithms.⁸

⁷Recently, an alternative version of the Potts method has been proposed that is able to deal with both positive and negative links [294]. Even more recently, a new framework of network quality functions based on modularity has been proposed that can deal with time-evolving networks, networks with multiple types of links, and multiple scales [214]; we discuss this method in Section 4.6.12

⁸See Ref. [105] for more details of these and other modularity (energy) optimization heuristics.

4.4 Edge communities

All of the techniques that we have described thus far define communities as groups of nodes. Recently, however, some community detection methods have been proposed in which communities are defined as sets of edges [5, 6, 90]. Edge communities are identified by considering *line graphs* [24]. A line graph is a representation of a network in which the nodes represent edges in the original network and two nodes in the line graph are connected if the corresponding edges in the original network are attached to the same node. Identifying communities of nodes in line graphs is equivalent to finding edge communities in the original network. In Ref. [90], Evans and Lambiotte present methods for identifying communities in line graphs by maximizing quality functions (derived from dynamical processes taking place on networks [177]) that are similar to modularity (see Section 4.3.2).

4.5 Clustering networks

In Chapter 6, we introduce a framework for clustering networks based on comparing their community structures at multiple resolutions. In this section, we review two notable prior attempts to cluster networks using mesoscopic structures.

In Ref. [210], Milo *et al.* clustered a set of networks based on the frequency at which certain small subgraphs they called *motifs* appeared in the networks. Motifs represent small mesoscopic structures and some motifs can be considered as small communities; for example, a 3-clique can be considered as a community because all possible connections exist between the members of the motif. Milo *et al.* created profiles for each network indicating the over- or under-representation of motifs compared to randomized networks with the same degree distribution and clustered the networks based on these profiles. They studied 19 directed networks and 16 undirected networks and identified four families for each type of network. The directed families included a family containing four gene transcription networks for microorganisms; a family containing a network of signal-transduction interactions in mammalian cells, two developmental transcription networks, and a network of synaptic wiring between neurons; a family of three social networks and three world wide web (WWW) networks; and a family including four language networks and a model of a bipartite network. The undirected network families consisted of a family containing a power grid network and a “geometric model” network; a family containing another geometric model network and three protein structure networks; a family of six networks of

the internet at the level of autonomous systems; and the final family included four Barabási-Albert preferential attachment networks.

In Ref. [142], Guimerà *et al.* clustered networks based on the over- or under-representation of nodes with particular network roles. Guimerà *et al.* first assigned each node a role based on the node's pattern of inter- and intra-community links and then created profiles indicating the under or over-representation of node roles within each network compared with randomized networks⁹. Based on these profiles, Guimerà *et al.* identified two clusters of networks. The first cluster included metabolic and airport networks, and the second cluster included protein interaction and internet networks. The authors hypothesized that the division of the networks into these two clusters might result from the fact that the networks in the first cluster are transportation networks, in which strong conservation laws must be obeyed, whereas the networks in the second cluster could be considered as signalling networks, which do not obey conservation laws. We discuss further the clustering in Refs. [210] and [142] in Section 6.6.4.

4.6 Community dynamics

In comparison with the number of papers investigating communities in static networks, there are relatively few studies of communities in dynamic networks [105]. An important reason for this comparatively small volume of work is the limited availability of data sets for time-evolving networks. However, in recent years, time-evolving data for large networks have become more widely available, in part because of the rapid expansion of online social communities such as social networking sites and blog communities. A desire to understand the evolution of these communities has led to more researchers (particularly computer scientists) studying dynamic networks and trying to answer some of the fundamental questions on community dynamics. These include: how do communities change over time; what community properties result in stable communities; and what features of a community determine whether an individual will join (or leave) that community? These questions are key to understanding the evolution of many systems: for example, the evolution of groups of employees within large organizations can provide insights into the organization's global decision-making behaviour; an understanding of the dynamics of sub-populations of people can help develop strategies for preventing the spread of diseases [23]; and an understanding of

⁹Guimerà *et al.* considered two different ensembles of random networks. In the first ensemble, they preserved only the degree distribution of the original network; in the second ensemble, they preserved both the degree distribution and the modular structure of each network.

the changes in correlations between groups of financial assets can lead to better risk management tools.

Although the study of dynamic communities is still in its infancy, several methods have been proposed for detecting and tracking communities in dynamic networks. In the remainder of this chapter, we describe the different techniques.

4.6.1 Early studies

In an early study of community dynamics, Toyoda and Kitsuregawa investigated the evolution of communities of web pages [290–293]. They first proposed a method to identify web page communities in static networks [290] using a modified version of the *Companion* algorithm proposed by Dean and Henzinger [78]. *Companion* finds web pages related to a particular URL by only exploiting the hyperlink-structure of the web; i.e., it does not use information about the content or usage levels of web pages. By following links from seed pages, the algorithm identifies web pages related to the seed page and considers seed pages to belong to the same community if they are related to similar sets of pages. In Refs. [291, 292], Toyoda and Kitsuregawa extended this work to track web communities through time. They mapped communities between consecutive time steps based on the overlap of nodes (i.e., URLs) and defined the descendant of a community $C(t)$ as the community $C(t + 1)$ that shared the most nodes with $C(t)$; if more than one community at $t + 1$ shared the same number of nodes with $C(t)$, they selected the community with the largest number of nodes as the descendant.

Toyoda and Kitsuregawa defined six types of community changes between consecutive time steps: *emerge* (a community $C(t + 1)$ emerged if it did not share any nodes with any of the communities in the network at time t), *dissolve* (a community $C(t)$ dissolved if it did not share any nodes with any of the communities in the network at $t + 1$), *grow*, *shrink*, *split*, and *merge*. A community $C(t)$ was only considered to grow or shrink if it shared all of its nodes with one community at $t + 1$; i.e., a community grew if the nodes that joined it were new to the network and a community shrunk if the nodes leaving it disappeared from the network. If a community $C(t + 1)$ contained nodes from more than one community at time t , it was considered to have merged; similarly, if more than one community at $t + 1$ contained nodes from a community $C(t)$, then $C(t)$ was considered to have split.

Based on these events, Toyoda and Kitsuregawa defined several quantities for describing community evolution, including a growth rate; a stability index; indices for measuring the rate at which nodes appeared in (disappeared from) communities;

and indices for measuring the rate at which split and merge events occurred. They applied this framework to an evolving sequence of networks of Japanese web archives for each of the years 1999–2002 and found that changes in the community structure were largely a result of merge and split events. This observation seems unsurprising given the tight constraints on nodes’ community membership for the other types of event. They also found that the distribution of community sizes and the distributions of the sizes of emerged and dissolved communities followed power laws.

In another early study [152], Hopcroft *et al.* employed a very different approach to study the evolution of weighted citation networks¹⁰ in which the nodes represented papers and the weights were given by the cosine similarity [84] between vectors representing each paper’s citations. Hopcroft *et al.* identified communities using agglomerative hierarchical clustering, but found that the clusters were very sensitive to random perturbations in the network. This led them to define “natural communities” as clusters that were robust to the random removal of nodes. To identify natural communities, Hopcroft *et al.* created n realizations of the network in which 5% of the nodes were randomly removed and compared clusters C in the original network with clusters C' in the perturbed networks using the similarity function

$$\min \left(\frac{|C \cap C'|}{|C|}, \frac{|C \cap C'|}{|C'|} \right), \quad (4.5)$$

where $|C \cap C'|$ indicates the cardinality of the intersection of nodes in the two clusters. They defined a natural community as a cluster in the original network whose similarity with any cluster in a perturbed network exceeded a pre-defined threshold p for a fraction f of the networks with nodes removed.¹¹

Hopcroft *et al.* tested their method by comparing citation data for the years 1990–1998 with data for 1990–2001, which enabled them to identify changes that occurred in the community structure during the period 1999–2001. They associated each community with a research topic by considering the most frequent words in the titles of the papers in the communities. They then classified the natural communities in the second period as either *established* or *emerging* depending on their overlap with communities in the first period. They found that some of the established communities grew rapidly while others stagnated, and that some of the communities that emerged had split from communities that existed in the first period. Based on the evolution

¹⁰The citation data covered the period 1990–2001 and was downloaded from the CiteSeer database, which is available at <http://citeseer.ist.psu.edu/>.

¹¹Hopcroft *et al.* created $n = 45$ networks in which 5% of nodes were removed and set $f = 0.6$; they set $p = 0.7$ for clusters containing fewer than 1,000 papers and $p = 0.5$ for larger clusters.

of the different communities, they identified new, expanding, and declining fields of research.

An important issue with the approach proposed by Hopcroft *et al.* is that hierarchical trees contain clusters at several different levels and their method does not identify the level at which the clusters are most appropriate. In addition, there are several parameters that the user must define, including the fraction of nodes to randomly remove from the original network to create the comparison networks; the overlap threshold p for a pair of clusters to be considered similar; and the fraction of perturbed networks f in which a cluster needs to match another cluster for it to be considered a natural community. The node compositions of the natural communities depend on all of these parameters.

4.6.2 Comparing and mapping communities

In Ref. [152], Hopcroft *et al.* used the similarity function defined in Eq. 4.5 to compare communities, but there are several other functions that can be used (some of which we describe later in this chapter). For many of the methods that compare communities using a similarity function, it is also necessary to select an appropriate overlap threshold that the similarity function must exceed for two clusters to be considered similar (the parameter p in Hopcroft *et al.*'s study). In most studies a formal procedure is not defined for selecting the threshold; instead this parameter is chosen using ad hoc methods or is simply set to a value that is found *a posteriori* to produce meaningful results.

Perhaps the most important issue with methods that identify descendent communities based on maximum node (or edge) overlap is that they can lead to equivocal mappings following splits and mergers. For example, consider a community $C^f(t)$ that splits into two communities $C^g(t+1)$ and $C^h(t+1)$. If the overlap between $C^f(t)$ and $C^g(t+1)$ is identical to the overlap between $C^f(t)$ and $C^h(t+1)$ then it is not obvious which community represents the descendent of $C^f(t)$. For the specific case of two communities with identical node overlaps with a community at the previous time step, Toyoda and Kitsuregawa [291,292] chose the descendant as the community containing the largest number of nodes. However, there are other plausible choices. For example, a tie in node overlap could be broken by selecting the community with the highest edge overlap as the descendant.

This highlights the more general question of whether communities should be mapped based on node or edge overlap. For example, consider a community $C^r(t)$ that splits into two communities $C^s(t+1)$ and $C^t(t+1)$, such that $C^s(t+1)$ has a greater

node overlap with $C^r(t)$, but $C^t(t+1)$ has a greater link weight in common with $C^r(t)$. In this case, either community could be identified as the descendant of $C^r(t)$ depending on whether one considers node or edge overlap to be a more important measure of community similarity. Most methods that we describe map communities based on node overlap; in practice, the choice between node or edge overlap is likely to depend on which measure is most appropriate for a particular analysis.

4.6.3 Dynamics of known partitions

Although in most work on community dynamics methods are presented both for community detection and community tracking, in some studies the communities are already known. In Ref. [23], Backstrom *et al.* investigated the evolution of communities of bloggers on the LiveJournal blogging website¹² and communities within a co-authorship network of computer scientists taken from the Digital Bibliography and Library Project (DBLP) website¹³. Backstrom *et al.* did not detect communities, but instead studied the evolution of known groups. In the case of LiveJournal the communities corresponded to blogging groups that the users joined; for the DBLP network, conferences were used as proxies for communities.

For both data sets, Backstrom *et al.* found that the probability of a person joining a community increased with the number of people that they knew in the community, but that there was a “diminishing return” property in which this probability rose at an increasingly slower rate as the number of friends already in the community increased. For the LiveJournal network, they also showed that an individual was more likely to join a community if the people that they knew in the community already knew each other, but that groups with a very large number of 3-cliques grew less quickly than groups with relatively few such cliques. These results imply that the tendency of an individual to join a community is not just influenced by the number of friends that individual has within the community, but crucially also by how those friends are connected to each other. Backstrom *et al.* hypothesized that the slower rate of growth of communities containing large numbers of 3-cliques could be because such “cliquishness” makes communities less attractive to join; alternatively, they suggested that many 3-cliques could indicate a community that has stopped gaining new members, but continues to gain new edges between existing members. Finding an explanation for this observation is an interesting open question because of

¹²See <http://www.livejournal.com/>.

¹³DBLP is a database of bibliographic information for computer science journals. See <http://www.informatik.uni-trier.de/~ley/db/>.

its implications for the potential rate of growth of online communities such as social networking websites.

Berger-Wolf and collaborators have proposed several different methods for studying dynamic communities [35]. In Ref. [36], Berger-Wolf and Saia presented a technique in which it was assumed that the community partition at each time step was already known. They created a network of these known communities in which two communities C and C' were linked if the similarity

$$\frac{2|C \cap C'|}{|C| + |C'|} \quad (4.6)$$

exceeded a pre-defined threshold β_m . Within this framework two communities could be connected irrespective of the number of time steps separating the networks in which they were observed. This is in contrast to other techniques that create networks of communities but only allow communities to be connected if they appear in networks separated by a specified number of time steps (e.g., Refs. [91, 93, 96, 97] which we discuss in Section 4.6.6.).

Using the network of communities, Berger-Wolf and Saia then defined a *metagroup* as any connected group of at least α_m communities and considered that an individual node was a member of a metagroup if it belonged to more than γ_m communities in that metagroup. They then defined the *most persistent metagroup* as the metagroup that contained the most communities; the *most stable metagroup* as the metagroup that contained the most links as a fraction of the number of time steps over which the group persisted; and the *largest metagroup* as the metagroup that contained the most nodes.

Berger-Wolf and Saia tested the metagroup framework on the southern women social network [76], which is a standard benchmark in social network analysis [112]. The southern women data set consists of details of the participation of 18 women in 14 social events in Mississippi in the 1930s; the network contains 14 communities corresponding to the groups of women that attended each of the 14 events. Berger-Wolf and Saia found good agreement between the membership of the most stable metagroups and the clusters identified in previous studies of the same data. They also considered the importance of communities and nodes to the existence of metagroups at different similarity thresholds β_m and length thresholds α_m and found that the metagroups were robust to the removal of particular communities and individuals from the population. Such observations are of practical interest in epidemiology; for example, targeted vaccination of individuals whose removal results in the break-up of metagroups might help to prevent the spread of diseases [10, 62, 151].

4.6.4 Dynamic subgraphs and cliques

There are several studies of dynamic networks in which motifs consisting of repeated subgraphs, such as cliques, are investigated. As we discussed in Section 4.3.1, a k -clique in an unweighted network is a set of k nodes that are connected with all $k(k-1)/2$ possible edges, so they represent particularly strong relationships between a group of nodes. Motifs need not contain all possible links between nodes, but if a subgraph appears regularly through time it indicates a persistent or recurrent relationship between a group of nodes.

In Ref. [175], Lahiri and Berger-Wolf defined *frequent* and *periodic* subgraphs as groups of nodes that had the same intra-group links for more than a pre-defined fraction of observed time steps, and groups of nodes that had the same relationships in networks separated by a constant number of time steps, respectively. For example, a 3-clique that appeared every fifth time step was considered to be a periodic subgraph. Lahiri and Berger-Wolf investigated subgraph dynamics for a social network of zebras [283], a network of e-mail exchanges within Enron¹⁴, a co-appearance network for celebrities in photos on the Internet Movie Database (IMDB)¹⁵, and a contact network of mobile phone users at MIT [85]¹⁶. Lahiri and Berger-Wolf identified many frequent and periodic subgraphs for each of these data sets, including a periodic subgraph of actresses from the television show *Desperate Housewives* in the IMDB network. This subgraph had a period of 364 days and is likely to result from the joint appearance of these actresses at annual awards shows.

In Ref. [311], Yoneki *et al.* also studied the MIT contact network data set as well as three other dynamic contact networks. Yoneki *et al.* focused on the distribution of the durations of meetings between particular groups and the distribution of the times between these meetings. They took a stricter approach than Lahiri and Berger-Wolf [175] by only investigating cliques – this meant that every node in the studied groups had to be connected to every other node. They analyzed k -cliques with $k = \{3, \dots, 8\}$ nodes and found that the durations of meeting times for the cliques were power-law distributed, but the intervals between these meetings were not.

In another study of dynamic motifs [157], Jin *et al.* investigated the evolution of weighted subgraphs. They analyzed networks in which there was a time series associated with each node and the edge weights were a function of the time-dependent

¹⁴The data for the Enron e-mail network is available at <https://www.cs.cmu.edu/~enron/>.

¹⁵See <http://www.imdb.com/>.

¹⁶The contact networks were constructed using mobile phones fitted with proximity tracking technology that recorded when two individuals were located near to each other.

pairwise correlations between these time series. Community detection in networks of this kind is equivalent to the problem of clustering multivariate time series [187]. Jin *et al.* defined a trend motif as any subgraphs whose edge (or node) weights consistently increased (or decreased) by more than a threshold amount over a specified time period. They investigated a network of trade between countries, in which the node weights represented each country's share of global gross domestic product (GDP) [122], a stock market network [230], and a protein interaction network [27, 278], and found several examples of trend motifs in each case. For example, they identified a subgraph in the trade network over the period 1980–1990 containing the U.K., Japan, and the U.S. in which each country's share of global GDP was trending upwards. In another subgraph for the period 1981–1989 containing the U.S., Mexico, Argentina, and South Africa, the U.S.'s share of global GDP was trending upwards while the share of each of the other countries was trending downwards.

Jdidia *et al.* [154] also identified stable cliques in an evolving co-authorship network for the Infocom conference on computer communications over the period 1985–2007. They investigated cliques with three or more nodes and considered a clique to be stable if it appeared in three or more networks. Using this approach, they identified many stable cliques of collaborators based on their conference publications.

In the same paper, Jdidia *et al.* also proposed a method for detecting communities in dynamic networks based on the behaviour of random walkers.¹⁷ They first created an aggregate network consisting of a combination of the networks for individual time steps coupled through additional links. They introduced two types of links between consecutive networks: (1) a node in a network at time t was connected to itself if it also appeared at $t + 1$, i.e., a link was added between node i at time step t and node i at time step $t + 1$; (2) a link was added between node i at time step t and node j at $t + 1$ if there existed a node k such that i and k were linked at time step t and j and k were linked at $t + 1$; these edges were called *transversal edges*.

Jdidia *et al.* detected communities in this network by maximizing modularity using a variant of the walktrap algorithm proposed by Pons and Latapy [240]. This algorithm identifies communities based on the observation that random walkers on a graph tend to get “trapped” in densely connected parts of the graph that correspond to communities. Jdidia *et al.* presented an example of an evolving community of collaborators in which a stable clique of researchers gained and lost additional collaborators through time. They also investigated the probability of an author joining the conference program committee board as a function of the number of their co-authors

¹⁷We describe other methods based on random walkers in Section 4.6.8.

already on the board and found that the probability of an author joining the committee increased with the number of their co-authors already on it. This result is consistent with Backstrom *et al.*'s [23] observation that the probability of a person joining a community increases with the number of people that they know in that community.

4.6.5 Dynamic clique percolation

All of the studies that we described in Section 4.6.4 uncovered recurrent relationships between groups of nodes by detecting frequent subgraphs and cliques. The CPM method described in Section 4.3.1 extends the idea of cliques by defining communities as groups of overlapping cliques. This method is based on the observation that intra-community edges are likely to form cliques as a result of their high density, but inter-community edges are not. In Ref. [233], Palla *et al.* extended the CPM framework to investigate community dynamics.

As we discussed in Section 4.3.1, communities detected using CPM can overlap (i.e., share nodes), which can lead to additional problems when trying to identify community descendants using node overlap. For example, consider the situation in which a community $C(t)$ increases in size between time steps t and $t + 1$ and the resulting community $C(t+1)$ overlaps with another community $C'(t+1)$. The overlap between $C(t + 1)$ and $C'(t)$ might be larger than the overlap between $C(t + 1)$ and $C(t)$ resulting in $C(t + 1)$ being identified as the descendant of $C'(t)$ and not $C(t)$. Palla *et al.* tackled this problem by considering the graph $\mathcal{G}(t, t + 1)$, which consisted of the union of nodes and edges from the two graphs $\mathcal{G}(t)$ and $\mathcal{G}(t + 1)$. The rationale for this approach is as follows. Let $\mathcal{P}(t)$ denote the set of communities from graph $\mathcal{G}(t)$, $\mathcal{P}(t + 1)$ the set of communities from graph $\mathcal{G}(t + 1)$, and $\mathcal{P}(t, t + 1)$ the set of communities identified for the combined graph $\mathcal{G}(t, t + 1)$. For any community in $\mathcal{P}(t)$ or $\mathcal{P}(t + 1)$ there is exactly one community in $\mathcal{P}(t, t + 1)$ containing it, which is found by comparing edges. The descendant of $C(t)$ is then the community contained in the same community $C(t, t + 1)$ as $C(t)$ with which $C(t)$ has the largest edge overlap.

Palla *et al.* applied this method to a call network of mobile phone users and to a co-authorship network of condensed matter physicists. For both networks, they found that the age of a community was positively correlated with its size (i.e., older communities tended to be larger on average) and also found that the membership of large communities varied more than small communities, which tended to be almost static. They further found that communities whose members had relatively strong connections with nodes outside their community were more likely to break up, and

that nodes that were only loosely connected to their community were more likely to leave that community than nodes with strong intra-community connections. The observation that nodes are more likely to leave a community if they are only weakly connected to that community is complementary to the observation made by Backstrom *et al.* [23] and Jdida *et al.* [154] that the probability of an individual joining a community increases with the number of people they know in that community.

Reference [233] provides answers to several of the fundamental questions relating to community dynamics, but the results should be validated using other techniques. This is important because there are some issues with the CPM method; for example, there are several possible choices for the clique size; and the definition of a community is very stringent (see Section 4.3.1). It would also be interesting to investigate if similar results are observed for other types of network.

4.6.6 Edge betweenness methods

In contrast to the motif-based methods described in Sections 4.6.4 and 4.6.5, edge betweenness methods do not require the user to specify the structures to identify. In Ref. [92], Falkowski *et al.* investigated community dynamics using the Girvan-Newman edge betweenness method (see Section 4.3) and a method proposed by Radicchi *et al.* [247]. The Radicchi method is similar to the Girvan-Newman method but, instead of iteratively removing edges with the lowest betweenness centrality, edges with the lowest *edge-clustering coefficient* are removed. The edge-clustering coefficient is analogous to the the node-clustering coefficient [305] and is defined as the number of 3-cliques to which an edge belongs divided by the total number of 3-cliques the edge could potentially belong to based on the degrees of the nodes it connects. The basic idea is that edges with a low edge-clustering coefficient belong to fewer small cliques than edges with high edge-clustering coefficient, so these edges are considered to be more likely to run between communities.

To create dynamic networks, Falkowski *et al.* split their network data into time periods and constructed a network for the interactions within each period.¹⁸ Falkowski *et al.* mapped communities between consecutive time steps based on the percentage node overlap exceeding a threshold and defined several community events: *persists*, *disappears*, *merges*, and *splits*. They further divided the persist events into *grows* and *declines* transitions. A community grew if the number of members increased between

¹⁸This is in contrast to other studies, such as the work of Hopcroft *et al.* [152], in which community dynamics were investigated by cumulatively adding data to a network and identifying changes in the aggregated network.

time steps; a community declined if the number of members decreased and/or the number of edges, or the edge weights, decreased between time steps. In contrast to the grow and shrink events defined by Toyoda and Kitsuregawa in Refs. [291, 292], the grow and decline events defined by Falkowski *et al.* allowed nodes to join from existing communities, or leave to join other communities; i.e., the nodes joining a community did not have to be nodes not previously in the network and the nodes leaving a community were not required to be nodes leaving the network. Falkowski *et al.* also introduced software for visualizing community dynamics in Ref. [92], but they did not provide details of any results found using their method.

Falkowski *et al.* extended the work of Ref. [92] in a series of papers [91, 93, 96, 97] in which they matched two communities C and C' at different time steps if the overlap function

$$\frac{|\mathcal{C} \cap \mathcal{C}'|}{\min(|\mathcal{C}|, |\mathcal{C}'|)} \quad (4.7)$$

exceeded a threshold ρ_m . Instead of simply comparing communities at consecutive time steps, they matched communities between all networks within τ_p time steps of each other. They then constructed a graph in which each community observed over the full evolution of the network represented a node and they connected all nodes that appeared in networks within τ_p time steps of each other for which the community overlap exceeded ρ_m . Finally, they found groups of similar communities in this network of communities using the Girvan-Newman edge betweenness algorithm. An issue with this method is that it suffers from two of the weaknesses that we described in Section 4.6.2; namely that the user is required to select values for the parameters ρ_m and τ_p and the detected communities are sensitive to these choices.

Using this method to track dynamic communities, in Ref. [97] Falkowski *et al.* defined several quantities that described the relationships between nodes and their communities. These included the *involvement* of a node, which measured the number of intra-community interactions of nodes at a single time step; the *participation*, which measured the involvement of nodes in a particular community over all time steps as a fraction of the total interactions of the node; and the *relevance*, which measured the involvement of nodes in a community as a fraction of the total interactions over a specified period. Falkowski *et al.* used this framework to perform a “preliminary set of proof-of-concept experiments” on a social network.¹⁹

¹⁹Although the network is not specified in Ref. [97], this paper extends the work presented in Ref. [93] in which an online social network of students from the University of Magdeburg is studied, so it seems likely that this network is also used in Ref. [97].

4.6.7 Density methods

Other authors have proposed techniques for detecting communities based on the density of nodes in different regions of the network, where the precise definition of density depends on the method. In Refs. [94, 95], Falkowski *et al.* proposed a density-based method for detecting communities in graphs that are growing both in terms of the number of nodes and the number of edges. They assigned nodes to the same cluster if they were *density connected*; nodes were described as density connected if their was some overlap in their *neighbourhoods*, where a node's neighbourhood was all nodes on the graph within a specified distance. Dense regions of the graph therefore had many nodes within a small distance of each other.

Falkowski *et al.* designed this approach with the analysis of graphs that evolve incrementally (i.e., only a few nodes join or disappear from the network at a time) in mind because the insertion (or deletion) of nodes was only considered to affect the clustering in the neighbourhood of the inserted (deleted) nodes. Because of this property, this method is potentially useful for uncovering the changes in communities in networks constructed from generative models involving attachment mechanisms in which new nodes are iteratively added to the network. Falkowski *et al.* applied this technique to the Enron e-mail network and compared the communities with those obtained using the edge betweenness method discussed in Section. 4.6.6. They found that the density-based algorithm tended to detect small dense communities whereas the edge betweenness method often merged small groups. This highlights that different community detection methods often identify different communities. These differences are important because they can affect the conclusions regarding the properties of dynamic communities. Given this, the most rigorous approach that is currently available to assess the reliability of the outputs of different dynamic community techniques is only to consider features that are similar across multiple methods as meaningful.

In Ref. [126], Goldberg *et al.* proposed another density-based method and used it to investigate the dynamics of a directed network of blogs from the Russian section of LiveJournal. They first constructed networks of bloggers in which each node represented a blogger and there was a directed edge from the author of any comment to the author of the blog where the comment was posted. They then investigated the evolution of several microscopic (e.g., mean clustering coefficient) and macroscopic (e.g., the fraction of nodes in the largest connected component) properties of the network as well as the community dynamics.

Goldberg *et al.* defined a community C as a set of nodes \mathcal{C} for which for every node $i \in \mathcal{C}$ (resp. $i \notin \mathcal{C}$), removing i from \mathcal{C} (resp. adding i to \mathcal{C}) resulted in a

community C with a smaller value of a “density function” $\Psi(C)$ given by

$$\Psi(C) = \frac{w_{in}}{w_{in} + w_{out}} + \mu \frac{2w_{in}}{|\mathcal{C}|(|\mathcal{C}| - 1)}, \quad (4.8)$$

where w_{in} is the number of edges connecting two nodes in C , w_{out} is the number of edges with only one end connected to a node in C , and μ is a user-defined parameter. Goldberg *et al.* then considered a community $C(t + 1)$ to be the descendant of a community $C(t)$ if the similarity function

$$\frac{|\mathcal{C}(t) \cap \mathcal{C}(t + 1)|}{|\mathcal{C}(t) \cup \mathcal{C}(t + 1)|} \quad (4.9)$$

exceeded a threshold α_t , which they set to $1/3$ because it was found to produce meaningful results. They discovered that the number of blogger communities that persisted for more than a few weeks was very small, which is unsurprising given that they also observed that 25% of the nodes changed between some time steps. However, the persistence of communities determined using this method is affected by the value of the threshold α_t , so the results might have been different for other values of this parameter. The dependence of the results on α_t highlights why it can be undesirable for dynamic community detection methods to incorporate user-defined parameters.

4.6.8 Random walkers

In Section 4.6.4, we described a dynamic community detection algorithm that identifies communities using random walkers [154]; several other methods have been proposed that investigate community dynamics using similar techniques.

In Ref. [22], Asur *et al.* investigated the evolving relationships between nodes and communities. They detected communities at each time step using the Markov cluster algorithm introduced by van Dongen [300] and defined five types of community evolution events: *continue* (the community contained the same nodes at consecutive time steps, but not necessarily the same edges), κ -*merge* (two communities merged if a community existed at the next time step that included more than $\kappa\%$ of the nodes belonging to the two communities), κ -*split* (a community split if more than $\kappa\%$ of nodes were in different communities at the next time step), *form* (no pair of nodes in a community $C(t + 1)$ were in the same community at t), *dissolve* (no pair of nodes in a community $C(t)$ were in the same community at $t + 1$). The final two events are equivalent to the emerge and dissolve events defined by Toyoda and Kitsuregawa in Refs. [291, 292].

Asur *et al.* also defined four types of events involving nodes: *appear* (a node joined the network), *disappear* (a node left the network), *join* (a node joined a community), and *leave* (a node left a community). Based on these events, they defined four indices that measured the behaviour of the nodes in relation to the communities: the *stability index* (the tendency of a node to interact with the same nodes over time), the *sociality index* (the number of different interactions in which a node was involved), the *popularity index* (the number of nodes attracted by a community in a time interval), and the *influence index* (the number of nodes that left or joined a community at the same time as a node).

Asur *et al.* used these measures to describe the community evolution of a co-authorship network taken from DBLP database and a network of clinical drug trial patients in which the weights of the edges were based on the correlation in patients' liver toxicity levels during the trial. For the drug network, they identified several patients with a low stability index and suggested that this implied that these patients were suffering from side effects from the drugs. The reasoning behind this suggestion was that patients with a low stability index regularly switched between communities because of large variations in their response to the trial drugs, and these variations implied that they were responding badly to the treatment. Asur *et al.* also used the influence index to predict the appearance of links within clusters.

In another method utilizing random walkers, Lin *et al.* [190] proposed a technique that identified communities by finding the partition of the network that minimized the number of steps that the walkers needed to take to reach other nodes within the same community and maximized the number of steps required to move between communities. In contrast to many of the methods that we discuss, instead of mapping communities between time steps based on node or edge overlap, Lin *et al.* compared vectors representing the interactions between members of a community at different time steps. They then defined five types of community evolution: *one-to-one mapping*, *merge*, *split*, *extinct*, and *emerge*. Each of these events corresponds to one of the five events defined in Ref. [22] by Asur *et al.*

Lin *et al.* tested their method on a blog network in which each node represented a blogger and there was a directed edge from the author of any comment to the author of the blog where the comment was posted. Based on this network, they then constructed weighted networks for several different search queries in which the edge weights in a network for a particular query were based on the relevancy of a post to that query. For example, they studied the community evolution in a network based on the query "London bombing" and found that there were initially two distinct political

blog communities, with different political interests, which joined together when their interests converged – in this case, when both communities began to discuss terrorist-related issues, such as the investigation of terrorist suspects.

The major weakness of the method proposed by Lin *et al.* which is common to several of the methods that we discuss, is that the user is required to input the number of communities to identify at each time step. In almost all situations, it is desirable that the appropriate number of communities is determined by the community-detection algorithm from the structure of the data, rather than being specified by the user.

Random walkers have also been used to investigate communities in dynamic networks using methods based on modularity maximization (see Section 4.3.2). In Ref. [177], Lambiotte *et al.* demonstrated the equivalence of modularity-like quality functions and Laplacian dynamics of populations of random walkers. Recently, Mucha *et al.* extended this framework to study the community structure of *multislice* networks, which are combinations of individual networks coupled through additional links that connect each node in one network slice to itself in other slices [214].²⁰ Their generalization includes an additional parameter that controls the strength of the coupling between slices. The different connections between the network slices are flexible and can represent connections between time slices, connections between networks including different types of links, or connections across different resolutions. The method allows one to simultaneously identify communities at different time steps and to systematically track the development of communities through time.

Mucha *et al.* tested their method on an evolving roll call voting network for the U.S. Senate over the period 1789–2008 (see Refs. [241, 306] and Chapter 6). They uncovered details about the group voting dynamics of U.S. Senators that would not be captured by simply considering the union of the partitions for the different networks. In particular, their analysis identified several important changes in U.S. politics, such as the formation of political parties and the beginning of the Civil War. The method proposed by Mucha *et al.* is particularly appealing because it can simultaneously deal with multiple time steps, multiple types of edge, and multiple resolutions. However, the user is again required to make a parameter choice; in this case to choose an appropriate value for the parameter controlling the coupling between different network slices.

²⁰This approach bears similarities to the method proposed by Jdidia *et al.* in Ref. [154] (see Section 4.6.4).

4.6.9 Graph colouring

The investigation of community dynamics has also been cast as a graph colouring problem. In Ref. [286], Tantipathananandh *et al.* defined a method for investigating community dynamics in which the colour of a node at a time step represented the node's community affiliation. To derive an optimization formulation for the community detection problem, they made three explicit assumptions about the behaviour of nodes: (1) a node tends not to change its community affiliation very frequently (i.e., a node does not change colour very often); (2) if a node does change its community affiliation (colour), it will usually move between only a few communities; (3) nodes in the same community interact more than nodes in different communities. They then assigned costs to penalize deviations from each of these behaviours and defined an optimization problem in which the community affiliation was determined by minimizing the sum of these costs; they also assigned parameters to each of these costs that could be tuned by the user to adjust the relative importance of assumptions (1)–(3). The resulting optimization problem is NP-hard, so in Ref. [286] Tantipathananandh *et al.* proposed several computational heuristics to identify approximate solutions and they presented further heuristics in Ref. [285].

Tantipathananandh *et al.* tested this framework on the southern women's data set [76] and on a social network of zebras [283] and found good agreement between the communities they identified and the communities found in prior studies. However, clearly the assumptions about node and community behaviour used to define the graph colouring problem are very strong and in general they are not valid for other networks.

4.6.10 Graph segmentation and change points

In several of the studies we have discussed, events have been defined to describe changes in individual communities (e.g., merge and split events). In this section, we describe two methods that identify time steps at which the overall community partition of a network changed.

In Ref. [282], Sun *et al.* investigated dynamic communities in bipartite networks using methods of information compression. Instead of identifying communities in the network for each time step independently and then comparing communities across time steps, Sun *et al.* separated the sequence of networks into *segments* such that the optimal community partitions of the networks in each segment were similar. The

networks in a segment were then considered to represent the same stage of the evolution of the network and were characterized by the same partition of the nodes into communities. Furthermore, the boundaries between segments were considered to correspond to “change points” in the evolution of the network. Sun *et al.* determined the partitions of the sequence of networks into segments and of the segments into communities using the minimum description length principle [136, 257], which is a formalization of Occam’s Razor [80] in which the best description of a data set is the one that results in the largest compression of the data. They calculated an encoding cost for the description of the communities in each segment and summed this value over all segments to give a total encoding cost for the sequence of networks. The optimal partition of the sequence of networks into segments and of the segments into communities was the partition that minimized the total encoding cost. Sun *et al.* applied this technique to several data sets, including the Enron e-mail network, for which they identified a change point at the time when the investigation into document shredding at the company began and the CEO resigned.

Duan *et al.* used a different approach to partition evolving, directed, weighted networks into segments in which all of the networks had similar optimal partitions into communities [83]. They began by partitioning the first two instances $\mathcal{G}(t = 1)$ and $\mathcal{G}(t = 2)$ of the network into community partitions $\mathcal{P}(1)$ and $\mathcal{P}(2)$, respectively, by maximizing modularity for each network.²¹ They compared the two partitions $\mathcal{P}(1)$ and $\mathcal{P}(2)$ using a similarity function based on the intersection of the communities at the two time steps. They then proceeded in different ways depending on the value of this similarity:

1. If the similarity exceeded a pre-defined threshold, the two networks were considered to belong to the same segment. Duan *et al.* then constructed an aggregate network $\mathcal{G}(1, 2)$, containing all of the nodes and the total edge weight in $\mathcal{G}(1)$, and $\mathcal{G}(2)$ and identified communities in this new network. They compared the community partition $\mathcal{P}(3)$ of the third network $\mathcal{G}(3)$ with the partition for the aggregate network $\mathcal{G}(1, 2)$ to determine if this network was sufficiently similar to also join the segment. If it was, they integrated $\mathcal{G}(3)$ into the aggregate graph $\mathcal{G}(1, 2)$; if it was not, there was a change point and $\mathcal{G}(3)$ began a new segment.
2. If the similarity of the first two partitions $\mathcal{P}(1)$ and $\mathcal{P}(2)$ did not exceed the threshold, they were considered to belong to different segments, so there was a

²¹See Ref. [184] for details of the generalization of modularity to directed networks.

change point between time steps 1 and 2 and the community partition $\mathcal{P}(3)$ of the third network was then only compared to the second partition $\mathcal{P}(2)$.

They repeated this process for each of the time steps of the evolving network. Duan *et al.* also applied their method to the Enron e-mail network and identified stable and fluctuating periods during which there were few and many changes points, respectively.

4.6.11 Node-centric methods

In Section 4.6.1, we highlighted problems with mapping communities between consecutive time steps following splits and mergers using methods based on node (or edge) overlap. One approach to tackling this issue is to identify descendant communities according to the community membership of particular nodes.

In Ref. [303], Wang *et al.* proposed a method for mapping communities between time steps based on the community membership of *core* nodes. For each node, they first summed the difference between the node's degree and the degree of each of its nearest neighbours. They then defined a core node as any node for which this sum was greater than zero; this meant that a community could contain more than one core node. They defined the descendants of a community $C(t)$ as all communities at $t + 1$ that contained any of the core nodes in $C(t)$ and identified four possible community events: *split*, *merge*, *birth*, and *death*. All of these events are variants of the events defined by other authors that we have already discussed.

Wang *et al.* applied this technique to several data sets, including three co-authorship networks [216]; a network of mobile phone users in China; the Enron email network; a collaboration network of film actors taken from IMDB; an internet network; a word adjacency network of computer related vocabulary in which nodes represented words and nodes were connected by edges if the words appeared in the same article on the Engineering Village website; and three software networks in which nodes represented classes and nodes were connected if an invoking relationship existed between the classes. For each of these networks, Wang *et al.* uncovered dynamic communities and calculated correlation coefficients between the size of each community and its age (they called this correlation coefficient *growth*) and between the lifetime of each community and its stability (they called this coefficient *metabolism*). They found positive growth values for social networks and negative values for all other networks; they further found negative values of the metabolism coefficient for social networks and positive values for the other networks.

The positive value of the growth coefficient for social networks is in agreement with the findings of Palla *et al.* [233] (see Section 4.6.5). However, Palla *et al.* only investigated social networks, so it would be interesting to test whether their methods also find that the age of a community is negatively correlated with its size in other types of network. If this difference between the two types of network is verified using other methods, a further question of interest is what properties of the networks lead to these differences?

There are, however, several problems with Wang *et al.*'s approach. For example, it is possible that a community could split in half such that one half contains all of the core nodes and the other none. In this case, although the two new communities contain the same fraction of nodes of the original community, only one will be labelled as a descendant. A second possibility is that a community $C(t)$ with three core nodes could split into three communities, two of which contain significantly fewer nodes than the third community. In this case, all three new communities would be considered to be descendants of the original community; however, it would perhaps be more reasonable to only consider the largest community as the descendant of $C(t)$.

In another node-centric approach, Asur and Parthasarthy [20, 21] tracked the evolution of groups of nodes in the local neighbourhood of individual nodes. For each node i , they defined a *viewpoint neighbourhood* as the network of nodes rooted at i that contained only nodes (and their connections) with some degree of importance to i . To identify the viewpoint neighbourhood of a node, Asur and Parthasarthy proposed an activation spread model defined as follows. They began at a node i with an amount M of some resource to allocate; they then distributed this resource amongst the immediate neighbours of i , assigning the proportion of the resource to each node based on an *activation function*. They described any node that received some of the resource as *activated*. The activated nodes retained some amount of the resource for themselves and assigned the rest to their neighbours. This activation process proceeded with the amount of resource to be allocated decaying as the number of steps from i increased until a minimum threshold was reached, at which point the resource was considered indivisible and the activation ceased. Asur and Parthasarthy defined the viewpoint neighbourhood of node i as the set of all activated nodes. They considered three activation functions for determining the fraction of the resource allocated to the nodes at each level: one based on the degree of a node, another based on edge betweenness, and a third based on the semantic similarity of keywords with which the nodes were annotated.

Asur and Parthasarthy used this technique to investigate the dynamics of a DBLP co-authorship network and a network of Wikipedia pages. They identified five evolution events for viewpoint neighbourhoods, which are similar to the events identified in Ref. [22] by Asur *et al.* These events are *growth*, *shrinkage*, *continuity* (the nodes in a viewpoint neighbourhood remained unchanged, but there were possibly changes in the edges), *mutate* (a growth or shrinkage event in which more than half of the nodes in a viewpoint neighbourhood changed between consecutive time steps), κ -*attraction* ($\kappa\%$ of the nodes in a viewpoint neighbourhood moved closer), and κ -*repulsion* ($\kappa\%$ of the nodes in a viewpoint neighbourhood moved further apart). These events are not mutually exclusive so, for example, a viewpoint neighbourhood could grow and attract at the same time. Asur and Parthasarthy found that, for both the DBLP and Wikipedia networks, growth and shrinkage events were frequent, while continuity events were rare in the DBLP network, but quite frequent in the Wikipedia network.

Asur and Parthasarthy also defined four indices (which are again similar to the indices in Ref. [22]) for measuring the changes in a node's viewpoint neighbourhood: *stability* (how much a neighbourhood changed over time), *sociability* (how many different nodes were affected by a particular node over time), *popularity* (how many nodes were attracted to a node's neighbourhood), and *impact* (for identifying nodes that had the highest impact on most viewpoint neighbourhoods). Perhaps unsurprisingly, the authors in the DBLP network with the highest impact scores were those that were regarded as most influential within their field. Finally, Asur and Parthasarthy identified stable and short-lived subgraphs within viewpoint neighbourhoods.

Kampis *et al.* [162] also proposed a method for tracking communities from the point of view of individual nodes. In Ref. [162], they suggested a community tracking method based on *identifier* nodes, which they defined as the nodes within communities with the highest betweenness centrality. A community was then considered to evolve from another community if the communities shared the same identifier node. However, Ref. [162] is a work in progress and Kampis *et al.* have not produced any results yet using this framework.

A primary objective of node-centric techniques for investigating community dynamics is to make the mapping of communities between consecutive time steps unequivocal. However, as we highlighted at the beginning of this section when discussing the method proposed by Wang *et al.* in Ref. [303], this mapping can still be ambiguous for community mappings based on the properties of individual nodes. In Chapter 5, we introduce an alternative node-centric method for tracking communities in dynamical networks.

4.6.12 Evolutionary clustering

Most of the methods described thus far are essentially two-step procedures in which one first independently partitions the network into communities at each time step and then uncovers community dynamics by comparing the partitions across time steps. For noisy data, this can often result in significant variations in the communities detected in consecutive partitions; however, the community changes can then simply be an artefact of the data rather than the result of major changes in the underlying community structure of the network.

To overcome this problem, Chakrabarti *et al.* introduced the idea of *evolutionary clustering* [65], which seeks to simultaneously optimize two criteria: first, the clustering obtained at any time step should closely reflect the data at that time step; second, the clustering should not change drastically between consecutive time steps. More formally, if we let $\mathcal{P}(t)$ denote the clustering at time step t and $M(t)$ denote a similarity matrix²² for the objects to be clustered, one can define a snapshot quality function $s_{\text{quality}}[\mathcal{P}(t), M(t)]$ that gives the quality of the clustering $\mathcal{P}(t)$ at time t with respect to $M(t)$. One can then also define a history cost function $h_{\text{cost}}[\mathcal{P}(t-1), \mathcal{P}(t)]$ that gives the history cost of the clustering at time step t . Within this framework, a good partition should have a high snapshot quality (i.e., the clusters at time step t should closely reflect the data at this time step) and a low history cost (i.e., the clustering at time step t should be similar to the clustering at $t-1$).

Chakrabarti *et al.* identified optimal sequences of clusters by finding the partition $\mathcal{P}(t)$ at each time step t that maximized the quality function

$$s_{\text{quality}}[\mathcal{P}(t), M(t)] - \nu h_{\text{cost}}[\mathcal{P}(t-1), \mathcal{P}(t)], \quad (4.10)$$

where ν is a tunable parameter that adjusts the relative weights of the snapshot quality and history cost. This framework is flexible and one can define quality functions and history costs that are appropriate for a particular problem. In Ref. [65], Chakrabarti *et al.* derived evolutionary versions of hierarchical clustering and k -means clustering [84] and tested their algorithm under different parameter settings on a bipartite network of photos and photo-tags from the photo-sharing website `flickr.com`.

Using a similar approach, in Refs. [69] and [68], Chi *et al.* proposed two evolutionary spectral algorithms. In both algorithms, the optimal clustering was identified

²²Chakrabarti *et al.* defined the similarity of a pair of nodes in a bipartite network as a linear combination of their cosine similarity and the correlation between time series associated with each node. Their method, however, does not depend on this choice, so other similarity measures can be used.

by minimizing a cost function with both a snapshot and a history cost, similar to Eq. 4.10.²³ The two approaches proposed by Chi *et al.* differed in the data that was used to minimize the history cost. In the first approach, the clustering $\mathcal{P}(t)$ was compared to the similarity data at $t - 1$, whereas in the second approach the clustering $\mathcal{P}(t)$ was compared to the clustering $\mathcal{P}(t - 1)$. Chi *et al.* tested their methods on an evolving blog network and found that, for certain values of the parameter weighting the snapshot and history costs, the clusters were stable in the short-term, but evolved over longer time horizons.

The evolutionary spectral framework proposed by Chi *et al.* allowed for changing numbers of clusters, but they also extended it to allow for changing numbers of nodes. However, the number of clusters required at each time step is not determined automatically in this method, but must be input by the user. This is also true of the evolutionary k -means and hierarchical clustering algorithms proposed by Chakrabarti *et al.* [65]. Another issue with these evolutionary clustering techniques is that they do not include a method for automatically selecting the parameter weighting the snapshot and history costs; instead, the value of this parameter again needs to be chosen by the user.

In another paper on evolutionary clustering, Lin *et al.* [188] proposed an algorithm called *FacetNet*, that produces a *soft* assignment of nodes to communities, i.e., instead of each node belonging to a single community at each time step, the algorithm returns a probability that a node belongs to a community, so nodes can be considered to belong to more than one community. Lin *et al.* defined the snapshot cost as the Kullback-Leibler divergence²⁴ [173] between the similarity matrix at time t and the matrix describing the community structure of the network at t ; they defined the history cost as the Kullback-Leibler divergence between the matrices describing the community structures at t and $t - 1$. They also extended the framework to deal with the insertion and deletion of nodes and changing numbers of communities. To determine the number of communities at each time step, they defined a soft modularity and selected the partition that maximized this function. However, the user is still required to input an appropriate range of candidate values for the number of

²³Note that Chi *et al.* [69] minimized a cost function whereas Chakrabarti *et al.* [65] maximized a quality function. Of course, the two optimizations are closely related: the higher the quality, the lower the cost.

²⁴The Kullback-Leibler divergence is a non-symmetric measure of the distance between two probability distributions. For two matrices \mathbf{X} and \mathbf{Y} with elements x_{ij} and y_{ij} , respectively, the Kullback-Leibler divergence is given by $D(X||Y) = \sum_{i,j} (x_{ij} \log \frac{x_{ij}}{y_{ij}} - x_{ij} + y_{ij})$.

communities because evaluating the modularity over all possible community numbers is computationally expensive.

Lin *et al.* tested the method on a blog network and a DBLP co-authorship network and concluded that the identified communities were robust with respect to data noise. In Ref. [189], they extended this work and provided more detailed algorithms and proofs. The main problems with FacetNet are that it is not able to deal with the appearance and disintegration of communities and the computation time needed to find communities does not scale well with network size. These issues were addressed in a recent paper by Kim *et al.* [167].

Evolutionary clustering algorithms have also been developed for multipartite networks. In Ref. [284], Tang *et al.* developed an evolutionary spectral clustering algorithm for multipartite networks and applied this technique to a tripartite representation of the Enron e-mail network (in which nodes corresponded to users, e-mails and words, and edges connected users to e-mails and e-mails to words) and to a four-mode DBLP co-authorship network (in which nodes corresponded to papers, authors, words in the title, and conferences/journals). For the co-authorship network, they found that the method was able to successfully detect community changes. For example, it identified the shift in focus of the Neural Information Systems Processing conference from neural networks to machine learning between 1995 and 2004. The main shortcomings of this approach are that the user must provide weightings indicating the relevant importance of each edge type in the community detection and the number of communities to identify in each mode.

Finally, in Ref. [319], Zhou *et al.* proposed an evolutionary spectral clustering algorithm for identifying dynamic communities in tripartite networks. The algorithm allows the nodes in the network to change through time, but the user is required input the number of communities to identify. They applied the method to a co-authorship network derived from the CiteSeer website in which nodes represented authors, words, and venues, and they successfully identified communities corresponding to scientific disciplines.

4.6.13 Summary

Although the study of community dynamics is still in its infancy, many methods have already been proposed for detecting and tracking communities in dynamic networks. In this section, we have described several techniques and discussed their application to different networks. We have also highlighted the problems with some of these methods; in particular, the difficulty of mapping communities between different time

steps. A problem that we have not discussed is the issue of using these methods to provide insights into data. With a few notable exceptions, the studies that we have described in this section present a method for detecting dynamic communities and then validate the method by checking that the communities it identifies in a real-world network are reasonable. However, many of the studies stop there. They do not then go on to investigate the mechanisms driving the community evolution or try to answer some of the fundamental questions that we posed at the beginning of this section, such as what properties of a community lead to stability. For many of the studies that we discussed, answering such question was probably not the authors' objective, but it seems that this is where real insights into these evolving systems can be gained and this is an obvious direction for future research.

In Chapter 5, we try to answer some of these questions for the FX market. We begin by presenting a node-centric method for tracking dynamic communities which side-steps the issue of mapping communities between different time steps. We then investigate some of the properties of these evolving communities and use them to provide insights into the changing structure of the FX market.

Chapter 5

Dynamic Communities in the Foreign Exchange Market

The work described in this chapter has been published in reference [P1] and a further paper that extends this publication is under review [P3]. The techniques we present are complementary to the methods described in Chapter 3 and provide an alternative approach for investigating evolving correlation matrices. In this chapter, we consider an FX market network in which each node represents an exchange rate and each weighted edge represents a time-dependent correlation between the rates and we use community detection to study the temporal evolution of these correlations.

5.1 Introduction

An investigation of a financial market can be formulated as a network problem. In the most common network description of a market, each node represents an asset, and each weighted link is a function (the same function for all links) of the pairwise temporal correlations between the two assets it connects [198]. A wide range of financial assets have been investigated using network techniques, including equities, e.g., [197, 198, 229], currencies, e.g., [133, 204, 205], commodities, e.g., [272], bonds, e.g., [41], and interest rates, e.g., [79]. However, because the network adjacency matrix is a function of the correlation matrix, a network for N assets contains $\frac{1}{2}N(N - 1)$ links (i.e., the network is fully-connected) so, as with the correlation matrices we analyzed in Chapter 3, simultaneous investigation of the interactions is difficult for even moderate N and some simplification is necessary to attain an understanding of the market system.

The most prevalent method for reducing the complexity of a financial network is to construct a minimum spanning tree (MST), e.g., [53, 197, 198, 229, 231]. The MST

is generated using a hierarchical clustering algorithm (see Section 4.3) and reduces the network to $N - 1$ of its most important microscopic interactions. This approach has resulted in many useful financial applications, including the construction of a visualization tool for portfolio optimization [229] and a means for identifying the effect of news and major events on market structure [205]. Nevertheless, the MST approach has a number of limitations which we discuss in Section 5.6.

An alternative simplification method is to coarse-grain the network and consider it at various mesoscopic scales. The properties of the market can then be understood by considering the dynamics of small groups of similar nodes (communities). From a financial perspective, communities correspond to groups of closely-related assets, so this treatment has the potential to suggest possible formulations for coarse-grained models of markets.

Most prior studies of financial networks find groups of closely-related assets using traditional hierarchical clustering techniques, e.g., [198, 204, 229] or by thresholding to create an unweighted network, e.g., [99]. In contrast, in this chapter, we identify communities using the Potts method described in Section 4.3.3. To the best of my knowledge, other studies that uses similar approaches to study financial networks have not examined longitudinal networks or have considered networks of equities rather than exchange rates, e.g., [148].

To provide insights into the clustering of the exchange rate time series, we introduce a new approach for investigating dynamic communities in networks. Community detection in fully-connected networks of the type studied is equivalent to the problem of clustering multivariate time series [187]. We propose a method to track communities from the perspective of individual nodes, which removes the undesirable requirement of determining which community at each time step represents the descendant of a community at the previous time step that we discussed in Section 4.6. We demonstrate that exchange rate community dynamics provide insights into the correlation structures within the FX market and uncover the most important exchange rate interactions. Although we focus on the FX market, the techniques that we present in this chapter are general and can be applied to other systems for which an evolving similarity between the constituent elements can be defined.

5.2 Data

The FX networks we construct have $N = 110$ nodes, each of which represents an exchange rate of the form XXX/YYY (with $XXX \neq YYY$), where $XXX, YYY \in \{\text{AUD},$

CAD, CHF, GBP, DEM, JPY, NOK, NZD, SEK, USD, XAU} and we note that DEM→EUR after 1998. Other authors have recently studied the FX market by constructing networks in which all nodes represent exchange rates with the same base currency, implying that each node can then be considered to represent a single currency [133]. Exchange rate networks formed with reference to a single base currency are somewhat akin to ego-centred networks studied in the social networks literature [304]. Ego-centred networks include links between a number of nodes that all have ties to an *ego* which is the focal node of the network. However, this approach has two major problems for FX networks. First, it neglects a large number of exchange rates that can be formed from the set of currencies studied and consequently also ignores the interactions between these rates. Second, the network properties depend strongly on the choice of base currency and this currency is, in effect, excluded from the analysis. We therefore construct a network including all exchange rates that can be formed from the studied set of currencies.

5.2.1 Returns

We take the price $p_i(t)$ at discrete time t as the mid-price of the bid and ask prices, so that

$$p_i(t) = \frac{1}{2} [p_i^{\text{bid}}(t) + p_i^{\text{ask}}(t)] . \quad (5.1)$$

We define the logarithmic return of an exchange rate with price $p_i(t)$ as (see Eq. 3.3)

$$z_i(t) = \ln \left[\frac{p_i(t)}{p_i(t-1)} \right] ,$$

and we use the last posted price within an hour to represent the price for that hour. To calculate a return at time t , one needs to know the price at both t and $t-1$. To minimize the possibility of a price not being posted in a given hour, we focus on the FX market's most liquid period: 07:00-18:00 U.K. time. Nevertheless, there are still hours for which we do not have price data (this usually occurs as a result of problems with the data feed). One can calculate a return for hours with missing price data by assuming the last posted price or interpolating between prices at the previous and next time step [73]. However, to ensure that all time steps included in the study are ones at which a trade can actually be made, we take the stricter approach of omitting all returns for which one of the prices is not known. In order to ensure that the time series of exchange rates are directly comparable, we consequently remove a return from all exchange rates if it is missing from any rate.

For the period 1991–2003, we derive each exchange rate XXX/YYY with $XXX, YYY \neq \text{USD}$ from two USD rates. For example, we find the CAD/CHF price at each time step by dividing the USD/CHF price by the USD/CAD price. For the period 2005–2008, we derive each exchange rate not included in the set $\{\text{AUD/USD}, \text{EUR/NOK}, \text{EUR/SEK}, \text{EUR/USD}, \text{GBP/USD}, \text{NZD/USD}, \text{USD/CAD}, \text{USD/CHF}, \text{USD/JPY}, \text{USD/XAU}\}$ from pairs of exchange rates in this set. For example, we find the USD/NOK price at each time step by dividing the EUR/NOK price by the EUR/USD price. Although this approach appears somewhat artificial, it matches the way in which many exchange rates are calculated in the actual FX market. For example, a bank customer wishing to convert CAD to NZD (or vice versa) will need to be quoted the CAD/NZD prices. Because this is not a standard conversion, the bank will not be able to quote a direct market price but will instead calculate a price using the more widely traded USD/NZD and USD/CAD exchange rates. Calculating the exchange rates in this way implies that there is some intrinsic structure inherent in the FX market. However, as shown in Ref. [204] and demonstrated further in Sections 5.5.2 and 5.5.3 of this chapter, this “triangle effect” does not dominate the results.

5.2.2 Adjacency matrix

We determine the weights of the edges connecting pairs of nodes in the network using a function of the linear correlation coefficient r between the return time series for the corresponding exchange rates. This is the same correlation coefficient defined in Eq. 3.6, but we reproduce the definition here for clarity of exposition. The correlation between the returns of exchange rates z_i and z_j over a time window of T returns is given by

$$r(i, j) = \frac{\langle z_i z_j \rangle - \langle z_i \rangle \langle z_j \rangle}{\sigma_i \sigma_j}, \quad (5.2)$$

where $\langle \dots \rangle$ indicates a time-average over T returns and σ_i is the standard deviation of z_i over T . We use the linear coefficient $r(i, j)$ to measure the correlation between pairs of exchange rates because of its simplicity, but one could use alternative measures that are capable of detecting more general dependencies [265]. The weighted adjacency matrix \mathbf{A} representing the network then has components

$$A_{ij} = \frac{1}{2} [r(i, j) + 1] - \delta_{ij}, \quad (5.3)$$

where the Kronecker delta δ_{ij} removes self-edges. The matrix elements A_{ij} (which take values in the interval $[0, 1]$) quantify the similarity of each pair of exchange rates i

and j . For example, two exchange rates i and j whose return time series are perfectly correlated will be connected by a link of unit weight.

We exclude self-edges in order to deal with simple graphs. This approach was also taken in a previous study of a stock network derived from a correlation matrix [148]. We note that if we include self-edges, the node compositions of the identified communities are identical if one makes a small parameter change in the community detection algorithm. We discuss the the effect of including self-edges in Sections 5.4 and 5.2.2.

Similarly to Section 3.2.3, we create a longitudinal sequence of networks by consecutively displacing the time windows by $\Delta t = 20$ hours (approximately 2 trading days) and fix $T = 200$ hours (approximately 1 month of data). This choice of T , motivated in part by the example data in Fig. 5.1, represents a trade-off between over-smoothing for long time windows and overly-noisy correlation coefficients for small T [227, 229]. Figure 5.2 demonstrates that the choice of Δt has a similar, but less pronounced, effect on the standard deviation of the edge weights and we again select a compromise value. The time windows we use to construct the networks overlap, so the single-time networks are not independent but rather form an evolving sequence through time.

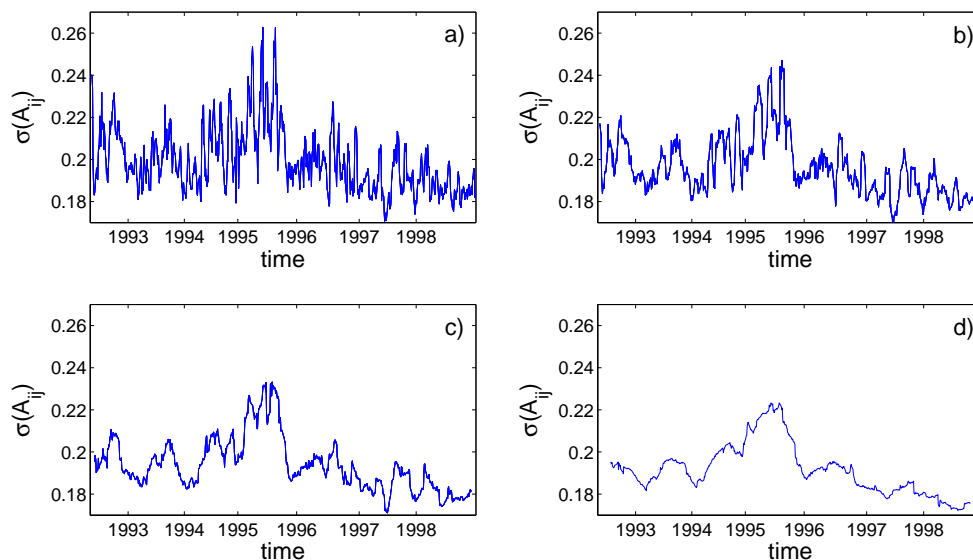


Figure 5.1: The standard deviation of the edge weights A_{ij} as a function of time for the period 1991–1998. For each panel, $\Delta t = 20$ (approximately 2 days), and (a) $T = 100$ hours, (b) $T = 200$ hours, (c) $T = 400$ hours, and (d) $T = 1200$ hours (approximately 0.5, 1, 2, and 6 months, respectively).

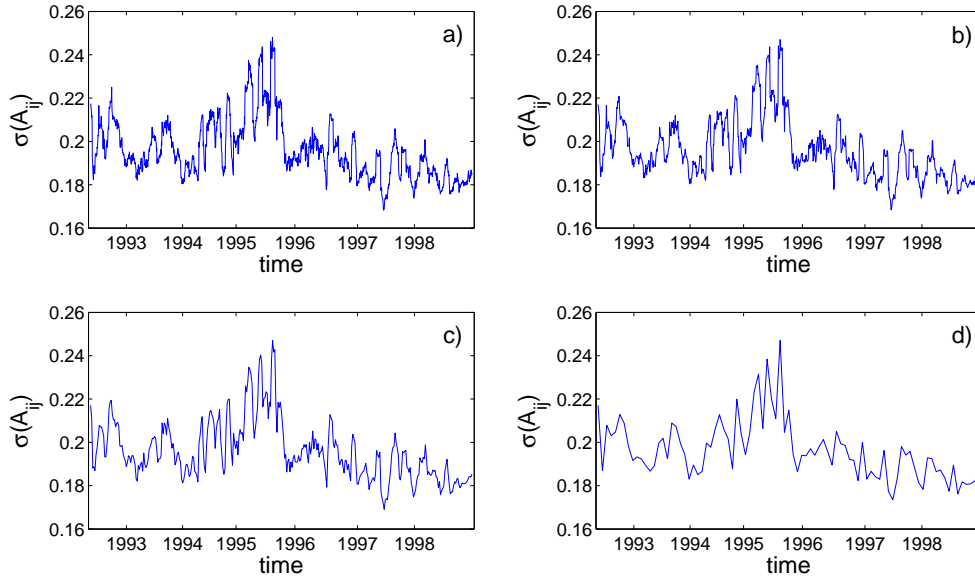


Figure 5.2: The standard deviation of the edge weights A_{ij} as a function of time for the period 1991–1998. For each panel, $T = 200$ hours, and (a) $\Delta t = 10$, (b) $\Delta t = 20$, (c) $\Delta t = 50$, and (d) $\Delta t = 200$ (approximately 1 day, 2 days, 5 days, and 2 weeks, respectively).

5.3 Detecting communities

We detect communities using the Potts method described in Section 4.3.3. Recall from Eq. 4.3 that the Hamiltonian of the N -state Potts spin glass is given by

$$\mathcal{H}(\lambda) = - \sum_{ij} J_{ij} \delta(C_i, C_j),$$

where C_i is the state of spin i and J_{ij} is the interaction energy between spins i and j . The coupling strength J_{ij} is given by $J_{ij} = A_{ij} - \lambda P_{ij}$, where P_{ij} denotes the expected weight of the link with which nodes i and j are connected in a null model and λ is a resolution parameter. We employ the standard null model of random link assignment $P_{ij} = k_i k_j / 2m$, which preserves the degree distribution of the network.

We construct FX networks by calculating a correlation coefficient between every pair of exchange rates, resulting in a weighted, fully-connected network. We include each exchange rate XXX/YYY and its inverse rate YYY/XXX in the network, because one cannot infer *a priori* whether a rate XXX/YYY will form a community with a rate WWW/ZZZ or its inverse ZZZ/WWW . However, the return of an exchange rate XXX/YYY is related to the return of its inverse YYY/XXX by $z_{\frac{XXX}{YYY}} = -z_{\frac{YYY}{XXX}}$. This

implies that the correlation coefficients between these rates and a rate WWW/ZZZ are related by $r\left(\frac{XXX}{YYY}, \frac{WWW}{ZZZ}\right) = -r\left(\frac{YYY}{XXX}, \frac{WWW}{ZZZ}\right)$. Consequently, every node has the same strength

$$k_i = \sum_j A_{ij} = \frac{1}{2}(N - 2), \quad (5.4)$$

so the probability of connection in the standard null model $P_{ij} = k_i k_j / 2m$ is also constant and is given by

$$P_{ij} = \frac{N - 2}{2N}. \quad (5.5)$$

In the case of the FX network, the standard null model $P_{ij} = k_i k_j / 2m$ and the uniform null model are thus equivalent. However, the methods we present are general and can be applied to networks with non-uniform strength distributions.

If we include self-edges in the network, the strength of each node increases by one. This, in turn, leads to a constant increase in the expected edge weight in the null model. For a network with self-edges, the expected edge weight is given by $P_{ij}^s = N/[2(N+2)]$, a shift by a constant value of $P_{ij}^s - P_{ij} = 2/[N(N+2)] \doteq 1.62 \times 10^{-4}$ relative to the network in which self-edges are excluded. Self-edges always occur within a community, so they will always contribute to the summation in Eq. 4.3 irrespective of exactly how the nodes are partitioned into communities. This implies that self-edges play no role when determining the community partition that minimizes the interaction energy at a particular resolution.

Additionally, every community has an equivalent inverse community. For example, if there is a community consisting of the three exchange rates XXX/YYY, XXX/WWW, and ZZZ/WWW in one half of the network, there must be an equivalent community formed of YYY/XXX, WWW/XXX, and WWW/ZZZ in the other half. The existence of an equivalent inverse community for each community means that at each time step, the network is composed of two equivalent halves. However, the exchange rates residing in each half change in time as the correlations evolve.

5.4 Robust community partitions

In many networks, the same community structure persists across a range of resolutions [17, 107, 254]. As one increases the resolution parameter in the Potts method one is providing an incentive for nodes to belong to smaller clusters; community partitions that are robust across a range of resolutions are therefore significant because the communities do not break up despite an increasing incentive to do so. Communities in robust partitions have been found to correspond to the communities imposed by

construction in simulated networks and to known groupings in real-world networks [17, 107]. This suggests that the communities in partitions that persist over a large range of resolutions potentially represent important substructures.¹

We compare community partitions using the normalized variation of information \hat{V} [207, 295]. The entropy of a partition \mathcal{P} of the N nodes in \mathbf{A} into η communities \mathcal{C}^k ($k \in \{1, \dots, \eta\}$) is

$$S(\mathcal{P}) = - \sum_{k=1}^{\eta} q(k) \log q(k), \quad (5.6)$$

where $q(k) = |\mathcal{C}^k|/N$ is the probability that a randomly-selected node belongs to community k and $|\mathcal{C}^k|$ is the size of communities.² For a partition \mathcal{P} , the entropy therefore indicates the uncertainty in the community membership of a randomly-chosen node. Given a second partition \mathcal{P}' of the N nodes into η' communities, the mutual information $I(\mathcal{C}, \mathcal{C}')$ is given by

$$I(\mathcal{C}, \mathcal{C}') = \sum_{k=1}^{\eta} \sum_{k'=1}^{\eta'} q(k, k') \log \frac{q(k, k')}{q(k)q(k')}, \quad (5.7)$$

where $q(k, k') = |\mathcal{C}^k \cap \mathcal{C}^{k'}|/N$. The mutual information is the amount by which knowledge of a node's community in \mathcal{P} reduces the uncertainty about its community membership in \mathcal{P}' (averaged over all nodes). The normalized variation of information \hat{V} between \mathcal{P} and \mathcal{P}' is then given by

$$\hat{V}(\mathcal{P}, \mathcal{P}') = \frac{S(\mathcal{P}) + S(\mathcal{P}') - 2I(\mathcal{P}, \mathcal{P}')}{\log N}. \quad (5.8)$$

The factor $\log N$ normalizes $\hat{V}(\mathcal{P}, \mathcal{P}')$ to the interval $[0, 1]$, with 0 indicating identical partitions and 1 indicating that all nodes are in individual communities in one partition and in a single community in the other. We will use Eq. 5.8 to compare partitions in networks with the same number of nodes and remark that one should not normalize by $\log N$ when comparing the variation of information in data sets with different sizes [207].

¹In order to find equivalent communities in the network in which self-edges are included, it is necessary to decrease the resolution parameter to compensate for the increase in the constant expected edge weight in the null model. If we identify communities in the network in which self-edges are excluded using the resolution parameter λ , then we find identical communities in the corresponding network with self-edges using a resolution parameter $\lambda^s = \lambda P_{ij}/P_{ij}^s = \lambda(N+2)(N-2)/N^2$. For example, if we identify communities in the network without self-edges using a resolution of $\lambda = 1.4500$, then we identify equivalent communities in the network with self-edges with a resolution parameter of $\lambda_s = 1.4495$.

²Recall that the quantity \mathcal{C}^k represents the set of communities indexed by k but that \mathcal{C}_i is the set of nodes in the same community as node i .

The variation of information is a desirable measure for quantifying the difference between partitions of a network because it satisfies the triangle inequality; therefore, if two partitions are close to a third partition, they cannot differ too much from each other. It is also a local measure, so the contribution to $\hat{V}(\mathcal{P}, \mathcal{P}')$ from changes in a single community does not depend on how the rest of the nodes are clustered [164, 207].

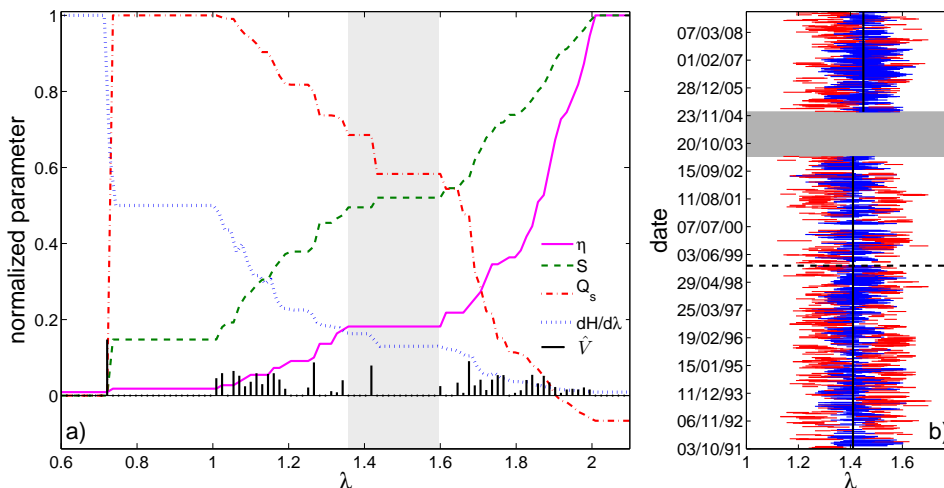


Figure 5.3: (a) The quantities η , S , Q , and $d\mathcal{H}/d\lambda$ (defined in the text), normalized by their maximum values, versus the resolution parameter λ for a single time window beginning on 17/03/1992. The shaded grey area highlights the main plateau. The bottom curve gives the normalized variation of information between partitions at resolutions separated by $\Delta\lambda = 0.015$. (b) The position of the main plateau at each time step for the full period 1991–2008. Main plateaus (blue) containing the fixed resolution (set at $\lambda = 1.41$ for 1991–2003 and to $\lambda = 1.45$ for 2005–2008) and (red) not containing the fixed resolution. The grey block corresponds to 2004, for which we do not have data.

One can identify robust communities by detecting communities at multiple resolutions and calculating $\hat{V}(\mathcal{P}, \mathcal{P}')$ between the community partitions for consecutive values of the investigated resolutions. Robust communities are revealed by intervals in which there are few spikes in $\hat{V}(\mathcal{P}, \mathcal{P}')$. In Fig. 5.3(a) we show $\hat{V}(\mathcal{P}, \mathcal{P}')$ between community partitions at resolutions λ in the interval $[0.6, 2.1]$. We focus on this interval in this example because at $\lambda = 0.6$ all of the nodes are assigned to the same community and at $\lambda = 2.1$ all of the nodes are assigned to singleton communities. We investigate 100 resolutions in this interval as a compromise between having too few resolutions to make meaningful comparisons and the computational costs of investigating more. The resolutions that we study are then separated by $\Delta\lambda = 0.015$. One

can also identify robust communities by examining summary statistics that describe the community structure as a function of the resolution parameter. We consider the number of communities η , the modularity Q (see Eq. 4.1), the entropy S (see Eq. 5.6), and the rate of change of the energy with resolution $d\mathcal{H}/d\lambda$. Robust communities correspond to plateaus (constant values) in curves of any of these quantities as a function of the resolution parameter. In Fig. 5.3(a), we plot curves for each of the summary statistics as a function of λ .

Figure 5.3(a) contains four principal plateaus, corresponding to partitions of the network into $\eta = 1, 2, 20,$ and 110 communities. The first and last plateaus, respectively, represent all nodes in a single community and all nodes in individual communities. The second plateau represents one community of exchange rates and a corresponding community of inverse rates. The $\eta = 20$ plateau occurs over the interval $\lambda = [1.34, 1.57]$, in which there is a single plateau in the η plot and a few smaller plateaus in each of the other plots. In contrast to the other plateaus, this one was not expected, so the robust communities over this interval can potentially provide new insights into the correlation structure of the FX market. Although the community configuration over this interval does not have maximal Q (i.e., it is not the community configuration corresponding to the maximum value of the traditional modularity, which is the scaled energy [see Eq. 4.4] with $\lambda = 1$), it provides an appropriate resolution at which to investigate community dynamics due to its resolution robustness and the financially-interesting features of the detected communities. For the remainder of this chapter, we will refer to this plateau as the “main” plateau.

5.5 Community detection in dynamic networks

5.5.1 Choosing a resolution

To investigate the community dynamics, we first choose a resolution parameter at which to detect communities at each time step. One approach is to always select a resolution λ in the main plateau; as shown in Figs. 5.3(b) and 5.4(a), this plateau occurs over different λ intervals at different time steps and has different widths. These intervals need not share common resolution values, so this method seems inappropriate because one would then be comparing communities obtained from many different resolutions. Therefore, we fix the resolution at the value that occurs within the largest number of main plateaus. As shown in Fig. 5.4(a), this corresponds to $\lambda = 1.41$ for the period 1991–2003 and $\lambda = 1.45$ for the period 2005–2008.

In order to demonstrate the validity of this technique, we show in Fig. 5.4(b) the distribution of the λ distance from the fixed resolution to the main plateau and in Fig. 5.4(c) the distribution of the normalized variation of information between the community configuration obtained at the fixed resolution and that corresponding to the main plateau. Both distributions are peaked at zero. The fixed resolution is a λ distance of less than 0.05 from the main plateau 91% of the time for the period 1991–1998, 93% of the time for 1999–2003, and 88% of the time for 2005–2008. The community configurations of the main plateau and the fixed resolution differ in the community assignments of fewer than five nodes in 78% of time steps for the period 1991–1998, in 83% of time steps for 1999–2003, and in 88% of time steps for 2005–2008. For the majority of time steps, the community configuration at the fixed resolution is hence identical or very similar to the configuration corresponding to the main plateau. This supports the proposed method of investigating the community dynamics at a fixed λ for each period.

5.5.2 Testing community significance

The scaled energy Q_s (see Eq. 4.4) measures the strength of communities compared with some null model, so large scaled energies indicate more significant communities. To ensure that the identified communities are meaningful, we perform a permutation test [129] and compare the scaled energies of the observed community partitions with the scaled energies for community partitions derived from shuffled data. For the period 1991–2003, we generate shuffled data for each of the USD exchange rates by randomly reordering the returns of the corresponding time series. We create shuffled data for each of the non-USD exchange rates using the shuffled USD time series and the triangle relations described in Section 5.2. We then calculate new correlation matrices for these shuffled time series, form new adjacency matrices and find the communities and scaled energies for each of the new networks. Similarly for the period 2005–2008, we shuffle the returns for each of the exchange rates in the set {AUD/USD, EUR/NOK, EUR/SEK, EUR/USD, GBP/USD, NZD/USD, USD/CAD, USD/CHF, USD/JPY, USD/XAU} and calculate the return time series for each of the rates not in this set by applying the triangle relations to these shuffled time series. This procedure conserves the return distribution for each of the original USD exchange rates for the period 1991–2003 and for each of the rates in the above set for 2005–2008. The shuffling, however, destroys the temporal correlations; any structure in the shuffled data therefore emerges as a result of the triangle relationships. The shuffled data thus

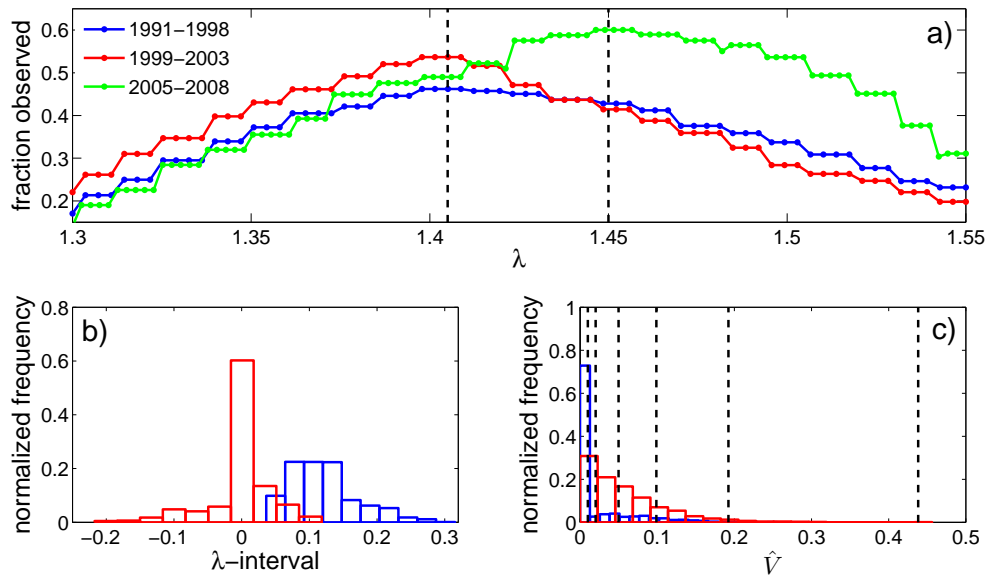


Figure 5.4: (a) Observed fraction of time steps that the resolution λ lies on the main plateau. The vertical lines indicate $\lambda = 1.41$, which lies in the highest number of main plateaus for the period 1991–2003, and $\lambda = 1.45$, which lies in the highest number of main plateaus for 2005–2008. These are the resolutions at which we investigate the community dynamics over the two periods. For the full period 1991–2008, we show in panel (b) the normalized sampled distribution of the main plateau width (blue) and the normalized sampled distribution of the λ -distance between the main plateau and the fixed resolution (red). The distance is exactly zero for 53% of the time steps. Again for 1991–2008, we show in panel (c) the normalized variation of information distribution between the community configuration at the fixed resolution and the configuration corresponding to the main plateau (blue) and the normalized variation of information distribution between consecutive time steps (red). The value of \hat{V} is exactly zero for 64% of the time steps. The vertical lines give the mean \hat{V} when (left to right) 1, 2, 5, 10, 20, and 50 nodes are randomly reassigned to different communities (averaged over 100 reassignments for each time step).

provides some insights into the effects of the triangle relations on the properties of the actual data.

By inspection, Fig. 5.5(b) shows that the communities identified for the actual data are stronger than those generated using shuffled data. The sample mean scaled energy for the actual data is 0.011 (with a standard deviation of 0.0061) and for shuffled data the sample mean is 0.0039 (with a standard deviation of 0.0013). The communities observed for the actual data are therefore stronger than the communities for randomized data in which the structure results from the triangle effect. This provides strong evidence that the communities represent meaningful structures within the FX market, so these communities can provide insights into the correlation structure of the market. We now consider properties of these communities in detail.

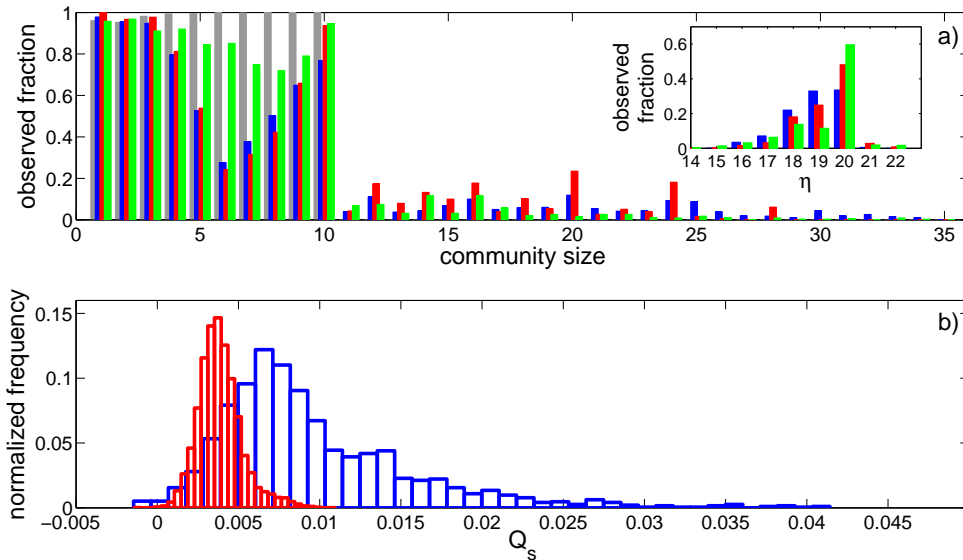


Figure 5.5: (a) The fraction of time steps at which a community of a given size is observed for 1991–1998 (blue), 1999–2003 (red), 2005–2008 (green), and shuffled data (grey). The shuffled data distribution combines the results for the period 1991–2003 and for 2005–2008. The distributions were almost identical for the two periods. The inset shows the fraction of time steps at which η communities are observed for 1991–1998 (blue), 1999–2003 (red), and 2005–2008 (green). (b) Comparison of the distribution of the scaled energy for 1991–2003 for market data (blue) and 100 realizations of shuffled data (red).

5.5.3 Community properties

The inset of Fig. 5.5(a) shows that the number of communities into which the network is partitioned exhibits only small fluctuations from 1991–2008. Nevertheless,

as shown in Fig. 5.4(c), there is a considerable variation in the extent of community reorganization between consecutive time steps. No nodes change community between some steps, whereas more than twenty nodes change communities between others. Figure 5.5(a) shows that the community size distribution is bimodal for all three periods, with a tail extending to large community sizes. There is therefore a large variation in the sizes of the communities observed at each time step for all three periods. However, the minimum between the two peaks is not as deep for the period 2005–2008 and has shifted from a community size of six nodes to a community size of eight nodes.

The peak in the size distribution for communities with 10 members occurs as a result of the the number of currencies in the network. For each of the eleven currencies $XXX \in \{\text{AUD, CAD, CHF, GBP, DEM, JPY, NOK, NZD, SEK, USD, XAU}\}$, there are ten exchange rates XXX/YYY with XXX as the base currency (and ten equivalent inverse rates YYY/XXX). We derive most of the exchange rates in a set of rates with the same base currency by applying the triangle relation (see Section 5.2) to pairs of exchange rate time series; one of the rates is common across across all of the exchange rates in the base currency set and the other rate is different for each rate in the set. For example, for the period 1991–2003, we derive the CAD/DEM exchange rate from the USD/CAD and USD/DEM rates while we derive the CAD/GBP rate from the USD/CAD but with the USD/GBP. Exchange rates with the same base currency are, therefore, often correlated and consequently they have a tendency to form communities with ten members. If there is no additional structure beyond these base-currency correlations that emerge as a result of the triangle relation, then one would expect to observe communities with $1, 2, \dots, 10$ members at each time step (and equivalent communities of inverse rates). Figure 5.5(a) shows that this size distribution is indeed observed for shuffled data. However, Fig. 5.5(a) also shows that the community size distribution for market data is significantly different, so the community detection techniques are uncovering additional structure in the FX market correlations. This again demonstrates that the triangle effect is not dominating the results.

The frequently-observed communities shown in Table 5.1 demonstrate the variation in community size. Some of the most common communities are single exchange rates, such as USD/CAD, which are formed of two closely-related currencies. Table 5.1 also highlights that communities often consist of exchange rates with the same base currency. In Ref. [205], McDonald *et al.* used the relative clustering strengths of groups of exchange rates with the same base currency to provide insights into the

effects of important news and events on individual currencies. The relative size of different base-currency communities can provide similar information. For example, if we observe a community of ten CHF/YYYY exchange rates and a community of three DEM/YYYY, the larger size of the CHF/YYYY community suggests that the CHF is more dominant than the DEM in the market at this time.

It is also worth noting that the most frequently observed community of ten exchange rates with the same base currency is the gold (XAU) community. We include gold because there are many similarities between it and a currency. However, gold also tends to be more volatile than most currencies, so the gold exchange rates tend to have relatively high correlations and strong links in the network. Given this, it is unsurprising that the gold rates often form their own community; the absence of a large gold community at a time step is often a good indication that another currency is particularly influential.

Importantly, the identified communities do not always contain exchange rates with the same base currency, providing insights into changes in the inherent values of different currencies. For example, consider a community containing several exchange rates with CHF as the base currency and several rates with DEM as the base currency. The fact that the exchange rates are in the same community suggests that they are correlated. The structure of this community also provides information about the inherent values of the CHF and DEM. Exchange rates of the form XXX/YYYY quote the value of one currency in terms of another currency, so if the price of XXX/YYYY increases it is not clear whether this is because XXX has become more valuable or because YYY has become less valuable. However, if one observes that the price of XXX increases against a range of different YYY over the same period, then one expects that the value of XXX has increased. Therefore, returning to the example, if one observes a community of several CHF/YYYY and DEM/YYYY exchange rates for many different YYY then this suggests that these rates are positively correlated. Because the values of CHF and DEM have increased against a range of other currencies, we expect that the inherent values of both CHF and DEM are increasing.

5.6 Minimum spanning trees

Perhaps the best-known approach for studying networks of financial assets is to consider the minimum spanning tree (MST) of the network. MSTs have been used regularly in studies of equity markets to identify clusters of stocks that belong to the same market sector, e.g., [53, 197, 229, 231]. In this section, we briefly consider

Table 5.1: Examples of frequently-observed communities for the pre-euro period 1991–1998 and for the two post-euro periods (1999–2003 and 2005–2008). The quantity Fr denotes the fraction of time steps at which each community is observed. The notation $XXX/\{YYY,ZZZ\}$ indicates the set of exchange rate $\{XXX/YYY,XXX/ZZZ\}$.

Period	Community	Fr
1991–1998	USD/CAD	0.62
	DEM/CHF	0.45
	NZD/{CAD,USD}	0.33
	AUD/{CAD,NZD,USD}	0.32
	XAU/{AUD,CAD,CHF,DEM,GBP,JPY,NOK,NZD,SEK,USD}	0.28
	SEK/{AUD,CAD,CHF,DEM,GBP,JPY,NOK,NZD,USD,XAU}	0.17
	DEM/NOK	0.16
	AUD/{CAD,NZD,USD,XAU}	0.14
	GBP/{CHF,DEM,NOK}	0.12
1999–2003	EUR/CHF	0.88
	USD/CAD	0.67
	XAU/{AUD,CAD,CHF,EUR,GBP,JPY,NOK,NZD,SEK,USD}	0.64
	NOK/{CHF,EUR}	0.59
	SEK/{CHF,EUR,NOK}	0.51
	GBP/{CAD,USD}	0.24
	NZD/{AUD,CAD,CHF,EUR,GBP,JPY,NOK,SEK,USD}	0.21
	JPY/{CAD,GBP,USD}	0.17
	AUD/{CAD,CHF,EUR,GBP,JPY,NOK,SEK,USD}	0.14
2005–2008	XAU/{AUD,CAD,CHF,EUR,GBP,JPY,NOK,NZD,SEK,USD}	0.91
	EUR/CHF	0.65
	AUD/NZD	0.39
	CAD/{AUD,CHF,EUR,GBP,JPY,NOK,NZD,SEK,USD}	0.39
	GBP/{CHF,EUR}	0.35
	SEK/{CHF,EUR}	0.33
	NZD/{AUD,CAD,CHF,EUR,GBP,JPY,NOK,SEK,USD}	0.26
	NOK/{CHF,EUR,SEK}	0.21
	GBP/{CHF,EUR,NOK,SEK}	0.20

the limitations of this approach for community detection and describe the additional information that the Potts method can provide.

MSTs are constructed using the agglomerative hierarchical clustering technique known as single-linkage clustering [84, 244]. Agglomerative methods start with N singleton clusters and create a hierarchy by sequentially linking clusters based on their similarity. At the first step, the two nodes separated by the smallest distance are joined in a cluster. At each subsequent step, the distance between the new cluster and each of the old clusters is recomputed and the two clusters again joined. This can be repeated until all clusters are connected. The similarity of clusters \mathcal{C} and \mathcal{C}' is usually expressed as a distance that is determined by considering the distance d_{ij} between each node $i \in \mathcal{C}$ and each node $j \in \mathcal{C}'$. In single-linkage clustering, the distance between clusters is given by

$$d_{\text{sing}}(\mathcal{C}, \mathcal{C}') = \min_{\substack{i \in \mathcal{C} \\ j \in \mathcal{C}'}} d_{ij}. \quad (5.9)$$

Single-linkage clustering thus represents an extreme because it joins clusters based on the minimum distance between nodes in each cluster. An alternative is average-linkage clustering, for which

$$d_{\text{ave}}(\mathcal{C}, \mathcal{C}') = \frac{1}{|\mathcal{C}||\mathcal{C}'|} \sum_{i \in \mathcal{C}} \sum_{j \in \mathcal{C}'} d_{ij}. \quad (5.10)$$

For financial networks, the standard measure used for d_{ij} is the nonlinear transformation of the correlation coefficient $r(i, j)$ given by [197, 198]

$$d_{ij} = \sqrt{2[1 - \rho(i, j)]}. \quad (5.11)$$

The distance takes values d_{ij} in the interval $[0, 2]$.

In constructing MSTs, the merging of clusters \mathcal{C} and \mathcal{C}' corresponds to adding an edge between the closest nodes in \mathcal{C} and \mathcal{C}' . The edges must always link clusters, so that the network never has any closed loops. If the agglomeration is continued until there is a path from every node to every other node, one obtains a spanning tree. Because the clusters are joined using the minimum distance between pairs of nodes, MSTs necessarily possess the minimum total edge length of any possible spanning tree. A minimum spanning tree is, therefore, a simply connected, acyclic graph that connects the N nodes in a network with $N - 1$ links, which is appealing because its $N - 1$ links make it much simpler to analyze than the full network with $\frac{1}{2}N(N - 1)$ links. An alternative representation of the output of a linkage clustering

algorithm, which shows the full hierarchical structure, is a dendrogram (or hierarchical tree) [84, 244]. At the first level of the dendrogram, there are N singleton clusters. As one climbs the vertical distance scale of the dendrogram, clusters are combined consecutively until all nodes are contained in a single community at the top of the dendrogram.

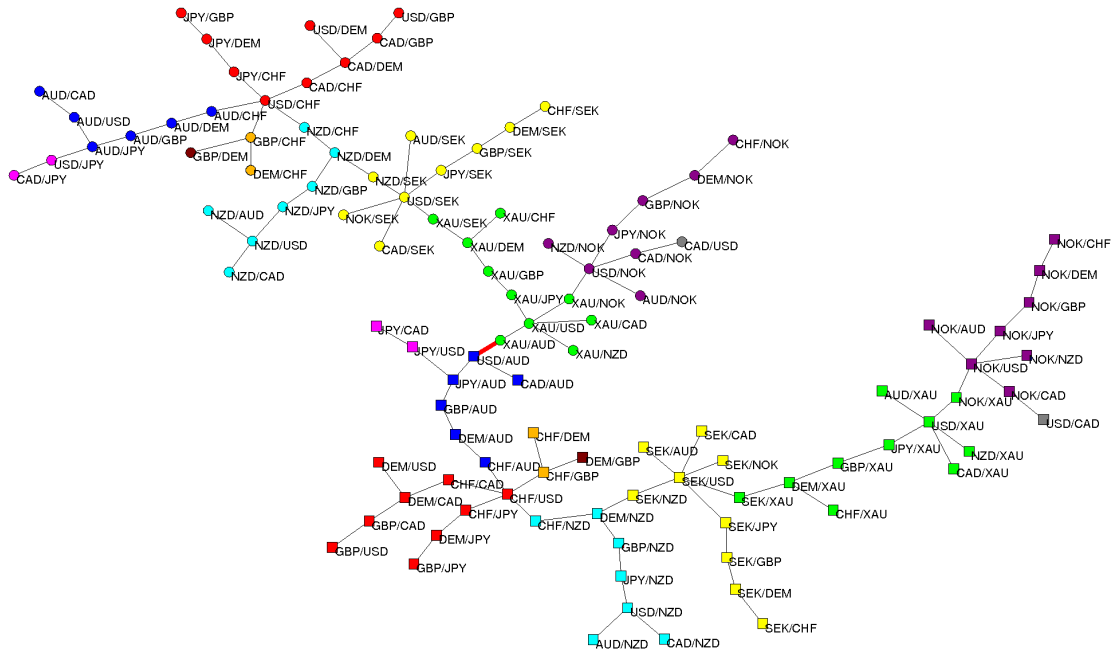


Figure 5.6: The minimum spanning tree for the network formed from a time window of returns beginning on 18/09/1991. The tree is split into two identical halves (indicated by \circ and \square), which are connected via the edge (shown in red) between the XAU/USD and USD/AUD exchange rates. For each community of exchange rates, there is an equivalent community of inverse rates in the other half of the tree. We colour each node according to its community membership determined using the Potts method with $\lambda = 1.41$, and we show each community of exchange rates in the same colour as the corresponding community of inverse rates.

In earlier studies of equity markets, clusters of closely-related assets were identified by their proximity on the branches of the MST, e.g., [197, 229, 231] and by finding the disconnected groups of assets that remained when all tree links weaker than some threshold were removed, e.g., [53]. Similar analyses have been performed that find clusters of assets by considering the whole network and removing edges below some threshold or alternatively by starting with a network with no links and iteratively adding links above an increasing threshold, e.g., [118, 231]. In Fig. 5.6, we show an example of an MST of exchange rates. We colour the nodes in this tree according

to their community membership as determined using the Potts method. The MST is partitioned into two halves with communities of exchange rates in one half and equivalent communities of inverse exchange rates in the other. In this example, nodes belonging to the same community are always linked in the MST, but this is not always the case.

The main problem with single-linkage clustering (and, as a consequence, with MSTs) is that clusters can be joined as a result of single pairs of elements being close to each other even though many of the elements in the two clusters have large separations. The MST then contains weak links that might be misinterpreted as being more financially meaningful than they actually are [231]. It is also difficult to determine where the community boundaries lie on the MST. For example, a branch of an MST might include nodes belonging to a single community or the nodes might belong to several communities. As an example of this phenomenon, and of the additional clustering information provided by the Potts method, consider the branch at the far right of the tree shown in Fig. 5.6. By simply considering the MST, one might have inferred the existence of a cluster that includes all of the NOK/YYY rates and USD/CAD. However, the Potts method highlights the fact that USD/CAD forms a singleton community and that NOK/XAU belongs to a community with the XXX/XAU rates. This observation might provide information as to the relative importance of NOK and XAU in the market over this period.

In Fig. 5.7(a), we show the dendrogram generated using the same single-linkage clustering algorithm used to produce the MST in Fig. 5.6. If the distances between different dendrogram levels are reasonably uniform, then no clustering appears more “natural” than any other [84]. However, large distances between levels (i.e., the same clusters persist over a large range of distances) might indicate the most appropriate level at which to view the clusters. This is analogous to investigating communities that are robust over a range of resolutions. The clusterings observed at some levels of Fig. 5.7(a) correspond quite closely with the communities identified using the Potts method, but there is no level at which they correspond exactly. The levels are also reasonably evenly distributed along the distance axis. In the dendrogram in Fig. 5.7(b), which was generated using average-linkage clustering, there is a range of distances over which the clustering does not change. The clustering observed over this interval is identical to the community configuration corresponding to the main plateau found using the Potts method. Therefore, in this case, average-linkage clustering and the Potts method identify the same robust communities.

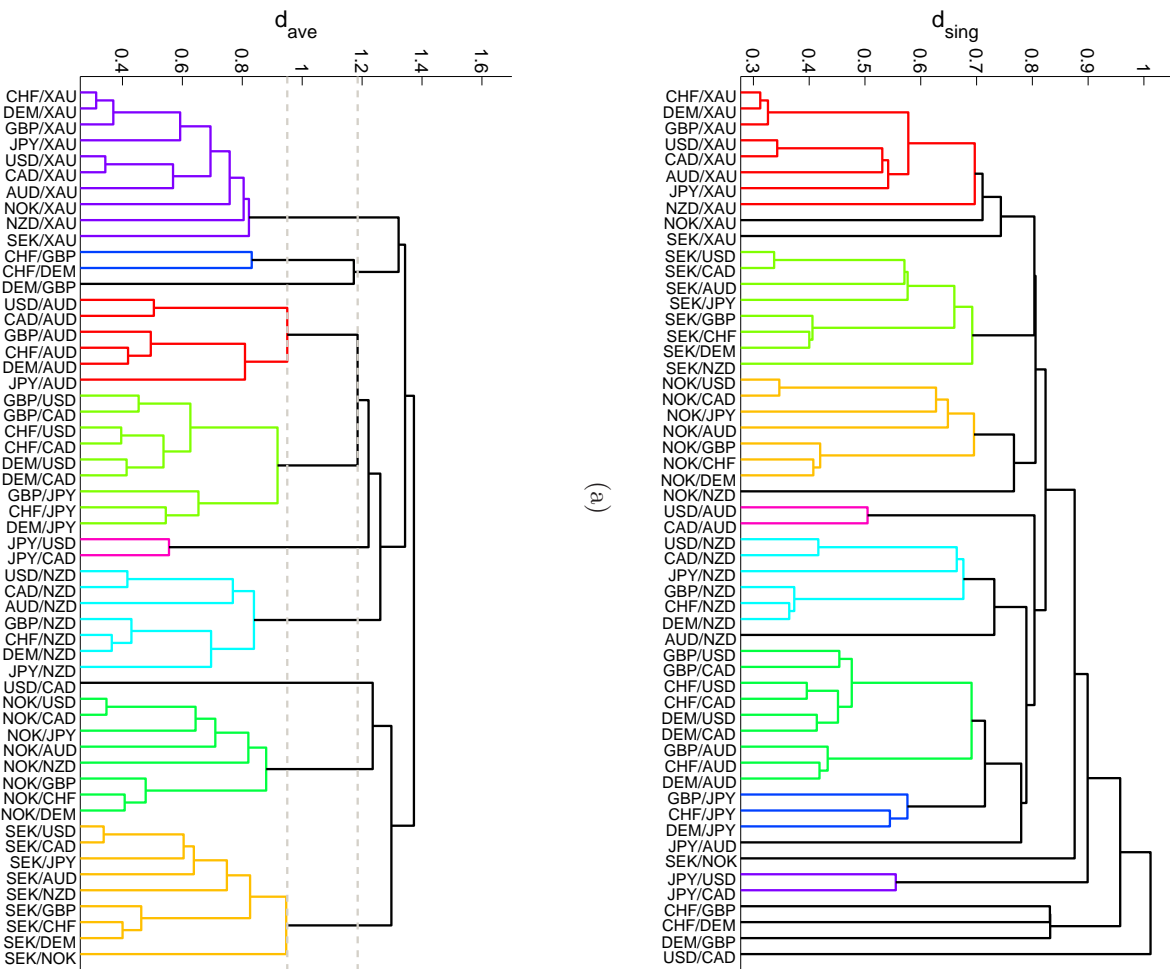


Figure 5.7: Dendrograms showing the hierarchical clustering of exchange rates for one half of the network for a time window of returns beginning on 18/09/1991. We colour each exchange rate according to its community membership determined using the Potts method with $\lambda = 1.41$. We generated the dendrograms using (a) single-linkage clustering and (b) average-linkage clustering. The dashed grey lines in panel (b) highlights the range over which the communities correspond to the communities of the main plateau identified using the Potts method.

5.7 Exchange rate centralities and community persistence

Thus far, we have considered the properties of entire communities. We now investigate the roles of nodes within communities.

5.7.1 Centrality measures

We describe the relationship between a node and its community using various centrality measures. In the social networks literature, such measures are used to measure the roles of nodes within the network and to identify which nodes are the most important or most prominent [304]. Because there are many notions of importance, several different centrality measures have been proposed [299]. In the present context, we use centrality measures to identify exchange rates that occupy important positions within the FX market.

The *betweenness centrality* of nodes is defined using the number of geodesic paths between pairs of vertices in a network [110, 217]. We calculate node betweenness by taking the distance between nodes i and j as

$$d_{ij} = \begin{cases} 0 & \text{if } i = j \text{ or } A_{ij} = 1, \\ 1/A_{ij} & \text{otherwise.} \end{cases} \quad (5.12)$$

The betweenness centrality b_i of node i is then given by

$$b_i = \sum_s \sum_t \frac{g_{st}^i}{G_{st}}, \quad \text{for } s, t \neq i \text{ and } s \neq t, \quad (5.13)$$

where G_{st} is the total number of shortest paths from node s to node t and g_{st}^i is the number of shortest paths from s to t passing through i . Betweenness centrality is widely used in social network analysis to quantify the extent to which people lie on paths that connect others. Nodes with high betweenness can be considered to be important for facilitating communication between others in the network, so betweenness is used to help measure the importance of nodes for the spread of information around the network [299].

We also consider the community centrality of each node [220]. We employ the scaled energy matrix \mathbf{J} , with components $J_{ij} = A_{ij} - \lambda P_{ij}$, where we again set $P_{ij} = k_i k_j / 2m = (N - 2) / 2N$. Following the notation in Ref. [220], the energy matrix can be expressed as $\mathbf{J} = \mathbf{U} \mathbf{D} \mathbf{U}^T$, where $\mathbf{U} = (\mathbf{u}_1 | \mathbf{u}_2 | \dots)$ is the matrix of eigenvectors of

\mathbf{J} and \mathbf{D} is the diagonal matrix of eigenvalues β_i . If \mathbf{D} has q positive eigenvalues, then one can define a set of node vectors $\{\mathbf{x}_i\}$ of dimension q by

$$[\mathbf{x}_i]_j = \sqrt{\beta_j} U_{ij}, \quad j \in \{1, 2, \dots, q\}, \quad (5.14)$$

where $[\mathbf{x}_i]_j$ indicates the j th ($j \in 1, \dots, q$) element of the node vector of node i . The magnitude $|\mathbf{x}_i|$ is the *community centrality*. Nodes with high community centrality play an important role in their local neighbourhood, irrespective of the community boundaries.

One can also define a community vector

$$\mathbf{w}_k = \sum_{i \in \mathcal{C}^k} \mathbf{x}_i \quad (5.15)$$

for each community k with members \mathcal{C}^k . Nodes with high community centrality are strongly attached to their community if their node vector is also aligned with their community vector. Continuing to use the definitions in Ref. [220], a *projected community centrality* y_i is defined by

$$y_i = \mathbf{x}_i \cdot \hat{\mathbf{w}}_k = |\mathbf{x}_i| \cos \theta_{ik} \quad (5.16)$$

and we refer to the quantity $\cos \theta_{ik}$ as the *community alignment*. The community alignment is near 1 when a node is at the centre of its community and near 0 when it is on the periphery. Nodes with high community alignment are located near the centre of their community and have a high projected community centrality, so they are strongly attached to their community and can be considered to be highly influential within it. The number of positive eigenvalues of \mathbf{J} can vary between time steps, so we normalize $|\mathbf{x}_i|$ and y_i by their maximum value at each time step.

5.7.2 Community tracking

In Section 4.6, we reviewed the dynamic communities literature and discussed different methods for tracking communities through time. Many methods identify descendant communities based on maximum node or edge overlap; however, as we highlighted in Section 4.6, this can lead to equivocal mappings following community splits and mergers. In order to avoid these ambiguities, instead of tracking whole communities, we identify communities from the perspective of individual nodes.

We investigate the persistence through time of nodes' communities by defining a community autocorrelation. For a node i with community $C_i(t)$ at time t , the

autocorrelation $a_i^t(\tau)$ of its community after τ time steps is defined by

$$a_i^t(\tau) = \frac{|\mathcal{C}_i(t) \cap \mathcal{C}_i(t + \tau)|}{|\mathcal{C}_i(t) \cup \mathcal{C}_i(t + \tau)|}. \quad (5.17)$$

This is a node-centric version of a quantity considered in Ref. [233] and importantly does not require one to determine which community at each time step represents the descendant of a community at the previous time step.

5.7.3 Exchange rate roles

In Fig. 5.8(a), we show the mean normalized community centrality of exchange rates as a function of community size (averaging over all nodes belonging to the same-size community). The community centrality increases with community size up to sizes of about 10 members. For larger communities, $|\mathbf{x}_i|$ remains approximately constant. Nodes with high $|\mathbf{x}_i|$ therefore tend to belong to large communities, so exchange rates with high community centrality tend to be closely linked with many other rates. Table 5.2 shows the ten exchange rates that have the highest betweenness centrality, community centrality, and projected community centrality. For all three periods, CHF/NZD, CHF/XAU, and SEK/XAU have one of the ten highest community centralities, so they are closely tied to many other rates. For 1991–2003, exchange rates formed from one of the major European currencies—DEM (and then EUR, after its introduction) or CHF—and one of the commodity currencies³ also tend to have high community centrality. For 2005–2008, however, XAU rates encompass nearly all of the exchange rates with the highest $|\mathbf{x}_i|$.

Figure 5.8(b) shows the mean betweenness centrality versus the community alignment. We calculate the mean community alignment by splitting the range of b into 10 bins containing equal numbers of data points and then averaging over all community alignments falling within these bins. (The observed relationships are robust with respect to variations in the number of bins.) Nodes with high betweenness centrality tend to have small values for their community alignment, implying that nodes that are important for information transfer are usually located on the edges of communities. Table 5.2 shows that for all three periods, NOK/SEK, AUD/NZD, and AUD/CAD all tend to have high betweenness centrality on average. They are therefore located on the edges of communities and are important for information transfer. Interestingly, for the post-euro period (1999–2008), several USD exchange rates are also important for information transfer, but no USD rates regularly have high betweenness for

³A country is said to have a “commodity currency” if its export income depends heavily on a commodity. For example, AUD, NZD and CAD are all considered to be commodity currencies.

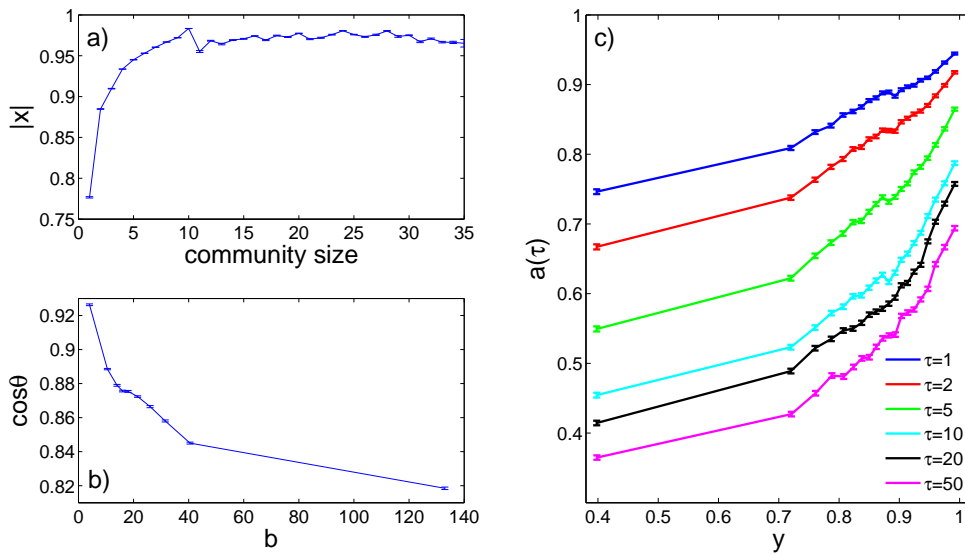


Figure 5.8: (a) Mean community centrality versus the size of the community to which the node belongs. (b) Mean community alignment versus the betweenness centrality of nodes. (c) Mean community autocorrelation versus the projected community centrality. (All error bars indicate the standard error [42].)

the pre-euro period. In contrast, XAU exchange rates are important for information transfer for the pre-euro period but not after the euro was introduced.

In Fig. 5.8(c), we show the mean community autocorrelation versus the projected community centrality. We calculate the mean autocorrelation by splitting the range of y into 15 bins containing equal numbers of data points and then averaging over all autocorrelations falling within these bins. (Again, the observed relationships are robust with respect to variations in the number of bins.) As one would expect, the community autocorrelation for the projected community centrality of a given node is smaller for larger τ . More interesting is that for all values of τ , the mean community autocorrelation increases with y . This suggests that nodes that are strongly connected to their community are likely to persistently share that community membership with the same subset of nodes. In contrast, exchange rates with a low y experience regular changes in the set of rates with which they are clustered. This result agrees with the observation in Ref. [233] for social networks that nodes that are only loosely connected to their community were more likely to leave that community than nodes with strong intra-community connections (see Section 4.6.5).

Table 5.2 shows the exchange rates with the highest projected community centrality, which in turn reveals the most persistent communities. For 1991–2003, approxi-

mately half of the ten exchange rates with the highest projected community centrality also appear in the list of the ten rates with the highest community centrality. For 2005–2008, however, the lists of exchange rates with the highest community centrality and projected community centrality are dominated by the same set of XAU exchange rates (though the rankings differ). For 1991–2003, the exchange rates with the highest projected community centrality again includes rates formed of DEM (and EUR) or CHF and one of the commodity currencies. However, there are also a number of USD exchange rates with high projected community centrality that don't have high community centrality. This suggests that these USD rates do not have strong links with a large number of other exchange rates, but that they strongly influence the rates within their community.

5.8 Major community changes

We now investigate the insights that short-term community dynamics can provide into changes in the FX market. Figure 5.9(a) shows a contour plot of the normalized distribution of the link weights at each time step. The mean link strength remains constant through time because of the inclusion in the network of each exchange rate and its inverse but [as one can see in Figs. 5.9(a) and 5.9(b)] there is a large variation in the standard deviation of the link strengths. The scaled energy and standard deviation of link weights are closely related. This is expected because the standard deviation increases as a result of the strengthening of strong ties and the weakening of weak ties.

In Fig. 5.9(c), we also show \hat{V} between the community configurations at consecutive time steps. Large spikes in \hat{V} indicate significant changes in the community configuration over a single time step and potentially also indicate important market changes. The correlation coefficient between \hat{V} and the absolute change in Q_s between consecutive time steps is 0.39 over the period 1991–2003 and 0.47 over the period 2005–2008. The correlation between \hat{V} and the absolute change in $\sigma(A_{ij})$ is 0.28 over the period 1991–2003 and 0.27 from 2005–2008. Changes in Q_s are thus a better indicator than changes in $\sigma(A_{ij})$ that there has been a change in the community configuration of the network.

In Fig. 5.10, we show three example community reorganizations—two in which \hat{V} is more than four standard deviations larger than its mean and a third in which it is over two standard deviations above the mean.

Rank	1991–1998			1999–2003			2005–2008		
	b	$ x $	y	b	$ x $	y	b	$ x $	y
1	NOK/SEK	CHF/AUD	USD/DEM	AUD/NZD	SEK/XAU	USD/XAU	USD/CAD	JPY/XAU	EUR/XAU
2	AUD/XAU	CHF/NZD	USD/CHF	NZD/CAD	CHF/CAD	EUR/USD	AUD/NZD	USD/XAU	GBP/XAU
3	AUD/NZD	CHF/XAU	USD/XAU	AUD/CAD	EUR/XAU	EUR/XAU	AUD/CAD	NZD/XAU	CHF/XAU
4	AUD/CAD	CHF/CAD	CHF/CAD	JPY/CAD	NOK/XAU	GBP/XAU	NOK/SEK	CAD/XAU	EUR/CAD
5	CHF/SEK	DEM/AUD	CHF/AUD	NOK/SEK	CHF/NZD	EUR/CAD	USD/GBP	GBP/XAU	SEK/XAU
6	NZD/XAU	SEK/AUD	CHF/NZD	USD/AUD	CHF/XAU	USD/CHF	NZD/CAD	SEK/XAU	USD/XAU
7	CAD/XAU	DEM/XAU	DEM/CAD	USD/NZD	EUR/CAD	CHF/XAU	USD/JPY	CHF/XAU	EUR/NZD
8	DEM/SEK	SEK/XAU	DEM/AUD	USD/JPY	EUR/NZD	NOK/XAU	USD/AUD	NOK/XAU	JPY/XAU
9	NZD/CAD	NOK/AUD	USD/AUD	GBP/JPY	SEK/NZD	EUR/NZD	CHF/NOK	CHF/NZD	AUD/XAU
10	DEM/NOK	DEM/NZD	DEM/NZD	CHF/SEK	NOK/NZD	CHF/NZD	GBP/AUD	AUD/XAU	NOK/XAU

Table 5.2: The ten exchange rates with the highest betweenness centrality b , community centrality $|x|$, and projected community centrality y for each of the three periods. We rank the exchange rates for each centrality according to their average rank over all time steps. For each exchange rate XXX/YYYY the equivalent inverse rate YYY/XXX had the same betweenness centrality, community centrality, and projected community centrality.

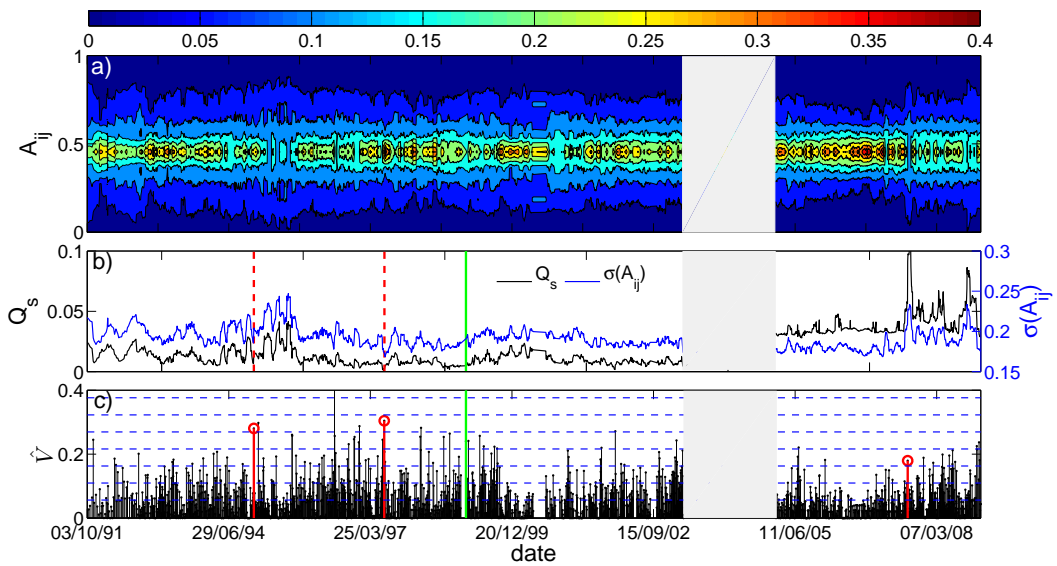


Figure 5.9: (a) Normalized distribution of the link weights at each time step. (b) Scaled energy Q_s (black line) and standard deviation of the link weights (blue line). (c) Normalized variation of information \hat{V} between the community configurations at consecutive time steps. The horizontal lines show (from bottom to top) the mean of \hat{V} and 1, 2, 3, 4, 5, and 6 standard deviations above the \hat{V} mean. The green vertical line in panels (b) and (c) separates the pre- and post-euro periods. The red vertical lines show the time steps when 22/12/94, 07/02/97, and 15/08/07 enter the rolling time window. These dates correspond, respectively, to the devaluation of the Thai baht during the Asian currency crisis, the flotation of the Mexican peso following its sudden devaluation during the tequila crisis, and significant unwinding of the carry trade during the 2007–2008 credit crisis. The grey blocks mark 2004 (for which we have no data).

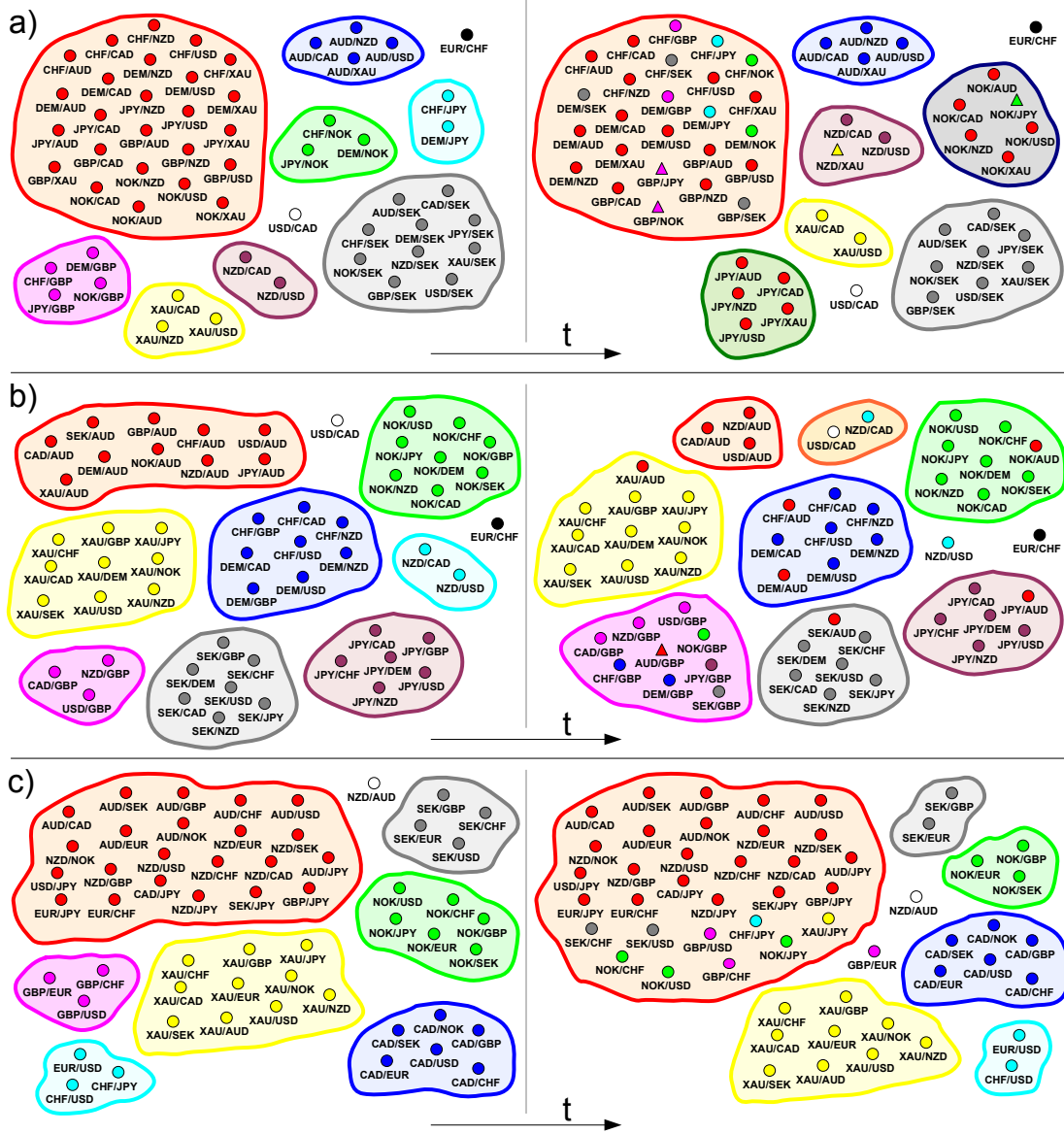


Figure 5.10: Schematic representation of the change in the community structure in one half of the FX market network for several events. (a) The Mexican tequila crisis: the depicted reorganization followed 22/12/94, when the Mexican peso was allowed to float after a sudden devaluation. (b) The Asian currency crisis: the depicted reorganization followed 02/07/97, when Thailand devalued the baht. (c) Carry trade unwinding: the depicted reorganization followed 15/08/07, when there was significant unwinding of the carry trade during the 2007–2008 credit and liquidity crisis. The node colours after the community reorganization correspond to their community before the change. If the parent community of a community after the reorganization is obvious, we draw it using the same colour as its parent. The nodes drawn as triangles resided in the opposite half of the network before the community reorganization.

5.8.1 Mexican peso crisis

Figure 5.10(a) shows the reorganization on 22/12/1994 when the Mexican peso was floated following its sudden devaluation.⁴ This change is accompanied by an increase in the scaled energy. Although we do not include the Mexican peso in the set of investigated exchange rates, it appears that its devaluation was a sufficiently serious event to cause major changes in the community relationships of the studied rates. Before 22/12/1994, the largest community consisted of a group of exchange rates constructed from currencies from the set {AUD, CAD, NZD, USD, XAU} versus currencies from {CHF, DEM, GBP, JPY, NOK}. After the flotation, the largest community consisted of a set of exchange rates formed from the major European currencies (CHF, DEM, and GBP). It is also noteworthy that there is only a small gold (XAU) community during this period which, as noted previously, often indicates that another currency is particularly important in the market.

5.8.2 Asian currency crisis

Figure 5.10(b) shows the community changes following 02/07/1997 when the Thai baht was devalued during the Asian currency crisis. As with the peso, although we did not include the baht in the set of studied rates, its devaluation appears to have had a significant effect on the whole market. There is a large stable gold cluster during the whole period. Before 02/07/1997, there is also a large AUD cluster, but after the devaluation, this cluster breaks up and the previously-small GBP cluster increases in size. This suggests that the GBP is playing a more prominent market role after the devaluation. Although the reasons for the changes in the sizes of the AUD and GBP communities are not obvious, both adjustments suggest a sharp and significant change in the correlation structure of the market.

5.8.3 Credit crisis

The final example in Fig. 5.10(c) shows the community changes following 15/08/07 when there was a significant community reorganization and reveals one of the major effects on the FX network of the recent credit and liquidity crisis. This example also demonstrates community changes that occurred as a result of a trading change that affected the studied rates directly.

⁴For a floating exchange rate, the value of the currency is allowed to fluctuate according to the FX market. Prior to its flotation the peso had been pegged to the US dollar, so the value of the peso tracked the value of the dollar.

The most important effect of the credit crisis on the FX market during the period 2005–2008 was its impact on the carry trade. The carry trade consists of selling low interest rate *funding currencies* such as the JPY and CHF and investing in high interest rate *investment currencies* such as the AUD and NZD. It yields a profit if the interest rate differential between the funding and investment currencies is not offset by a commensurate depreciation of the investment currency [59]. The carry trade is one of the most commonly used FX trading strategies and requires a strong appetite for risk, so the trade tends to “unwind” during periods in which there is a decrease in available credit. A trader unwinds a carry trade position by selling his/her holdings in investment currencies and buying funding currencies.

One approach to quantifying carry trade activity is to consider the returns that can be achieved using a carry trade strategy. In Fig. 5.11(b) we show the cumulative return index Υ for a common carry trade strategy. We consider a strategy in which one buys equal weights of the three major currencies with the highest interest rates and sells equal weights of the three currencies with the lowest interest rates. This is a dynamic trading strategy because the relative interest rates of currencies change over time. For example, consider the situation in which the interest rate of currency A (which initially has the third highest interest rate) decreases below the rate of currency B (which initially has the fourth highest interest rate). In order to maintain the strategy of only holding the three currencies with the highest interest rates at any time, one would re-balance the carry portfolio by selling the holding of currency A and buying currency B . The frequency at which such re-balances occur will depend on the frequency at which the relative interest rates change. The returns from a carry strategy like this are widely seen by market participants to provide a good gauge of carry trade activity. Large negative returns result in large decreases in Υ which are therefore likely to indicate significant unwinding of the carry trade.

In Fig. 5.11(a) we focus on the period 2005–2008 from Fig. 5.9(c). Again, large spikes indicate significant changes in the community configuration over a single time step. Figure 5.11(a) shows that a significant community reorganization occurred on 15/08/07 and in Fig. 5.10(c) we show the observed communities before and after this date. This community change is a result of massive unwinding of the carry trade. Figure 5.11(b) shows that leading up to 15/08/07 there was some unwinding of the carry trade so the initial configuration includes a community containing exchange rates of the form AUD/YYY, NZD/YYY, and XXX/JPY (which all involve one of the key carry-trade currencies). In Fig. 5.11(b) it is also clear that following this date there is a sharp increase in carry unwinding. The second community partition

in Fig. 5.10(c) highlights this increase as the carry community increases in size by incorporating other XXX/JPY rates as well as some XXX/CHF and XXX/USD rates. The presence of a large number of exchange rates involving one of the key carry-trade currencies in a single community clearly demonstrates the significance of the trade over this period. Importantly, some of the exchange rates included in the carry community are also somewhat surprising and provide insights into the range of currencies used in the carry trade over this period.

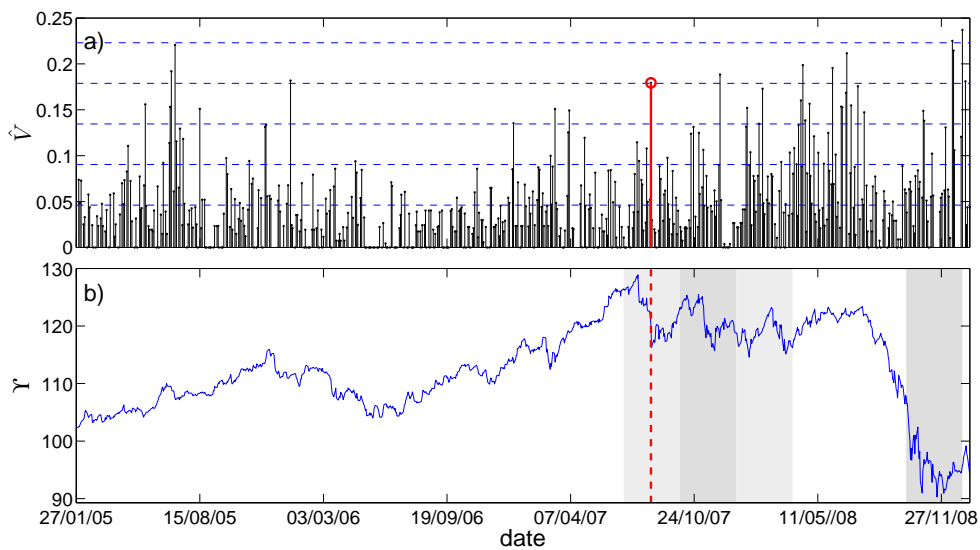


Figure 5.11: (a) Normalized variation of information between the community configuration at consecutive time steps for 2005–2008. The horizontal lines show (from bottom to top) the mean of \hat{V} and 1, 2, 3, and 4 standard deviations above the mean. The red vertical line in (a) shows the 15/08/07 when there was a marked increase in unwinding of the carry trade. (b) Carry trade index Υ . The vertical line again shows 15/08/07 and the shaded blocks (from left to right) Q3 2007, Q4 2007, Q1 2008, and Q4 2008.

The analysis above demonstrates that one can identify major changes in the correlation structure of the FX market by finding large values of \hat{V} between time steps. Having identified significant changes, one can gain a better understanding of the nature of these changes and potentially also gain insights into trading changes taking place in the market by investigating the adjustments in specific communities. We have discussed three examples in which the observed changes are obviously attributable to a major FX market event. However, there are also a number of time steps when significant community reorganizations occur for which the cause is much less obvious,

and the analysis of dynamic communities might help shed light on related market changes.

5.9 Visualizing changes in exchange rate roles

We now investigate changes in the relationships between specific exchange rates and their communities. We begin by defining within-community z -scores, which directly compare the relative importances of different nodes to their community [139]. We describe the roles of individual nodes at each time step using the within-community projected community centrality z -score κ^y and within-community betweenness centrality z -score κ^b . If a node i belongs to community C_i and has projected community centrality y_i , then

$$\kappa_i^y = \frac{y_i - \bar{y}_{C_i}}{\sigma_{C_i}^y}, \quad (5.18)$$

where \bar{y}_{C_i} is the mean of y over all nodes in C_i and $\sigma_{C_i}^y$ is the standard deviation of y in C_i . The quantity κ_i^y measures how strongly connected node i is to its community compared with other nodes in the same community. Similarly, if the same node has betweenness centrality b_i , then

$$\kappa_i^b = \frac{b_i - \bar{b}_{C_i}}{\sigma_{C_i}^b}, \quad (5.19)$$

where \bar{b}_{C_i} is the average of b over all nodes in C_i and $\sigma_{C_i}^b$ is the standard deviation of b in C_i . The quantity κ_i^b indicates the importance of node i to the spread of information compared with other nodes in its community.⁵ The positions of nodes in the (κ^b, κ^y) plane thereby illuminate the roles of the associated exchange rates in the FX market and provide information that cannot be gained by simply considering individual exchange rate time series.

We remark that the methods are robust with respect to the choice of measures used to construct the parameter plane: we obtain similar results using other notions, such as dynamical importance [256] instead of the betweenness centrality and the within-community strength z -score [139] instead of the projected community centrality.

5.9.1 Average roles

In Fig. 5.12, we show the mean position of each exchange rate over the three periods and highlight some rates that play particularly prominent roles. For example, the

⁵Note that in order for a within-community z -score to be well defined, a node must belong to a community containing two or more nodes.

USD/DEM (and then EUR/USD after the introduction of the euro) regularly had the strongest connection to its community from 1991–2003, but EUR/XAU was more strongly connected to its community from 2005–2008. The importance of USD/DEM and EUR/USD is unsurprising given that these rates had the highest daily trading volume [117]. This provides a reality check that the methods uncover useful information about the roles of minor exchange rates. Other exchange rates, such as NOK/SEK and AUD/NZD, were less influential within their communities but were very important for the transfer of information around the network.

The (κ^b, κ^y) plots also highlight exchange rates that play similar roles in the FX market. For example, exchange rates formed from one of the major European currencies—DEM or CHF—and one of the commodity currencies—AUD, CAD, and NZD (or the commodity XAU)—are located close together in the upper left quadrant of the (κ^b, κ^y) plane for 1991–2003. This prominent similarity is not present for 2005–2008.

5.9.2 Annual roles

We can also gain insights into the time dynamics of exchange rate roles by examining changes in the positions of the rates in the (κ^b, κ^y) plane over different time periods. Changes in a node’s position in the (κ^b, κ^y) plane reflect changes in the membership of a node’s community as well as changes in b and y . In Fig. 5.13, we show six example annual role evolutions. We determine the annual roles by averaging κ^y and κ^b over all time steps in each year. We see, for example, that the NZD/JPY exchange rate maintained a consistently influential role within its community over the full period and similarly the EUR/USD rate also maintained the same influential role played by the USD/DEM rate before the introduction of the euro.

Other rates changed role over the studied period. The GBP/USD and GBP/CHF exchange rates evolved in a similar manner, as they changed from being strongly influential within their communities before 1994 to being less influential within their communities but more important for information transfer after 1994. The role of both GBP/AUD and USD/JPY varied significantly from 1991–2008: From 2001 onwards the GBP/AUD became less influential within its community but more important for information transfer. Interestingly, the USD/JPY had its highest within-community influence in the late 1990s during a period of Japanese economic turmoil. One can construct similar plots to study the change in the role of other exchange rates. These role plots provide a useful tool for visualizing the changes in the exchange rate correlations.

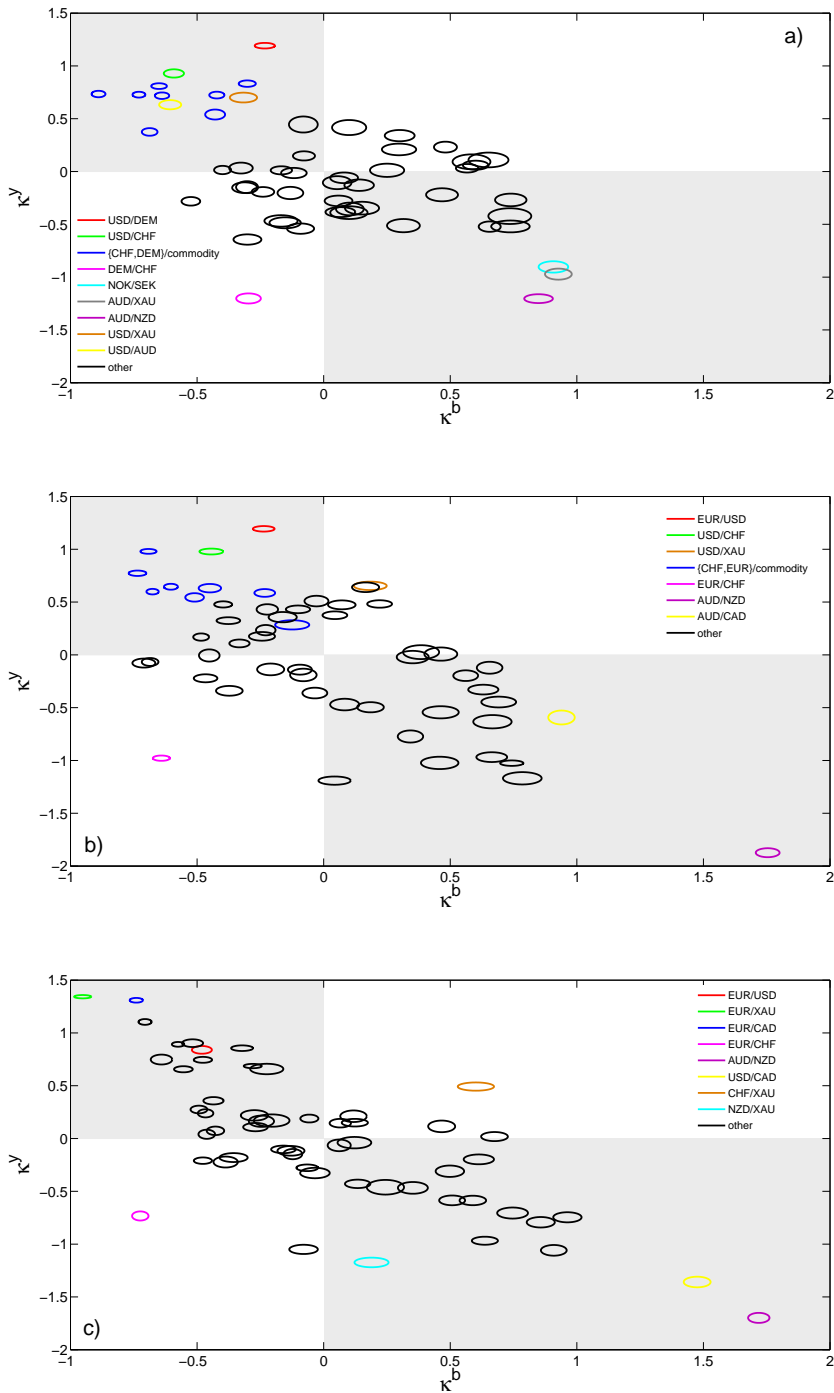


Figure 5.12: Node positions in the (κ^b, κ^y) plane averaged over all time steps for the periods (a) 1991–1998, (b) 1999–2003, and (c) 2005–2008. The radii of each elliptical marker equal the standard deviations in the parameters for the corresponding node scaled by a factor of 1/15 for visual clarity.

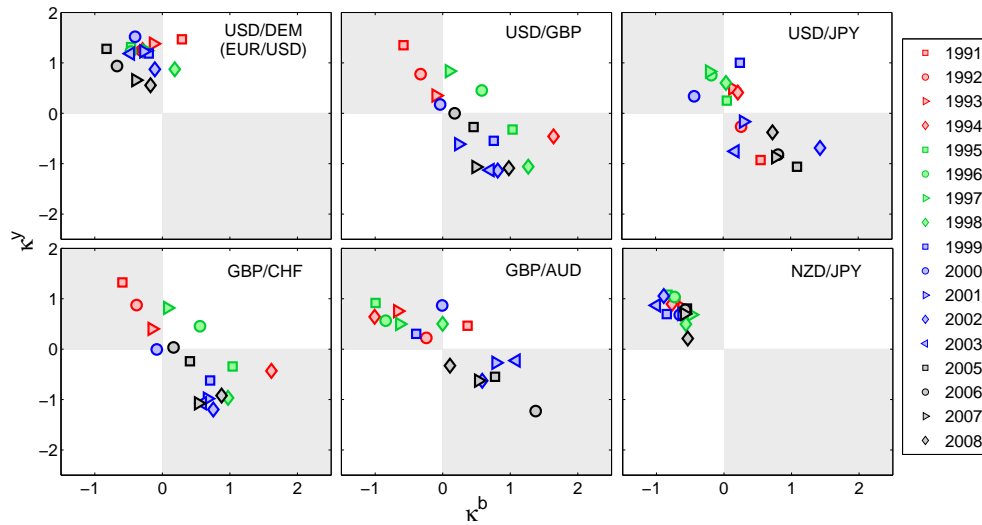


Figure 5.13: Annual node role evolutions in the (κ^b, κ^y) plane for the full period 1991–2008.

5.9.3 Quarterly roles

We also investigate higher-frequency changes in exchange rate market role over shorter time intervals. In Fig. 5.14 we show quarterly roles changes over the period 1995–1998 for six exchange rates including USD/DEM and GBP/USD for which we also show the annual changes in Fig. 5.13. Both exchange rates show similar role variations over both time-scales, with the USD/DEM always playing a relatively influential role within its community and the GBP/USD role varying significantly. We also show other examples for which we did not show annual changes. The role of DEM/JPY varied considerably from 1995–1998: In particular, it was an important information carrier for the last two quarters in 1996, but was influential within its community throughout 1998. In contrast the AUD/JPY moves from being unimportant for information transfer to being an information carrier during 1998. In further contrast, the AUD/NZD and AUD/XAU were both always information carriers to different extents, with AUD/NZD being particularly important for information transfer during 1998.

Finally, we consider some examples of quarterly role evolutions for the period 2005–2008. Figure 5.15, shows quarterly role changes for four exchange rates from 2005–2008. The USD/XAU rate provides an interesting example due to the persistence of its community over this period. From 2005–2008, the USD/XAU node shifted from being an important information carrier within the XAU community to

being more central to this community. This period of higher influence coincides closely with the period of financial turmoil during 2007–2008. The CHF is widely regarded as a “safe haven” currency [248], so one might expect USD/CHF to behave in a similar manner to USD/XAU. However, the CHF is also a key carry trade currency. Because CHF is used both as a safe haven and as a carry trade currency, the USD/CHF node does not move in the same direction as USD/XAU in the (κ^b, κ^y) plane. Instead, the USD/CHF exchange rate is an important information carrier during the 2007–2008 credit crisis. Over the same period, the AUD/JPY and NZD/JPY exchange rates change from being important for information transfer to being influential within their communities. The AUD/JPY and NZD/JPY were most influential within their community during Q3 and Q4 2007 and during Q1 and Q4 2008. Figure 5.11(b) shows that over all of these periods there was significant carry trade activity so it is unsurprising that two exchange rates that are widely used for this trade should increase in importance. This, however, is a further demonstration that the positions of exchange rates in the (κ^b, κ^y) parameter plane can provide important insights into the role of exchange rates in the FX market.

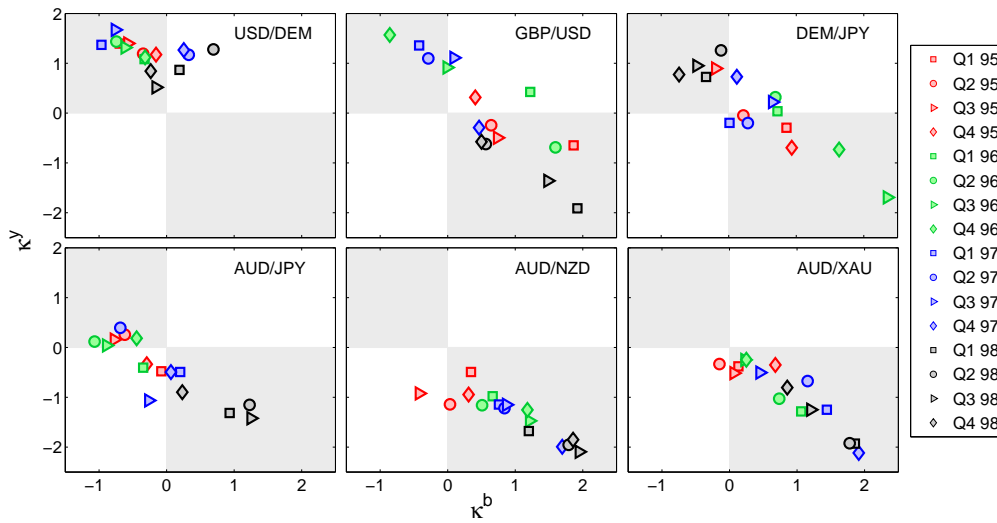


Figure 5.14: Quarterly node role evolutions in the (κ^b, κ^y) plane for the period 1995–1998.

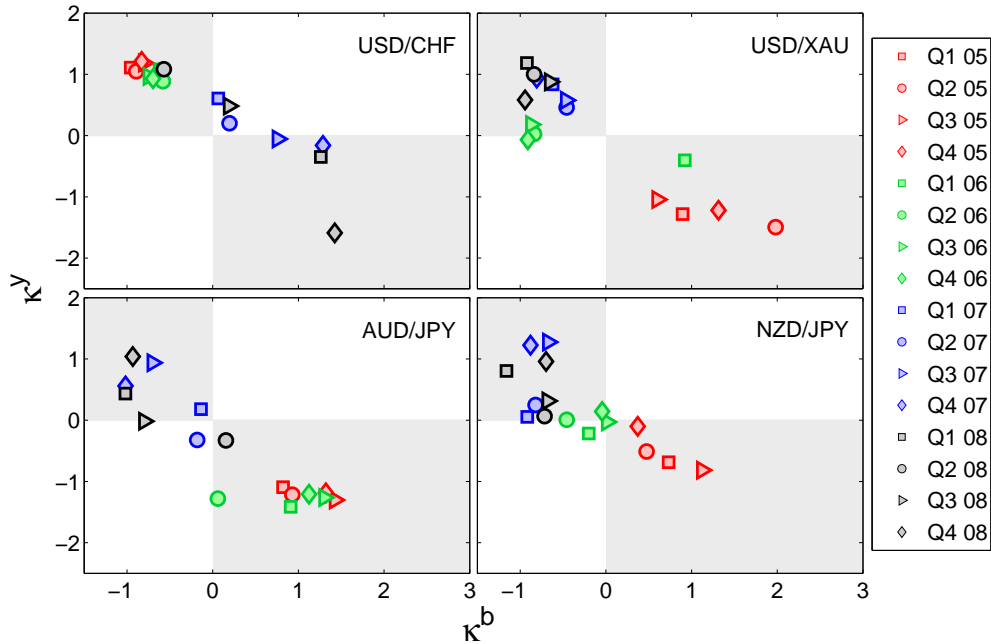


Figure 5.15: Quarterly node role evolutions in the (κ^b, κ^y) plane for the period 2005–2008.

5.10 Robustness of results: alternative computational heuristics

Thus far, we have detected all communities using a greedy algorithm [44]. However, as we noted in Chapter 4, several alternative heuristics exist. In Ref. [128], Good *et al.* demonstrated that there is extreme degeneracy in the energy function (Eq. 4.3), with an exponential number of high-energy solutions. Given this, it is unsurprising that, in some instances, different energy-optimization heuristics have been found to yield very different partitions for the same network. Good *et al.* suggest that the reason for this behaviour is that different heuristics sample different regions of the energy landscape. Because of the potential sensitivity of results to the choice of heuristic, one should treat individual partitions output by particular heuristics with caution. However, one can have more confidence in the validity of the partitions if different heuristics produce similar results.

With this in mind, we compared the results for the greedy algorithm [44] with those for a spectral algorithm [221] and simulated annealing [141] for the 563 networks we constructed for the period 2005–2008. We found that, although there are differences in the communities identified using different optimization heuristics, the aggregate

conclusions are the same. We identify the same changes taking place in the FX market whether we use the greedy algorithm or simulated annealing to minimize energy. The fact that we obtain very similar results using different optimization techniques, despite these techniques sampling different regions of the energy landscape, gives confidence that the effects that we uncover are genuine and that the results are robust. We present the results of the comparison of the computational heuristics in detail in Appendix B.

5.11 Summary

We have demonstrated that a network analysis of the FX market is useful for visualizing and providing insights into the correlation structure of the market. In particular, we investigated community structure at different times to provide insights into the clustering dynamics of exchange rate time series. We focused on a node-centric community analysis that allows one to follow the time dynamics of the functional role of exchange rates within the market, demonstrating that there is a relationship between an exchange rate's functional role and its position within its community. We indicated that exchange rates that are located on the edges of communities are important for information transfer in the FX market, whereas exchange rates that are located in the centre of their community have a strong influence on other rates within that community. We also demonstrated that the community structure of the market can be used to determine which exchange rates dominate the market at each time step and identified exchange rates that experienced significant changes in market role.

Our analysis successfully uncovered significant structural changes that occurred in the FX market, including ones that resulted from major market events that did not impact the studied exchange rates directly. We further demonstrated that community reorganizations at specific time steps can provide insights into changes in trading behaviour and highlighted the prevalence of the carry trade during the 2007–2008 credit and liquidity crisis. Although we focused on networks of exchange rates, the methodology should be similarly insightful for multivariate time series of other asset classes. Importantly, the results are robust with respect to the choice of optimization heuristic.

Chapter 6

A Taxonomy of Networks

We now expand the scope of our analysis beyond financial markets and investigate the community structure of networks from a wide variety of other fields. We have submitted a paper based on this work for publication [P4].

6.1 Introduction

The study of networks is an interdisciplinary endeavour, with contributions from researchers in the natural, social, and information sciences [9, 60, 217, 223]. Often the questions asked by researchers in these different fields are quite similar; however, techniques have sometimes had difficulty penetrating disciplinary boundaries, perhaps because the relevance or applicability of the methods from other disciplines is not always clear. In this chapter, we attempt to connect disciplines by introducing a framework for clustering networks and using this technique to establish a network taxonomy. The clustering scheme and taxonomy serve several purposes. First, if networks from two different fields are close together in the taxonomy, this implies that there are some similarities in their structure and that techniques from one field might be insightful in the other field. Second, a taxonomy might help to determine how an unstudied network might best be analyzed once its position within the taxonomy is known. Third, the taxonomy can be used to highlight differences within disciplines. For example, if a network that is expected to be similar to a group of networks based on their origin is not clustered with those networks, this suggests that the network is not typical of its family.

In aiming to cluster networks, it is necessary to consider a scale at which to investigate their structure. Much prior research on networks has focused on microscopic properties (such as the degree) or macroscopic properties (such as the average

path length), typically finding that most empirically observed networks have heavy-tailed degree distributions and possess the small-world property (see Section 1.1 and Refs. [9, 60, 217, 223]). The interpretations of both approaches often implicitly assume that networks are homogeneous and have no mesoscopic structure; however, as discussed in detail in Chapter 4 and demonstrated in Chapter 5, many networks possess community structures. The ubiquity of heavy-tailed degree distribution and the small-world property across a wide variety of networks from different domains suggests that mesoscopic heterogeneities should be exploited to differentiate effectively between networks. This has led some researchers to try to cluster networks based on mesoscopic structures, e.g., [142, 210]. In Ref. [142], Milo *et al.* compare the statistics of *a priori* specified subgraphs in networks from different fields, while in Ref. [142] Guimerà *et al.* investigate the relationships between individual nodes and communities (see Section 4.5 for a detailed discussion of these methods). Both approaches focus on a single mesoscopic scale.

In this chapter, we introduce a framework for clustering networks by identifying communities at multiple mesoscopic scales and create a taxonomy of networks using this approach. In addition to the fact that mesoscopic heterogeneities enable us to differentiate between networks, we focus on mesoscopic scales because structures at this scale have been shown to have a strong bearing on functional units in many networks [105, 244]. In contrast to Ref. [210], we do not specify the topology or sizes of the structure that we investigate *a priori*. Networks from different domains can possess very different sizes and connectivities, which makes comparison difficult [210]. The technique that we propose therefore involves a normalization that enables us to compare networks of significantly different sizes and connectivities.¹ Using this approach, we create a taxonomy of 714 networks from a variety of disciplines including sociology, biology, politics, technology, and finance, and include many synthetic model and benchmark networks. As well as creating an aggregate taxonomy, we also create taxonomies for sub-sets of networks that represent multiple realizations of the same type of system and temporal snapshots of time-dependent systems. In the latter case, we demonstrate that the framework we propose can detect changes in time-ordered sequences of evolving networks.

¹We study networks that range in size from 34 to over 40,000 nodes and possess from 0.1% to 100% of possible edges.

6.2 Multi-resolution community detection

In order to compare networks, we create profiles that characterize each network's structures across multiple mesoscopic scales. The first step in constructing these profiles is to select a community detection method. As in the earlier chapters in this thesis, we detect communities using the the multi-resolution Potts method described in Section 4.3.3. The Hamiltonian of the infinite-range N -state Potts spin glass is given by

$$\mathcal{H}(\lambda) = - \sum_{i \neq j} J_{ij} \delta(C_i, C_j) = - \sum_{i \neq j} (A_{ij} - \lambda P_{ij}) \delta(C_i, C_j), \quad (6.1)$$

where C_i indicates the state (community) of spin i , λ is a resolution parameter, and we again use the standard random null model $P_{ij} = k_i k_j / (2m)$, where k_i denotes the degree of node i for an unweighted network (the strength for a weighted network) and m is the number of edges for an unweighted network (or the total edge weight for weighted networks) [224].² By tuning the resolution parameter λ , we detect communities across multiple scales.

6.2.1 Resolution matrix

The second step is to determine the range of values of λ to investigate. We study a wide variety of networks containing different numbers of nodes and edges; to ensure that the profiles for different networks are comparable, we sweep λ from the minimum value Λ_{\min} to the maximum value Λ_{\max} , so that the number of communities η into which the network is partitioned varies from 1 to the number of nodes N in the network.

More formally, we define a coupling matrix $\mathbf{J}(\lambda)$ with entries $J_{ij}(\lambda)$ that represent the interaction strength between node i and j in the Potts Hamiltonian in Eq. 6.1. For each pair of nodes i and j , we find the resolution $\lambda = \Lambda_{ij}$ at which the interaction J_{ij} between them becomes antiferromagnetic by writing $J_{ij} = A_{ij} - \Lambda_{ij} P_{ij} = 0$ and solving to get $\Lambda_{ij} = A_{ij} / P_{ij}$. We then define a matrix $\mathbf{\Lambda}$ with entries Λ_{ij} and define three resolutions:

$$\Lambda_{\min} = \max_{ij} \{ \Lambda_{ij} | \eta(\lambda) = 1 \}, \quad (6.2)$$

$$\Lambda_{\max} = \max_{ij} \{ \Lambda_{ij} \} + \epsilon, \quad (6.3)$$

$$\Lambda^* = \min_{ij} \{ \Lambda_{ij} | A_{ij} > 0 \}, \quad (6.4)$$

²In Chapter 5, we summed over all i and j in the Potts Hamiltonian (see Eq. 4.3). In contrast, in this chapter, we only sum over all $i \neq j$. We explain the reason for this difference in Section D.1.

where $\epsilon > 0$ is a small number that ensures that all links are antiferromagnetic at resolution $\lambda = \Lambda_{\max}$. In other words, Λ_{\min} is the largest value of the resolution parameter λ for which the network still forms a single community. However, note that this is not necessarily the minimum non-zero value of Λ_{ij} . We do not simply sweep over the interval $[\Lambda^*, \Lambda_{\max}]$ because for some sparse networks $\eta > 1$ at Λ^* , whereas for fully-connected networks η does not become greater than one until a resolution $\lambda \gg \Lambda^*$. By sweeping λ from Λ_{\min} to Λ_{\max} , and exploring the full range of partitions from $\eta = 1$ to $\eta = N$, we ensure that the profiles are comparable for different networks.

6.2.2 Problems with comparing networks using resolution

The most common method for studying network community structure across multiple mesoscopic scales is to consider plots of networks summary statistics as a function of the resolution parameter, e.g., [17, 105, 244, 254].³ However, there are problems with this approach for some networks. Consider, Fig. 6.1(a), which shows the cumulative distribution $P(\Lambda_{ij} \leq x)$ for an (unweighted) network of Facebook users at Caltech [295].⁴ The vast majority of Λ_{ij} values are less than 100, but there are a few interactions with $\Lambda_{ij} > 8000$. The large Λ_{ij} values are the result of two low degree nodes being connected. Using the standard null model $P_{ij} = k_i k_j / (2m)$, the interaction between two nodes i and j becomes antiferromagnetic when $\lambda > A_{ij} / P_{ij} = 2m A_{ij} / (k_i k_j)$. If there are a large number of edges in the network, but both i and j have very low degrees, λ needs to be large to make the interaction antiferromagnetic. Figure 6.1(b) demonstrates the effect of these interactions on a plot of the number of communities η as a function of λ over the interval $[\Lambda_{\min}, \Lambda_{\max}]$ for the Caltech network. The network breaks up into just under N communities over a small range of λ , but there is then a long plateau as a few interactions with large λ become antiferromagnetic and the remaining communities break up. These few interactions dominate the figure and obscure the structure at small resolutions.

One way of avoiding this problem is only to sweep λ over a range such that the number of communities varies between $\eta \in [1, fN]$, where fN is some fraction of the total number of nodes in the network. Using this approach, it would not be necessary to force the nodes with large Λ_{ij} into individual communities, so the range of λ would be significantly smaller. However, there are obvious problems with this method: first, the choice of f is arbitrary; second, in general, the value of f that avoids the long

³In Chapter 5 we use this approach to study communities in FX market networks.

⁴We enumerate all of the networks that we study in Table C.1 in Appendix C.

plateaus is different for different networks; if one wishes to use plots of summary statistics versus resolution to compare networks, the value of f ought to be constant. Therefore, this seems like an unsuitable solution.

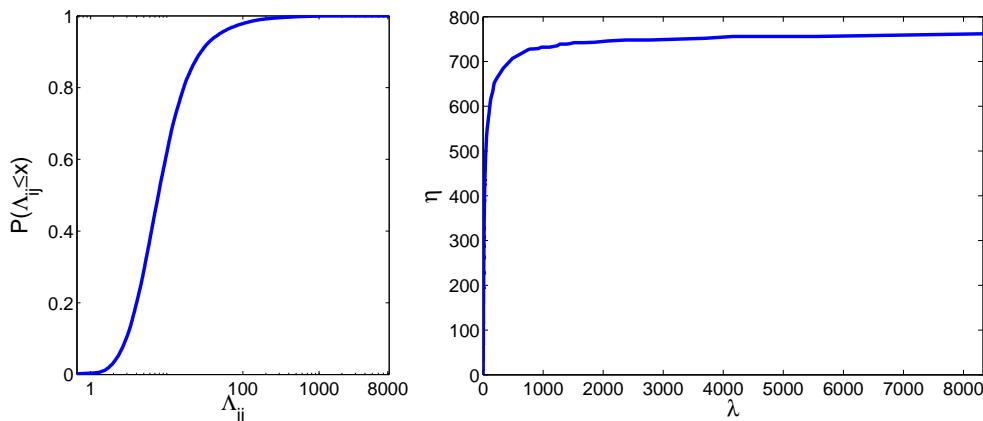


Figure 6.1: A demonstration using the Caltech Facebook network [295] of the problem of using the resolution parameter for networks with low-degree nodes that are connected to each other. The left figure shows the cumulative distribution of Λ_{ij} values $P(\Lambda_{ij} \leq x)$; the majority of Λ_{ij} are less than 100, but there are a few nodes with $\Lambda_{ij} > 8000$. The right figure shows the number of communities as a function of λ and demonstrates that the presence of low strength nodes that are connected to each other results in a long plateau. Only a few interactions then dominate the plot and obscure the structure at smaller λ .

Of course, the problem of having interactions that require large λ to become antiferromagnetic stems initially from our choice of null model. An alternative choice of null model that avoids this problem is one in which P_{ij} is constant for all i and j . In contrast to the standard null model $P_{ij} = k_i k_j / (2m)$, however, this model does not preserve the strength distribution of the original network. Given this appealing property of the null model $P_{ij} = k_i k_j / (2m)$ and its ubiquity within the literature, we persevere with this model.

6.2.3 Effective fraction of antiferromagnetic links

To avoid the issues arising from a few interactions requiring large resolutions to become antiferromagnetic, instead of considering network properties as a function of the resolution parameter, we work in terms of the *effective fraction of antiferromagnetic links* ξ . We define ξ as

$$\xi = \xi(\lambda) = \frac{\ell^A(\lambda) - \ell^A(\Lambda_{\min})}{\ell^A(\Lambda_{\max}) - \ell^A(\Lambda_{\min})}, \quad (6.5)$$

where $\ell^A(\lambda)$ is the total number of antiferromagnetic interactions ($J_{ij} < 0$) in the system for the given value of λ and $\ell^A(\Lambda_{\min})$ is the largest number of antiferromagnetic interactions for which the network still forms a single community. The effective number of antiferromagnetic interactions $\xi(\lambda)$ is therefore the number of antiferromagnetic interactions in excess of $\ell^A(\Lambda_{\min})$ (normalized to the unit interval) and is a monotonically increasing function of λ .

To simplify the discussion of the fraction of antiferromagnetic links, it is also useful to divide the elements of the adjacency matrix \mathbf{A} into links ($A_{ij} > 0$) and non-links ($A_{ij} = 0$). Based on the values Λ_{ij} , we further distinguish between two types of links: links with $0 < \Lambda_{ij} \leq \Lambda_{\min}$ are called Λ^- -links, and links with $\Lambda_{ij} > \Lambda_{\min}$ are called Λ^+ -links. The sum of the number of Λ^- -links and Λ^+ -links is then equal to L , the number of links in the network.⁵ When $\lambda = \Lambda_{\min}$ all of the Λ^- -links are antiferromagnetic, but the network nevertheless consists of a single community.

We illustrate the differences between the different types of links in Fig. 6.2 in which we show examples of the cumulative distributions of links $P(\Lambda_{ij} \leq x)$ for a fully-connected, weighted network and for an unweighted network. For the unweighted network, $\Lambda_{\min} < \Lambda^*$, so the network does not possess any Λ^- -links. As one increases the resolution parameter, the network begins to break up into communities before any of the Λ^+ -links become antiferromagnetic. In contrast, for the fully-connected, weighted network $\Lambda^* < \Lambda_{\min}$.

6.2.3.1 Properties of the fraction of antiferromagnetic links

In the definition of ξ that we select, we sweep over the values $\lambda \in [\Lambda_{\min}, \Lambda_{\max}]$, so that the number of communities varies between 1 and N . Although the regime $\lambda < \Lambda_{\min}$ affects the energy $\mathcal{H}(\lambda)$ (see Eq. 6.1), there are no further changes in the partition into communities and, consequently, only the region $\lambda \in [\Lambda_{\min}, \Lambda_{\max}]$ is interesting. The normalization in our definition of ξ accounts for the existence of antiferromagnetic Λ^- -links, which do not cause the network to break up into communities and ensures that $0 \leq \xi \leq 1$. Note that ξ is equal to the fraction of antiferromagnetic Λ^+ -links.

By working in terms of ξ rather than λ , we ensure that interactions that require a large resolution to become antiferromagnetic do not dominate plots of community summary statistics. The existence of such interactions also implies that we do not necessarily sweep λ uniformly over the interval $[\Lambda_{\min}, \Lambda_{\max}]$. As demonstrated in Fig. 6.1, some networks have several orders of magnitude between Λ_{\min} and Λ_{\max} and most interactions become antiferromagnetic at $\lambda \approx \Lambda_{\min}$. To ensure that ξ is sampled

⁵In an unweighted network $L = m$, the total link weight in the network.

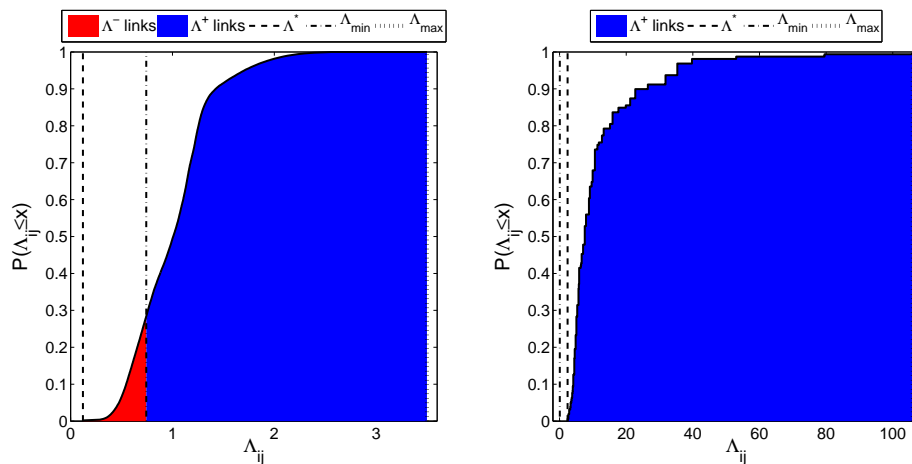


Figure 6.2: The cumulative distribution $P(\Lambda_{ij} \leq x)$ for: (left) the 100th U.S. House of Representatives roll-call voting network [203,241,306], (right) the dolphins network [192]. We show the proportions of Λ^+ and Λ^- links in the distributions and highlight the position of Λ^* , Λ_{\min} , and Λ_{\max} . For the House network, $\Lambda_{\min} > \Lambda^*$, so there are both Λ^+ and Λ^- links. For the dolphins network, $\Lambda_{\min} < \Lambda^*$, so all links are Λ^+ links and the network begins to break up into communities at a resolution $\lambda \leq \Lambda_{\min}$.

uniformly, we select the values of λ using the cumulative distribution of Λ_{ij} for Λ^+ -links, instead of simply sampling λ uniformly over the interval $[\Lambda_{\min}, \Lambda_{\max}]$.⁶

In Appendix D we provide further technical details of the Potts Hamiltonian and of the structure of the networks that we study.

6.3 Mesoscopic response functions

The third step in creating multi-resolution profiles to characterize a network's mesoscopic structures is to select summary statistics to examine as a function of ξ . We choose to investigate the number of communities η , the energy \mathcal{H} (given by Eq. 6.1) and the partition entropy S (given by Eq. 5.6).⁷ The values of these quantities vary across networks; for example, as we show in Section D.1, the energy \mathcal{H} is determined

⁶As we noted in Section 4.3.3, the number of possible community partitions grows rapidly with the number of nodes [218], so finding communities in large networks is computationally intensive [55]. As a result, one cannot find the optimal community configuration at every resolution and, accordingly, the values of Λ_{\min} that we find are necessarily approximate.

⁷We focus on the energy, entropy and number of communities because, as we discuss later in this section, each statistic provides information on a key property of the community structure of the networks. One could examine other summary statistics as a function of ξ ; however, in the interests of parsimony, it is desirable to limit the number of summary statistics. In Section 6.4.1 we use PCA to construct a single measure that summarize the three statistics.

by the resolution λ , and Λ_{\max} depends strongly on the link structure of the network. As a result, for it to be possible to compare networks using profiles of the summary statistics versus ξ , we need to normalize \mathcal{H} , S , and η . Therefore, we define an *effective energy* as

$$\mathcal{H}_{\text{eff}}(\lambda) = \frac{\mathcal{H}(\lambda) - \mathcal{H}_{\min}}{\mathcal{H}_{\max} - \mathcal{H}_{\min}} = 1 - \frac{\mathcal{H}(\lambda)}{\mathcal{H}_{\min}}, \quad (6.6)$$

where $\mathcal{H}_{\min} = \mathcal{H}(\Lambda_{\min})$ and $\mathcal{H}_{\max} = \mathcal{H}(\Lambda_{\max})$. Similarly, we define an *effective entropy*

$$S_{\text{eff}}(\lambda) = \frac{S(\lambda) - S_{\min}}{S_{\max} - S_{\min}} = \frac{S(\lambda)}{\log N}, \quad (6.7)$$

where $S_{\min} = S(\lambda_{\min})$ and $S_{\max} = S(\lambda_{\max})$, and an *effective number of communities*

$$\eta_{\text{eff}}(\lambda) = \frac{\eta(\lambda) - \eta_{\min}}{\eta_{\max} - \eta_{\min}} = \frac{\eta(\lambda) - 1}{N - 1}, \quad (6.8)$$

where $\eta_{\min} = \eta(\Lambda_{\min})$ and $\eta_{\max} = \eta(\Lambda_{\max})$. In sweeping ξ from 0 to 1, the number of communities increases from $\eta(\xi = 0) = 1$ to $\eta(\xi = 1) = N$, producing a signature that we call the *mesoscopic response function* (MRF). Because $\mathcal{H}_{\text{eff}} \in [0, 1]$, $S_{\text{eff}} \in [0, 1]$, $\eta_{\text{eff}} \in [0, 1]$, and $\xi \in [0, 1]$ for any network, we can compare the response functions across networks and use the MRFs to identify groups of networks with similar mesoscopic structures.

For a given network, at each resolution, \mathcal{H}_{eff} , S_{eff} , and η_{eff} respectively provide a measure of the frustration level of the spin system, the disorder in the associated community size distribution (whether most nodes are in a few large communities or are spread across many small communities), and the number of communities. The MRFs indicate the way in which these quantities change as the resolution parameter is increased – at higher resolutions there is a larger incentive for nodes to belong to smaller communities, so communities fragment. The shapes of the MRFs (gradient, concavity/convexity, points of inflection etc.) are the non-trivial result of many factors, including the fraction of possible edges in the network; the relative weights of inter- versus intra-community edges; the edge weights compared with the expected edge weights in the random null model; the number of edges that need to become antiferromagnetic for a community to fragment; and the way in which the communities fragment (e.g., whether a single node leaves a community if an edge becomes antiferromagnetic or a community splits in half). The effects of some of these factors on the shapes of the MRFs can be better understood by considering some examples.

6.3.1 Example MRFs

Figure 6.3 shows the Zachary karate club network [315] for different values of the effective fraction of antiferromagnetic links ξ and highlights that, as more links become antiferromagnetic (as the resolution parameter λ is increased), the network fragments into communities. The nature of this fragmentation process then determines the shapes of the MRFs shown in the lower half of Fig. 6.3.

In Fig. 6.4, we show example MRFs for several other networks. Figure 6.4 demonstrates that, although there are large variations in the shapes of the response functions, there are also common features. Of particular interest are plateaus in the η_{eff} and S_{eff} curves that are accompanied by large increases in \mathcal{H}_{eff} . Some plateaus in plots of network summary statistics as a function of ξ have a similar interpretation to plateaus in plots of summary statistics as a function of resolution λ (see Section 5.4). The NYSE: 1980–1999 network [229] provides an example of this behaviour [see Fig. 6.4(b)]. The plateaus imply that as the resolution λ is increased (leading to an increase in \mathcal{H}_{eff}), the number of antiferromagnetic interactions also increases even though the number of communities remains constant. As λ is increased, and more interactions become antiferromagnetic, there is an increased energy incentive for communities to break up. The plateaus demonstrate that, despite this incentive, the communities remain intact. Community partitions corresponding to these plateaus are therefore very robust and potentially represent interesting structures [17, 105, 244, 254]. The large increase in \mathcal{H}_{eff} shows that such partitions are robust over a large range of resolutions.

The MRF for the Fractal: (10,2,8) network [279] [Fig. 6.4(k)] also demonstrates that there can be plateaus in the η_{eff} and S_{eff} MRFs that are not accompanied by significant changes in \mathcal{H}_{eff} . Such plateaus can be explained by considering the distribution of Λ_{ij} . If several interactions have identical Λ_{ij} , then the interactions all become antiferromagnetic at exactly the same resolution. This leads to a significant increase in ξ , but only a small change in \mathcal{H}_{eff} . If these interactions do not lead to additional communities, there are plateaus in the η_{eff} and S_{eff} curves.

Another common feature is a sharp increase in the \mathcal{H}_{eff} and S_{eff} curves at $\xi = 0$. Some networks initially break into two communities at a resolution $\Lambda_{\text{min}} < \Lambda^*$. As λ is increased, the communities then continue to split before Λ^* is reached, at which point another interaction becomes antiferromagnetic. In these networks, the number of communities increases to $\eta \geq 2$ at $\xi = 0$. This usually occurs in sparse networks in which the non-links play a significant role in determining the community structure.

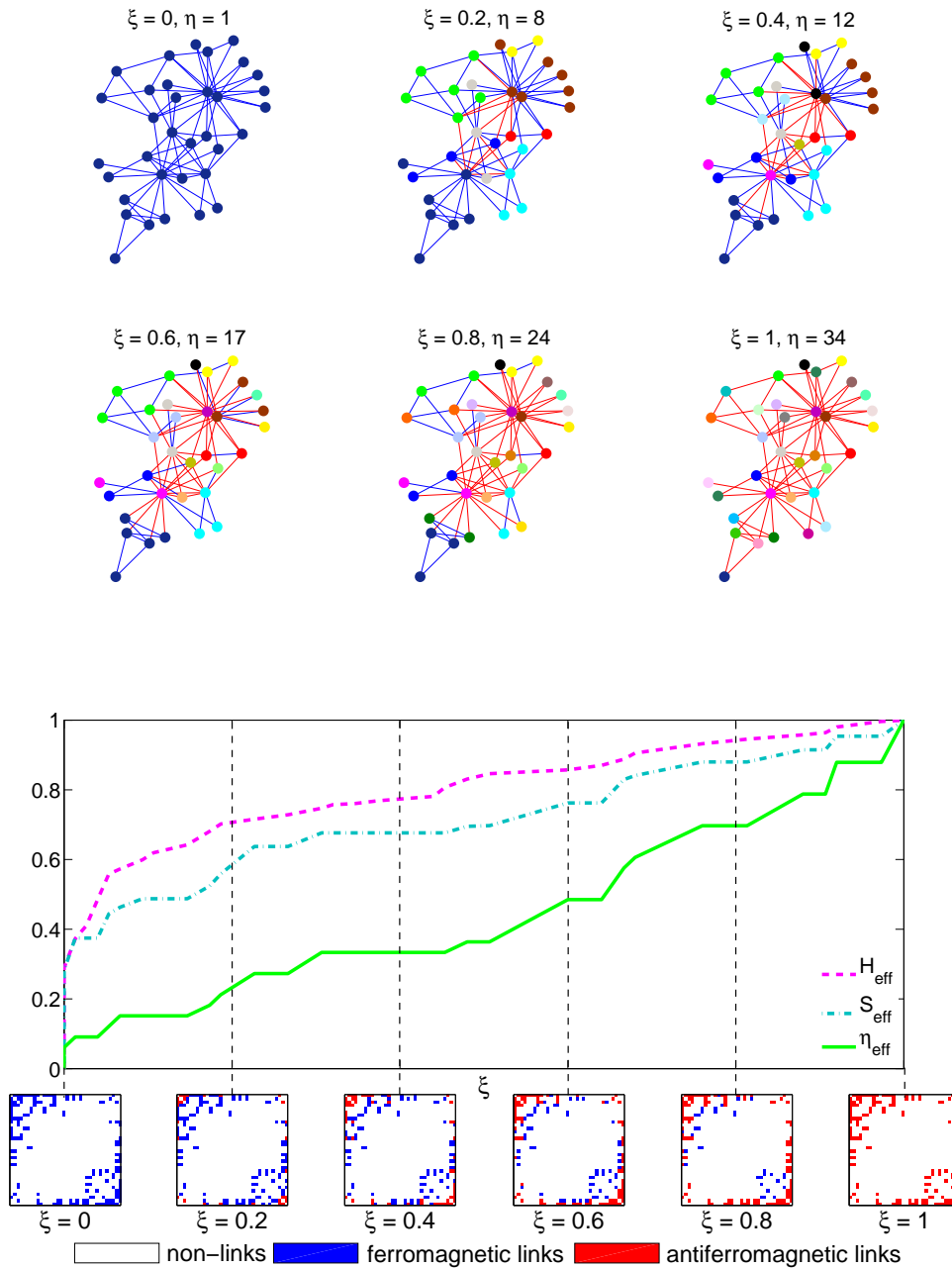


Figure 6.3: The upper half of the figure shows the Zachary karate club network [315] for different values of the effective fraction of antiferromagnetic links ξ . The edges are coloured blue if the corresponding interaction is ferromagnetic or red if the interaction is antiferromagnetic. The nodes are coloured according to their community membership. In the lower half of the figure, we show the \mathcal{H}_{eff} , S_{eff} , and η_{eff} MRFs and the interaction matrix \mathbf{J} for different values of ξ . We have coloured elements of the interaction matrix corresponding to non-links white and elements corresponding to ferromagnetic and antiferromagnetic links blue and red, respectively.

The Biogrid *D. melanogaster* [280] and the Garfield Scientometrics citation [119] MRFs demonstrate this effect [Fig. 6.4(e) and Fig. 6.4(m), respectively].

The MRFs for the voting network of the U.K. House of Commons over the period 2001–2005 [104] [Fig. 6.4(g)] and the roll-call voting network for the 108th U.S. House of Representatives (2003–2004) [203, 241, 306] [Fig. 6.4(q)] also reveal that sharp increases in \mathcal{H}_{eff} can be accompanied by small changes in η_{eff} and S_{eff} . This observation can also be explained by considering the distribution of Λ_{ij} . If the Λ_{ij} distribution is multi-modal, there can be a large difference between consecutive Λ_{ij} values. A large increase in λ is then needed to increase ξ , which leads to a large change in \mathcal{H}_{eff} . However, because this only results in a single additional antiferromagnetic interaction, the change in η_{eff} is small. We discuss the distribution of Λ_{ij} for U.S. House of Representative roll-call voting networks in more detail in Section 6.9.1.3.

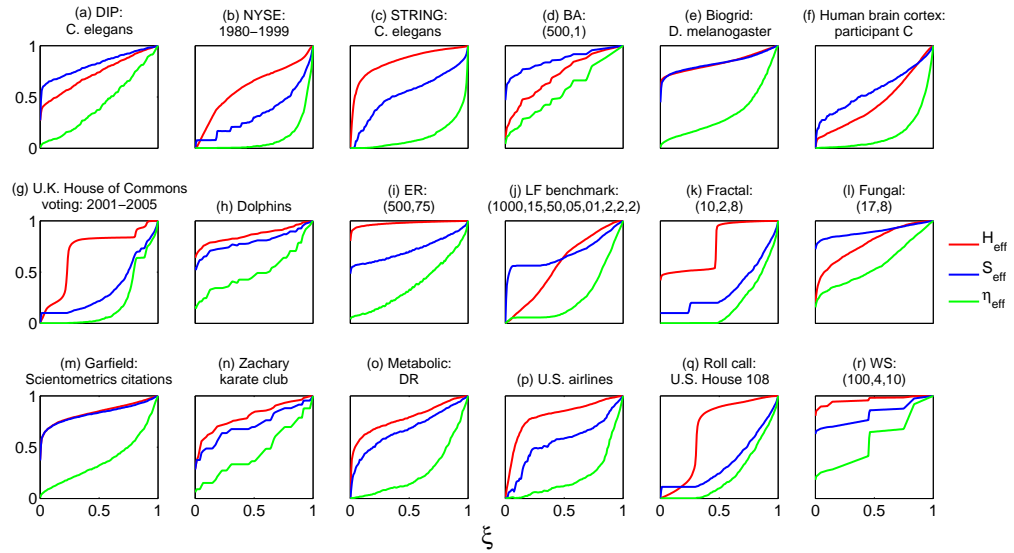


Figure 6.4: Example MRFs. The curves show \mathcal{H}_{eff} (red), S_{eff} (blue), and η_{eff} (green) as a function of the effective fraction of antiferromagnetic links ξ for the following networks: (a) DIP: *C. elegans* [262,310] (b) New York Stock Exchange (NYSE): 1980–1999 [229] (c) STRING: *C. elegans* [155] (d) Barabási-Albert (BA): (500,1) [26] (e) Biogrid: *D. melanogaster* [280] (f) Human brain cortex: participant C [144] (g) U.K. House of Commons Voting: 2001–2005 [104] (h) Dolphins [192] (i) Erdős-Rényi (ER): (500,75) [86] (j) LF benchmark: (1000,15,50,05,01,2,2,2) [180] (k) Fractal: (10,2,8) [279] (l) Fungal: (17,8) [33, 113, 114, 288] (m) Garfield: Scientometrics citations [119] (n) Zachary karate club [315] (o) Metabolic: DR [156] (p) U.S. airlines [29, 77] (q) Roll call: U.S. House 108 [203, 241, 306] (r) Watts-Strogatz (WS): (100,4,10) [305]. See Table C.1 for more details on the networks.

6.3.2 MRFs for Erdős-Rényi networks

We can gain further understanding of the shapes of the MRFs by comparing multiple realizations of synthetic networks with different parameter values. In this section, we consider the \mathcal{H}_{eff} , S_{eff} , and η_{eff} curves for Erdős-Rényi (ER) networks with different numbers of nodes N and fractions f_e of possible edges.⁸ In Fig. 6.5, we show MRFs for $N = 50, 100, 500$ and 1000 and $f_e = 0.25, 0.5$ and 0.75 ; although the shapes of the MRFs for the different ER networks are similar, important differences result from the different values of N and f_e .

6.3.2.1 Varying the fraction of possible edges

Figure 6.5 shows that for a fixed number of nodes N , as the fraction of possible edges f_e is increased, the maximum value of η_{eff} at $\xi = 0$ decreases. This can be explained by considering the number of non-links for each network (i.e., the number of elements of the adjacency matrix for which $A_{ij} = 0$). For any resolution $\lambda > 0$, the interaction strength J_{ij} between pairs of spins joined by non-links is less than zero, so the spins seek to align in different spin-states (join different communities). For some networks, as the resolution λ is increased, the negative interaction strength between nodes joined by non-links can become so strong that the network breaks up into communities before any of the links ($A_{ij} > 0$) become antiferromagnetic (i.e., for some networks $\eta(\xi = 0) \geq 2$). This effects explains the different levels of $\eta_{\text{eff}}(\xi = 0)$ for different values of f_e . For a set of ER networks with the same number of nodes N , networks with smaller fractions of possible edges f_e possess more non-links than networks with higher f_e ; this results in more negative elements in the interaction matrix \mathbf{J} for $\lambda > 0$, which in turn causes networks with lower f_e to break up into more communities at $\xi = 0$ than networks with higher f_e . Hence, $\eta_{\text{eff}}(\xi = 0)$ reaches a higher level for networks with smaller fractions of possible edges. For example, in Fig. 6.5, for networks with $N = 50$ nodes, when $f_e = 0.25$ the maximum value of $\eta(\xi = 0)$ is 15, and when $f_e = 0.75$ the maximum value is 4; similarly, for networks with $N = 1000$ nodes, when $f_e = 0.25$ the maximum value of $\eta(\xi = 0)$ is 176, and when $f_e = 0.75$ the maximum value is 48.

The number of communities at $\xi = 0$ also affects the energy and entropy MRFs: for larger values of f_e , because there are fewer communities at $\xi = 0$, the S_{eff} and \mathcal{H}_{eff} MRFs reach lower levels.

⁸Strictly, we generate ER networks with different probabilities for connecting each pair of nodes, but this probability is generally equal (or almost equal) to the fraction of possible edges present.

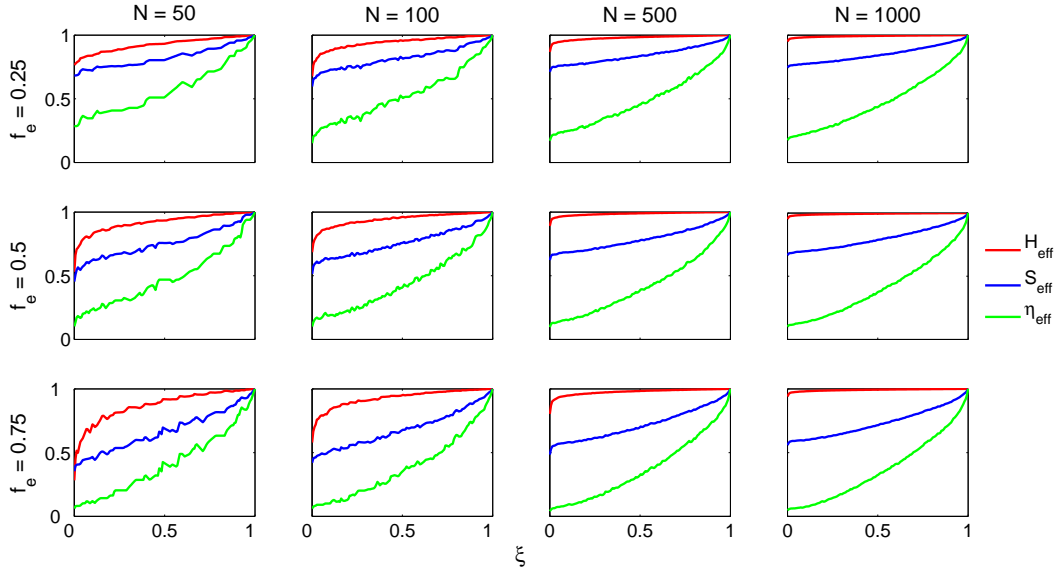


Figure 6.5: A comparison of the \mathcal{H}_{eff} , S_{eff} , and η_{eff} MRFs for Erdős-Rényi networks with different numbers of nodes N and fractions of possible edges f_e .

6.3.2.2 Varying the number of nodes

Figure 6.5 also shows that as the number of nodes increases, for the same fraction of possible edges, the maximum value of η_{eff} at $\xi = 0$ decreases. For larger values of N , the network breaks up into more communities at $\xi = 0$ than for smaller N ; however, the number of communities as a fraction of the number of nodes in the network is lower, hence $\eta_{\text{eff}}(\xi = 0)$ is lower. For example, for networks with $f_e = 0.25$, when $N = 50$ the maximum value of $\eta(\xi = 0)$ is 15, which corresponds to $\eta/N = 0.3$, and when $N = 1000$ the maximum value is 176, which corresponds to $\eta/N = 0.18$.

In contrast to the η_{eff} MRFs, for larger values of N at the same value of f_e S_{eff} reaches a higher value at $\xi = 0$. The entropy can be considered as the uncertainty in the community membership of a particular node. For a larger number of communities there is generally greater uncertainty in the community membership of a randomly chosen node, which results in a higher entropy and is consistent with the observation that $S_{\text{eff}}(\xi = 0)$ is higher for larger N . However, because we normalize the entropy using the transformation $S_{\text{eff}} = (S - S_{\text{min}})/(S_{\text{max}} - S_{\text{min}}) = S/\log N$ (see Eq. 6.7), more precisely, the higher value of S_{eff} at $\xi = 0$ for higher N indicates that there is greater uncertainty in the community membership of a node relative to the maximum possible uncertainty (which occurs when all nodes are in singleton communities and is given by $S_{\text{max}} = \log N$).

Finally, Fig. 6.5 shows that for larger N the maximum value of \mathcal{H}_{eff} at $\xi = 0$ is higher. This is again explained in part by the fact that networks with larger numbers of nodes fragment into more communities at $\xi = 0$ than smaller networks. Recall from Eq. 4.3 that the Hamiltonian of the Potts spin glass is given by $\mathcal{H} = \sum_{i \neq j} J_{ij} \delta(C_i, C_j) = -\sum_{i \neq j} (A_{ij} - \lambda P_{ij}) \delta(C_i, C_j)$. The Kronecker delta $\delta(C_i, C_j)$ means that the interaction energies $J_{ij} = (A_{ij} - \lambda P_{ij})$ are only summed over nodes that belong to the same community. Therefore, as the networks fragment, the summation includes fewer terms so \mathcal{H} becomes progressively less negative and \mathcal{H}_{eff} increases. The higher values \mathcal{H}_{eff} at $\xi = 0$ for networks with more nodes can be further explained by considering the distribution of Λ_{ij} for the different networks. In Fig. 6.6, we show that for larger N the distribution of Λ_{ij} values is concentrated in a sharper peak, which means that the resolution λ only needs to be swept over a small range of values for all of the links to become antiferromagnetic. The small range of λ also means that there is a relatively small change in energy as the network breaks up into N communities, which explains the small difference in energy that we observe between $\xi = 0$ and $\xi = 1$ in the \mathcal{H}_{eff} MRFs for larger networks in Fig. 6.5.

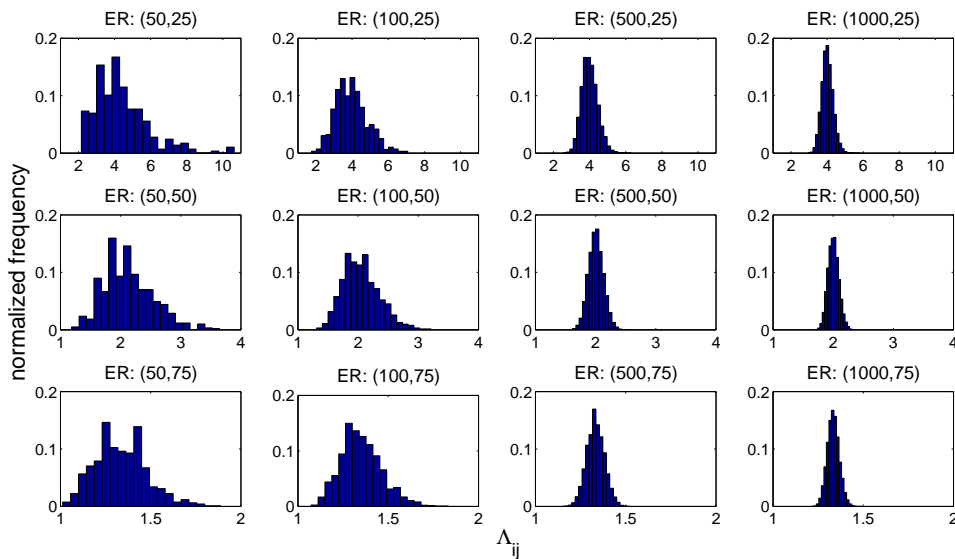


Figure 6.6: A comparison of the distribution of Λ_{ij} values for Erdős-Rényi networks with different numbers of nodes N and fractions of possible edges f_e .

6.3.3 Synthetic MRFs

The shapes of the MRFs reflect the manner in which the network splits into communities as the resolution is increased. To provide further insights into the mesoscopic heterogeneities leading to different MRFs it is therefore instructive to consider the effect of different community fragmentation mechanisms on the MRFs. In this section, we do not assume any network structure or detect communities; instead, we create synthetic η_{eff} and S_{eff} MRFs by considering different rates of community fragmentation as a function of ξ and different community size distributions.

We begin by assuming a fixed shape for the η_{eff} response function. Figure 6.4 suggests that most of the η_{eff} curves are either approximately linear or some convex function so, as a first approximation, we assume that the η_{eff} MRFs are either linear, quadratic, or cubic.⁹ We create synthetic η_{eff} MRFs for each of these cases as follows. We assume that as the resolution λ is increased, the number of communities increases as

$$\eta(i) = \left\lceil \frac{i^k}{N^{k-1}} \right\rceil, \quad (6.9)$$

where $\lceil x \rceil = \min\{j \in \mathbb{Z} | j \geq x\}$, with j denoting an integer, is the ceiling function, $i \in \{1, \dots, N\}$, N is the number of nodes in the network and we investigate $k \in \{1, 2, 3\}$. The normalization N^{k-1} ensures that the number of communities does not exceed N and the ceiling function ensures that we have only integer numbers of communities. We normalize these values to effective numbers of communities η_{eff} lying in the unit interval through the transformation

$$\eta_{\text{eff}}(i) = \frac{\eta(i) - \eta_{\min}}{\eta_{\max} - \eta_{\min}} = \frac{\eta(i) - 1}{N - 1}. \quad (6.10)$$

We then construct synthetic S_{eff} MRFs based on the number of communities η at each value of i in the η_{eff} MRFs. We investigate two extreme cases for the community fragmentation process:

1. We consider the case in which each increase in the number of communities η results from a single node leaving the largest community. For example, at $\eta = 2$ we assume that one community contains a single node and the other community contains $N - 1$ nodes; at $\eta = 3$, we assume that there are two communities containing single nodes and a third community containing $N - 2$ nodes; and so on.

⁹Although this assumption is not strictly true for most networks, it is nevertheless a reasonable starting point.

2. We examine the case in which each increase in η results from the largest community splitting in half. For example, at $\eta = 2$ we assume that each community contains $N/2$ nodes; at $\eta = 3$, we assume that there are two communities containing $N/4$ nodes and a third community containing $N/2$ nodes; at $\eta = 4$, we assume that each community contains $N/4$ nodes; and so on.¹⁰

To plot the MRFs we assume that the ξ are uniformly distributed over the interval $[0, 1]$ such that the i^{th} value is given by

$$\xi(i) = \frac{i - 1}{N - 1}, \quad (6.11)$$

where $i = 1, \dots, N$. We show in Section 6.3.1 that the number of communities increases to $\eta > 1$ at $\xi = 0$ for many networks, so for each splitting regime we examine two behaviours for the MRFs at $\xi = 0$:

1. The number of communities does not exceed $\eta = 1$ at $\xi = 0$. (See columns A and C in Fig. 6.7.)
2. The number of communities initially increases without an increase in the effective fraction of antiferromagnetic interactions ξ , i.e., $\eta > 1$ at $\xi = 0$. (See columns B and D in Fig. 6.7.)

We create MRFs that represent the second type of behaviour by setting the first ι elements of the ξ vector to zero; increasing ι results in the MRFs reaching a higher values at $\xi = 0$.

In Fig. 6.7, we show synthetic MRFs for networks with $N = 500$ nodes and $\iota = 20$.¹¹ For all of the curves where we assume that each increase in η results from a single node leaving the largest community, the S_{eff} MRF closely tracks the η_{eff} MRF. For each example in which increases in η result from the largest community splitting in half, the entropy increases faster than in the equivalent MRF for single nodes splitting from the largest community. This is because in the former case there is greater uncertainty in the community membership of individual nodes. Figure 6.7 also demonstrates that for the fragmentation mechanism in which communities split in

¹⁰When splitting the k^{th} community into two, if $n_k/2$ is not an integer (where n_k is the number of nodes in the k^{th} community), we assume that one of the communities contains $\lfloor n_k/2 \rfloor$ nodes and that the other community contains $\lceil n_k/2 \rceil$ nodes. If two communities contain the same number of nodes, we choose one at random to split – this choice has no effect on the resulting MRF.

¹¹We have also investigated networks with different numbers of nodes N and observe similar differences in the MRFs for different sized networks to those described in Section 6.3.2 for ER networks.

half the MRFs have very different shapes for the different assumptions. For example, there is a plateau in some, but not all, of the S_{eff} MRFs and there is a large variation in the amount by which the S_{eff} MRFs increase at $\xi = 0$.

This is just a simple demonstration of how different fragmentation processes lead to different shaped MRFs. For real-world networks, the community splitting mechanism is likely to be somewhere between these two extreme cases, with single nodes leaving communities for some changes in ξ and communities splitting more equally at other values.

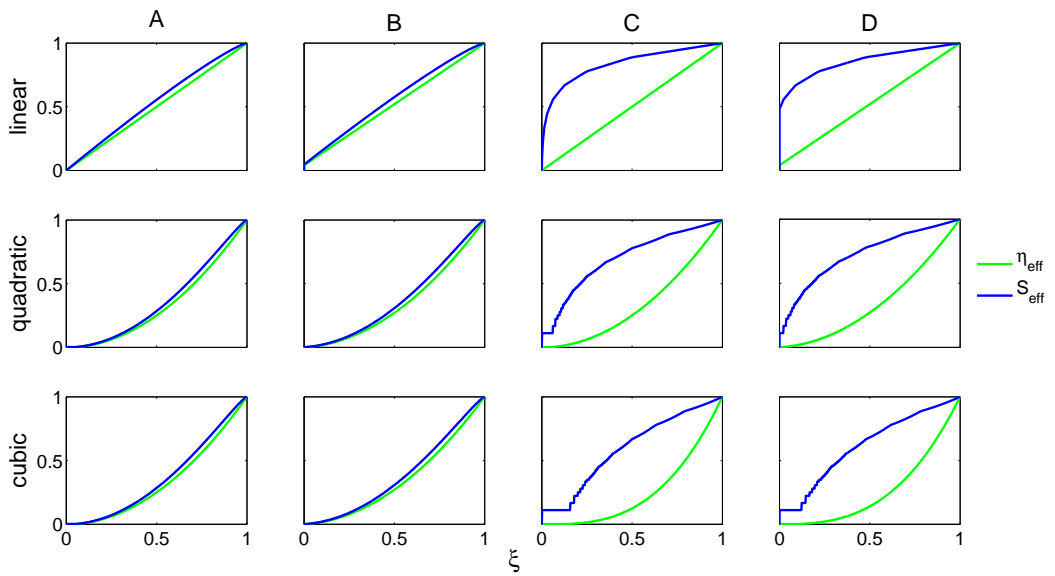


Figure 6.7: Synthetic MRFs for η_{eff} and S_{eff} . We assume that the η_{eff} response functions are either linear, quadratic, or cubic. We also consider that: (A) Each increase in the number of communities η results from a single node leaving the largest community. (B) Again, each increase in η results from a single node leaving the largest community, but we make the additional assumption that, as the resolution is increased, η initially increases without there being an increase in the effective number of antiferromagnetic interactions ξ . (C) Each increase in the number of communities η results from the largest community splitting in half. (D) Each increase in the number of communities η results from the largest community splitting in half and there is an initial increase in η without an increase in ξ . We assume that each network has $N = 500$ nodes.

6.4 Distance measures

In Section 6.3, we demonstrated that there are significant variations in the shapes of the MRFs for different networks. This variety reflects the diverse range of possible mesoscopic network structures; if two networks have similar MRFs, this suggests that the networks have similar mesoscopic properties. We now define a distance measure that quantifies the differences in the behaviours of the MRFs.

There are several plausible choices of distance measure, but we add the constraint that the measure should compare MRFs across all network scales (i.e., for all values of ξ). With this in mind, we define the pairwise distance between networks with respect to one of the investigated properties as the area between the corresponding MRFs. For example, the distance between two networks i and j with respect to the effective energy MRF \mathcal{H}_{eff} is given by

$$d_{ij}^{\mathcal{H}} = \int_0^1 |\mathcal{H}_{\text{eff}}^i - \mathcal{H}_{\text{eff}}^j| d\xi. \quad (6.12)$$

Similarly, for the effective entropy and effective number of communities, the distances are given by

$$d_{ij}^S = \int_0^1 |S_{\text{eff}}^i - S_{\text{eff}}^j| d\xi \quad (6.13)$$

and

$$d_{ij}^{\eta} = \int_0^1 |\eta_{\text{eff}}^i - \eta_{\text{eff}}^j| d\xi. \quad (6.14)$$

We represent the three distances in matrix form as $\mathbf{D}^{\mathcal{H}}$, \mathbf{D}^S , and \mathbf{D}^{η} . This definition of distance between MRFs has several desirable properties. First, as required, it compares MRFs across all network scales (i.e., for all values of ξ); second, the measure is bounded between 0 and 1; third, it is simple and transparent, in that the distances correspond to the geometric area between a pair of MRFs; finally, we find *a posteriori* that it seems to cluster networks accurately. We illustrate the distance measures in Fig. 6.8 using the NYSE: 1984–1987 [229] and Fungal: (4,8) networks [33,113,114,288].

We analyze MRFs for the energy \mathcal{H} , entropy S , and number of communities η , but the techniques that we present work similarly for other summary statistics. However, if two statistics provide very similar information, then one of them can be excluded without a significant loss of information. We check whether the summary statistics that we investigate are sufficiently different for it to be worthwhile to include all of them in our analysis by calculating the correlation between their distance measures. In Fig. 6.9, we show scatter density plots for each pairwise combination of the

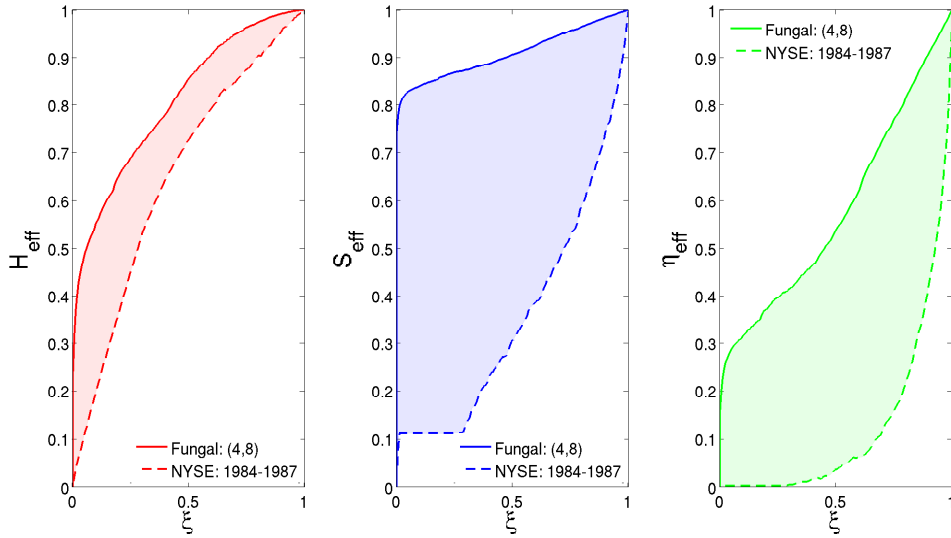


Figure 6.8: A comparison of the MRFs for the NYSE (1984–1987) [229] and fungal (4,8) networks. For each figure, the shaded area between the curves equals the distance between the networks for the corresponding measure. In this example, the distance are: $d^{\mathcal{H}} \doteq 0.1594$, $d^S \doteq 0.5496$, and $d^\eta \doteq 0.4524$.

distances $d_{ij}^{\mathcal{H}}$, d_{ij}^S , and d_{ij}^η . From these plots, it is clear that the most significant correlation is between d_{ij}^S and d_{ij}^η and the linear correlation between these two measures is only $r(d_{ij}^S, d_{ij}^\eta) \doteq 0.58$. The correlations between the other pairs of distances are $r(d_{ij}^{\mathcal{H}}, d_{ij}^S) \doteq 0.36$ and $r(d_{ij}^{\mathcal{H}}, d_{ij}^\eta) \doteq 0.24$. None of these correlations are sufficiently high to justify excluding one of the summary statistics, so we use all three.

6.4.1 PCA distance

We have defined three response functions and have shown that each MRF contains different information; in the interests of parsimony, we now reduce the number of distance measures using PCA [159]. As described in Chapter 3, PCA is a standard dimensionality-reduction technique that transforms multiple correlated variables into uncorrelated variables in which the first component accounts for as much of the variance in the original data as possible. Subsequent components then account for as much of the remaining variance as possible. We create an $\frac{1}{2}N(N-1) \times 3$ matrix in which each column corresponds to the vector representation of the upper triangle of one of the distance matrices $\mathbf{D}^{\mathcal{H}}$, \mathbf{D}^S , \mathbf{D}^η and we perform a PCA on this matrix. We then define a distance matrix \mathbf{D}^p with elements $d_{ij}^p = w_{\mathcal{H}}d_{ij}^{\mathcal{H}} + w_S d_{ij}^S + w_\eta d_{ij}^\eta$, where the weights are the PC coefficients for the first component, and we normalize the d_{ij}^p

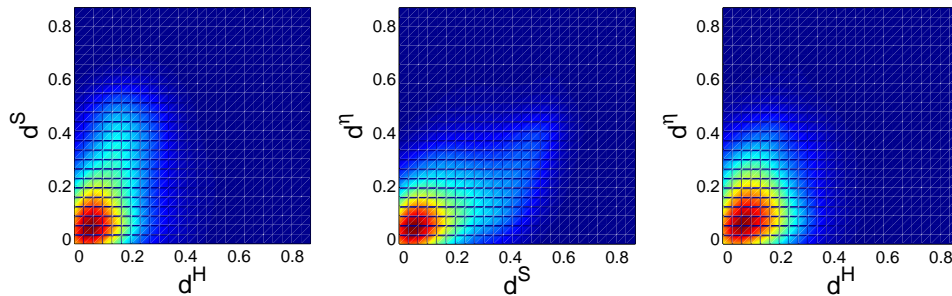


Figure 6.9: Scatter density plots showing the correlation between the distances measures $d_{ij}^{\mathcal{H}}$, d_{ij}^S , and d_{ij}^{η} . The linear correlations r between the distances are: $r(d_{ij}^{\mathcal{H}}, d_{ij}^S) \doteq 0.36$, $r(d_{ij}^S, d_{ij}^{\eta}) \doteq 0.58$, and $r(d_{ij}^{\mathcal{H}}, d_{ij}^{\eta}) \doteq 0.24$.

to the unit interval. The PC coefficients are $w_{\mathcal{H}} \doteq 0.24$, $w_S \doteq 0.79$, and $w_{\eta} \doteq 0.57$. The first component accounts for 69% of the variance of the system, so the distances \mathbf{D}^p provide a reasonable single-variable representation of the distances $\mathbf{D}^{\mathcal{H}}$, \mathbf{D}^S , and \mathbf{D}^{η} .

6.4.2 Distance matrices

In Fig. 6.10, we show the distribution of distances for all of the 714 networks studied (see Table C.1 for the full list of networks). The distribution d_{ij}^S for the entropy MRF has more weight at larger distances than the $d_{ij}^{\mathcal{H}}$ and d_{ij}^{η} distributions, which suggests that the entropy MRFs distinguish the networks slightly better than the other response functions. This is reflected in the fact that the weight w_S is larger than $w_{\mathcal{H}}$ and w_{η} .

In Fig. 6.11, we show the distance matrices $\mathbf{D}^{\mathcal{H}}$, \mathbf{D}^S , \mathbf{D}^{η} , and \mathbf{D}^p . We have block-diagonalized the distance matrices by reordering the nodes to maximize the cost function

$$\Phi = \frac{1}{N} \sum_{i,j=1}^N X_{ij} |i - j|, \quad (6.15)$$

which weights each matrix element with its distance to the diagonal ($X \in \{d^{\mathcal{H}}, d^S, d^{\eta}, d^p\}$). Figure 6.11 also suggests that the distance d_{ij}^S better separates the networks than the distances $d_{ij}^{\mathcal{H}}$ and d_{ij}^{η} and it appears from this figure that d_{ij}^S might separate the networks better than the PCA distance d_{ij}^p . However, we demonstrate in Section 6.5.4 that this is not the case: the PCA distance d_{ij}^p provides the best measure that we have investigated for separating the networks into categories.

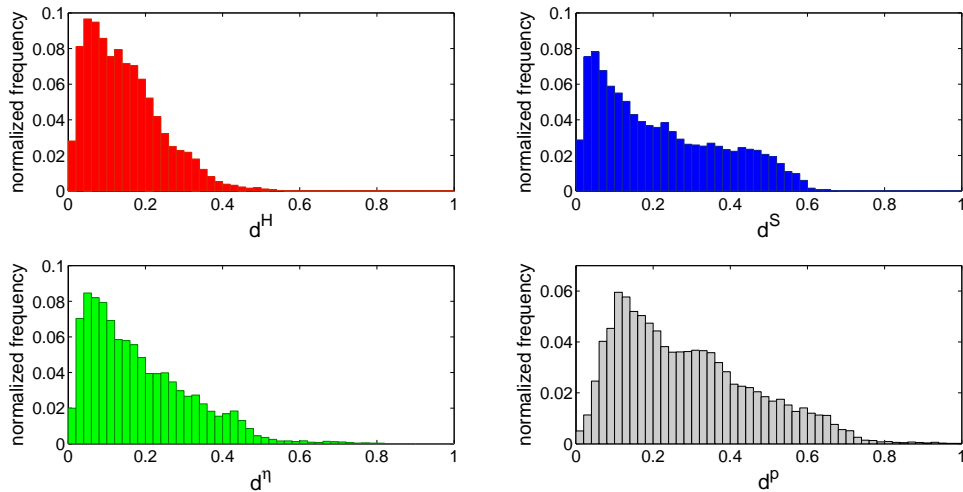


Figure 6.10: Distributions of the distances d_{ij}^H , d_{ij}^S , d_{ij}^η , and d_{ij}^p .

The block structure of the distance matrices in Fig. 6.11 suggests the existence of different clusters of networks. However, for these clusters to be meaningful it is important that the distance measures we define for comparing networks are robust to small perturbations in network structure. Because many networks are obtained empirically, it is expected that the network data will contain false positive and negative links; that is, there will be links erroneously included in the network that do not exist, and links that do actually exist will be erroneously omitted from the network.

To test the robustness of our distance measures with respect to such false positive and negatives, we recalculate the MRFs for a subset of unweighted networks in which some percentage of the links have been rewired. We investigate two rewiring mechanisms: one in which the degree distribution and connectivity of each network is maintained and another in which only the connectivity is maintained. We provide details of the analysis of the sensitivity of the distance measures to false positive and negative links in Appendix E. We find in both cases that the block structure in the distance matrices is robust to random perturbations of the networks. This implies that the MRF distance measures we define in Section 6.4 are robust and can be used to identify networks with similar mesoscopic structures across multiple scales.

6.5 Clustering networks

We now use the distance matrices \mathbf{D}^H , \mathbf{D}^S , \mathbf{D}^η , and \mathbf{D}^p to cluster networks. Before presenting network taxonomies, we provide some additional details that we use to

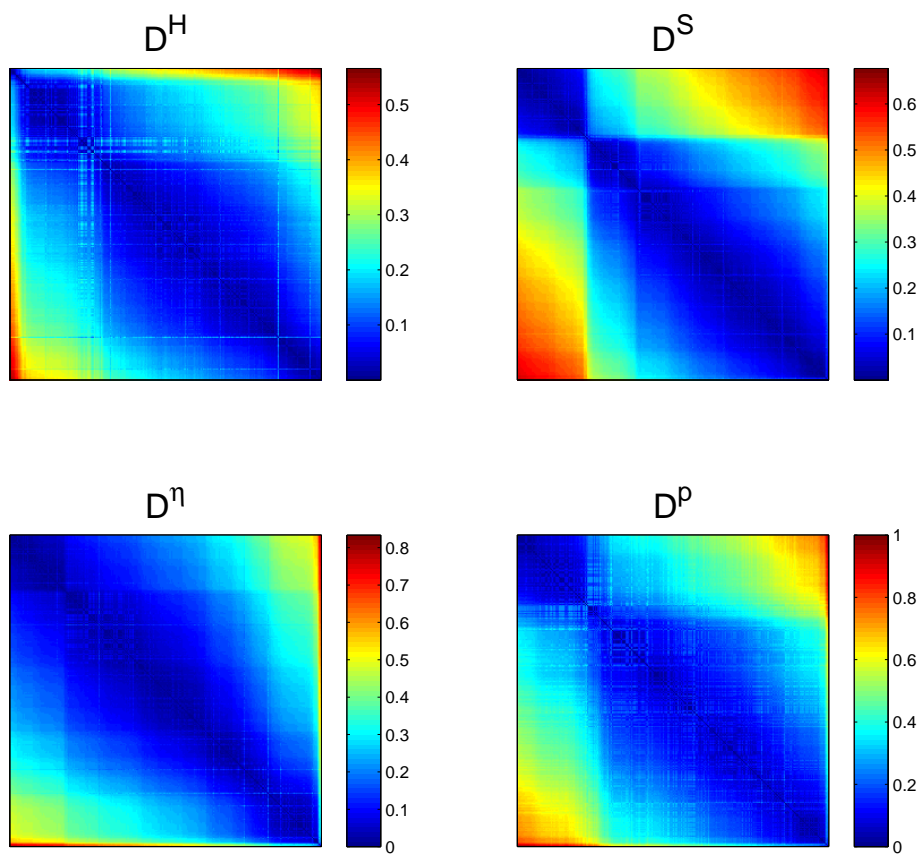


Figure 6.11: Block-diagonalized distance matrices D^H , D^S , D^η , and D^p .

study the clusters.

6.5.1 Network categories

We assign each of the networks to a family group that describes the type of network (see Table 6.1). One of the primary reasons for assigning each network to a category is to use this external categorization to help assess the quality of the taxonomy that is produced by the unsupervised MRF clustering. The assignment of the networks to one of these groups is subjective because several of the networks could belong to more than one category. For example, one could categorize the network of hyperlinks between blogs on U.S. politics [3] as a WWW network or a citation network, and one could categorize the network of jazz musicians [125] as a collaboration network or a social network. The initial selection of network categories is of course then also subjective. One could argue that if one has a social network category, then it is not necessary to have a collaboration network category as well because collaboration networks are merely a subset of social networks. However, in choosing the network categories, we have attempted to maintain a balance between having enough categories to make it possible to understand the differences that lead to the network clusters without having so many categories that it is impossible to discern the essential differences.

6.5.2 Selecting a subset of networks

We analyze a total of 714 networks (see Table C.1 for the full list); because of the data that is available, the networks are not evenly distributed across categories (see Table 6.1). Many of these networks are either different time-snapshots of the same network or different realizations of the same type of network.¹² For example, we include 110 roll-call voting networks for different sessions of the U.S. House of Representatives [203, 241, 306] and 100 Facebook networks for different U.S. universities [295]. In some of the analysis we present, we only study a subset of networks to have a more balanced set across different categories. One of the primary reasons for doing this is to keep the dendrograms readable. However, it is also true that to understand where a particular type of networks lies in the taxonomy it is often necessary only to include a representative subset of networks of that type. Therefore, for some of the analysis, we focus on a subset of 270 networks (which we highlight in Table C.1).

¹²We analyze intra-category taxonomies in Section 6.9.

Table 6.1: Network categories and the number of networks assigned to each category. See Table C.1 for the identities of the networks.

Category	No. of networks
Synthetic	64
Social	26
Facebook	100
Political: voting	285
Political: cosponsorship	26
Political: committee	16
Protein interaction	22
Metabolic	43
Brain	12
Fungal	12
Financial	69
Language	8
Collaboration	8
WWW	3
Electronic circuit	3
Citation	3
Trade	3
Other	11

6.5.3 Choosing a linkage clustering algorithm

For each distance measure, we construct a dendrogram for the subset of networks used in Section 6.5.2 using linkage clustering. As described in Sections 4.3 and 5.6, linkage clustering is an agglomerative hierarchical clustering technique [84, 244]. The three most common linkage clustering algorithms are single, average, and complete linkage clustering, which join clusters of objects based on the smallest, average, and largest distance between objects in the clusters, respectively. We compare dendrograms constructed with the different linkage clustering algorithms using the cophenetic correlation coefficient ζ . We define t_{ij} as the distance in the dendrogram between networks i and j . For example, for a dendrogram constructed from the PCA-distance matrix \mathbf{D}^p with elements d_{ij}^p using single-linkage clustering, the distance t_{ij} between a node i in cluster \mathcal{C} and a node j in cluster \mathcal{C}' is given by (see Eq. 5.9)

$$t_{ij} = d_{\text{sing}}(\mathcal{C}, \mathcal{C}') = \min_{\substack{i \in \mathcal{C} \\ j \in \mathcal{C}'}} d_{ij}^p. \quad (6.16)$$

Similarly, for a dendrogram constructed using average-linkage clustering the distance t_{ij} is given by (see Eq. 5.10)

$$t_{ij} = d_{\text{ave}}(\mathcal{C}, \mathcal{C}') = \frac{1}{|\mathcal{C}||\mathcal{C}'|} \sum_{i \in \mathcal{C}} \sum_{j \in \mathcal{C}'} d_{ij}^p, \quad (6.17)$$

and for complete-linkage clustering by

$$t_{ij} = d_{\text{comp}}(\mathcal{C}, \mathcal{C}') = \max_{\substack{i \in \mathcal{C} \\ j \in \mathcal{C}'}} d_{ij}^p. \quad (6.18)$$

The cophenetic correlation, which measures how well each dendrogram preserves the pairwise distances between the networks, is defined as [276]

$$\zeta = \frac{\sum_{i < j} (d_{ij}^p - \bar{d}^p)(t_{ij} - \bar{t})}{\sqrt{\left[\sum_{i < j} (d_{ij}^p - \bar{d}^p)^2 \right] \left[\sum_{i < j} (t_{ij} - \bar{t})^2 \right]}}, \quad (6.19)$$

where \bar{d}^p is the mean of the distances d_{ij}^p and \bar{t} the mean value of the t_{ij} .

The cophenetic correlations for the different linkage clustering algorithms are: $\zeta_{\text{sing}} \doteq 0.65$, $\zeta_{\text{ave}} \doteq 0.78$, and $\zeta_{\text{comp}} \doteq 0.62$. This implies that dendrograms constructed using average linkage clustering preserve the distances in \mathbf{D}^p better than those constructed using the other clustering techniques, so we use average linkage clustering to construct all dendrograms in the remainder of this chapter.

6.5.4 Comparison of clusterings for different distances

We defined the PCA-distance \mathbf{D}^p as a parsimonious representation of the three distance matrices \mathbf{D}^h , \mathbf{D}^S , \mathbf{D}^η . In this section, we justify using the distance \mathbf{D}^p instead of one of the alternative distances by demonstrating that it is the most effective measure for clustering networks of the same type. To ensure that the dendrograms we construct are readable, we analyze the subset of networks described in Section 6.5.2.

6.5.4.1 Visual comparison

In Figs. 6.12–6.15, we show dendrograms that we obtained from the distance-matrices \mathbf{D}^h , \mathbf{D}^S , \mathbf{D}^η , and \mathbf{D}^p . The coloured rectangle underneath each leaf indicates the network category. Contiguous blocks of colour demonstrate that networks from the same category have been grouped together using the MRF clustering method and the presence of such contiguous colour blocks is a good indication of the success of the MRF clustering scheme. One would not always expect networks in the same category to be clustered together (especially given the subjective nature of the categories described in Section 6.5.1) and, in fact, it can sometimes be more insightful to understand why superficially similar networks are not clustered together. However, in many cases, it is reasonable to assume that closely related networks should be clustered together. A visual comparison of the dendrogram leaf colours therefore provides an indication of the effectiveness of different distance measures at clustering the networks.

An inspection of the dendrograms in Figs. 6.12–6.14 reveals that for \mathbf{D}^h all of the networks are clustered at a smaller distance than for \mathbf{D}^S and \mathbf{D}^η . By examining the dendrogram leaf colours, it appears that each measure clusters some of the categories better than the other measures. For example, \mathbf{D}^h groups the synthetic networks and fungal networks well, \mathbf{D}^S groups the brain and metabolic networks well, and \mathbf{D}^η groups the political voting and fungal networks well.

In Fig. 6.15, we show the dendrogram for the distance \mathbf{D}^p . An examination of the leaf colours in this figure demonstrates that this distance groups together networks from a variety of categories, including political voting networks, political committee networks, Facebook networks, metabolic networks, and fungal networks. Using the simple visual criterion that a reasonable distance measure is one that leads to large blocks of contiguous colour in the dendrogram, it appears that the PCA distance \mathbf{D}^p provides the best measure for separating the networks into known clusters.

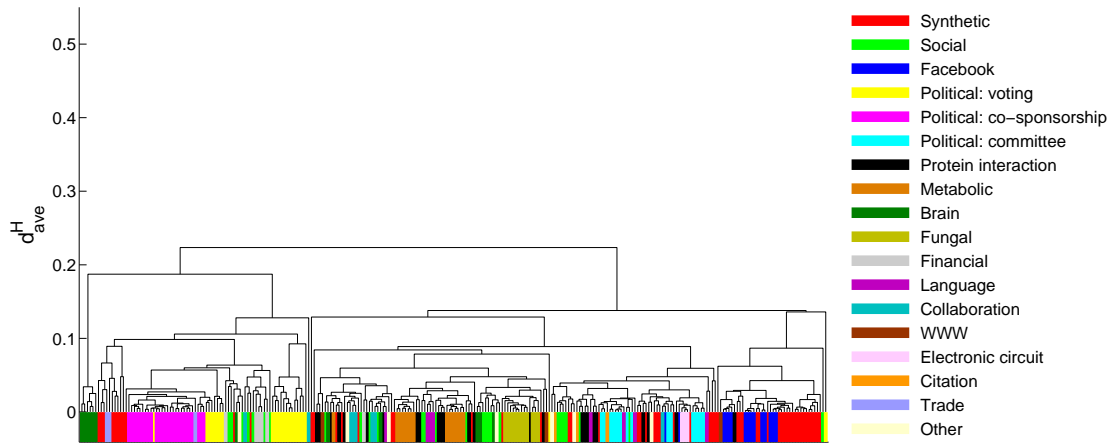


Figure 6.12: Dendrogram for the 270 networks constructed using the distance \mathbf{D}^H and average linkage clustering. We order the leaves of the dendrogram to minimize the distance between adjacent nodes and colour the leaves to indicate the type of network. The vertical scale in the dendrogram is set to the interval $[0, 0.55]$ to facilitate a visual comparison with the \mathbf{D}^S and \mathbf{D}^n dendrograms in Figs. 6.13 and 6.14. The distance d_{ave}^H at which clusters combine is given by Eq. 6.17.

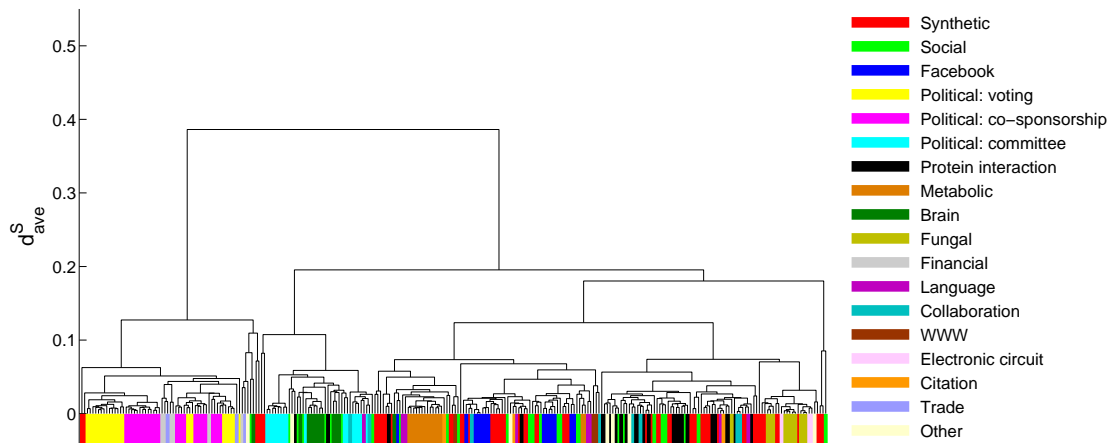


Figure 6.13: Dendrogram for the 270 networks constructed using the distance \mathbf{D}^S and average linkage clustering. We order the leaves of the dendrogram to minimize the distance between adjacent nodes and colour the leaves to indicate the type of network. The vertical scale in the dendrogram is set to the interval $[0, 0.55]$ to facilitate a visual comparison with the \mathbf{D}^H and \mathbf{D}^n dendrograms in Figs. 6.12 and 6.14. The distance d_{ave}^S at which clusters combine is given by Eq. 6.17.

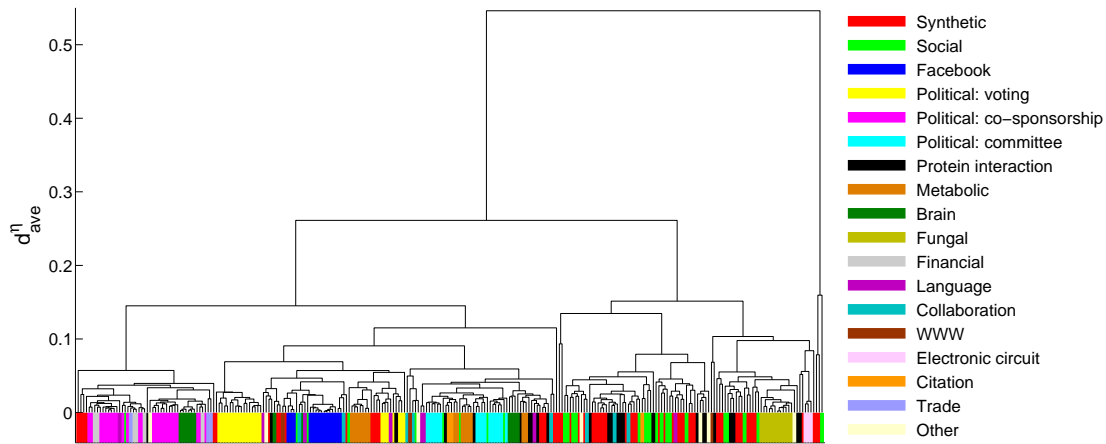


Figure 6.14: Dendrogram for the 270 networks constructed using the distance \mathbf{D}^n and average linkage clustering. We order the leaves of the dendrogram to minimize the distance between adjacent nodes and colour the leaves to indicate the type of network. The vertical scale in the dendrogram is set to the interval $[0, 0.55]$ to facilitate a visual comparison with the $\mathbf{D}^{\mathcal{H}}$ and \mathbf{D}^S dendrograms in Figs. 6.12 and 6.13. The distance d_{ave}^n at which clusters combine is given by Eq. 6.17.

6.5.4.2 Metric comparison

A visual comparison is a good starting point for assessing the effectiveness of different distance measures at clustering networks, but it is a subjective assessment. We therefore introduce a metric to quantify how effectively each distance measure clusters networks of the same type.

The assignment of networks to family categories is also subjective and some of the categories include networks of very different types (see Section 6.5.1), so it is inappropriate to assess the effectiveness of a distance measure based on how well it clusters all types of networks. Instead, we focus only on groups of networks that are clustered together in any one of the dendrograms in Figs. 6.12–6.15. This includes the following 8 categories: Facebook, metabolic, political co-sponsorship, political committee, political voting, financial, brain, and fungal networks.

For each distance measure, we construct a dendrogram and for each level of the dendrogram we calculate the maximum fraction of networks of a particular type that appear in the same cluster. That is, for a particular level of the dendrogram, we take a network category and find all clusters that contain at least one network from that category. We then calculate the fraction of networks from that category in each

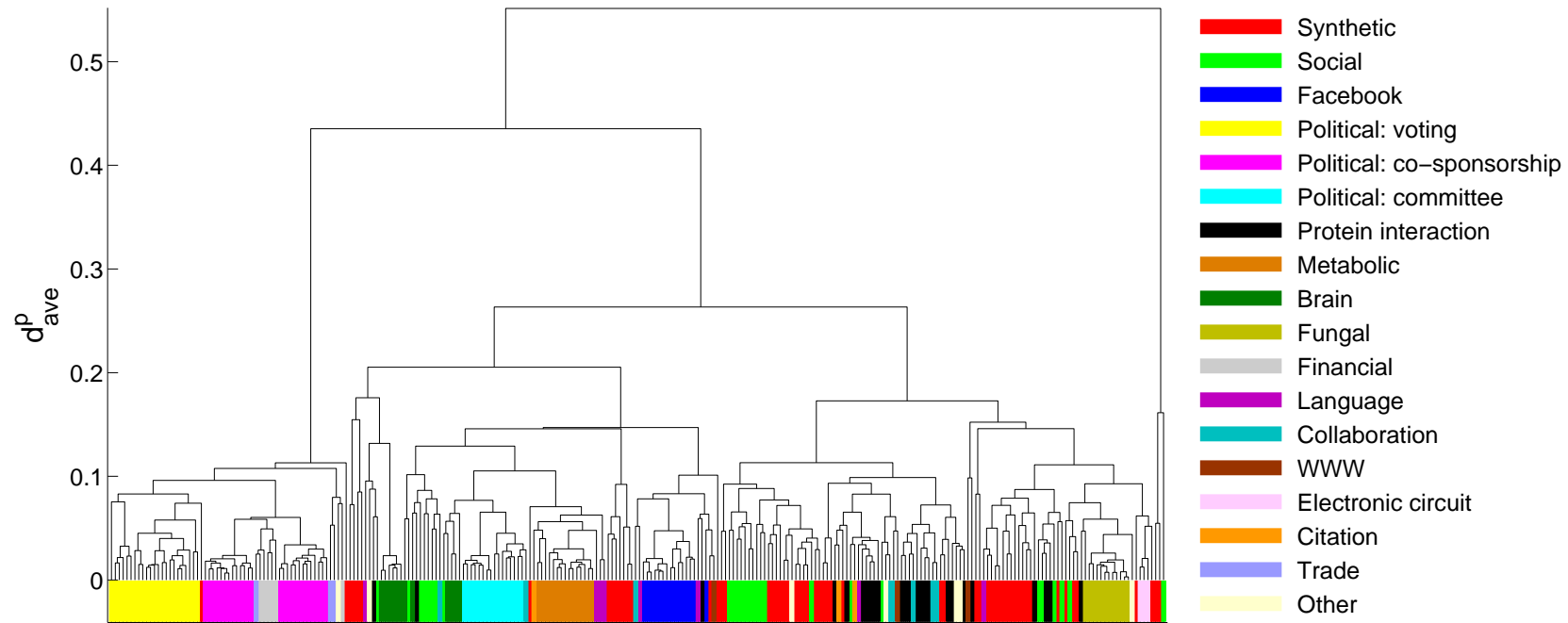


Figure 6.15: Dendrogram for the 270 networks constructed using the distance \mathbf{D}^p and average linkage clustering. We order the leaves of the dendrogram to minimize the distance between adjacent nodes and colour the leaves to indicate the type of network. A visual comparison with the \mathbf{D}^h , \mathbf{D}^s , and \mathbf{D}^n dendrograms in Figs. 6.12, 6.13, and 6.14 shows that the distance matrix \mathbf{D}^p provides a better separation of the networks into their groups. The distance d_{ave}^p at which clusters combine is given by Eq. 6.17.

of the identified clusters and find the cluster that contains the maximum fraction of networks of that type. We repeat this calculation for each network category and sum the maximum fraction over all categories. We perform similar calculations for each level of the dendrogram and use the value of the summation at each level to assess the effectiveness of the different distance measures at clustering the networks. For example, at the root of the dendrogram all of the networks are in a single cluster, so for every type of network the maximum fraction of networks in the same cluster is 1 and the value of the metric is 8 (the number of categories). However, as one moves to lower levels of the dendrogram (i.e., towards the leaves of the dendrogram) the clusters break up, so the maximum fraction of networks of each type in the same cluster decreases. If one compares the same level for dendrograms constructed using different distance measures, the sum of the maximum fraction of networks of each type in the same cluster will be larger for the more effective distance measure.

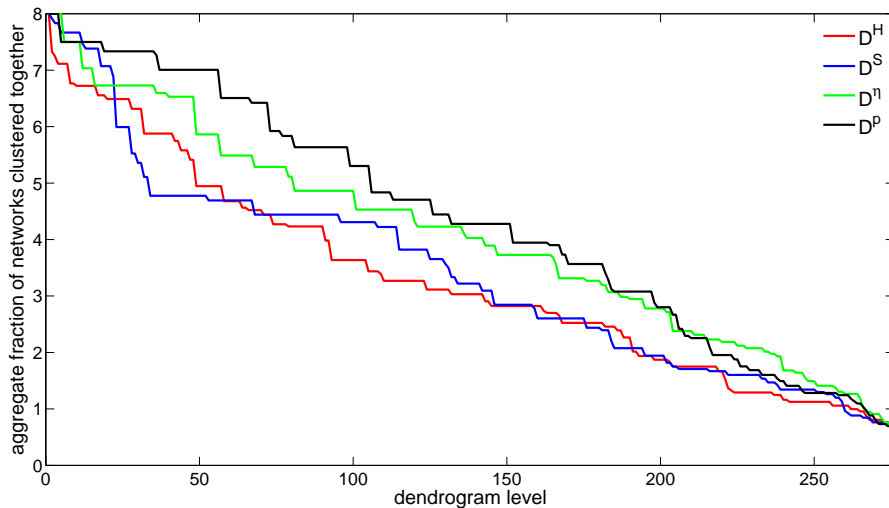


Figure 6.16: Comparison of the effectiveness of each distance measure at clustering networks of the same type. For each level of the dendrograms shown in Figs. 6.12–6.15, we calculate the maximum fraction of networks of a certain type that appear in a single cluster and we sum this fraction for networks from the following groups: Facebook, Metabolic, Political: co-sponsorship, Political: committee, Political: voting, Financial, Brain, and Fungal.

In Fig. 6.16, we compare the total fraction of networks clustered together at each level of the dendrogram for D^H , D^S , D^η , and D^P . Over most of the dendrogram levels, the PCA-distance D^P is the most effective at clustering networks of the same type,

which agrees with our visual assessment of the different distances in Section 6.5.4.1.¹³ We therefore focus on PCA-distance dendrograms for the remainder of this chapter.

6.6 Network taxonomies

6.6.1 Taxonomy of all networks

As we noted in Section 6.5.1, there is some subjectivity in selecting categories of networks and assigning networks to these categories. However, for many of the studied networks the category assignment is unequivocal, so it is insightful to consider how networks within categories are distributed across the branches of the dendrogram. In Fig. 6.17 we show a dendrogram containing leaves for all of the 714 networks studied. In this dendrogram, there are several large contiguous blocks of leaves that correspond to networks belonging to the same category. For example, there are large contiguous blocks of fungal, Facebook, metabolic, political committee, political voting, and financial networks. These blocks do not always include all of the networks within a category; when there are separate contiguous blocks for the same category, the blocks sometimes correspond to different types of networks within a category. For example, there are separate blocks of FX networks and New York Stock Exchange networks for the financial networks category. However, because of the number of networks that we include in the study and the imbalance in the spread of networks across categories, Fig. 6.17 is quite difficult to interpret and the smaller categories are obfuscated by the larger categories. Therefore, for a clearer view of the relationships between the different categories of networks, we return to considering the dendrogram in Fig. 6.15 for the subset of 270 networks.

6.6.2 Taxonomy of a sub-set of networks

In the dendrogram in Fig. 6.15 all of the networks in some categories appear in blocks of adjacent leaves. For example, there is a cluster of political voting networks at the far left of the dendrogram. This cluster includes voting networks from the U.S. Senate, the U.S. House of Representatives, the U.K. House of Commons, and the

¹³Figure 6.16 shows that at the highest and lowest levels of the dendrogram the PCA distance does not have the largest value of the metric used to assess the effectiveness of the different distances. These extreme levels correspond to most nodes in individual clusters and most nodes in the same cluster, respectively, and are not particularly insightful. The clusters that we observe over the intermediate levels of the dendrogram provide more insights into the relationships between the different types of networks; over these intermediate dendrogram levels the PCA distance is the most effective at clustering the networks.

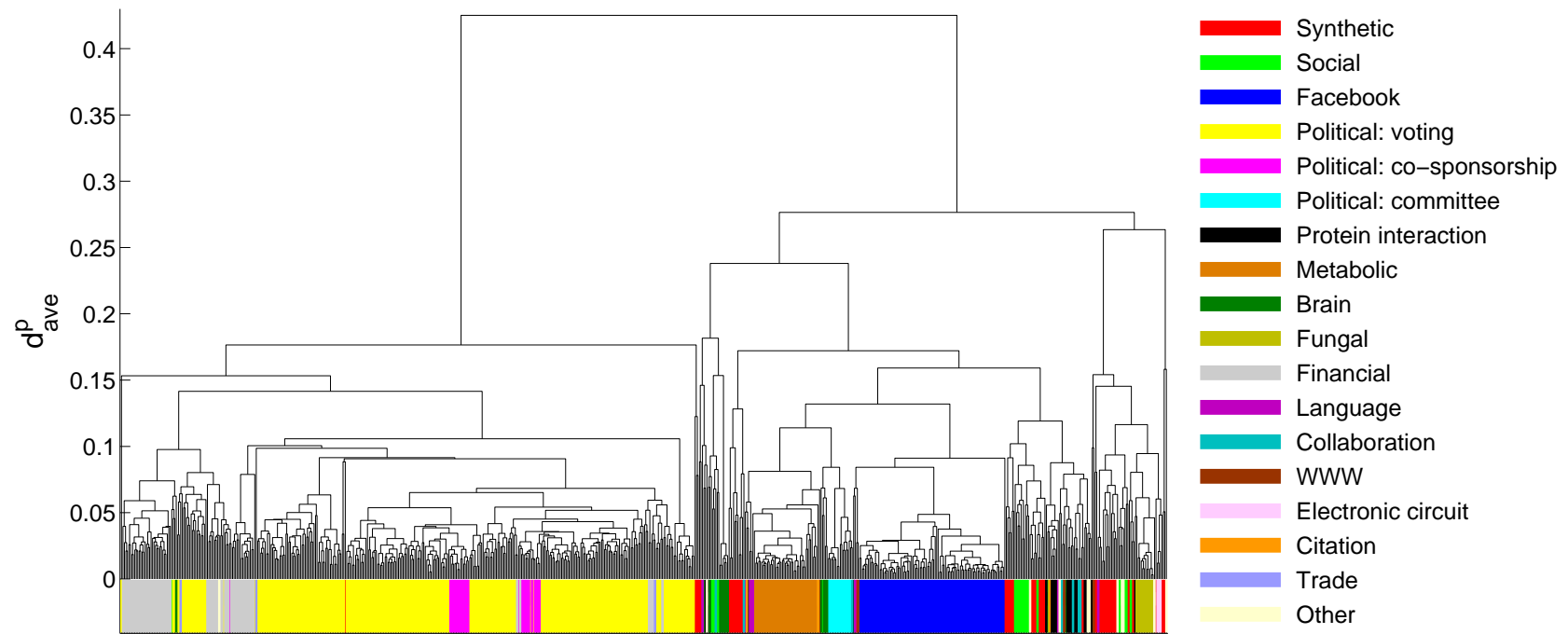


Figure 6.17: Dendrogram for the 714 networks constructed using the distance \mathbf{D}^p and average linkage clustering. We order the leaves of the dendrogram to minimize the distance between adjacent nodes and colour the leaves to indicate the type of network.

United Nations General Assembly. The clustering of these voting networks suggests that there are some common features in the MRFs that represent universal properties of the different parliaments and legislatures. We also obtain single blocks that consist of all political committee networks and all metabolic networks.

The political cosponsorship networks are split into two blocks that are separated by a cluster of financial and trade networks. The leftmost block of political cosponsorship networks consists of all of the House of Representatives cosponsorship networks, and the rightmost cluster consists of all of the Senate cosponsorship networks. There are also several categories for which all except one or two networks are clustered together in a contiguous block. For example, all but two of the fungal networks appear in the same block and all but one of the Facebook networks are clustered together. The isolated Facebook network is the Caltech network (which is the smallest network of this type), and it appears in a cluster next to the cluster containing all of the other Facebook networks.

There are other categories of network that do not appear in near-contiguous blocks. For example, protein interaction networks appear in several clusters. These networks represent interactions within several different organisms, so one might not expect all of them to be clustered together. However, there are also examples of protein interaction networks for the same organism in which the interactions were identified using different experimental techniques that are not clustered together. This supports previous work that suggests that the properties of protein interaction networks are extremely sensitive to the experimental procedure used to identify the interactions, e.g., [145, 313].

Social networks are also distributed throughout the dendrogram. This is unsurprising given the extremely broad nature of the category: the social network category includes networks of very different sizes with links representing a rather diverse range of social interactions (see Table C.1 for details of the different networks). The leftmost outlying social network is the network of Marvel comic book characters, which is arguably not a typical social network. Finally, the synthetic networks appear in clusters in different regions of the dendrogram, which is again unsurprising given that many of these graphs were developed to model systems with very different characteristics.

It is also worth highlighting the initial split of the dendrogram into two clusters. One of the clusters contains only three networks, whereas the other cluster contains all of the other networks. This suggests that the three networks in the smaller cluster possess unusual mesoscopic structures. The three networks are the NCAA football

schedule network [61] and two fractal networks [279]. The key feature that distinguishes these networks from most of the other networks are their degree distributions. For each of the networks in the small cluster all of the nodes have one of a limited number of possible degrees; for example, in the NCAA football networks, all but one of the nodes have a degree of 12 or 13. Such degree distributions result in MRFs that contain several plateaus (see Section 6.3.1) and lead to large distances between these networks and the other networks in the taxonomy.

The observations in this section demonstrate that the MRF framework is able to cluster categories of networks that are known to have similar structures, which verifies the effectiveness of this technique. However, sometimes networks that one might expect to be similar are not clustered together. These outliers might correspond to anomalous members of a class of networks, so understanding the differences in their structure is potentially insightful.

6.6.3 Taxonomy of network categories

In the previous sections, we applied the MRF clustering framework to individual networks. We now establish a taxonomy of network categories. We consider all empirical network categories for which we have 8 or more networks.¹⁴ In Fig. 6.18, we show the range of the \mathcal{H}_{eff} , S_{eff} , and η_{eff} MRF curves for each category. Figure 6.18 demonstrates that the MRFs for some classes of networks (such as political co-sponsorship and metabolic networks) are very similar, whereas there are large variations in the MRFs for other categories (such as social and protein interaction networks). The range of different MRFs for the social and protein interactions explains why these networks are scattered throughout the dendrogram in Fig. 6.15. Despite these differences, it is instructive to create a taxonomy of network categories.

We compute average intra-class MRFs for each category by calculating the mean of \mathcal{H}_{eff} , S_{eff} , and η_{eff} over all networks within the category, and create a PCA-distance matrix and taxonomy using the MRFs. At the highest level, the dendrogram in Fig. 6.19 is split into two clear clusters. The lower of the two clusters contains financial, political voting, and political cosponsorship networks. All of these networks are constructed from measures that characterize the similarity of nodes in the networks; as this measure can be computed between any two nodes, these networks are typically weighted and fully connected. The upper cluster contains all of the other categories. The clear outlier in this cluster is the fungal networks, which are not closely related

¹⁴We do not consider synthetic networks because these networks are designed to model networks with very different characteristics, so do not form a coherent category.

to any of the other categories. This observation is unsurprising given the tree-like structure of fungal networks [33]. The other categories of networks within this cluster appear to be more closely related. For example, protein interaction networks cluster with collaboration networks, Facebook networks cluster with language networks, and metabolic networks cluster with social networks.

It is tempting to speculate on the reasons for these similarities, but the taxonomy needs to be treated with some caution because of the differences in the intra-class MRFs highlighted in Fig. 6.18. Nonetheless, Fig. 6.19 does suggest that networks that are clustered together have some similarities in their mesoscopic structures; consequently, a detailed comparison of the properties of networks from related categories might help to identify common structures that support the functions of the different types of networks. In addition, the taxonomy in Fig. 6.19 might also help to identify network analysis techniques that might fruitfully be applied to a particular network. For example, if biologists have developed techniques that provide insights into protein interactions networks, the same techniques might successfully be applied to collaboration networks.

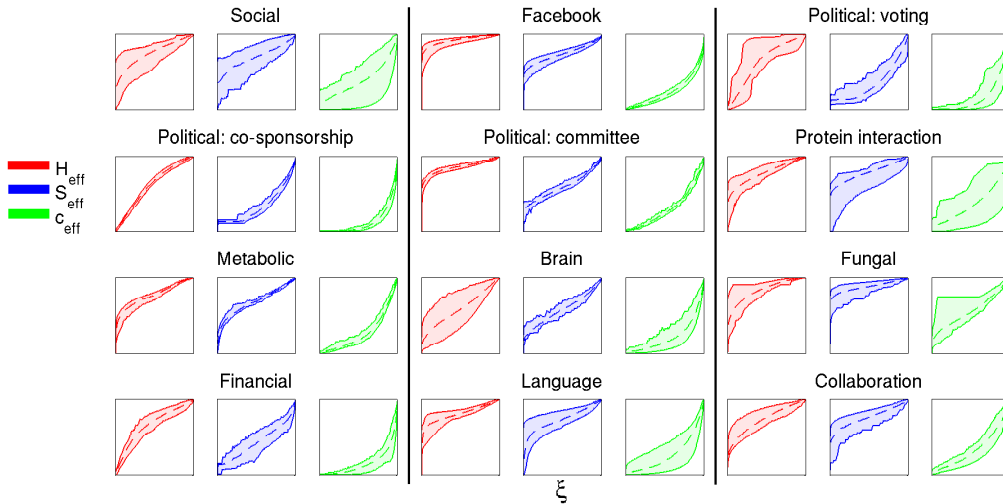


Figure 6.18: MRFs for all of the network categories containing 8 or more networks (see Table 6.1). At each value of ξ , the upper curve shows the maximum value of \mathcal{H}_{eff} , S_{eff} , or η_{eff} for all networks in the category, the dashed curve shows the mean, and the lower curve shows the minimum value.

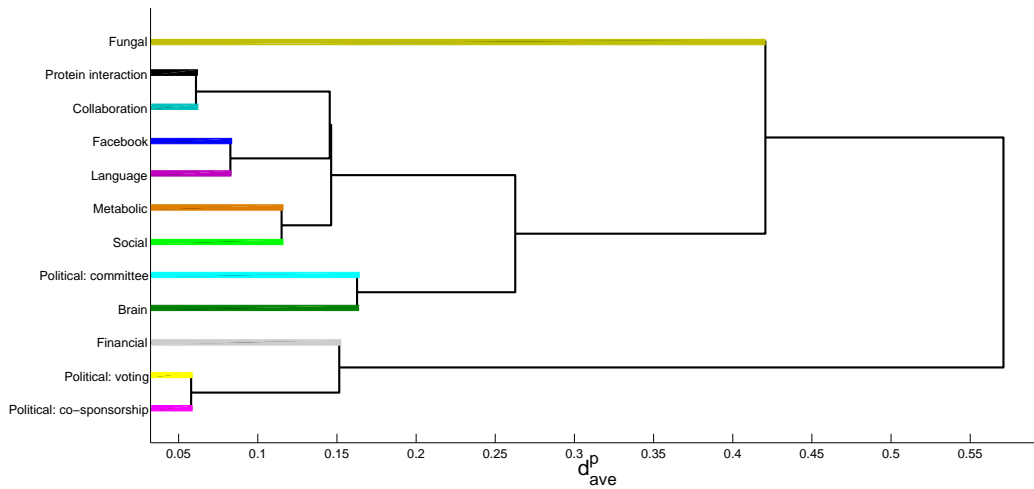


Figure 6.19: Taxonomy of network categories based on the average intra-class MRFs. The dendrogram is constructed using the distance \mathbf{D}^p and average linkage clustering. We order the leaves of the dendrogram to minimize the distance between adjacent nodes

6.6.4 Comparison with prior clusterings

It is also worthwhile to compare the clusters that we identify with those found in the prior studies of Milo *et al.* [210] and Guimerà *et al.* [142] discussed in Section 4.5. Such a comparison is difficult because, although we study many more networks, we do not include all of the networks used in the other studies because they are not all publicly available. Nevertheless, we can make some comparisons of the clusterings. We cluster all but one of the language networks studied by Milo *et al.* in the same cluster, but we study the undirected versions of these networks whereas Milo *et al.* studied the directed networks.¹⁵ These networks are not clustered with other networks in the language category, which are distributed throughout the dendrogram. However, scrutiny of the language category in Table C.1 shows that the language networks are constructed from very different sources, so it is unsurprising that they are not clustered. We only include a single airline network but, in contrast to the study of Guimerà *et al.*, this network is not clustered with the metabolic networks. In further contrast to the work of Guimerà *et al.*, the MRF framework does not cluster all protein interaction networks in the same cluster. Importantly, as stated above, we include protein networks that have been derived using different experimental techniques, so

¹⁵The network that appears in a different cluster is the English word adjacency network [210].

their appearance in different clusters is unsurprising.

We are only able to make a few comparisons of the different clustering frameworks because of the differences in the networks used in each study. To perform a more meaningful comparison it would be necessary to repeat the analyses of Refs. [210] and [142] using a larger set of networks.

6.6.5 Synthetic networks

It is also insightful to consider the cluster membership of the synthetic networks. The set of synthetic networks we study includes a wide range of networks models and benchmark networks introduced to test community detection algorithms (see Appendix C for a detailed description of the networks). An understanding of the similarities between the MRFs for real and synthetic networks is important because if a synthetic network has a similar MRF to a real-world network, the generative mechanism used to produce the synthetic network might help in understanding the structure of the real-world network.

In Fig. 6.20, we redraw the dendrogram in Fig. 6.15 with two colour bars under each leaf: the upper bar indicates the network category and the lower bar indicates the type of synthetic network. Figure 6.20 shows that the fractal networks are distributed throughout the dendrogram, whereas the other synthetic networks tend to be localized in particular clusters. There is only one synthetic network in the left-most cluster of the dendrogram, which contains weighted, fully-connected networks constructed from similarity measures. We include random fully-connected networks in the study but, despite having similar fractions of edges present, the MRFs of these networks are not similar to those for real-world fully-connected networks. Many of the synthetic networks lie in similar regions of the dendrogram. For example, there is a group including LF benchmark, LFR benchmark, KOSKK model, ER, and H13-4 benchmark networks near the centre of the dendrogram. We study a wide range of synthetic networks (and many of the most widely studied models), but we have not included an exhaustive set and consequently we need to be careful not to make any too strong statements based on the synthetic networks¹⁶. However, the absence of any synthetic networks in many regions of the dendrograms suggests that, in terms of mesoscopic structure, current network models are not representative of the full set of real-world networks.

¹⁶Of course, this is also true of the real-world networks.

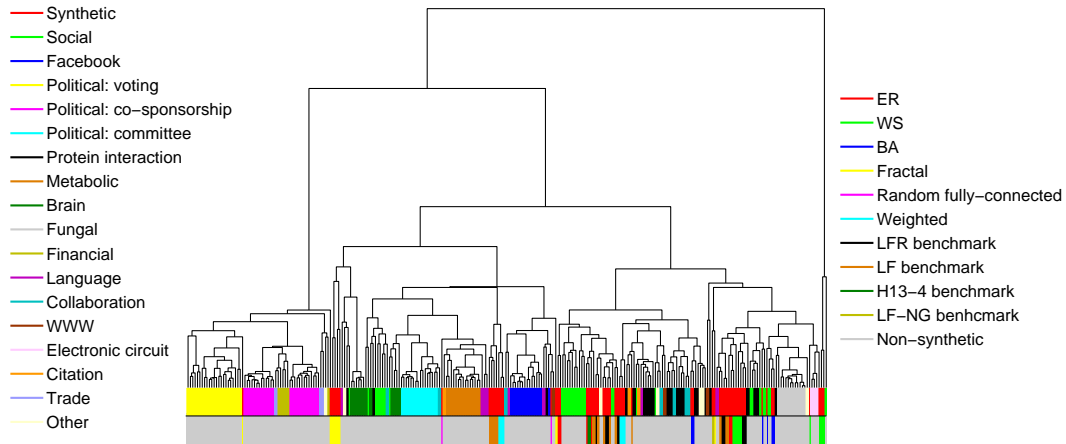


Figure 6.20: Dendrogram for the 270 networks constructed using the distance d_{ij}^p and average linkage clustering. We order the leaves of the dendrogram to minimize the distance between adjacent nodes. The upper colour bar indicates the type of network and the lower colour bar shows all non-synthetic networks in grey and highlights the position in the dendrogram of different types of synthetic network (see Appendix C for a description of the networks).

6.7 Clustering networks using other properties

Having established that the MRF framework produces a sensible clustering of networks, we now check that the observed taxonomy cannot be explained using simpler summary statistics.

6.7.1 Simple network statistics

Perhaps the three simplest properties of an undirected network are whether it has weighted or unweighted links, the number of nodes N , and the fraction of possible edges that are present (which is given by $2L/[N(N-1)]$). In Fig. 6.21, we again reproduce the dendrogram in Fig. 6.15 but now include a coloured bar under the leaves for each of these properties. The top coloured row in Fig. 6.21 indicates that many of the weighted networks are clustered together at the far left of the dendrogram. However, there are also weighted networks scattered throughout the dendrogram, so whether a network is weighted or unweighted does not explain the observed clustering. The third coloured row provides a clearer explanation for the leftmost cluster: these are not simply weighted networks, they are in fact weighted networks that contain all

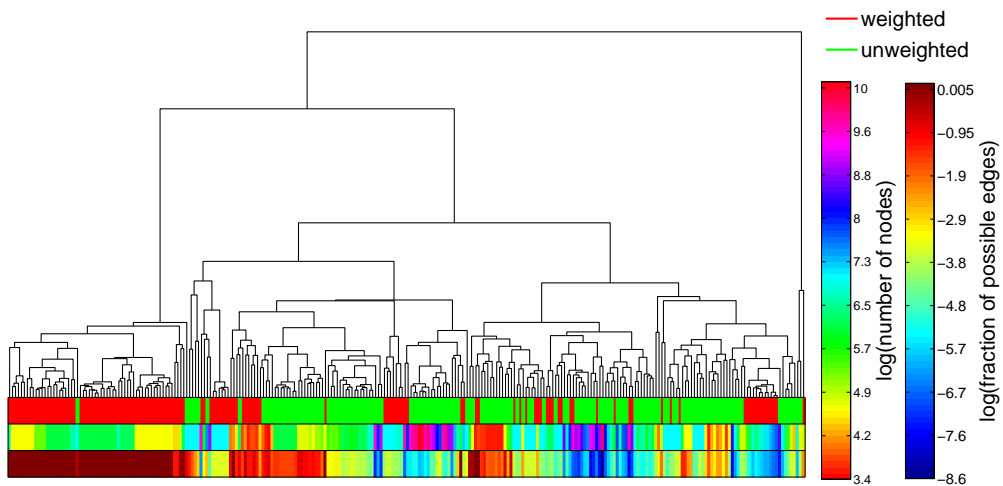


Figure 6.21: Dendrogram for the 270 networks constructed using the distance d_{ij}^p and average linkage clustering. We order the leaves of the dendrogram to minimize the distance between adjacent nodes. The three colour bars below the dendrogram indicate (top): whether the network corresponding to each leaf is weighted or unweighted, (middle) the number of nodes in the networks, and (bottom) the fraction of possible edges that are present. These colour bars clearly demonstrate that although some of the clustering in the dendrogram is attributable to these simple properties, they cannot explain much of the observed structure.

(or nearly all) possible edges¹⁷. Again, however, this property alone cannot explain the observed clusters, as several of the weighted networks that possess nearly all possible links do not appear in the leftmost cluster of the dendrogram. In fact, there are many clusters in the dendrogram that contain networks with very different fractions of possible edges. The third property we consider, the number of nodes, again explains some of the clustering as networks with similar numbers of nodes are clustered together in some regions of the dendrogram; however, there are also numerous examples in which networks with the same number of nodes appear in different clusters. Therefore, none of these simple network metrics can explain the observed clustering.

6.7.2 Strength distribution

We also consider whether we can obtain a better taxonomy using microscopic network properties. Of course, our original objective was to cluster networks based on their mesoscopic structure, but it is nonetheless informative to compare the MRF clustering with a clustering obtained using microscopic properties. The most widely studied microscopic property is the vertex degree which has been found to follow a heavy-tailed distribution in many empirically observed networks [9, 217]. Here we use the strength distribution (i.e., the generalization of the degree distribution to weighted networks) to compare networks. We denote the cumulative strength distribution of the network i as $F_i(k)$, which is the probability that the strength of a randomly sampled node is greater than or equal to k . We then define the distance d_{ij}^d between the strength distributions of networks i and j as the Kolmogorov-Smirnov statistic [42]

$$d_{ij}^d = \sup_k |F_i(k) - F_j(k)|, \quad (6.20)$$

where \sup denotes the supremum, and we represent these distances in matrix form as \mathbf{D}^d .

In Fig. 6.22, we show the dendrogram constructed using \mathbf{D}^d . In Fig. 6.23, we use the metric described in Section 6.5.4.2 to compare the effectiveness of \mathbf{D}^d and the PCA-distance \mathbf{D}^p at clustering groups of networks belonging to the same category (see Section 6.5.4.2). Figure 6.23 demonstrates that the PCA-distance performs better than the strength distribution distance. In addition, the wealth of similar heights of the branches in the dendrogram in Fig. 6.22 indicates that the strength distribution

¹⁷This cluster contains the networks constructed from similarity measures that we discussed in Sections 6.6.5 and 6.6.3.

clustering is not very robust because very slight methodological differences might lead to large differences in the clusters.

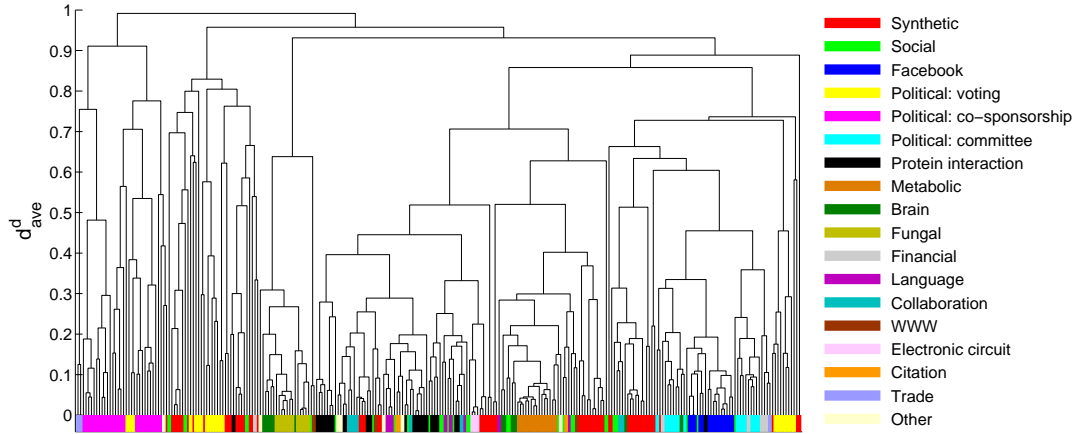


Figure 6.22: Dendrogram for the 270 networks constructed using the distance between the strength distributions of the networks and average-linkage clustering. We order the leaves of the dendrogram to minimize the distance between adjacent nodes and colour them to indicate the type of network. The dendrogram demonstrates that clustering using the strength distribution does not separate the networks into their groups as effectively as the distance matrix \mathbf{D}^p that we obtained using MRFs. The distance d_{ave}^d at which clusters combine is given by Eq. 6.17.

6.8 Robustness of MRFs for different heuristics

In this chapter we have detected all communities by minimizing the Hamiltonian in Eq. 6.1 using a greedy algorithm [44]. However, as we noted in Sections 4.3.3 and 5.10, several alternative computational heuristics exist, so it is important to check that the MRFs and taxonomies that we produce are robust with respect to the choice of heuristic. In Appendix F, we provide a detailed analysis of the effects on the MRFs and taxonomies of using spectral [221] and simulated annealing algorithms [141] to minimize Eq. 6.1. We find small variations in the MRFs generated for the different algorithms, but these differences have very little effect on the resulting dendrograms. The taxonomies that we observe are therefore robust with respect to the choice of optimization heuristic.

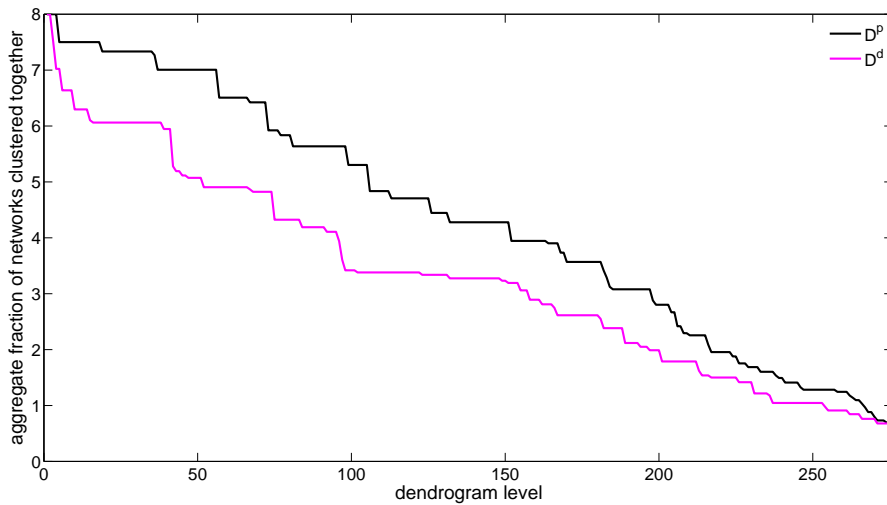


Figure 6.23: Comparison of the effectiveness of the PCA-distance \mathbf{D}^p and the strength distribution distance \mathbf{D}^d at clustering networks of the same type. For each level of the dendrograms shown in Figs. 6.15 and 6.22, we calculate the maximum fraction of networks of a certain type that appear in a single cluster and we sum this fraction for networks from the following groups: Facebook, Metabolic, Political: co-sponsorship, Political: committee, Political: voting, Financial, Brain, and Fungal.

6.9 Case studies

Thus far, we have used the MRF framework to create taxonomies of large sets of networks of different types. We now cluster individual families of networks in order to demonstrate that our method can generate meaningful intra-class taxonomies. We present a number of case studies in which we cluster groups of networks that represent different time snapshots of the same system and groups of network that represent multiple realizations of the same system. Networks in each of these families could be studied using field-specific methods, but this approach would not make it possible to relate different families to each other. By comparing the results of the MRF framework with those obtained using methods specific to the relevant field we can further verify that the MRF approach produces meaningful results.

6.9.1 U.S. Congressional roll-call voting

We first consider roll-call voting in the U.S. Congress, which is the legislative branch of the U.S. federal government. Congress is formed of two chambers: the Senate and the House of Representatives. The current Congress consists of 100 senators and

435 members of the House. We analyze roll-call voting for the 1st–110th Congresses, covering the period 1789–2008. We construct networks from the roll call data [241] for each two-year Congress as follows [306]. The roll calls for each chamber are encoded in an $N \times b$ matrix \mathbf{M} , in which each element M_{ik} equals 1 if legislator i voted yea on bill k , -1 if the legislator voted nay, and 0 otherwise. We are interested in characterizing the similarities between legislators, so we transform \mathbf{M} into an $N \times N$ adjacency matrix \mathbf{A} with elements

$$A_{ij} = \frac{1}{b_{ij}} \sum_k \alpha_{ijk}, \quad (6.21)$$

where $\alpha_{ijk} = 1$ if legislators i and j voted the same on bill k and 0 otherwise, and b_{ij} is the total number of bills on which i and j both voted [243, 306]. The elements A_{ii} all equal 1, indicating the perfect similarity between each legislator’s voting record with himself/herself. We set all $A_{ii} = 0$ to remove self-edges. The matrix \mathbf{A} , with elements A_{ij} in the interval $[0, 1]$, then represents a network of weighted ties between legislators, where the weights are determined by the similarity of their roll-call voting over a single two-year Congress. Following Ref. [241], we only consider “non-unanimous” roll call votes, where a roll call vote is considered “non-unanimous” if more than 3% of the legislators are in the minority.

6.9.1.1 Party polarization

For each Congress, we calculate MRFs for both the House and Senate and cluster the Congresses for each chamber by comparing the MRFs. In Figs. 6.24(a) and 6.24(b), we show dendrograms for the House of Representatives and Senate, respectively. Much work on the U.S. Congress has been devoted to the extent of partisan polarization, the influence of party on roll-call voting, and the degree to which this has varied over time (see Refs. [203, 306] and references therein). In highly-polarized legislatures, representatives tend to vote along party lines, so there are strong similarities in the voting patterns of members of the same party, and strong differences between members of different parties. In contrast, during periods of low polarization, the party lines become blurred and there are greater similarities in the voting patterns of members of different parties.

We use the notion of party polarization to understand the taxonomy of Congresses shown in Figs. 6.24(a) and 6.24(b). We consider two measures of polarization. The first uses DW-Nominate scores, a multi-dimensional scaling technique that is very popular among political scientists [203, 241]. The DW-Nominate polarization is

given by the absolute value of the difference between the mean first-dimension DW-Nominate scores for members of one party and the same mean for members of the other party (see Refs. [203, 241] for a detailed description of DW-Nominate scores). The problem with the DW-Nominate polarization is that it assumes a competitive two-party system and therefore cannot be calculated prior to the 46th Congress. The second measure we consider is the modularity Q , which was recently shown to be a good measure of polarization [306], even for Congresses without a clear division into parties. Modularity is given, in terms of the energy \mathcal{H} in Eq. 6.1 as

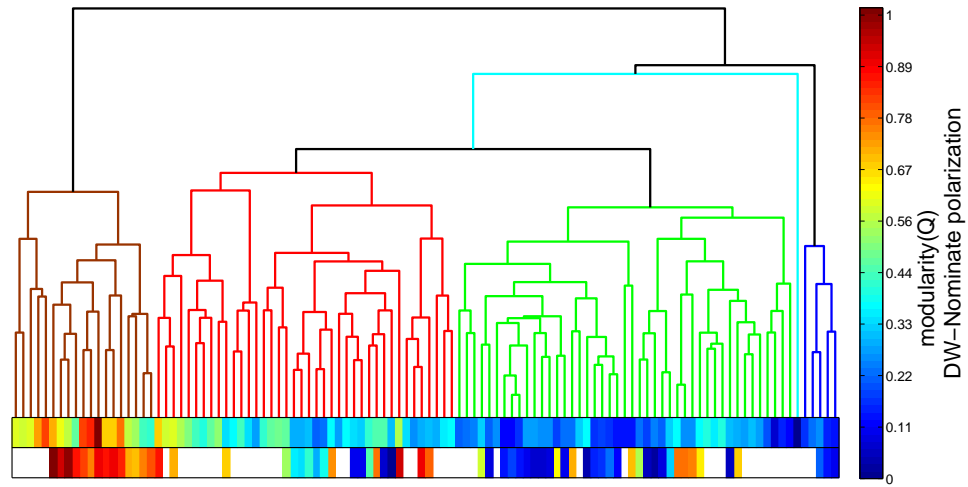
$$Q = -\frac{\mathcal{H}(\lambda = 1)}{2m}. \quad (6.22)$$

The two measures agree fairly closely on the level of polarization of each Congress for which they can both be calculated, although there are some differences [306].

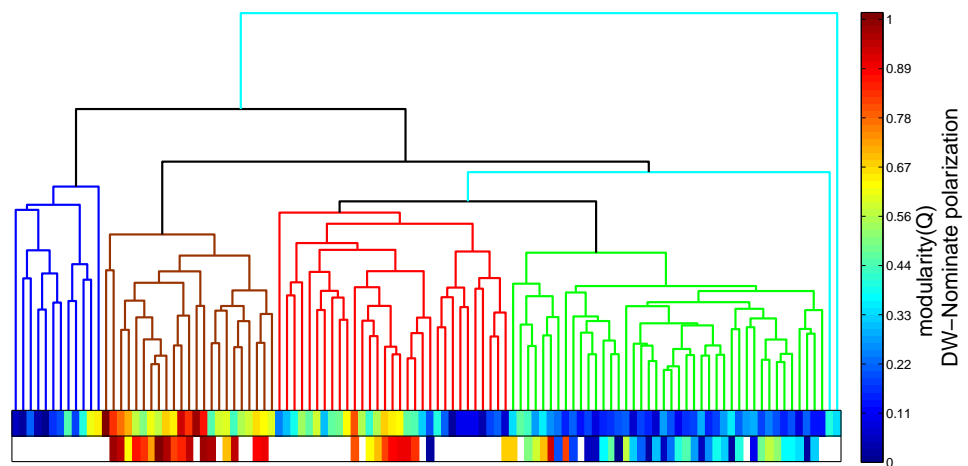
In Figs. 6.24(a) and 6.24(b), we include bars under the dendrograms that represent these polarization measures (we have normalized both measures to the interval $[0, 1]$). The bars demonstrate that (for both the House and Senate) Congresses with similar levels of polarization, as measured using both modularity and DW-Nominate, usually appear in the same cluster. This suggests that our MRF clustering technique groups Congresses based on the polarization of roll call votes. We have also coloured branches in the same cluster in the dendrogram according to the level of polarization of the corresponding Congresses, where brown indicates highly-polarized Congresses and blue less polarized Congresses.

6.9.1.2 Using MRFs to identify periods of polarization

We now consider in more detail, the Congresses lying within each cluster. In Figs. 6.25(a) and 6.25(b), we show the variation in the polarization measured using both DW-Nominate scores and modularity as a function of time. For each Congress, the height of each stem indicates the level of polarization measured using modularity. The colour of each stem indicates the cluster membership of each Congress in the dendrograms. The black curve, running from the 46th Congress onwards, shows the DW-Nominate polarization. The DW-Nominate and modularity curves suggest that the periods of maximal polarization in the House and Senate do not correspond exactly. In both chambers, the 104th – 110th Congresses are highly polarized (the 104th immediately followed the 1994 “Republican Revolution” in which the Republicans earned majority status in the House for the first time in more than 40 years [203]). However, the House has a second polarization peak from the 55th – 58th Congresses, and the Senate has a high polarization for the 46th – 51st Congresses. The MRF clustering scheme is



(a) House of Representatives



(b) Senate

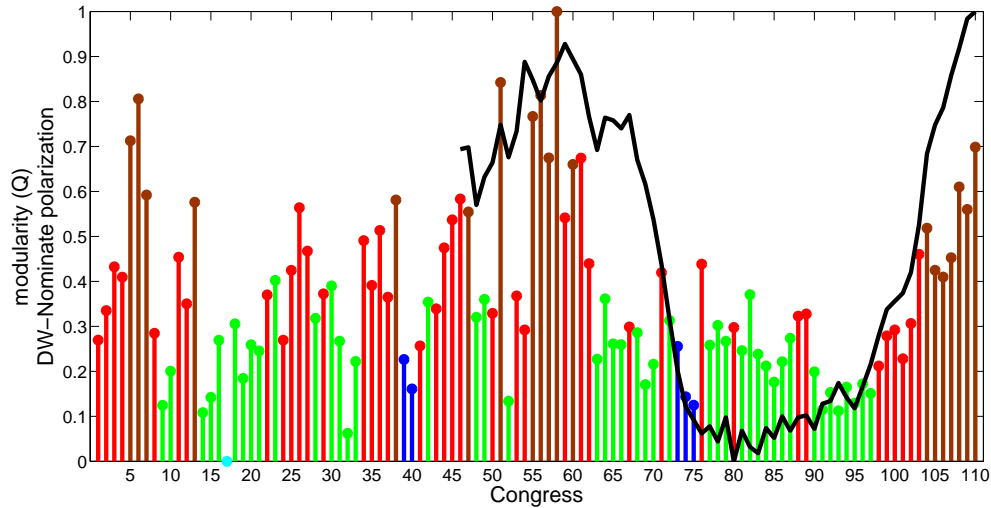
Figure 6.24: Dendrograms for (a) House of Representatives and (b) Senate roll-call voting networks for the 1st–110th Congresses (covering the period 1789–2008). Each leaf in the dendrograms represents a single Congress. The upper colour bar below the dendrograms show the polarization of the Congresses measured using modularity. The lower colour bar shows the polarization measured using DW-Nominate scores. The DW-Nominate polarization assumes a competitive two-party system and therefore cannot be calculated prior to the 46th Congress. We do not include rectangles at the leaf nodes corresponding to these earlier Congresses in the DW-Nominate colour bar. We also colour groups of branches in the dendrogram that correspond to periods of similar polarization (see the discussion in the text).

able to detect these differences. In Figs. 6.25(a) and 6.25(b), the brown stems highlight a group of Congresses that lie within the same cluster in the dendrogram. The clusters for both the House and Senate closely match the periods of high polarization identified using modularity and DW-Nominate.

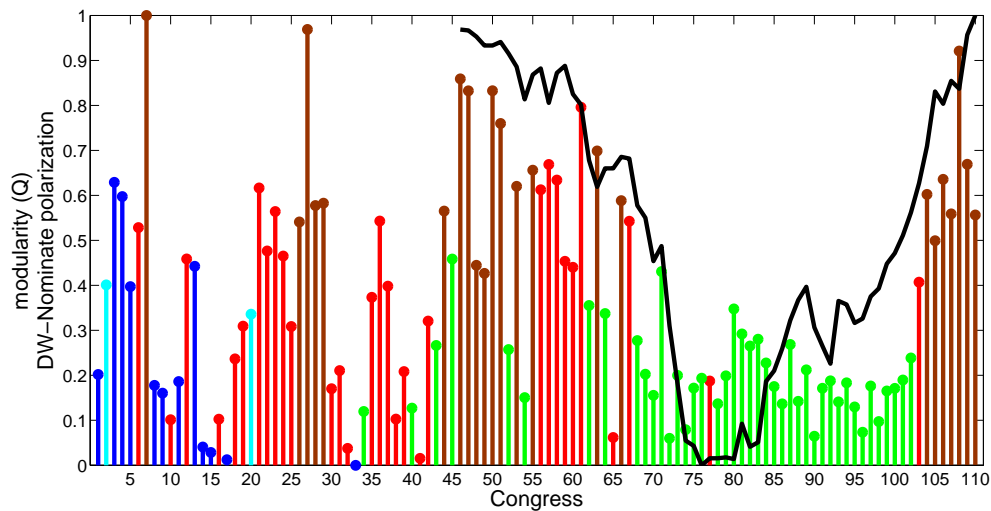
For both the House and Senate, the 104th – 110th and 55th Congresses are identified in the high-polarization cluster. As mentioned above, this first set corresponds to a period of high polarization following the 1994 elections. The 55th Congress corresponds to a period when a third party known as the Populist Party was strong. There are also several other Congressional sessions that are part of the highly polarized cluster for the House but not the Senate (and vice versa). For example, the House was also highly polarized for the 5th – 7th Congresses, which is a period following George Washington’s resignation during which John Adams headed a divided Federalist Party. The same cluster includes the 38th Congress, which occurred during the Civil War, and the 56th – 58th Congresses, when the Populist party was again strong. The highly-polarized cluster for the Senate includes the 26th – 29th Congresses. The 25th Congress saw the emergence of the Whigs and the Democratic Party and during this period, the abolitionist movement was also prevalent, with the Amistad seizure occurring in 1839 during the 26th Congress. The cluster also includes the 46th – 51st Congresses (1879-1891), which occurred during the period immediately following Reconstruction.

The MRF clustering also identifies periods during which polarization was low. We highlight these periods in green in Figs. 6.24(a)–6.25(b). The 75th – 95th Congresses are recognized as a period of party decline, during which fractionalization decreased [71]. For the House, we find that the 77th – 97th Congresses are all grouped within the same cluster. For the Senate, there is a cluster that includes the 68th – 102nd Congresses. Although this includes all of the Congresses during the period of party decline, interestingly, the cluster spans a much longer period. The House cluster also includes most of the 15th – 21st Congresses, which corresponds to the period 1817–1825 and is known as the “Era of Good Feeling” because of the decline of partisan politics. One can make similar observations for each of the other clusters identified in the dendrogram.

For each legislative chamber, it is also worth commenting on the Congresses that are not assigned to a cluster. For the House, the 17th Congress forms an isolated cluster. Using modularity, this House, which occurred during the Era of Good Feeling, seems to have an extremely low polarization. For the Senate, the 2nd and 20th Congresses form isolated clusters. The 20th Congress took place from 1827–1829 and



(a) House of Representatives



(b) Senate

Figure 6.25: Variation in the polarization of (a) the U.S. House of Representatives (b) the Senate as a function of time. The height of each stem indicates the level of polarization measured using modularity. The colour of each stem indicates the cluster membership of each Congress in the dendrograms in Fig. 6.24(a) and 6.24(b). The black curve shows the DW-Nominate polarization. We have rescaled the modularity and the DW-Nominate polarization to the interval $[0, 1]$.

included the election of 1828, which was a significant benchmark in the trend towards broader voter participation.

6.9.1.3 Effect of polarization on the MRFs

The Congresses are assigned to clusters in the dendrograms based on a comparison of their MRFs. In Figs. 6.26(a) and 6.26(b), we show the \mathcal{H}_{eff} , \mathcal{S}_{eff} , and η_{eff} response functions for the main clusters identified in the dendrograms in Figs. 6.24(a) and 6.24(b). The MRFs are assigned the same colours as the clusters in the dendrograms. For each group of Congresses, the MRFs for the House have similar shapes to the corresponding MRFs for the Senate. Figures 6.26(a) and 6.26(b) demonstrate that the main differences between clusters occur for the \mathcal{H}_{eff} response functions. For the most polarized Congresses, there is a sharp shoulder in the \mathcal{H}_{eff} MRF, which becomes less pronounced as the polarization decreases.

Figure 6.27 helps to explain this behaviour. We compare the \mathcal{H}_{eff} MRFs for the 85th and 108th Houses, which have very low and very high polarization, respectively. The shoulder in the \mathcal{H}_{eff} curve for the highly polarized 108th House is very pronounced, which can be explained by considering the distribution of Λ_{ij} values. Figure 6.27 shows that for the highly polarized 108th House, the Λ_{ij} distribution is bimodal, with the trough between the peaks occurring at $\Lambda_{ij} = 1$. Recall that $\Lambda_{ij} = A_{ij}/P_{ij}$, so Λ_{ij} compares the observed voting similarity A_{ij} of legislators i and j with the similarity $P_{ij} = k_i k_j / (2m)$ expected from random voting. Any $\Lambda_{ij} < 1$ then correspond to legislators i and j that vote differently a large fraction of the time, and any $\Lambda_{ij} > 1$ to legislators that vote the same a large fraction of the time. The two peaks in the Λ_{ij} distribution above and below 1 therefore correspond, respectively, to intra-party and inter-party voting similarities. For a Congress with low polarization, legislators from different parties often vote in the same manner, so there is no separation of the distribution on either side of $\Lambda_{ij} = 1$. These differences in the Λ_{ij} distributions are reflected in different \mathcal{H}_{eff} curves, which can then be used to cluster the Congresses.

6.9.2 United Nations General Assembly voting

In this section, we consider voting on resolutions in the United Nations General Assembly (U.N.G.A.) [194, 302]. The U.N.G.A. is one of the five principal organs of the United Nation (U.N.) and the only one in which all member nations have equal representation. Most General Assembly (G.A.) resolutions are not legally or practically enforceable because the G.A. lacks enforcement powers on most issues, so

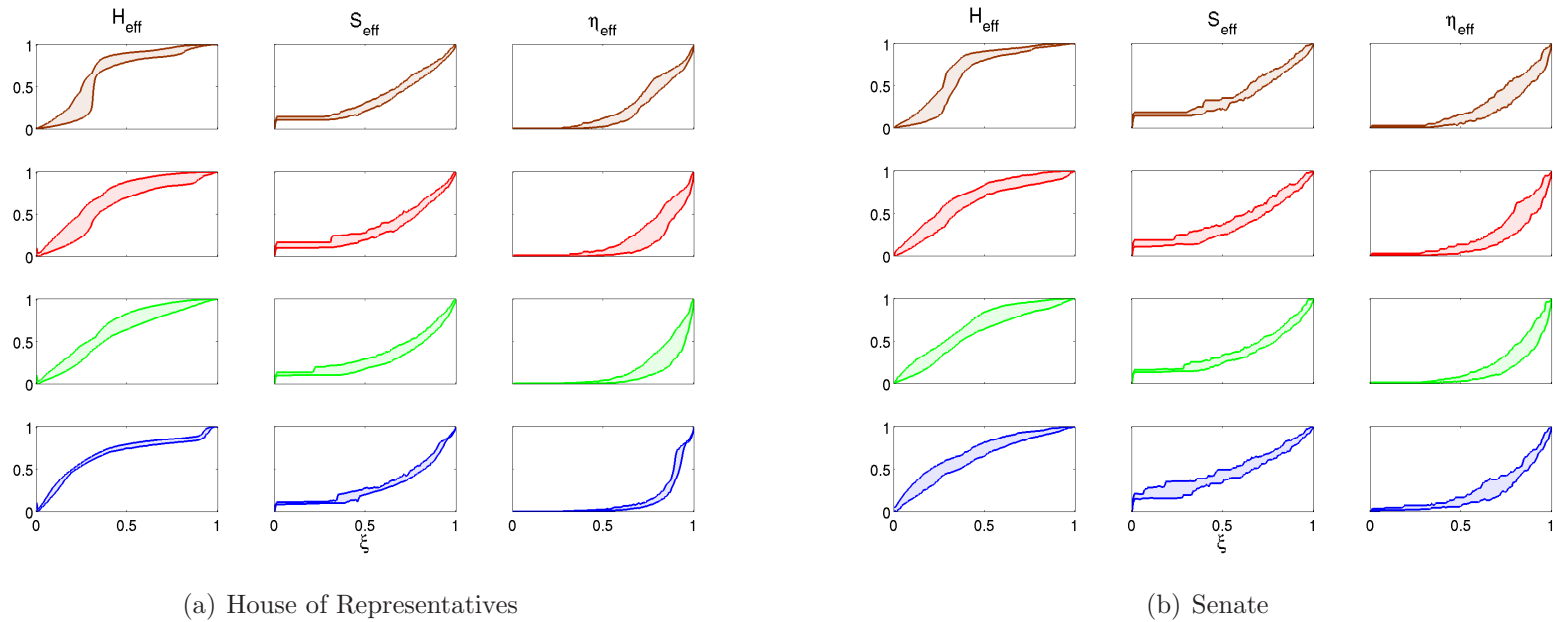


Figure 6.26: (a) MRFs for all Houses lying in each of the main clusters in the dendrogram in Fig. 6.24(a) (b) MRFs for all Senates lying in each of the main clusters in the dendrogram in Fig. 6.24(b). The colour of each set of MRFs indicates the cluster membership of each House or Senate in the corresponding dendrogram. At each value of ξ , the upper curve shows the maximum value of \mathcal{H}_{eff} , S_{eff} , or η_{eff} for all Houses/Senates in the cluster and the lower curve shows the minimum value.

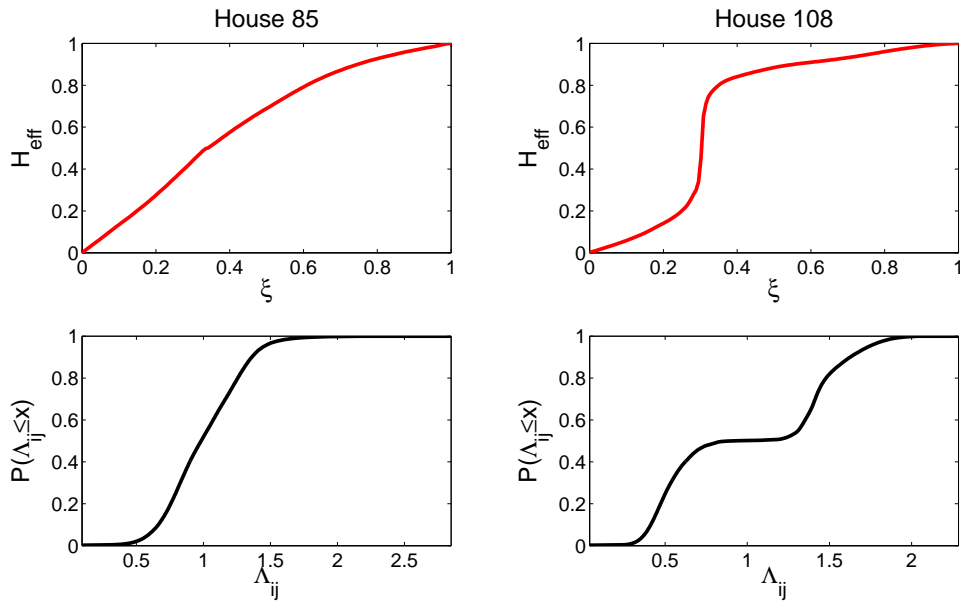


Figure 6.27: Comparison of the 85th (low polarization) and 108th (high polarization) House of Representatives. The upper curves show the \mathcal{H} MRFs, and the lower curves show the cumulative distribution of Λ_{ij} values $P(\Lambda_{ij} \leq x)$.

voting in the U.N.G.A. is considered by some to be merely symbolic. Nevertheless, it is the only forum in which a large number of states meet and vote regularly on international issues.

We analyze voting for the 1st–63rd sessions, covering the period 1946–2008, where each session corresponds to a year.¹⁸ For each session, we then define an adjacency matrix \mathbf{A} with elements A_{ij} giving the number of times countries i and j cast the same vote in a session (i.e., the sum of the number of times both countries voted yea on the same resolution, both countries voted nay on the same resolution, or both countries abstained from voting on the same resolution), normalized by the total number of times a country could have voted in a session. The matrix \mathbf{A} , with elements $A_{ij} \in [0, 1]$, then represents a network of weighted ties between countries, with weights determined by the similarity of their voting over a single G.A. session.

We cluster U.N.G.A. sessions by comparing MRFs for the corresponding voting networks. In Fig. 6.28, we plot a dendrogram of the U.N.G.A. sessions and highlight some of the clusters. The red cluster in the middle of the dendrogram consists of all post Cold War assemblies (1992–2008) except 1995. This group forms a larger cluster

¹⁸We exclude the 19th session from our analysis because there was only one resolution voted on by the U.N.G.A.

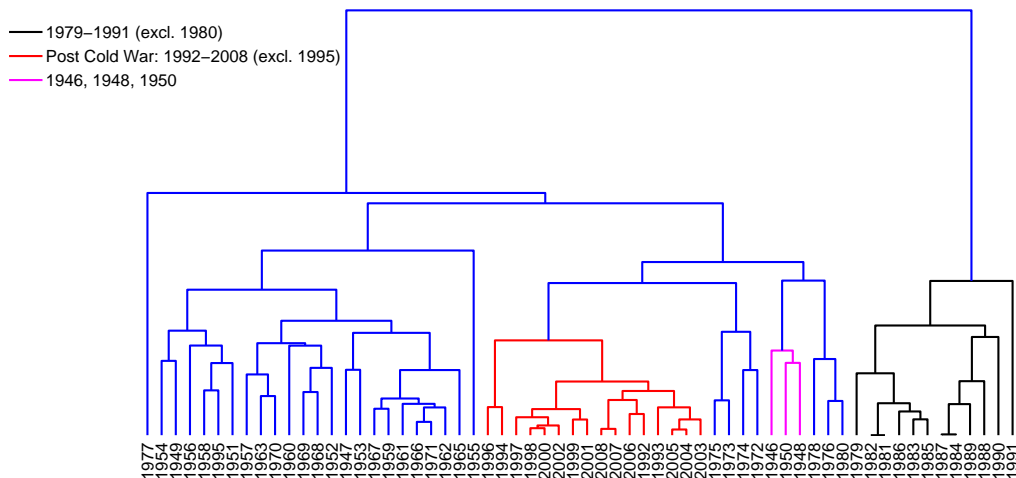


Figure 6.28: Dendrogram for the United Nations General Assembly roll-call voting for the 1st-63rd sessions, covering the period 1946–2008 (excluding the 19th session). Each leaf in the dendrogram represents a single session. We colour groups of branches in the dendrogram (see the discussion in the text).

with some assemblies from the 1970s and a cluster consisting of 1946, 1948, and 1950, which we highlight in magenta. These assemblies are all noteworthy: 1946 was the first assembly; during the 1948 assembly, the universal declaration of human rights was introduced; and in 1950, the “Uniting for Peace” resolution was passed. At the right of the dendrogram, we highlight in black a group consisting of all assemblies from 1979–1991 (excluding 1980). The end of this period marks the end of the Cold War; the beginning marks the end of the period of *Détente* between the Soviet Union and the U.S. following the former’s invasion of Afghanistan at the end of 1979. The large blue cluster at the left of the dendrogram consists primarily of sessions from before 1971, but also includes the sessions in 1977 and 1995.

6.9.3 Facebook

We now consider networks of the online social networking site Facebook for 100 U.S. universities [295]. The nodes in the network represent users of the site, and the links represent reciprocated “friendships” between users at a single-time snapshot in September 2005. We consider only links between students at the same university, which allows us to compare the structure of the networks at the different institutions. These networks represent complete data sets that we obtained from Facebook. We

provide details of these networks in Table C.1. In contrast to the previous examples, we are not comparing snapshots of the same network at different times but rather are comparing multiple realizations of the same type of network that have evolved independently.

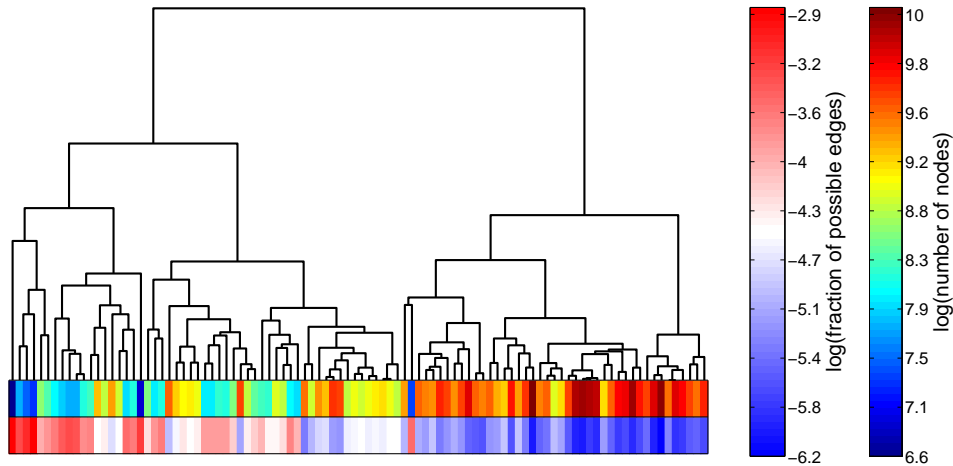


Figure 6.29: Dendrogram for 100 Facebook networks of U.S. universities at a single-time snapshot in September 2005. We order the leaves of the dendrogram to minimize the distance between adjacent nodes. The colour bars below the dendrogram indicate: (top) the number of nodes in the networks and (bottom) the fraction of possible edges that are present.

In Fig. 6.29, we show the dendrogram for Facebook networks that we produced by comparing MRFs. The two colour bars below the dendrogram indicate the number of nodes in each network and the fraction of possible edges that are present. It is clear that, in this case, these two simple network properties explain most of the observed cluster structure. In Fig. 6.30, we show the distribution of MRFs for all of the networks. For each of the properties \mathcal{H}_{eff} , S_{eff} , and η_{eff} , the MRFs are very similar in shape and lie within a narrow range. If we consider that the Facebook networks range in size from 762 to 41,536 nodes and that the fraction of possible edges present varies from 0.2% to 6%, this similarity is surprising and implies that all of the networks have very similar mesoscopic features. However, it is quite possible that there are heterogeneities in the mesoscopic structures of the Facebook networks that we do not uncover using the MRF framework. Equally, there might be other differences in these networks at the microscopic and macroscopic scales that we do not detect.

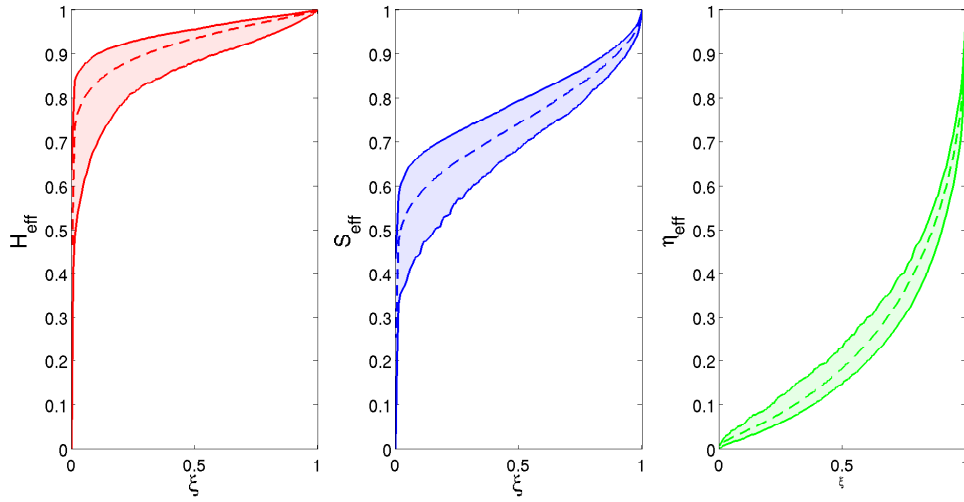


Figure 6.30: Distribution of MRFs for 100 Facebook networks of U.S. universities at a single-time snapshot in September 2005. At each value of ξ , the upper curve shows the maximum value of \mathcal{H}_{eff} , S_{eff} , or η_{eff} for all of the networks, the lower curve shows the minimum value, and the dashed line shows the mean.

6.9.4 New York Stock Exchange

We now return to financial networks and begin by studying a set of correlation networks for the New York Stock Exchange (NYSE) [1], which is the largest stock exchange in the world in terms of the U.S. dollar value of the securities listed on it. We construct networks of N nodes for the NYSE in which each node represents a stock [229]. We define the strength of the link connecting stocks i and j using the time series of daily exchange rate returns $z_i(t)$ ($i = 1, 2, \dots, N$) over the period 1985–2008. Recall from Section 3.2.2 that the return of an exchange rate with price $p_i(t)$ at discrete time t is given by $z_i(t) = \ln[p_i(t)/p_i(t-1)]$. We then represent the resulting fully-connected, weighted networks by an adjacency matrix \mathbf{A} with components

$$A_{ij} = \frac{[r(i, j) - \min_{ij} r(i, j)]}{[\max_{ij} r(i, j) - \min_{ij} r(i, j)]} - \delta(i, j), \quad (6.23)$$

where $r(i, j) = [\langle z_i z_j \rangle - \langle z_i \rangle \langle z_j \rangle] / \sigma_i \sigma_j$ is the linear correlation coefficient (see Chapters 3 and 5) between exchange rates i and j over a window of T returns, the Kronecker delta $\delta(i, j)$ removes self-edges, $\langle \cdot \rangle$ indicates a time-average over T , and σ_i is the standard deviation of z_i over T . The matrix elements $A_{ij} \in [0, 1]$ thereby quantify the similarity of two stocks.

As we discussed in Sections 3.2.3 and 5.2.2, the choice of T is a compromise between overly noisy and overly smoothed correlation coefficients [227, 229]: if T is

too small the correlation coefficients can be noisy; on the other hand, large values of T can mask interesting market changes. For example, a value of $T = 250$ days corresponds to one year, but a single year might include a market crash followed by a period of recovery. We set $N = 100$ and construct networks for each half year period over 1985–2008. This corresponds to time windows of $T \simeq 125$ returns, yielding $\Theta = T/N \doteq 1.25$.¹⁹ In contrast to the U.S. Congress and U.N. voting networks, the evolving NYSE network always has the same number of nodes, which always represent the same stocks.

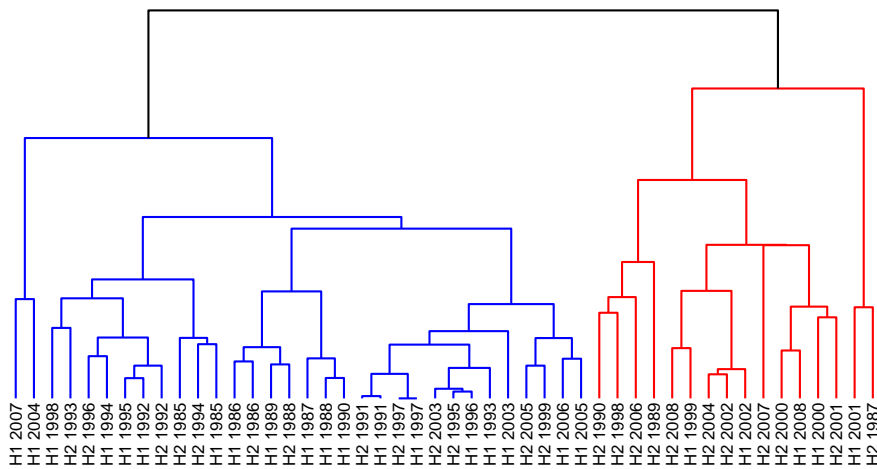


Figure 6.31: Dendrogram for 48 networks of the NYSE over the period 1985–2008. Each network represents the correlations between the returns of 100 stocks over each half year during this period. We order the leaves of the dendrogram to minimize the distance between adjacent nodes. The dendrogram is clearly split into two clusters (see the discussion in the text).

6.9.4.1 NYSE composite index

In Fig. 6.31, we show a dendrogram for the NYSE networks constructed using the MRF method. There are two clear clusters (which we highlight in red and blue). Networks in the red cluster appear to correspond to periods of market turmoil. For example, the cluster contains the networks for the second half of 1987 (July–December

¹⁹We note that we have return data for 235 stocks over this period, but we select 100 stocks at random for our analysis so that $\Theta > 1$. This ensures that the correlation coefficients are not overly noisy (see Section 3.2.3 and 5.2.2). We have reproduced the analysis that we present in this section using 10 other random stock selections and find similar results for the different selections.

1987), which includes the Black Monday stock market crash of October 1987; all of 2000–2002, following the bursting of the dot-com bubble; and the second half of 2007 and all of 2008, which includes the recent credit and liquidity crisis.

We provide support for the hypothesis that the constituents of the red cluster are networks for periods of market turmoil by considering the NYSE composite index (NYSECI). The NYSECI measures the performance of all common stocks listed on the NYSE by calculating the changes in their aggregate market value adjusted to eliminate the effects of capitalization changes, new listings, and delistings. In Fig. 6.32, we show the NYSECI as a function of time over the period 1985–2008 and highlight the time periods that correspond to networks in the red cluster in the dendrogram in Fig. 6.31. In Fig. 6.33, we show the volatility of the NYSECI over each half year period. Volatility is usually high during periods of market turmoil. If we let $\chi(t)$ represent the value of the index at time t , we can define a log-return z_χ for the index as $z_\chi(t) = \ln[\chi(t)/\chi(t-1)]$. We then define the volatility ν_χ of the NYSECI over a window of T returns as [73]

$$\nu_\chi = \frac{1}{T} \sum_{t=1}^T |z_\chi(t)|. \quad (6.24)$$

Figure 6.33 demonstrates that the networks assigned to the red cluster in Fig. 6.31 correspond (with one or two exceptions) to the periods of highest volatility. As we noted above, the time window for a single network might include periods of both high and low volatility, so it is unsurprising that the networks assigned to the red cluster do not correspond exactly to the half year periods with the highest volatilities. This remains true for all choices of T .

Although we study the same stocks over the full period 1985–2008, it is worth noting that many of the companies might have changed significantly during these years. For example, some of the companies might have expanded through acquisitions, while others might have grown organically (i.e., through increased output, sales, or both). Both of these processes could have altered the industries in which these companies operate and led to significant changes in the nature of the stocks that we investigate. The fact that we uncover a cluster corresponding to periods of market turmoil (and do not simply uncover clusters corresponding to similar time periods) despite such non-stationarities in the data is a testament to the effectiveness of the MRF clustering framework.

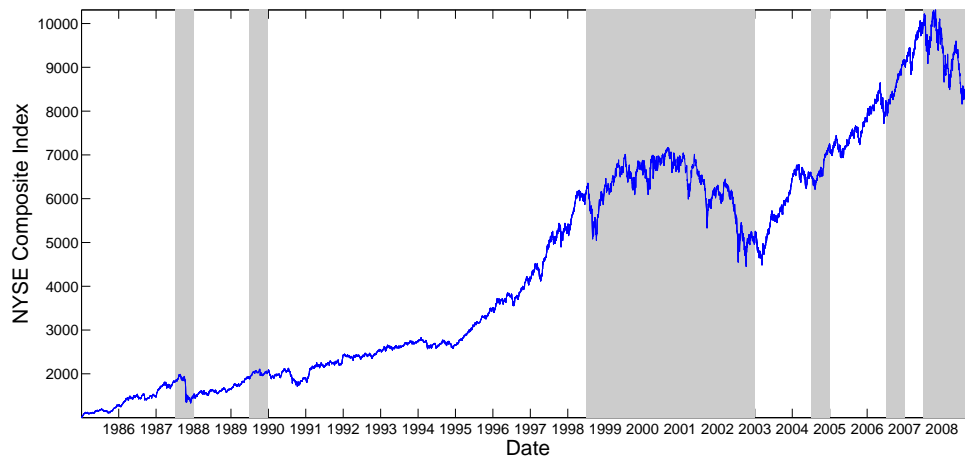


Figure 6.32: The NYSE composite index over the period 1985–2008. The grey blocks indicate the time periods corresponding to networks in the red cluster in the dendrogram in Fig. 6.31.

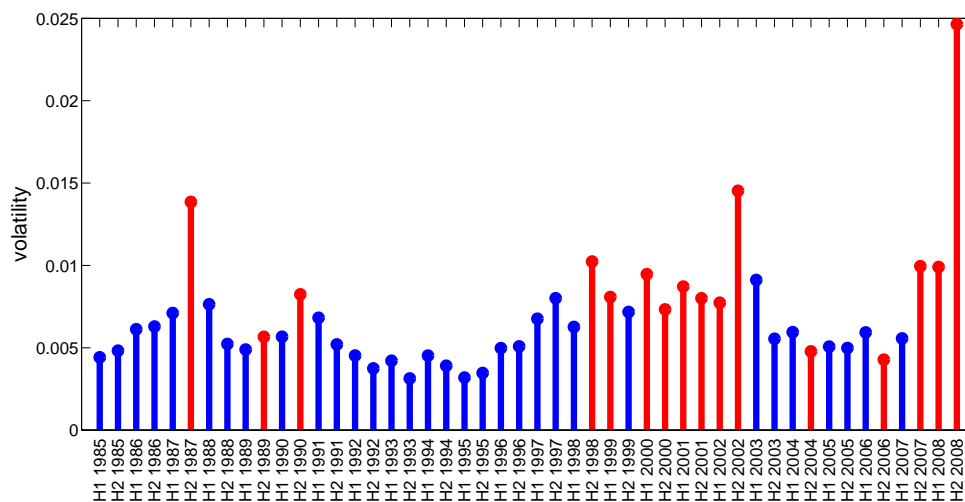


Figure 6.33: The average daily volatility of the NYSE composite index over each half year period from 1985–2008. We have coloured each stem according to the cluster membership of the corresponding network in the dendrogram in Fig. 6.31.

6.9.5 Foreign exchange market

Our final example is a set of foreign exchange market networks. We use the data described in Chapter 5 and define each network using Eq. 5 from Chapter 5. Each network represents the correlations between the returns of 110 exchange rates over each year during the period 1992–2008.²⁰

In Fig. 6.34, we show the dendrogram of annual FX networks, which is clearly split into two clusters. We highlight in green a sub-cluster within one of these clusters for which the networks are particularly closely related. The years within this green cluster are all years during which there was a major financial crisis: the Mexican tequila crisis in 1994; the Asian crisis in 1997; the beginning of the Argentine crisis and the devaluation of the Brazilian real in 1999; and the credit and liquidity crisis in 2007/2008. As a result, one could argue that this cluster represents years of financial crisis. However, there are years during which there were major crises that are not included in this cluster. For example, the withdrawal of the UK pound from the European exchange rate mechanism in 1992 and the Russian rouble crisis in 1998. There therefore seems to be an additional reason for the grouping of the networks in the green cluster beyond the fact that they are all crisis years.

To further explain the clusters in the dendrogram, we consider the carry trade return index Υ described in Section 5.8.3. We let $\Upsilon(t)$ represent the value of the index at time t and define a log-return z_Υ for the index as $z_\Upsilon(t) = \ln[\Upsilon(t)/\Upsilon(t-1)]$. We then define the volatility ν_Υ of the carry trade return index over a window of T returns as

$$\nu_\Upsilon = \frac{1}{T} \sum_{t=1}^T |z_\Upsilon(t)|. \quad (6.25)$$

In Fig. 6.34, we add a coloured bar under each leaf indicating the volatility ν_Υ of the carry return index each year. For all of the years in the rightmost cluster (which we highlight in red), the volatility of carry returns was low. Although other clusters contain years during which the carry trade return volatility was low, the fact that all years in the red cluster all have low volatility suggests that the carry trade explains some of the observed structure in the dendrogram. Given the prevalence and importance of the carry trade in the FX market, this observation is perhaps unsurprising.

²⁰We exclude 2003 and 2004 because we do not have data for these years.

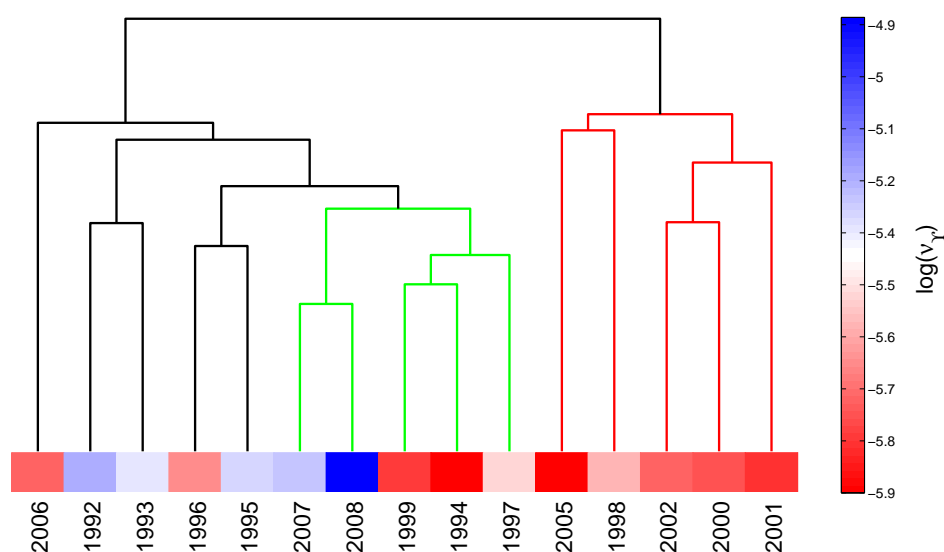


Figure 6.34: Dendrogram for 15 foreign exchange market networks over the period 1992–2008. Each network represents the correlations between the returns of 110 exchange rates over each year during this period. We order the leaves of the dendrogram to minimize the distance between adjacent nodes. The dendrogram is split into two clusters. We highlight one of these clusters in red and we highlight in green a sub-cluster within one of these clusters for which the networks are particularly closely related. The colour bar under the dendrogram shows the volatility in the carry trade return index ν_T .

6.9.6 Case studies summary

In this section, we have considered four case studies to demonstrate that the MRF clustering scheme is able to produce meaningful taxonomies for a diverse range of networks. In these examples, we can explain many of the observed clusters by properties that are unique to each type of network, but the MRF method can be applied successfully in all of these cases. The wide range of areas for which the MRF clustering is successful thereby provides supporting evidence that the clusters that we see in the aggregate taxonomy are meaningful.

6.10 Summary

We have developed a framework based on MRFs for comparing and clustering networks using their mesoscopic structures. We used this framework to create a taxonomy of networks and to identify groups of closely related networks and anomalous networks that were not grouped with members of their class. In addition to clustering networks of different types, we also created taxonomies for sub-sets of networks that represent multiple realizations of the same type of system (Facebook networks) and temporal snapshots of time-dependent systems (Congressional roll-call voting, U.N. resolution, NYSE, and FX networks). For each example of time-ordered sequences of networks, we identified periods during which there were significant changes in mesoscopic structure.

Chapter 7

Conclusions

We began this thesis by investigating triangular arbitrage in the spot foreign exchange market in Chapter 2. The aim of Chapter 2 was twofold: first, to answer a question of interest to market practitioners, namely whether triangular arbitrage opportunities exist; second, to demonstrate that when investigating financial markets it is essential to ensure that one is using data that is appropriate to the question being posed. Using executable price data, we demonstrated that although triangular arbitrage opportunities appear to exist in the foreign exchange market, most of these opportunities are very short in duration and represent very small profit opportunities. We further showed that, when one also considers the strong competition for each arbitrage and trading and technology costs, a trader would need to beat other market participants to an unfeasibly large proportion of arbitrage opportunities for triangular arbitrage to remain profitable in the long-term. These results provide a limited verification of foreign exchange market efficiency.

In Chapter 3, we extended our analysis of financial markets beyond the foreign exchange market and considered a variety of other markets, including equities, bonds, and commodities. We investigated these markets by constructing correlation matrices for the time series of asset returns and analyzed the temporal changes in the structure of these correlations. The number of correlations scales as the square of the number of assets N , so some simplification was necessary to identify the key relationships. We coarse-grained the correlation matrix using principal component analysis to identify the important relationships and analyzed the evolution of the system by considering the changes in the principal components. We found that the percentage of the variance in market returns accounted for by the first principal component rose steadily between 1999 and 2008 but then increased sharply following the 2008 collapse of Lehman Brothers. We further found that during this period the number of significant components decreased and the number of assets making significant contributions

to the first principal component increased. To gain some insights into the relationships between the different assets, we considered the correlations between the asset return time series and the principal components. Initially, the first few components appeared to represent different asset classes. For example, the first component corresponded to bonds, the second to equities, and the third to currencies. However, later in the studied period these relationships began to break down. In fact, by January 2010 nearly all of the studied assets were significantly correlated with the first principal component and relatively few assets were significantly correlated with the other components. This suggests that there are more common features across markets in 2010 than there were in 1999.

In Chapter 4, we described some of the most widely used methods for detecting communities in networks and presented a relatively comprehensive review of the literature on communities in dynamic networks. In Chapter 5, we presented an alternative method for investigating evolving correlation matrices in which we represented the correlation matrices as time-dependent networks and investigated the dynamics of network communities. We proposed a method for tracking communities through time from the perspective of individual nodes, which removes the undesirable requirement of determining which community at each time step represents the descendant of a community at the previous time step. We applied this technique to foreign exchange market networks in which each node represents an exchange rate and each edge represents a time-dependent correlation between the rates. Our analysis successfully uncovered significant structural changes that occurred in the foreign exchange market, including ones that resulted from major market events, and we demonstrated that community reorganizations at specific time steps can provide insights into changes in trading behaviour. We also considered the evolving relationship between individual nodes and their community and demonstrated that an exchange rate's functional role is related to its position within its community, with exchange rates that are important for information transfer located on the edges of communities and exchange rate that have a strong influence on other rates within that community located at the centre of their community.

Finally, in Chapter 6, we introduced mesoscopic response functions to characterize the community structures of networks. Importantly, the response functions are normalized so that it is possible to compare networks of significantly different sizes and connectivities. We used the response functions to compare and cluster networks and created a taxonomy of networks from a wide variety of different fields. The taxonomy contained many clusters that included networks from the same family, but there

were also examples of networks not clustered with networks that were nominally of the same type. In this way, the framework that we propose can be used to identify anomalous members of a family of networks.

As well as creating a taxonomy of networks from different fields, we also created taxonomies for subsets of networks that represent multiple realizations of the same type of system and temporal snapshots of time-dependent systems. For example, we created a taxonomy for a time-sequence of New York Stock Exchange networks which was split into two clusters based on the volatility of the market over the corresponding period. We also created taxonomies of roll-call voting in the U.S. Senate and House of Representatives in which the cluster membership of the different Congressional sessions was determined by the levels of party polarization. Although we can explain many of the observed clusters by properties that are unique to each type of network in the intra-family taxonomies, the mesoscopic response function framework provides insights in all of the different case studies.

7.1 Outlook

For much of this thesis we focused on financial networks and network communities, so we conclude with some comments on the current state of both fields and we discuss potential directions for future research.

In Chapter 5, we studied communities in foreign exchange market networks, but the techniques that we presented are general and can be applied to networks for other asset classes. In fact, the Potts methods has already been used to study communities in a network of equities [148]. However, in Ref. [148] Heimo *et al.* only examine communities in a static network of stocks traded on the New York Stock Exchange and do not study longitudinal networks. A potential area for future research is, therefore, to investigate community dynamics in evolving networks of equities. In equity markets, stocks are usually assigned to industry sectors based on the business activities of the companies; these sectors provide a useful tool for sorting and comparing different companies. For example, it is often insightful to compare the performance of stocks within the same sector to find out if any are under-performing (or over-performing) compared with the rest of the sector. An interesting avenue for future research would be to compare the communities identified using the Potts method with the sector classifications to see if they line up well or if there are periods during which there are significant differences in the classifications.

One issue with using the Potts method to investigate communities in longitudinal equity networks is that in previous work [148] plateaus have not been observed in plots of the number of communities as a function of the resolution parameter (see Section 5.4).¹ The absence of a plateau means that it is not possible to use the approach described in Section 5.4 to select the resolution at which to investigate community dynamic, so other methods will need to be developed.

We have focused on financial networks constructed from correlation matrices of asset price time series, but other types of financial networks have also been studied (see Ref. [11] for an overview of the applications of networks in finance). For example, networks have been used to analyze the trade relationships between nations, e.g., [266,275], and the credit relationships between financial institutions, e.g., [31,52,116]. The latter subject has received particular attention in the last few years as a result of the 2007–2008 credit and liquidity crisis. During the credit crisis, difficulties in the U.S. subprime mortgage market soon spread to debt markets all over the world, and eventually resulted in credit drying up as banks became unwilling to lend as freely [11]. The market turmoil clearly demonstrated the interconnectedness of the global financial system and how this connectivity can lead to outcomes that are difficult to forecast. As a consequence, the study of credit networks is currently one of the most active areas of research in financial networks and is an important direction for future research.

In the standard representation of a credit network, the nodes represent financial institutions and the edges represent credit relationships. A key concern in the study of such networks is how the insolvency of particular institutions affects the network; in particular, whether the failure of individual banks is “contagious” and leads to a systemic crisis in which a large fraction of the firms in the system fail at the same time [31]. One of the most important questions for understanding this risk is how connectivity affects network robustness [31,116,202], which is closely related to questions asked in ecology [202]. In Ref. [12], Allen and Gale studied how the banking system responds to contagion when banks are connected under different network structures. They found that networks with higher connectivities are more resilient and have a lower likelihood of widespread default because the losses sustained by one bank are transferred to more banks through interbank agreements. However, Gai and Kapadia [116] reached a different conclusion. They agreed that greater connectivity

¹Recall that community partitions that are robust across a range of resolutions are significant because the communities do not break up despite an increasing incentive to do so. Communities that persist over a large range of resolutions thus potentially represent important substructures.

reduces the likelihood of contagion, but it also means that if a problem does occur the shocks could be on a significantly larger scale. Battiston *et al.* [31] make similar observations. They found that although increased connectivity can reduce the risk of the collapse of an individual node through risk sharing, it can also result in crises being more severe and more frequent.

The lack of a consensus on the most robust structure for banking networks means that this is a particularly crucial area for future research. One of the major questions in this context is whether networks organized into communities have lower systemic risk [31]. Ecologists have suggested that decoupling a system into relatively discrete components can promote robustness [202]; however, this is not a simple question because some partitions of financial networks into communities could potentially preclude stabilizing effects such as mechanisms for maintaining liquidity [161]. Some steps have been taken to investigate communities in credit networks, e.g., [195], but there are still many unanswered questions. An interesting direction for future research would be to apply the methods that we presented in Chapter 5 to directed networks representing the evolving credit relationships between financial institutions during the 2007–2008 credit crisis.²

In the wider study of community structure in networks, significant technical advances have been made in recent years, and it remains a thriving area of research [105, 244]. Typically, the first stage of community analysis is the identification of the communities; indeed, this is the subject of many of the papers in the literature and a wealth of different techniques have been proposed for the algorithmic detection of communities. However, researchers have not yet agreed on which methods are most appropriate or reliable or when particular methods should be adopted or avoided. The problem of assessing the reliability of the output of different algorithms is exacerbated by the fact that there is no rigorous definition of a community. The most rigorous approach that is currently available is to identify communities using different detection algorithms and only to consider structures that are similar across multiple methods as meaningful [244, 289]. In this way, one can be more sure that the identified structures are genuine features of the data and not simply byproducts of the detection algorithm.

Even with the focus on developing community detection algorithms, very little attention has been paid to validating the output of the detection algorithms and trying to understand what the communities mean, what they actually look like or

²Although we focused on undirected networks in Chapters 5 and 6, the techniques that we introduced in these chapters can easily be extended to directed networks.

how they can be used [105, 181, 222, 244]. Some steps have now been taken towards answering some of these questions. For example, in Ref. [295] the composition of communities is related to the demographic characteristics of nodes and in Ref. [181] the structure and properties of communities in a range of different networks, including biological, social, and communication networks, have been studied and compared. In this thesis, we have also contributed to this endeavour. For example, in Chapter 5 we used the composition of different communities to uncover changes taking place in trading behaviour within the foreign exchange market and in Chapter 6 we used communities to create a taxonomy of networks. However, much still remains to be done in this direction and this is arguably the most pressing area of research if we are to gain real insights from studies of network community structures.

There are similar open questions in the study of dynamic communities (see Section 4.6.13). With a few exceptions, the studies of dynamic communities present a method for detecting communities, check that the identified communities make sense, and then stop. There are very few studies that investigate the mechanisms that drive the community evolution or try to answer some of the fundamental questions relating to dynamic communities, such as what community properties result in stable communities and what features of a community determine whether an individual will join (or leave) that community. In Chapter 5, we attempted to answer some of these questions for the foreign exchange market. For example, we demonstrated that nodes that have strong connections with their communities tend to have more stable community relationships than nodes with weak connections. The limited progress in the study of the properties of dynamic communities is perhaps unsurprising given the relative infancy of the field; hence, it represents an important direction for future research [318].

Another direction for future research is the development of algorithms that can identify overlapping communities. Most existing community detection algorithms generate partitions in which each node is assigned to exactly one community. However, this does not reflect the structure of many real-world systems. For example, in social networks people can belong to communities of friends, communities of work colleagues, and family communities. Some methods have been developed that can identify overlapping communities, e.g., [32, 234]. Perhaps the most widely used is the clique percolation method [234] that we described in Section 4.3.1; however, as we highlighted, this approach has limitations, so alternative techniques need to be developed.

The methods in Refs. [32, 234] allow nodes to belong to more than one community, but do not give any indication of the community with which a node is most closely

associated. Therefore, another possibility is algorithms that do not assign nodes to one or to multiple communities, but instead assign each node a weight indicating the strength of its attachment to each community [215, 317]. By normalizing the sum of each node's community affiliation to unity, this measure can be interpreted as the probability that a node belongs to a particular community. Along similar lines, models have been proposed in the dynamic communities literature that give a probability that each node belongs to each community at different time steps, e.g., [186].

All of the community detection methods that we have discussed so far have focused on partitioning the entire network into communities, i.e., all of the methods associate every node in the network with at least one community. However, many real-world networks contain nodes that do not fit into any community particularly well. With this in mind, a recent paper [318] has proposed a method that broadens the community detection framework by allowing a network to contain not only communities but also *background* nodes that are not associated with any community.

Finally, the typical motivation for studies of communities is that the community structure of a network has some bearing on its function. Most studies then use structural communities as proxies for functional communities. However, the functional and structural properties of a system sometimes do not map onto each other, so it is likely that structural communities do not always correspond to functional communities [271]. For example, studies of neural networks have shown that it is fairly common for central pattern generators³ to change their functional organization, depending on the pattern that they are generating, while maintaining a constant anatomical structure [268]. Consequently, an important avenue for future research is the development of techniques that detect communities using both functional and structural information.

This represents just a small sample of open questions relating to networks communities, which is itself just a sub-area of the field of networks, and many other open questions exist in the wider field. It will be interesting to see how the analysis of communities and the field of networks matures over the next few years and whether it can maintain the current rate of development.

³Central pattern generators are the neuronal circuits that give rise to repetitive or oscillatory patterns of muscle activity that produce rhythmic movements, such as locomotion, breathing, and chewing [54].

Appendix A

Details of Financial Assets

Table A.1: Details of all of the financial assets studied in Chapter 3. The data that we use in this chapter was downloaded from Bloomberg. See <http://www.bloomberg.com/> for more information on the different financial instruments.

Ticker	Sector	Description
AEX	Equities	AEX Index (Netherlands)
AS30	Equities	Australian All Ordinaries Index
ASE	Equities	Athens Stock Exchange General Index
ATX	Equities	Austrian Traded Index
BEL20	Equities	BEL 20 Index (Belgium)
BVLX	Equities	PSI General Index (Portugal)
CAC	Equities	CAC 40 Index (France)
DAX	Equities	DAX Index (Germany)
FTSEMIB	Equities	FTSE MIB Index (Italy)
HEX	Equities	Helsinki Stock Exchange General Index
HSI	Equities	Hang Seng Index (Hong Kong)
IBEX	Equities	IBEX 35 Index (Spain)
INDU	Equities	Dow Jones Industrial Average Index (U.S.)
ISEQ	Equities	Irish Overall Index
KFX	Equities	OMX Copenhagen 20 Index
NDX	Equities	NASDAQ 100 Index (U.S.)
NKY	Equities	Nikkei 225 Index (Japan)
NZSE	Equities	New Zealand All Ordinaries Index
OBX	Equities	OBX Stock Index (Norway)
OMX	Equities	OMX Stockholm 30 Index
RTY	Equities	Russell 2000 Index (U.S.)
SMI	Equities	Swiss Market Index
SPTSX	Equities	S&P/Toronto Stock Exchange Index
SPX	Equities	Standard and Poor's 500 (U.S.)
UKX	Equities	FTSE 100 Index (U.K.)
GDDUEMEA	Equities	Emerging markets: Europe, Middle East, Africa
GDUEEGFA	Equities	Emerging markets: Asia
GDUEEGFL	Equities	Emerging markets: Latin America

continued on next page

Appendix A

Ticker	Sector	Description
ATGATR	Government bonds	Austrian government bonds
AUGATR	Government bonds	Australian government bonds
BEGATR	Government bonds	Belgian government bonds
CAGATR	Government bonds	Canadian government bonds
DEGATR	Government bonds	Danish government bonds
FIGATR	Government bonds	Finnish government bonds
FRGATR	Government bonds	French government bonds
GRGATR	Government bonds	German government bonds
IEGATR	Government bonds	Irish government bonds
ITGATR	Government bonds	Italian government bonds
JNGATR	Government bonds	Japanese government bonds
NEGATR	Government bonds	Netherlands government bonds
NOGATR	Government bonds	Norwegian government bonds
NZGATR	Government bonds	New Zealand government bonds
PTGATR	Government bonds	Portuguese government bonds
SPGATR	Government bonds	Spanish government bonds
SWGATR	Government bonds	Swedish government bonds
SZGATR	Government bonds	Swiss government bonds
UKGATR	Government bonds	U.K. government bonds
USGATR	Government bonds	U.S. government bonds
AUDUSD	Currencies	Australian dollar
CADUSD	Currencies	Canadian dollar
CHFUSD	Currencies	Swiss franc
CZKUSD	Currencies	Czech koruna
EURUSD	Currencies	Euro
GBPUSD	Currencies	Pounds sterling
IDRUSD	Currencies	Indonesian rupiah
JPYUSD	Currencies	Japanese yen
KRWUSD	Currencies	Korean won
MXNUSD	Currencies	Mexican peso
NOKUSD	Currencies	Norwegian krone
NZDUSD	Currencies	New Zealand dollar
PHPUSD	Currencies	Philippines peso
SEKUSD	Currencies	Swedish krona
ZARUSD	Currencies	South African rand
HG1	Metals	Copper
LA1	Metals	Aluminium
LL1	Metals	Lead
LN1	Metals	Nickel
LT1	Metals	Tin
XAG	Metals	Silver
XAU	Metals	Gold
XPD	Metals	Palladium
XPT	Metals	Platinum
CL1	Fuels	Crude oil, WTI

continued on next page

Details of Financial Assets

Ticker	Sector	Description
CO1	Fuels	Crude oil, brent
HO1	Fuels	Heating oil
NG1	Fuels	Natural gas
BO1	Commodities	Soybean oil
C 1	Commodities	Corn
CC1	Commodities	Cocoa
CT1	Commodities	Cotton
FC1	Commodities	Coffee
JN1	Commodities	Feeder cattle
JO1	Commodities	Orange juice
KC1	Commodities	Coffee
LB1	Commodities	Lumber
LC1	Commodities	Live cattle
LH1	Commodities	Lean hogs
O 1	Commodities	Oats
PB1	Commodities	Frozen pork bellies
QW1	Commodities	Sugar
RR1	Commodities	Rough rice
S 1	Commodities	Soybean
SM1	Commodities	Soybean meal
W 1	Commodities	Wheat
MOODCAAA	Corporate bonds	Moody's AAA corporate bonds
MOODCAA	Corporate bonds	Moody's AA corporate bonds
MOODCA	Corporate bonds	Moody's A corporate bonds
MOODCBAA	Corporate bonds	Moody's BAA corporate bonds

Appendix B

Robustness of FX Communities to Alternative Heuristics

In this section, we demonstrate that the results described in Chapter 5 are robust with respect to the choice of computational heuristic used to minimize the Hamiltonian in Eq. 4.3.

B.1 Comparison of partition energies

We begin by comparing the energy \mathcal{H} (see Eq. 4.3) of the optimal partitions at the studied resolution $\lambda = 1.45$. Figure B.1 shows the distribution of energies for the different algorithms and demonstrates that the greedy algorithm and simulated annealing find better partitions than the spectral algorithm. The spectral algorithm begins by splitting the network into two components, choosing the split that minimizes the energy, and then recursively partitions the smaller networks into two groups until no decrease in energy can be obtained through partitioning. At each step, the algorithm only finds the optimal partition of each community into two smaller communities, even though a split into more communities might yield a lower energy. Given this, it is unsurprising that the spectral algorithm identifies partitions further from the optimum than the other heuristics. For the remainder of this section, we will only compare the greedy and simulated annealing algorithms because of the lower quality of the spectral partitions.

B.2 Temporal changes in communities

First, we compare the community partitions identified by the two heuristics for each network. In Fig. B.2, we show the distribution of the variation of information be-

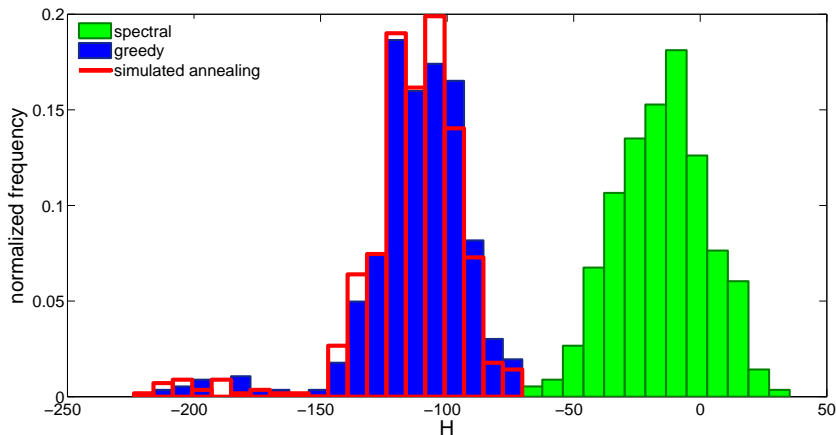


Figure B.1: Distribution of the energy \mathcal{H} of the optimal partition for networks over the period 2005–2008 for different optimization algorithms.

tween the community partitions identified using the greedy and simulated annealing algorithms. The two methods identify identical partitions for 19% of the networks; for 83% of the networks, the partitions differ in their assignment of nodes to communities by fewer than 10 nodes. Therefore, there is strong agreement between the partitions obtained by the two heuristics, but there are also differences that warrant further investigation.

In Section 5.8, we identified significant changes in the community configuration by comparing changes in the scaled energy Q_s (see Eq. 4.4) between consecutive time steps and by calculating the variation of information between community partitions at consecutive time steps (see Fig. 5.9). The correlation between Q_s as a function of time for the two heuristics is 0.99 and the correlation between the changes in Q_s is 0.93. The correlation between the variation of information between partitions at consecutive time steps is 0.36. The scaled energy correlations are clearly extremely high. However, there are differences in the timings of some major reorganizations identified by the variation of information. To compare the timings of major events, we identify time steps at which the variation of information between consecutive partitions is more than a certain number of standard deviations larger the mean variation of information between consecutive partitions. We find that the algorithms identify 40% of one standard deviation events at the same time steps and 33% of 2.5 standard deviation events. The methods therefore agree reasonably well, with one in three 2.5 standard deviation events identified at exactly the same time step. However, the differences also suggest that one should be cautious using variation of information to identify major community reorganizations.

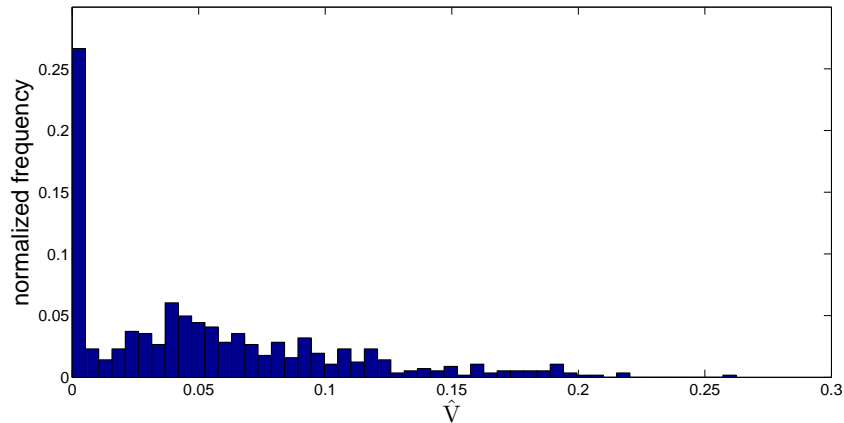


Figure B.2: The distribution of the variation of information between community partitions identified using the greedy algorithm and simulated annealing for networks over the period 2005–2008.

B.3 Example community comparison

One time step at which both heuristics identify a large community change is 15/08/07 which, as described in Section 5.8.3, was a day when there was a significant increase in carry trade unwinding. It is worth considering the communities at this time step in detail to help assess the similarity of the results for the two heuristics. In Fig. B.3(a), we show the communities that we identified using a greedy algorithm [44] immediately before and after 15/08/07; in Fig. B.3(b) we show communities that we identified using simulated annealing [141] for the same time steps. Figure B.3(a) shows that, leading up to 15/08/07, there was some unwinding of the carry trade, so the initial configuration includes a community containing exchange rates of the form AUD/YYYY, NZD/YYYY, and XXX/JPY (which all involve one of the key carry-trade currencies). After 15/08/07, as the volume of carry trade unwinding increases, this community incorporates other XXX/JPY rates as well as some XXX/CHF and XXX/USD rates. Although, the communities in Fig. B.3(b) for the simulated annealing algorithm are not identical to those in Fig. B.3(a), they are very similar. The main difference is that for the simulated annealing algorithm, there are two carry trade communities before 15/08/07: one community of exchange rates of the form AUD/YYYY, NZD/YYYY (which are all exchange rates that include a carry trade investment currency) and another community containing exchange rates of the form XXX/CHF and XXX/JPY (which are all exchange rates that include a carry trade funding currency). After 15/08/07, as carry trade unwinding increases, these two communities combine and

Appendix B

two other exchange rates also join the community. The resulting merged community is very similar to the largest community identified at the same time step using the greedy algorithm.

Figure B.3 therefore illustrates that there are only small differences in the community configurations that are identified by the two heuristics. In fact, as Fig. B.2 shows, the two algorithms agree in the assignment of all but about ten nodes approximately 80% of the time. Importantly, Fig. B.3 highlights that, even when there are differences in the exact community configurations, the communities that are identified by the two heuristics nonetheless indicate the same changes taking place in the FX market.

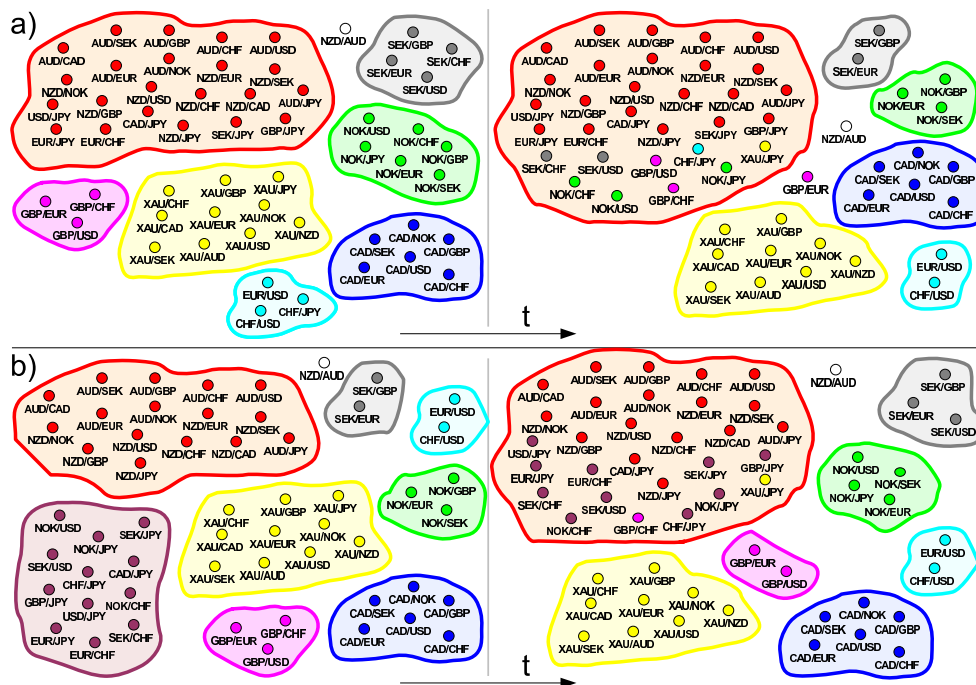


Figure B.3: Comparison of the change in community structure in one half of the FX market network over the same period for different optimization heuristics. We show a schematic of the communities for the period following 15/08/07, when there was significant unwinding of the carry trade during the 2007–2008 credit and liquidity crisis. We identified communities using (a) a greedy algorithm [44] and (b) a simulated annealing algorithm [141]. The node colours after the community reorganization correspond to their community before the change. If the parent community of a community after the reorganization is obvious, we draw it using the same colour as its parent. The nodes drawn as triangles resided in the opposite half of the network before the community reorganization.

B.4 Node role comparison

As a further comparison, we investigate the effect of different heuristics on exchange rate roles (see Section 5.9). In Fig. B.4, we compare quarterly role evolutions over the period 2005–2008 for the same exchange rates shown in Fig. 5.15. Although there are slight differences in the positions of the exchange rates in the (κ^b, κ^y) plane for some periods, we obtain the same aggregate conclusions. For example, for both heuristics, AUD/JPY is most influential within its community (high κ^b) during Q3 and Q4 2007 and during Q1 and Q4 2008; however, it is less influential, but more important for information transfer, during 2005 and 2006.

The positions in the (κ^b, κ^y) plane are similarly close for all of the other exchange rates. We quantify the differences in the positions for the two heuristics by calculating the mean and standard deviation of the change in position over all exchange rates and over all time periods. That is, we average the change in position of every node in the (κ^b, κ^y) plane over every quarter. The mean change in position in both the κ^b and κ^y directions is less than 10^{-4} ; the standard deviations are 0.15 and 0.17, respectively. However, because the changes in position are likely to cancel out (i.e., an increase in κ^b for one exchange rate is likely to be offset by a decrease in κ^b for another exchange rate), it is more informative to calculate the mean and standard deviation of the absolute changes in position in the κ^b and κ^y directions. In the κ^b direction, the mean absolute change in position is 0.08, with a standard deviation of 0.13; in the κ^y direction, the mean change is 0.09, with a standard deviation of 0.15. The mean differences in positions in the (κ^b, κ^y) are therefore very small for the two heuristics and, as Fig. B.4 demonstrates, both algorithms uncover the same role changes in the FX market for the different exchange rates.

Finally, we also checked the relationships shown in Fig. 5.8 between the community centrality and community size, between the community alignment and betweenness centrality, and between the community autocorrelation and projected community centrality. Using simulated annealing, we find the same relationships that we uncovered with the greedy algorithm.

The results of this section demonstrate that, although there are differences in the communities identified using different optimization heuristics, the aggregate conclusions are the same. We identify the same changes taking place in the FX market whether we use the greedy algorithm or simulated annealing to minimize energy. The fact that we obtain very similar results using different optimization techniques,

Appendix B

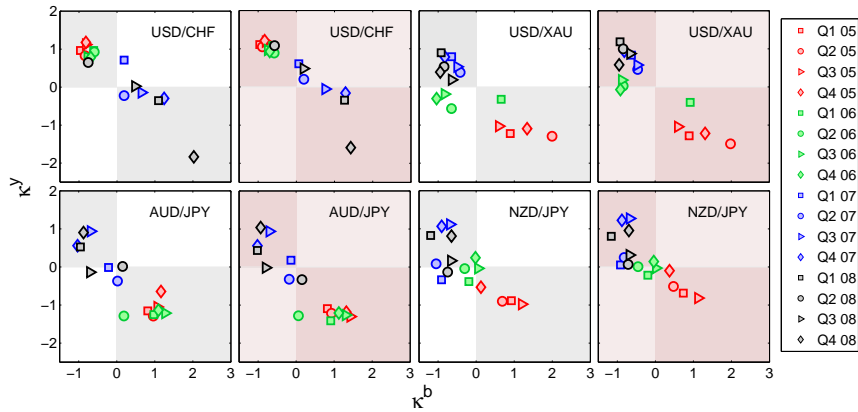


Figure B.4: Comparison of the quarterly node role evolutions in the (κ^b, κ^y) plane for the period 2005–2008 for communities identified using a greedy algorithm [44] and simulated annealing [141]. The white/grey shading plots show results for the greedy algorithm and the pink/dark pink plots show results for simulated annealing.

despite these techniques sampling different regions of the energy landscape, gives confidence that the effects that we uncover are genuine and that the results are robust. In practice, the greedy algorithm is preferable to simulated annealing because of the computational cost of the latter.

Appendix C

Network Details

In Table C.1, we provide details of the networks studied in Chapter 6. We include several synthetic network families and benchmark networks that were introduced to test community detection algorithms. For many of these, we include multiple realizations that we obtained using different parameter values. We briefly describe these networks and explain the notation we use to label them in Table C.1.

Erdős-Rényi (ER): In an ER network of N nodes, each pair of nodes is connected by an unweighted edge with probability p and not connected with probability $1 - p$ [86]. The degree of each node is distributed according to a binomial distribution. We label the ER networks using the notation “ER: (N,p) ”.

Watts-Strogatz (WS): We consider the small-world network of Watts and Strogatz [305] for a one-dimensional lattice of N nodes with periodic boundary conditions. The network consists of a ring in which each node is connected with an unweighted edge to all of its neighbours that are k or fewer lattice spacings away. Each edge is then visited in turn and one end is rewired with probability p to a different node selected uniformly at random, subject to the constraint that there can be no self-edges or double-edges. We label each Watts-Strogatz network as “WS: (N,k,p) ”.

Barabási-Albert (BA): BA networks [26] are obtained using a network growth mechanism in which nodes with degree m are added to the network and the other end of each edge attaches to another node with a probability proportional to the degree of that node. We label each BA network “BA: (N,m) ”.

Fractal: We generate fractal networks using the method described in Ref. [279]. We begin by generating an isolated group of 2^m fully-connected nodes, where m is

the size of the clusters. These groups correspond to the hierarchical level $h = 0$. We then create a second identical group and we link the two groups with a link density of E^{-h} ($h = 1$), where the link density is the number of links out of all possible links between the groups and E gives the connection density fall-off per hierarchical level. We then duplicate this network and connect the two duplicates at the level $h = 2$ with a link density E^{-2} . We repeat this until we reach the desired network size $N = 2^n$, where n is the number of hierarchical levels. At each step the connection density is decreased, resulting in progressively sparser interconnectivity at higher hierarchical levels. The resulting network exhibits self-similar properties. We label each network “Fractal: (n, m, E) ”.

Random fully-connected: We produce random, fully connected networks of N nodes by linking every node to every other node with an edge whose weight is chosen uniformly at random on the unit interval. The networks have $N(N-1)/2$ edges. We label each network “Random fully-connected: (N) ”.

Kumpula-Onnela-Saramäki-Kaski-Kertész (KOSKK) model: We generate weighted networks containing communities using the model described in [174]. We create links through two mechanisms: First, at each time step, each node i selects a neighbour j with probability w_{ij}/s_i , where w_{ij} is the weight of the link connecting i and j and $s_i = \sum_j w_{ij}$ is the strength of i . If j has other neighbours in addition to i , then one of them is selected with probability $w_{jk}/(s_j - w_{ij})$. If i and k are not connected, then a new link of weight $w_{ik} = w_0$ is created with probability p_n . If the link already exists, its weight is increased by an amount δ . In both cases, w_{ij} and w_{jk} are also increased by δ . This process is termed *local attachment*. Second, if a node has no links, with probability p_r , it creates a link of weight w_0 to a randomly selected node, which is termed *global attachment*. A node can be deleted with probability p_d , in which case all of its links are also removed and it is replaced by a new node, so that the total number of nodes N remains constant. The mechanism begins with an empty network, and links are added by running the local and global attachment mechanisms in parallel. We label each network “Weighted: $(N, w_0, \delta, p_n, p_r, p_d, t)$ ”, where t is the total number of simulation time steps.

Lancichinetti-Fortunato-Radicchi (LFR) benchmark: The LFR benchmarks, introduced in Ref. [180], are unweighted networks with non-overlapping communities. The networks are constructed by assigning each node a degree from a

power law distribution with exponent γ , where the extremes of the distribution k_{\min} and k_{\max} are chosen such that the mean degree is $\langle k \rangle$, and the nodes are connected using the configuration model [212] to maintain their degree distribution. Each node shares a fraction μ of its links with nodes in other communities and $1 - \mu$ with nodes in its own community. The community sizes are taken from a power law distribution with exponent β , subject to the constraint that the sum of all of the community sizes equals the number of nodes N in the network. The minimum and maximum community sizes (q_{\min} and q_{\max}) are then chosen to satisfy the additional constraint that $q_{\min} > k_{\min}$ and $q_{\max} > k_{\max}$, which ensures that each node is included in at least one community. We label each network “LFR: $(N, \langle k \rangle, k_{\max}, \gamma, \beta, \mu, q_{\min}, q_{\max})$ ”.

Lancichinetti-Fortunato (LF) benchmark: The LF benchmarks introduced in Ref. [178] are weighted networks that can contain overlapping communities, although we only consider non-overlapping communities. The node degrees are again taken from a power law degree distribution, but this time we label the exponent τ_1 , and the community sizes are taken from a power law degree distribution with exponent τ_2 . The strength s_i of each node is chosen so that $s_i = k_i^\beta$, where k_i again gives the degree of node i . There are also two mixing parameters: a topological mixing parameter μ_t , which measures the proportion of links outside a node’s community, and a mixing parameter μ_w , which measures the weight of a node’s links outside its community. We label each network “LF: $(N, \langle k \rangle, k_{\max}, \mu_t, \mu_w, \beta, \tau_1, \tau_2)$ ”. For all of the LF networks, we set $N = 1000$. One can alternatively set the minimum and maximum community sizes q_{\min} and q_{\max} . We always use $q_{\min} = 20$ and $q_{\max} = 50$, so we do not include these parameters when we label the networks.

LFR-Newman-Girvan benchmark: We also include a network with parameters $N = 128$, $\langle k \rangle = 16$, $k_{\max} = 16$, $\gamma = 1$, $\beta = 1$, $\mu = 0.2$, $q_{\min} = 32$, and $q_{\max} = 32$, which is similar to the NG benchmark [178, 224].¹

¹In this case, all of the nodes have the same degree and each community is constrained to contain the same number of nodes so the values of the exponent γ of the degree distribution and the exponent β of the community size distribution are unimportant.

Table C.1: Network summary statistics. We symmetrize all networks, remove self-edges, and only consider the largest connected component. We give the network category, whether it is weighted or unweighted, the number of nodes N in the largest connected component, the number of edges L , the fraction of possible edges present $f_e = 2L/[N(N-1)]$, and a reference providing details of the data source. We highlight in bold all of the networks included in the subset of 25 networks described in Appendix E and we colour red all of the networks included in the subset of 270 networks used to produce the results described in several sections in Chapter 6. We indicate with an asterisk * all networks used in Appendix F to test the robustness of the taxonomy to different optimization heuristics.

ID	Name	Category	Weighted	N	L	f_e	References
1	Human brain cortex: participant A1	Brain	Y	994	13,520	0.0274	[144]
2	Human brain cortex: participant A2	Brain	Y	987	14,865	0.0305	[144]
3	Human brain cortex: participant B	Brain	Y	980	14,222	0.0296	[144]
4	Human brain cortex: participant D	Brain	Y	996	14,851	0.0300	[144]
5	Human brain cortex: participant E	Brain	Y	992	14,372	0.0292	[144]
6	Human brain cortex: participant C	Brain	Y	996	14,933	0.0301	[144]
7	Cat brain: cortical*	Brain	Y	52	515	0.3884	[264]
8	Cat brain: cortical/thalamic*	Brain	Y	95	1,170	0.2620	[264]
9	Macaque brain: cortical*	Brain	N	47	313	0.2895	[102]
10	Macaque brain: visual/sensory cortex*	Brain	N	71	438	0.1763	[102]
11	Macaque brain: visual cortex 1*	Brain	N	30	190	0.4368	[312]
12	Macaque brain: visual cortex 2*	Brain	N	32	194	0.3911	[312]
13	Garfield: scientometrics citations	Citation	Y	2,678	10,368	0.0029	[119]
14	Garfield: Small and Griffith citations	Citation	Y	1,024	4,916	0.0094	[119]
15	Garfield: small-world citations	Citation	N	233	994	0.0368	[119]
16	Co-authorship: astrophysics	Collaboration	Y	14,845	119,652	0.0011	[216]
17	Co-authorship: comp. geometry	Collaboration	Y	3,621	9,461	0.0014	[34, 77]
18	Co-authorship: condensed matter	Collaboration	Y	13,861	44,619	0.0005	[216]
19	Co-authorship: Erdős	Collaboration	N	6,927	11,850	0.0005	[29]
20	Co-authorship: high energy theory	Collaboration	Y	5,835	13,815	0.0008	[216]
21	Co-authorship: network science	Collaboration	Y	379	914	0.0128	[220]
22	Hollywood film music*	Collaboration	Y	39	219	0.2955	[100]
23	Jazz collaboration	Collaboration	N	198	2,742	0.1406	[125]
24	Electronic circuit (s208)*	Electronic circuit	N	122	189	0.0256	[210]
25	Electronic circuit (s420)	Electronic circuit	N	252	399	0.0126	[210]

ID	Name	Category	Weighted	N	L	f_e	References
26	Electronic circuit (s838)	Electronic circuit	N	512	819	0.0063	[210]
27	Facebook: American	Facebook	N	6,370	217,654	0.0107	[295]
28	Facebook: Amherst	Facebook	N	2,235	90,954	0.0364	[295]
29	Facebook: Auburn	Facebook	N	18,448	973,918	0.0057	[295]
30	Facebook: Baylor	Facebook	N	12,799	679,815	0.0083	[295]
31	Facebook: BC	Facebook	N	11,498	486,961	0.0074	[295]
32	Facebook: Berkeley	Facebook	N	22,900	852,419	0.0033	[295]
33	Facebook: Bingham	Facebook	N	10,001	362,892	0.0073	[295]
34	Facebook: Bowdoin	Facebook	N	2,250	84,386	0.0334	[295]
35	Facebook: Brandeis	Facebook	N	3,887	137,561	0.0182	[295]
36	Facebook: Brown	Facebook	N	8,586	384,519	0.0104	[295]
37	Facebook: BU	Facebook	N	19,666	637,509	0.0033	[295]
38	Facebook: Bucknell	Facebook	N	3,824	158,863	0.0217	[295]
39	Facebook: Cal	Facebook	N	11,243	351,356	0.0056	[295]
40	Facebook: Caltech	Facebook	N	762	16,651	0.0574	[295]
41	Facebook: Carnegie	Facebook	N	6,621	249,959	0.0114	[295]
42	Facebook: Colgate	Facebook	N	3,482	155,043	0.0256	[295]
43	Facebook: Columbia	Facebook	N	11,706	444,295	0.0065	[295]
44	Facebook: Cornell	Facebook	N	18,621	790,753	0.0046	[295]
45	Facebook: Dartmouth	Facebook	N	7,677	304,065	0.0103	[295]
46	Facebook: Duke	Facebook	N	9,885	506,437	0.0104	[295]
47	Facebook: Emory	Facebook	N	7,449	330,008	0.0119	[295]
48	Facebook: FSU	Facebook	N	27,731	1,034,799	0.0027	[295]
49	Facebook: Georgetown	Facebook	N	9,388	425,619	0.0097	[295]
50	Facebook: GWU	Facebook	N	12,164	469,511	0.0063	[295]
51	Facebook: Hamilton	Facebook	N	2,312	96,393	0.0361	[295]
52	Facebook: Harvard	Facebook	N	15,086	824,595	0.0072	[295]
53	Facebook: Haverford	Facebook	N	1,446	59,589	0.0570	[295]
54	Facebook: Howard	Facebook	N	4,047	204,850	0.0250	[295]
55	Facebook: Indiana	Facebook	N	29,732	1,305,757	0.0030	[295]
56	Facebook: JMU	Facebook	N	14,070	485,564	0.0049	[295]
57	Facebook: Johns Hopkins	Facebook	N	5,157	186,572	0.0140	[295]
58	Facebook: Lehigh	Facebook	N	5,073	198,346	0.0154	[295]
59	Facebook: Maine	Facebook	N	9,065	243,245	0.0059	[295]
60	Facebook: Maryland	Facebook	N	20,829	744,832	0.0034	[295]

ID	Name	Category	Weighted	N	L	f_e	References
61	Facebook: Mich	Facebook	N	3,745	81,901	0.0117	[295]
62	Facebook: Michigan	Facebook	N	30,106	1,176,489	0.0026	[295]
63	Facebook: Middlebury	Facebook	N	3,069	124,607	0.0265	[295]
64	Facebook: Mississippi	Facebook	N	10,519	610,910	0.0110	[295]
65	Facebook: MIT	Facebook	N	6,402	251,230	0.0123	[295]
66	Facebook: MSU	Facebook	N	32,361	1,118,767	0.0021	[295]
67	Facebook: MU	Facebook	N	15,425	649,441	0.0055	[295]
68	Facebook: Northeastern	Facebook	N	13,868	381,919	0.0040	[295]
69	Facebook: Northwestern	Facebook	N	10,537	488,318	0.0088	[295]
70	Facebook: Notre Dame	Facebook	N	12,149	541,336	0.0073	[295]
71	Facebook: NYU	Facebook	Y	21,623	715,673	0.0031	[295]
72	Facebook: Oberlin	Facebook	N	2,920	89,912	0.0211	[295]
73	Facebook: Oklahoma	Facebook	N	17,420	892,524	0.0059	[295]
74	Facebook: Penn	Facebook	N	41,536	1,362,220	0.0016	[295]
75	Facebook: Pepperdine	Facebook	N	3,440	152,003	0.0257	[295]
76	Facebook: Princeton	Facebook	N	6,575	293,307	0.0136	[295]
77	Facebook: Reed	Facebook	N	962	18,812	0.0407	[295]
78	Facebook: Rice	Facebook	N	4,083	184,826	0.0222	[295]
79	Facebook: Rochester	Facebook	N	4,561	161,403	0.0155	[295]
80	Facebook: Rutgers	Facebook	N	24,568	784,596	0.0026	[295]
81	Facebook: Santa	Facebook	N	3,578	151,747	0.0237	[295]
82	Facebook: Simmons	Facebook	N	1,510	32,984	0.0290	[295]
83	Facebook: Smith	Facebook	N	2,970	97,133	0.0220	[295]
84	Facebook: Stanford	Facebook	N	11,586	568,309	0.0085	[295]
85	Facebook: Swarthmore	Facebook	N	1,657	61,049	0.0445	[295]
86	Facebook: Syracuse	Facebook	N	13,640	543,975	0.0058	[295]
87	Facebook: Temple	Facebook	N	13,653	360,774	0.0039	[295]
88	Facebook: Tennessee	Facebook	N	16,977	770,658	0.0053	[295]
89	Facebook: Texas80	Facebook	N	31,538	1,219,639	0.0025	[295]
90	Facebook: Texas84	Facebook	N	36,364	1,590,651	0.0024	[295]
91	Facebook: Trinity	Facebook	N	2,613	111,996	0.0328	[295]
92	Facebook: Tufts	Facebook	N	6,672	249,722	0.0112	[295]
93	Facebook: Tulane	Facebook	N	7,740	283,912	0.0095	[295]
94	Facebook: U. Chicago	Facebook	N	6,561	208,088	0.0097	[295]
95	Facebook: U. Conn.	Facebook	N	17,206	604,867	0.0041	[295]

ID	Name	Category	Weighted	N	L	f_e	References
96	Facebook: U. Illinois	Facebook	N	30,795	1,264,421	0.0027	[295]
97	Facebook: U. Mass.	Facebook	N	16,502	519,376	0.0038	[295]
98	Facebook: U. Penn.	Facebook	N	14,888	686,485	0.0062	[295]
99	Facebook: UC33	Facebook	N	16,800	522,141	0.0037	[295]
100	Facebook: UC61	Facebook	N	13,736	442,169	0.0047	[295]
101	Facebook: UC64	Facebook	N	6,810	155,320	0.0067	[295]
102	Facebook: UCF	Facebook	N	14,936	428,987	0.0038	[295]
103	Facebook: UCLA	Facebook	N	20,453	747,604	0.0036	[295]
104	Facebook: UCSB	Facebook	N	14,917	482,215	0.0043	[295]
105	Facebook: UCSC	Facebook	N	8,979	224,578	0.0056	[295]
106	Facebook: UCSD	Facebook	N	14,936	443,215	0.0040	[295]
107	Facebook: UF	Facebook	N	35,111	1,465,654	0.0024	[295]
108	Facebook: UGA	Facebook	N	24,380	1,174,051	0.0040	[295]
109	Facebook: UNC	Facebook	N	18,158	766,796	0.0047	[295]
110	Facebook: USC	Facebook	N	17,440	801,851	0.0053	[295]
111	Facebook: USF	Facebook	N	13,367	321,209	0.0036	[295]
112	Facebook: USFCA	Facebook	N	2,672	65,244	0.0183	[295]
113	Facebook: UVA	Facebook	N	17,178	789,308	0.0054	[295]
114	Facebook: Vanderbilt	Facebook	N	8,063	427,829	0.0132	[295]
115	Facebook: Vassar	Facebook	N	3,068	119,161	0.0253	[295]
116	Facebook: Vermont	Facebook	N	7,322	191,220	0.0071	[295]
117	Facebook: Villanova	Facebook	N	7,755	314,980	0.0105	[295]
118	Facebook: Virginia	Facebook	N	21,319	698,175	0.0031	[295]
119	Facebook: Wake	Facebook	N	5,366	279,186	0.0194	[295]
120	Facebook: Wash. U.	Facebook	N	7,730	367,526	0.0123	[295]
121	Facebook: Wellesley	Facebook	N	2,970	94,899	0.0215	[295]
122	Facebook: Wesleyan	Facebook	N	3,591	138,034	0.0214	[295]
123	Facebook: William	Facebook	N	6,472	266,378	0.0127	[295]
124	Facebook: Williams	Facebook	N	2,788	112,985	0.0291	[295]
125	Facebook: Wisconsin	Facebook	N	23,831	835,946	0.0029	[295]
126	Facebook: Yale	Facebook	N	8,561	405,440	0.0111	[295]
127	NYSE: 1980-1999	Financial	Y	477	113,526	1.0000	[229]
128	NYSE: 1980-1983	Financial	Y	477	113,526	1.0000	[229]
129	NYSE: 1984-1987	Financial	Y	477	113,526	1.0000	[229]
130	NYSE: 1988-1991	Financial	Y	477	113,526	1.0000	[229]

ID	Name	Category	Weighted	N	L	f_e	References
131	NYSE: 1992-1995	Financial	Y	477	113,526	1.0000	[229]
132	NYSE: 1996-1999	Financial	Y	477	113,526	1.0000	[229]
133	NYSE: H1 1985	Financial	Y	100	4,950	1.0000	[1]
134	NYSE: H2 1985	Financial	Y	100	4,950	1.0000	[1]
135	NYSE: H1 1986	Financial	Y	100	4,950	1.0000	[1]
136	NYSE: H2 1986	Financial	Y	100	4,950	1.0000	[1]
137	NYSE: H1 1987	Financial	Y	100	4,950	1.0000	[1]
138	NYSE: H2 1987	Financial	Y	100	4,950	1.0000	[1]
139	NYSE: H1 1988	Financial	Y	100	4,950	1.0000	[1]
140	NYSE: H2 1988	Financial	Y	100	4,950	1.0000	[1]
141	NYSE: H1 1989	Financial	Y	100	4,950	1.0000	[1]
142	NYSE: H2 1989	Financial	Y	100	4,950	1.0000	[1]
143	NYSE: H1 1990	Financial	Y	100	4,950	1.0000	[1]
144	NYSE: H2 1990	Financial	Y	100	4,950	1.0000	[1]
145	NYSE: H1 1991	Financial	Y	100	4,950	1.0000	[1]
146	NYSE: H2 1991	Financial	Y	100	4,950	1.0000	[1]
147	NYSE: H1 1992	Financial	Y	100	4,950	1.0000	[1]
148	NYSE: H2 1992	Financial	Y	100	4,950	1.0000	[1]
149	NYSE: H1 1993	Financial	Y	100	4,950	1.0000	[1]
150	NYSE: H2 1993	Financial	Y	100	4,950	1.0000	[1]
151	NYSE: H1 1994	Financial	Y	100	4,950	1.0000	[1]
152	NYSE: H2 1994	Financial	Y	100	4,950	1.0000	[1]
153	NYSE: H1 1995	Financial	Y	100	4,950	1.0000	[1]
154	NYSE: H2 1995	Financial	Y	100	4,950	1.0000	[1]
155	NYSE: H1 1996	Financial	Y	100	4,950	1.0000	[1]
156	NYSE: H2 1996	Financial	Y	100	4,950	1.0000	[1]
157	NYSE: H1 1997	Financial	Y	100	4,950	1.0000	[1]
158	NYSE: H2 1997	Financial	Y	100	4,950	1.0000	[1]
159	NYSE: H1 1998	Financial	Y	100	4,950	1.0000	[1]
160	NYSE: H2 1998	Financial	Y	100	4,950	1.0000	[1]
161	NYSE: H1 1999	Financial	Y	100	4,950	1.0000	[1]
162	NYSE: H2 1999	Financial	Y	100	4,950	1.0000	[1]
163	NYSE: H1 2000	Financial	Y	100	4,950	1.0000	[1]
164	NYSE: H2 2000	Financial	Y	100	4,950	1.0000	[1]
165	NYSE: H1 2001	Financial	Y	100	4,950	1.0000	[1]

ID	Name	Category	Weighted	N	L	f_e	References
166	NYSE: H2 2001	Financial	Y	100	4,950	1.0000	[1]
167	NYSE: H1 2002	Financial	Y	100	4,950	1.0000	[1]
168	NYSE: H2 2002	Financial	Y	100	4,950	1.0000	[1]
169	NYSE: H1 2003	Financial	Y	100	4,950	1.0000	[1]
170	NYSE: H2 2003	Financial	Y	100	4,950	1.0000	[1]
171	NYSE: H1 2004	Financial	Y	100	4,950	1.0000	[1]
172	NYSE: H2 2004	Financial	Y	100	4,950	1.0000	[1]
173	NYSE: H1 2005	Financial	Y	100	4,950	1.0000	[1]
174	NYSE: H2 2005	Financial	Y	100	4,950	1.0000	[1]
175	NYSE: H1 2006	Financial	Y	100	4,950	1.0000	[1]
176	NYSE: H2 2006	Financial	Y	100	4,950	1.0000	[1]
177	NYSE: H1 2007	Financial	Y	100	4,950	1.0000	[1]
178	NYSE: H2 2008	Financial	Y	100	4,950	1.0000	[1]
179	NYSE: H1 2008	Financial	Y	100	4,950	1.0000	[1]
180	NYSE: H2 2000	Financial	Y	100	4,950	1.0000	[1]
181	FX: 1992	Financial	Y	110	5,995	1.0000	[204, 205]
182	FX: 1993	Financial	Y	110	5,995	1.0000	[204, 205]
183	FX: 1994	Financial	Y	110	5,995	1.0000	[204, 205]
184	FX: 1995	Financial	Y	110	5,995	1.0000	[204, 205]
185	FX: 1996	Financial	Y	110	5,995	1.0000	[204, 205]
186	FX: 1997	Financial	Y	110	5,995	1.0000	[204, 205]
187	FX: 1998	Financial	Y	110	5,995	1.0000	[204, 205]
188	FX: 1999	Financial	Y	110	5,995	1.0000	[204, 205]
189	FX: 2000	Financial	Y	110	5,995	1.0000	[204, 205]
190	FX: 2001	Financial	Y	110	5,995	1.0000	[204, 205]
191	FX: 2002	Financial	Y	110	5,995	1.0000	[204, 205]
192	FX: 2005	Financial	Y	110	5,995	1.0000	[204, 205]
193	FX: 2006	Financial	Y	110	5,995	1.0000	[204, 205]
194	FX: 2007	Financial	Y	110	5,995	1.0000	[204, 205]
195	FX: 2008	Financial	Y	110	5,995	1.0000	[204, 205]
196	Fungal: (11,11)*	Fungal	Y	823	954	0.0028	[33, 113, 114, 288]
197	Fungal: (11,2)	Fungal	Y	117	136	0.0200	[33, 113, 114, 288]
198	Fungal: (11,5)	Fungal	Y	526	588	0.0043	[33, 113, 114, 288]
199	Fungal: (11,8)	Fungal	Y	721	821	0.0032	[33, 113, 114, 288]
200	Fungal: (17,11)	Fungal	Y	1,205	1,469	0.0020	[33, 113, 114, 288]

ID	Name	Category	Weighted	N	L	f_e	References
201	Fungal: (17,2)	Fungal	Y	232	240	0.0090	[33, 113, 114, 288]
202	Fungal: (17,5)	Fungal	Y	816	874	0.0026	[33, 113, 114, 288]
203	Fungal: (17,8)	Fungal	Y	1,113	1,303	0.0021	[33, 113, 114, 288]
204	Fungal: (4,11)	Fungal	Y	2,190	2,431	0.0010	[33, 113, 114, 288]
205	Fungal: (4,2)	Fungal	Y	461	490	0.0046	[33, 113, 114, 288]
206	Fungal: (4,5)	Fungal	Y	1,380	1,476	0.0016	[33, 113, 114, 288]
207	Fungal: (4,8)	Fungal	Y	1,869	2,061	0.0012	[33, 113, 114, 288]
208	AIDS blogs*	WWW	N	146	180	0.0170	[132]
209	Political blogs	WWW	Y	1,222	16,714	0.0224	[3]
210	WWW (Stanford)	WWW	N	8,929	26,320	0.0007	[124]
211	Online Dictionary of Computing	Language	Y	13,356	91,471	0.0010	[30]
212	Online Dictionary Of Information Science	Language	Y	2,898	16,376	0.0039	[77, 255]
213	Reuters 9/11 news	Language	Y	13,308	148,035	0.0017	[158]
214	Roget's thesaurus	Language	N	994	3,640	0.0074	[77, 168]
215	Word adjacency: English	Language	N	7,377	44,205	0.0016	[210]
216	Word adjacency: French	Language	N	8,308	23,832	0.0007	[210]
217	Word adjacency: Japanese	Language	N	2,698	7,995	0.0022	[210]
218	Word adjacency: Spanish	Language	N	11,558	43,050	0.0006	[210]
219	Metabolic: AA	Metabolic	N	411	1,818	0.0216	[156]
220	Metabolic: AB	Metabolic	N	386	1,691	0.0228	[156]
221	Metabolic: AG	Metabolic	N	494	2,173	0.0178	[156]
222	Metabolic: AP	Metabolic	N	201	857	0.0426	[156]
223	Metabolic: AT	Metabolic	N	296	1,231	0.0282	[156]
224	Metabolic: BB	Metabolic	N	175	628	0.0412	[156]
225	Metabolic: BS	Metabolic	N	772	3,611	0.0121	[156]
226	Metabolic: CA	Metabolic	N	483	2,274	0.0195	[156]
227	Metabolic: CE	Metabolic	N	453	2,025	0.0198	[156]
228	Metabolic: CJ	Metabolic	N	370	1,631	0.0239	[156]
229	Metabolic: CL	Metabolic	N	382	1,646	0.0226	[156]
230	Metabolic: CQ	Metabolic	N	187	663	0.0381	[156]
231	Metabolic: CT	Metabolic	N	211	772	0.0348	[156]
232	Metabolic: CY	Metabolic	N	537	2,503	0.0174	[156]
233	Metabolic: DR	Metabolic	N	800	3,789	0.0119	[156]
234	Metabolic: EC	Metabolic	N	762	3,683	0.0127	[156]
235	Metabolic: EF	Metabolic	N	375	1,721	0.0245	[156]

ID	Name	Category	Weighted	N	L	f_e	References
236	Metabolic: EN	Metabolic	N	374	1,617	0.0232	[156]
237	Metabolic: HI	Metabolic	N	505	2,325	0.0183	[156]
238	Metabolic: HP	Metabolic	N	365	1,703	0.0256	[156]
239	Metabolic: MB	Metabolic	N	418	1,850	0.0212	[156]
240	Metabolic: MG	Metabolic	N	199	783	0.0397	[156]
241	Metabolic: MJ	Metabolic	N	422	1,874	0.0211	[156]
242	Metabolic: ML	Metabolic	N	414	1,862	0.0218	[156]
243	Metabolic: MP	Metabolic	N	171	685	0.0471	[156]
244	Metabolic: MT	Metabolic	N	577	2,653	0.0160	[156]
245	Metabolic: NG	Metabolic	N	394	1,824	0.0236	[156]
246	Metabolic: NM	Metabolic	N	369	1,708	0.0252	[156]
247	Metabolic: OS	Metabolic	N	285	1,168	0.0289	[156]
248	Metabolic: PA	Metabolic	N	720	3,429	0.0132	[156]
249	Metabolic: PF	Metabolic	N	310	1,379	0.0288	[156]
250	Metabolic: PG	Metabolic	N	412	1,772	0.0209	[156]
251	Metabolic: PH	Metabolic	N	318	1,394	0.0277	[156]
252	Metabolic: PN	Metabolic	N	405	1,829	0.0224	[156]
253	Metabolic: RC	Metabolic	N	663	3,111	0.0142	[156]
254	Metabolic: RP	Metabolic	N	203	775	0.0378	[156]
255	Metabolic: SC	Metabolic	N	552	2,595	0.0171	[156]
256	Metabolic: ST	Metabolic	N	391	1,756	0.0230	[156]
257	Metabolic: TH	Metabolic	N	427	1,955	0.0215	[156]
258	Metabolic: TM	Metabolic	N	328	1,452	0.0271	[156]
259	Metabolic: TP	Metabolic	N	194	788	0.0421	[156]
260	Metabolic: TY	Metabolic	N	803	3,863	0.0120	[156]
261	Metabolic: YP	Metabolic	N	552	2,471	0.0162	[156]
262	U.S. political books co-purchase*	Other	N	105	441	0.0808	[171]
263	Power grid	Other	N	4,941	6,594	0.0005	[305]
264	Slovenian magazine co-purchase	Other	Y	124	5,972	0.7831	[28]
265	Transcription: <i>E. coli</i>	Other	N	328	456	0.0085	[196]
266	Transcription: Yeast	Other	N	662	1,062	0.0049	[211]
267	U.S. airlines	Other	Y	324	2,081	0.0398	[29, 77]
268	2008 NCAA football schedule*	Other	Y	121	764	0.1052	[61]
269	Internet: autonomous systems	Other	N	22,963	48,436	0.0002	[219]
270	Protein: serine protease inhibitor (1EAW)*	Other	N	53	123	0.0893	[210]

ID	Name	Category	Weighted	N	L	f_e	References
271	Protein: immunoglobulin (1A4J)*	Other	N	95	213	0.0477	[210]
272	Protein: oxidoreductase (1AOR)*	Other	N	97	212	0.0455	[210]
273	Bill cosponsorship: U.S. House 96	Political: cosponsorship	Y	438	95,529	0.9982	[108, 109]
274	Bill cosponsorship: U.S. House 97	Political: cosponsorship	Y	435	94,374	0.9998	[108, 109]
275	Bill cosponsorship: U.S. House 98	Political: cosponsorship	Y	437	95,256	0.9999	[108, 109]
276	Bill cosponsorship: U.S. House 99	Political: cosponsorship	Y	437	94,999	0.9972	[108, 109]
277	Bill cosponsorship: U.S. House 100	Political: cosponsorship	Y	439	96,125	0.9998	[108, 109]
278	Bill cosponsorship: U.S. House 101	Political: cosponsorship	Y	437	95,263	1.0000	[108, 109]
279	Bill cosponsorship: U.S. House 102	Political: cosponsorship	Y	437	95,051	0.9977	[108, 109]
280	Bill cosponsorship: U.S. House 103	Political: cosponsorship	Y	437	95,028	0.9975	[108, 109]
281	Bill cosponsorship: U.S. House 104	Political: cosponsorship	Y	439	95,925	0.9978	[108, 109]
282	Bill cosponsorship: U.S. House 105	Political: cosponsorship	Y	442	97,373	0.9991	[108, 109]
283	Bill cosponsorship: U.S. House 106	Political: cosponsorship	Y	436	94,820	0.9999	[108, 109]
284	Bill cosponsorship: U.S. House 107	Political: cosponsorship	Y	442	97,233	0.9977	[108, 109]
285	Bill cosponsorship: U.S. House 108	Political: cosponsorship	Y	439	96,104	0.9996	[108, 109]
286	Bill cosponsorship: U.S. Senate 96	Political: cosponsorship	Y	101	5,050	1.0000	[108, 109]
287	Bill cosponsorship: U.S. Senate 97	Political: cosponsorship	Y	101	5,050	1.0000	[108, 109]
288	Bill cosponsorship: U.S. Senate 98	Political: cosponsorship	Y	101	5,050	1.0000	[108, 109]
289	Bill cosponsorship: U.S. Senate 99	Political: cosponsorship	Y	101	5,049	0.9998	[108, 109]
290	Bill cosponsorship: U.S. Senate 100	Political: cosponsorship	Y	101	5,050	1.0000	[108, 109]
291	Bill cosponsorship: U.S. Senate 101	Political: cosponsorship	Y	100	4,950	1.0000	[108, 109]
292	Bill cosponsorship: U.S. Senate 102	Political: cosponsorship	Y	102	5,142	0.9983	[108, 109]
293	Bill cosponsorship: U.S. Senate 103	Political: cosponsorship	Y	101	5,050	1.0000	[108, 109]
294	Bill cosponsorship: U.S. Senate 104	Political: cosponsorship	Y	102	5,151	1.0000	[108, 109]
295	Bill cosponsorship: U.S. Senate 105	Political: cosponsorship	Y	100	4,950	1.0000	[108, 109]
296	Bill cosponsorship: U.S. Senate 106	Political: cosponsorship	Y	102	5,151	1.0000	[108, 109]
297	Bill cosponsorship: U.S. Senate 107	Political: cosponsorship	Y	101	5,049	0.9998	[108, 109]
298	Bill cosponsorship: U.S. Senate 108	Political: cosponsorship	Y	100	4,950	1.0000	[108, 109]
299	Committees: U.S. House 101, comms.	Political: committee	N	159	3,610	0.2874	[242, 243]
300	Committees: U.S. House 102, comms.	Political: committee	N	163	4,093	0.3100	[242, 243]
301	Committees: U.S. House 103, comms.	Political: committee	N	141	2,983	0.3022	[242, 243]
302	Committees: U.S. House 104, comms.	Political: committee	N	106	1,839	0.3305	[242, 243]
303	Committees: U.S. House 105, comms.	Political: committee	N	108	1,997	0.3456	[242, 243]
304	Committees: U.S. House 106, comms.	Political: committee	N	107	2,031	0.3581	[242, 243]
305	Committees: U.S. House 107, comms.	Political: committee	N	113	2,429	0.3838	[242, 243]

ID	Name	Category	Weighted	N	L	f_e	References
306	Committees: U.S. House 108, comms.	Political: committee	N	118	2,905	0.4208	[242, 243]
307	Committees: U.S. House 101, Reps.	Political: committee	N	434	18,714	0.1992	[242, 243]
308	Committees: U.S. House 102, Reps.	Political: committee	N	436	20,134	0.2123	[242, 243]
309	Committees: U.S. House 103, Reps.	Political: committee	N	437	18,212	0.1912	[242, 243]
310	Committees: U.S. House 104, Reps.	Political: committee	N	432	17,130	0.1840	[242, 243]
311	Committees: U.S. House 105, Reps.	Political: committee	N	435	18,297	0.1938	[242, 243]
312	Committees: U.S. House 106, Reps.	Political: committee	N	435	18,832	0.1995	[242, 243]
313	Committees: U.S. House 107, Reps.	Political: committee	N	434	19,824	0.2110	[242, 243]
314	Committees: U.S. House 108, Reps.	Political: committee	N	437	21,214	0.2227	[242, 243]
315	Roll call: U.S. House 1	Political: voting	Y	66	2,122	0.9893	[203, 241, 306]
316	Roll call: U.S. House 2	Political: voting	Y	71	2,428	0.9771	[203, 241, 306]
317	Roll call: U.S. House 3	Political: voting	Y	108	5,669	0.9811	[203, 241, 306]
318	Roll call: U.S. House 4	Political: voting	Y	114	6,342	0.9846	[203, 241, 306]
319	Roll call: U.S. House 5	Political: voting	Y	117	6,600	0.9726	[203, 241, 306]
320	Roll call: U.S. House 6	Political: voting	Y	113	6,222	0.9832	[203, 241, 306]
321	Roll call: U.S. House 7	Political: voting	Y	110	5,921	0.9877	[203, 241, 306]
322	Roll call: U.S. House 8	Political: voting	Y	149	10,888	0.9875	[203, 241, 306]
323	Roll call: U.S. House 9	Political: voting	Y	147	10,582	0.9861	[203, 241, 306]
324	Roll call: U.S. House 10	Political: voting	Y	149	10,857	0.9847	[203, 241, 306]
325	Roll call: U.S. House 11	Political: voting	Y	153	11,482	0.9874	[203, 241, 306]
326	Roll call: U.S. House 12	Political: voting	Y	146	10,535	0.9953	[203, 241, 306]
327	Roll call: U.S. House 13	Political: voting	Y	195	18,723	0.9898	[203, 241, 306]
328	Roll call: U.S. House 14	Political: voting	Y	195	18,540	0.9802	[203, 241, 306]
329	Roll call: U.S. House 15	Political: voting	Y	195	18,666	0.9868	[203, 241, 306]
330	Roll call: U.S. House 16	Political: voting	Y	197	19,118	0.9903	[203, 241, 306]
331	Roll call: U.S. House 17	Political: voting	Y	199	19,429	0.9862	[203, 241, 306]
332	Roll call: U.S. House 18	Political: voting	Y	221	23,812	0.9795	[203, 241, 306]
333	Roll call: U.S. House 19	Political: voting	Y	220	23,993	0.9960	[203, 241, 306]
334	Roll call: U.S. House 20	Political: voting	Y	219	23,666	0.9914	[203, 241, 306]
335	Roll call: U.S. House 21	Political: voting	Y	220	23,985	0.9956	[203, 241, 306]
336	Roll call: U.S. House 22	Political: voting	Y	217	23,404	0.9986	[203, 241, 306]
337	Roll call: U.S. House 23	Political: voting	Y	257	32,502	0.9880	[203, 241, 306]
338	Roll call: U.S. House 24	Political: voting	Y	255	32,062	0.9900	[203, 241, 306]
339	Roll call: U.S. House 25	Political: voting	Y	256	32,366	0.9916	[203, 241, 306]
340	Roll call: U.S. House 26	Political: voting	Y	255	32,067	0.9902	[203, 241, 306]

ID	Name	Category	Weighted	N	L	f_e	References
341	Roll call: U.S. House 27	Political: voting	Y	257	32,743	0.9953	[203, 241, 306]
342	Roll call: U.S. House 28	Political: voting	Y	234	26,788	0.9826	[203, 241, 306]
343	Roll call: U.S. House 29	Political: voting	Y	236	27,562	0.9939	[203, 241, 306]
344	Roll call: U.S. House 30	Political: voting	Y	236	27,669	0.9978	[203, 241, 306]
345	Roll call: U.S. House 31	Political: voting	Y	241	28,804	0.9960	[203, 241, 306]
346	Roll call: U.S. House 32	Political: voting	Y	239	28,318	0.9957	[203, 241, 306]
347	Roll call: U.S. House 33	Political: voting	Y	240	28,570	0.9962	[203, 241, 306]
348	Roll call: U.S. House 34	Political: voting	Y	236	27,545	0.9933	[203, 241, 306]
349	Roll call: U.S. House 35	Political: voting	Y	245	29,630	0.9913	[203, 241, 306]
350	Roll call: U.S. House 36	Political: voting	Y	243	29,312	0.9969	[203, 241, 306]
351	Roll call: U.S. House 37	Political: voting	Y	197	18,735	0.9704	[203, 241, 306]
352	Roll call: U.S. House 38	Political: voting	Y	187	17,326	0.9963	[203, 241, 306]
353	Roll call: U.S. House 39	Political: voting	Y	199	19,593	0.9945	[203, 241, 306]
354	Roll call: U.S. House 40	Political: voting	Y	233	26,605	0.9843	[203, 241, 306]
355	Roll call: U.S. House 41	Political: voting	Y	256	32,109	0.9837	[203, 241, 306]
356	Roll call: U.S. House 42	Political: voting	Y	253	31,626	0.9921	[203, 241, 306]
357	Roll call: U.S. House 43	Political: voting	Y	302	45,151	0.9934	[203, 241, 306]
358	Roll call: U.S. House 44	Political: voting	Y	308	46,723	0.9883	[203, 241, 306]
359	Roll call: U.S. House 45	Political: voting	Y	302	45,315	0.9970	[203, 241, 306]
360	Roll call: U.S. House 46	Political: voting	Y	301	44,987	0.9964	[203, 241, 306]
361	Roll call: U.S. House 47	Political: voting	Y	306	46,214	0.9903	[203, 241, 306]
362	Roll call: U.S. House 48	Political: voting	Y	338	56,484	0.9918	[203, 241, 306]
363	Roll call: U.S. House 49	Political: voting	Y	330	54,160	0.9977	[203, 241, 306]
364	Roll call: U.S. House 50	Political: voting	Y	326	52,907	0.9987	[203, 241, 306]
365	Roll call: U.S. House 51	Political: voting	Y	347	59,303	0.9879	[203, 241, 306]
366	Roll call: U.S. House 52	Political: voting	Y	340	57,285	0.9940	[203, 241, 306]
367	Roll call: U.S. House 53	Political: voting	Y	376	69,943	0.9921	[203, 241, 306]
368	Roll call: U.S. House 54	Political: voting	Y	368	67,085	0.9934	[203, 241, 306]
369	Roll call: U.S. House 55	Political: voting	Y	371	68,270	0.9947	[203, 241, 306]
370	Roll call: U.S. House 56	Political: voting	Y	369	67,059	0.9877	[203, 241, 306]
371	Roll call: U.S. House 57	Political: voting	Y	371	67,383	0.9818	[203, 241, 306]
372	Roll call: U.S. House 58	Political: voting	Y	397	75,891	0.9655	[203, 241, 306]
373	Roll call: U.S. House 59	Political: voting	Y	397	76,299	0.9707	[203, 241, 306]
374	Roll call: U.S. House 60	Political: voting	Y	398	77,921	0.9863	[203, 241, 306]
375	Roll call: U.S. House 61	Political: voting	Y	402	80,174	0.9947	[203, 241, 306]

ID	Name	Category	Weighted	N	L	f_e	References
376	Roll call: U.S. House 62	Political: voting	Y	408	82,442	0.9929	[203, 241, 306]
377	Roll call: U.S. House 63	Political: voting	Y	452	101,498	0.9958	[203, 241, 306]
378	Roll call: U.S. House 64	Political: voting	Y	441	96,780	0.9975	[203, 241, 306]
379	Roll call: U.S. House 65	Political: voting	Y	454	102,108	0.9930	[203, 241, 306]
380	Roll call: U.S. House 66	Political: voting	Y	453	101,199	0.9885	[203, 241, 306]
381	Roll call: U.S. House 67	Political: voting	Y	452	101,482	0.9956	[203, 241, 306]
382	Roll call: U.S. House 68	Political: voting	Y	442	96,885	0.9941	[203, 241, 306]
383	Roll call: U.S. House 69	Political: voting	Y	437	95,226	0.9996	[203, 241, 306]
384	Roll call: U.S. House 70	Political: voting	Y	443	97,497	0.9959	[203, 241, 306]
385	Roll call: U.S. House 71	Political: voting	Y	455	102,502	0.9924	[203, 241, 306]
386	Roll call: U.S. House 72	Political: voting	Y	447	99,028	0.9934	[203, 241, 306]
387	Roll call: U.S. House 73	Political: voting	Y	445	98,647	0.9986	[203, 241, 306]
388	Roll call: U.S. House 74	Political: voting	Y	440	96,170	0.9958	[203, 241, 306]
389	Roll call: U.S. House 75	Political: voting	Y	445	98,474	0.9968	[203, 241, 306]
390	Roll call: U.S. House 76	Political: voting	Y	456	102,495	0.9880	[203, 241, 306]
391	Roll call: U.S. House 77	Political: voting	Y	450	99,956	0.9894	[203, 241, 306]
392	Roll call: U.S. House 78	Political: voting	Y	450	100,513	0.9949	[203, 241, 306]
393	Roll call: U.S. House 79	Political: voting	Y	448	99,246	0.9912	[203, 241, 306]
394	Roll call: U.S. House 80	Political: voting	Y	448	99,902	0.9977	[203, 241, 306]
395	Roll call: U.S. House 81	Political: voting	Y	444	98,054	0.9970	[203, 241, 306]
396	Roll call: U.S. House 82	Political: voting	Y	447	99,281	0.9960	[203, 241, 306]
397	Roll call: U.S. House 83	Political: voting	Y	440	96,506	0.9992	[203, 241, 306]
398	Roll call: U.S. House 84	Political: voting	Y	437	95,253	0.9999	[203, 241, 306]
399	Roll call: U.S. House 85	Political: voting	Y	444	97,955	0.9960	[203, 241, 306]
400	Roll call: U.S. House 86	Political: voting	Y	443	97,377	0.9946	[203, 241, 306]
401	Roll call: U.S. House 87	Political: voting	Y	449	99,774	0.9920	[203, 241, 306]
401	Roll call: U.S. House 88	Political: voting	Y	443	97,842	0.9994	[203, 241, 306]
403	Roll call: U.S. House 89	Political: voting	Y	442	97,139	0.9967	[203, 241, 306]
404	Roll call: U.S. House 90	Political: voting	Y	437	95,251	0.9998	[203, 241, 306]
405	Roll call: U.S. House 91	Political: voting	Y	448	99,815	0.9969	[203, 241, 306]
406	Roll call: U.S. House 92	Political: voting	Y	443	97,579	0.9967	[203, 241, 306]
407	Roll call: U.S. House 93	Political: voting	Y	443	97,848	0.9994	[203, 241, 306]
408	Roll call: U.S. House 94	Political: voting	Y	441	96,837	0.9981	[203, 241, 306]
409	Roll call: U.S. House 95	Political: voting	Y	441	96,493	0.9946	[203, 241, 306]
410	Roll call: U.S. House 96	Political: voting	Y	440	96,379	0.9979	[203, 241, 306]

ID	Name	Category	Weighted	N	L	f_e	References
411	Roll call: U.S. House 97	Political: voting	Y	442	96,761	0.9928	[203, 241, 306]
412	Roll call: U.S. House 98	Political: voting	Y	439	95,922	0.9977	[203, 241, 306]
413	Roll call: U.S. House 99	Political: voting	Y	439	95,875	0.9972	[203, 241, 306]
414	Roll call: U.S. House 100	Political: voting	Y	440	96,544	0.9996	[203, 241, 306]
415	Roll call: U.S. House 101	Political: voting	Y	440	96,505	0.9992	[203, 241, 306]
416	Roll call: U.S. House 102	Political: voting	Y	441	96,811	0.9978	[203, 241, 306]
417	Roll call: U.S. House 103	Political: voting	Y	441	96,348	0.9931	[203, 241, 306]
418	Roll call: U.S. House 104	Political: voting	Y	445	98,720	0.9993	[203, 241, 306]
419	Roll call: U.S. House 105	Political: voting	Y	443	97,841	0.9994	[203, 241, 306]
420	Roll call: U.S. House 106	Political: voting	Y	440	96,557	0.9998	[203, 241, 306]
421	Roll call: U.S. House 107	Political: voting	Y	443	97,816	0.9991	[203, 241, 306]
422	Roll call: U.S. House 108	Political: voting	Y	440	96,561	0.9998	[203, 241, 306]
423	Roll call: U.S. House 109	Political: voting	Y	440	96,549	0.9997	[203, 241, 306]
424	Roll call: U.S. House 110	Political: voting	Y	448	99,603	0.9948	[203, 241, 306]
425	Roll call: U.S. Senate 1	Political: voting	Y	29	393	0.9680	[203, 241, 306]
426	Roll call: U.S. Senate 2	Political: voting	Y	31	449	0.9656	[203, 241, 306]
427	Roll call: U.S. Senate 3	Political: voting	Y	32	472	0.9516	[203, 241, 306]
428	Roll call: U.S. Senate 4	Political: voting	Y	43	760	0.8416	[203, 241, 306]
429	Roll call: U.S. Senate 5	Political: voting	Y	44	808	0.8541	[203, 241, 306]
430	Roll call: U.S. Senate 6	Political: voting	Y	37	644	0.9670	[203, 241, 306]
431	Roll call: U.S. Senate 7	Political: voting	Y	35	537	0.9025	[203, 241, 306]
432	Roll call: U.S. Senate 8	Political: voting	Y	44	864	0.9133	[203, 241, 306]
433	Roll call: U.S. Senate 9	Political: voting	Y	37	645	0.9685	[203, 241, 306]
434	Roll call: U.S. Senate 10	Political: voting	Y	37	660	0.9910	[203, 241, 306]
435	Roll call: U.S. Senate 11	Political: voting	Y	44	855	0.9038	[203, 241, 306]
436	Roll call: U.S. Senate 12	Political: voting	Y	37	663	0.9955	[203, 241, 306]
437	Roll call: U.S. Senate 13	Political: voting	Y	46	947	0.9150	[203, 241, 306]
438	Roll call: U.S. Senate 14	Political: voting	Y	44	898	0.9493	[203, 241, 306]
439	Roll call: U.S. Senate 15	Political: voting	Y	46	977	0.9440	[203, 241, 306]
440	Roll call: U.S. Senate 16	Political: voting	Y	51	1,249	0.9796	[203, 241, 306]
441	Roll call: U.S. Senate 17	Political: voting	Y	52	1,294	0.9759	[203, 241, 306]
442	Roll call: U.S. Senate 18	Political: voting	Y	52	1,304	0.9834	[203, 241, 306]
443	Roll call: U.S. Senate 19	Political: voting	Y	59	1,589	0.9287	[203, 241, 306]
444	Roll call: U.S. Senate 20	Political: voting	Y	53	1,343	0.9746	[203, 241, 306]
445	Roll call: U.S. Senate 21	Political: voting	Y	54	1,339	0.9357	[203, 241, 306]

ID	Name	Category	Weighted	N	L	f_e	References
446	Roll call: U.S. Senate 22	Political: voting	Y	53	1,348	0.9782	[203, 241, 306]
447	Roll call: U.S. Senate 23	Political: voting	Y	54	1,378	0.9630	[203, 241, 306]
448	Roll call: U.S. Senate 24	Political: voting	Y	61	1,732	0.9464	[203, 241, 306]
449	Roll call: U.S. Senate 25	Political: voting	Y	58	1,627	0.9843	[203, 241, 306]
440	Roll call: U.S. Senate 26	Political: voting	Y	60	1,689	0.9542	[203, 241, 306]
451	Roll call: U.S. Senate 27	Political: voting	Y	59	1,662	0.9714	[203, 241, 306]
452	Roll call: U.S. Senate 28	Political: voting	Y	57	1,575	0.9868	[203, 241, 306]
453	Roll call: U.S. Senate 29	Political: voting	Y	63	1,895	0.9703	[203, 241, 306]
454	Roll call: U.S. Senate 30	Political: voting	Y	72	2,320	0.9077	[203, 241, 306]
455	Roll call: U.S. Senate 31	Political: voting	Y	70	2,341	0.9694	[203, 241, 306]
456	Roll call: U.S. Senate 32	Political: voting	Y	73	2,511	0.9555	[203, 241, 306]
457	Roll call: U.S. Senate 33	Political: voting	Y	70	2,308	0.9557	[203, 241, 306]
458	Roll call: U.S. Senate 34	Political: voting	Y	64	2,002	0.9931	[203, 241, 306]
459	Roll call: U.S. Senate 35	Political: voting	Y	73	2,542	0.9673	[203, 241, 306]
460	Roll call: U.S. Senate 36	Political: voting	Y	70	2,370	0.9814	[203, 241, 306]
461	Roll call: U.S. Senate 37	Political: voting	Y	70	2,051	0.8493	[203, 241, 306]
462	Roll call: U.S. Senate 38	Political: voting	Y	54	1,402	0.9797	[203, 241, 306]
463	Roll call: U.S. Senate 39	Political: voting	Y	59	1,610	0.9410	[203, 241, 306]
464	Roll call: U.S. Senate 40	Political: voting	Y	69	2,274	0.9693	[203, 241, 306]
465	Roll call: U.S. Senate 41	Political: voting	Y	80	3,084	0.9759	[203, 241, 306]
466	Roll call: U.S. Senate 42	Political: voting	Y	75	2,773	0.9993	[203, 241, 306]
467	Roll call: U.S. Senate 43	Political: voting	Y	79	3,041	0.9870	[203, 241, 306]
468	Roll call: U.S. Senate 44	Political: voting	Y	82	3,261	0.9819	[203, 241, 306]
469	Roll call: U.S. Senate 45	Political: voting	Y	82	3,265	0.9831	[203, 241, 306]
470	Roll call: U.S. Senate 46	Political: voting	Y	81	3,219	0.9935	[203, 241, 306]
471	Roll call: U.S. Senate 47	Political: voting	Y	83	3,362	0.9880	[203, 241, 306]
472	Roll call: U.S. Senate 48	Political: voting	Y	78	2,998	0.9983	[203, 241, 306]
473	Roll call: U.S. Senate 49	Political: voting	Y	81	3,210	0.9907	[203, 241, 306]
474	Roll call: U.S. Senate 50	Political: voting	Y	76	2,850	1.0000	[203, 241, 306]
475	Roll call: U.S. Senate 51	Political: voting	Y	91	3,998	0.9763	[203, 241, 306]
476	Roll call: U.S. Senate 52	Political: voting	Y	93	4,249	0.9932	[203, 241, 306]
477	Roll call: U.S. Senate 53	Political: voting	Y	95	4,413	0.9884	[203, 241, 306]
478	Roll call: U.S. Senate 54	Political: voting	Y	90	4,000	0.9988	[203, 241, 306]
479	Roll call: U.S. Senate 55	Political: voting	Y	96	4,445	0.9748	[203, 241, 306]
480	Roll call: U.S. Senate 56	Political: voting	Y	93	4,201	0.9820	[203, 241, 306]

ID	Name	Category	Weighted	N	L	f_e	References
481	Roll call: U.S. Senate 57	Political: voting	Y	90	3,939	0.9835	[203, 241, 306]
482	Roll call: U.S. Senate 58	Political: voting	Y	93	4,174	0.9757	[203, 241, 306]
483	Roll call: U.S. Senate 59	Political: voting	Y	93	4,251	0.9937	[203, 241, 306]
484	Roll call: U.S. Senate 60	Political: voting	Y	95	4,382	0.9814	[203, 241, 306]
485	Roll call: U.S. Senate 61	Political: voting	Y	102	5,033	0.9771	[203, 241, 306]
486	Roll call: U.S. Senate 62	Political: voting	Y	109	5,719	0.9716	[203, 241, 306]
487	Roll call: U.S. Senate 63	Political: voting	Y	101	5,029	0.9958	[203, 241, 306]
488	Roll call: U.S. Senate 64	Political: voting	Y	100	4,931	0.9962	[203, 241, 306]
489	Roll call: U.S. Senate 65	Political: voting	Y	111	5,899	0.9663	[203, 241, 306]
490	Roll call: U.S. Senate 66	Political: voting	Y	101	5,005	0.9911	[203, 241, 306]
491	Roll call: U.S. Senate 67	Political: voting	Y	105	5,413	0.9914	[203, 241, 306]
492	Roll call: U.S. Senate 68	Political: voting	Y	102	5,081	0.9864	[203, 241, 306]
493	Roll call: U.S. Senate 69	Political: voting	Y	105	5,353	0.9804	[203, 241, 306]
494	Roll call: U.S. Senate 70	Political: voting	Y	102	5,082	0.9866	[203, 241, 306]
495	Roll call: U.S. Senate 71	Political: voting	Y	109	5,779	0.9818	[203, 241, 306]
496	Roll call: U.S. Senate 72	Political: voting	Y	103	5,220	0.9937	[203, 241, 306]
497	Roll call: U.S. Senate 73	Political: voting	Y	100	4,879	0.9857	[203, 241, 306]
498	Roll call: U.S. Senate 74	Political: voting	Y	100	4,933	0.9966	[203, 241, 306]
499	Roll call: U.S. Senate 75	Political: voting	Y	102	5,126	0.9951	[203, 241, 306]
500	Roll call: U.S. Senate 76	Political: voting	Y	104	5,106	0.9533	[203, 241, 306]
501	Roll call: U.S. Senate 77	Political: voting	Y	108	5,575	0.9649	[203, 241, 306]
502	Roll call: U.S. Senate 78	Political: voting	Y	104	5,304	0.9903	[203, 241, 306]
503	Roll call: U.S. Senate 79	Political: voting	Y	107	5,466	0.9639	[203, 241, 306]
504	Roll call: U.S. Senate 80	Political: voting	Y	97	4,655	0.9998	[203, 241, 306]
505	Roll call: U.S. Senate 81	Political: voting	Y	108	5,646	0.9772	[203, 241, 306]
506	Roll call: U.S. Senate 82	Political: voting	Y	98	4,748	0.9989	[203, 241, 306]
507	Roll call: U.S. Senate 83	Political: voting	Y	110	5,724	0.9548	[203, 241, 306]
508	Roll call: U.S. Senate 84	Political: voting	Y	99	4,845	0.9988	[203, 241, 306]
509	Roll call: U.S. Senate 85	Political: voting	Y	101	5,014	0.9929	[203, 241, 306]
510	Roll call: U.S. Senate 86	Political: voting	Y	103	5,246	0.9987	[203, 241, 306]
511	Roll call: U.S. Senate 87	Political: voting	Y	105	5,444	0.9971	[203, 241, 306]
512	Roll call: U.S. Senate 88	Political: voting	Y	103	5,249	0.9992	[203, 241, 306]
513	Roll call: U.S. Senate 89	Political: voting	Y	103	5,247	0.9989	[203, 241, 306]
514	Roll call: U.S. Senate 90	Political: voting	Y	101	5,048	0.9996	[203, 241, 306]
515	Roll call: U.S. Senate 91	Political: voting	Y	102	5,148	0.9994	[203, 241, 306]

ID	Name	Category	Weighted	N	L	f_e	References
516	Roll call: U.S. Senate 92	Political: voting	Y	102	5,147	0.9992	[203, 241, 306]
517	Roll call: U.S. Senate 93	Political: voting	Y	103	5,246	0.9987	[203, 241, 306]
518	Roll call: U.S. Senate 94	Political: voting	Y	101	5,049	0.9998	[203, 241, 306]
519	Roll call: U.S. Senate 95	Political: voting	Y	104	5,345	0.9979	[203, 241, 306]
520	Roll call: U.S. Senate 96	Political: voting	Y	101	5,049	0.9998	[203, 241, 306]
521	Roll call: U.S. Senate 97	Political: voting	Y	101	5,049	0.9998	[203, 241, 306]
522	Roll call: U.S. Senate 98	Political: voting	Y	101	5,049	0.9998	[203, 241, 306]
523	Roll call: U.S. Senate 99	Political: voting	Y	101	5,049	0.9998	[203, 241, 306]
524	Roll call: U.S. Senate 100	Political: voting	Y	101	5,049	0.9998	[203, 241, 306]
525	Roll call: U.S. Senate 101	Political: voting	Y	100	4,950	1.0000	[203, 241, 306]
526	Roll call: U.S. Senate 102	Political: voting	Y	102	5,148	0.9994	[203, 241, 306]
527	Roll call: U.S. Senate 103	Political: voting	Y	102	5,080	0.9862	[203, 241, 306]
528	Roll call: U.S. Senate 104	Political: voting	Y	103	5,247	0.9989	[203, 241, 306]
529	Roll call: U.S. Senate 105	Political: voting	Y	100	4,950	1.0000	[203, 241, 306]
530	Roll call: U.S. Senate 106	Political: voting	Y	102	5,148	0.9994	[203, 241, 306]
531	Roll call: U.S. Senate 107	Political: voting	Y	102	5,148	0.9994	[203, 241, 306]
532	Roll call: U.S. Senate 108	Political: voting	Y	100	4,950	1.0000	[203, 241, 306]
533	Roll call: U.S. Senate 109	Political: voting	Y	101	5,049	0.9998	[203, 241, 306]
534	Roll call: U.S. Senate 110	Political: voting	Y	102	5,147	0.9992	[203, 241, 306]
535	U.K. House of Commons voting: 1992-1997	Political: voting	Y	668	220,761	0.9909	[104]
536	U.K. House of Commons voting: 1997-2001	Political: voting	Y	671	223,092	0.9925	[104]
537	U.K. House of Commons voting: 2001-2005	Political: voting	Y	657	215,246	0.9988	[104]
538	U.N. resolutions 1	Political: voting	Y	54	1,431	1.0000	[302]
539	U.N. resolutions 2	Political: voting	Y	57	1,594	0.9987	[302]
540	U.N. resolutions 3	Political: voting	Y	59	1,711	1.0000	[302]
541	U.N. resolutions 4	Political: voting	Y	59	1,711	1.0000	[302]
542	U.N. resolutions 5	Political: voting	Y	60	1,770	1.0000	[302]
543	U.N. resolutions 6	Political: voting	Y	60	1,768	0.9989	[302]
544	U.N. resolutions 7	Political: voting	Y	60	1,770	1.0000	[302]
545	U.N. resolutions 8	Political: voting	Y	60	1,770	1.0000	[302]
546	U.N. resolutions 9	Political: voting	Y	60	1,770	1.0000	[302]
547	U.N. resolutions 10	Political: voting	Y	65	2,037	0.9793	[302]
548	U.N. resolutions 11	Political: voting	Y	81	3,239	0.9997	[302]
549	U.N. resolutions 12	Political: voting	Y	82	3,317	0.9988	[302]
550	U.N. resolutions 13	Political: voting	Y	82	3,294	0.9919	[302]

ID	Name	Category	Weighted	N	L	f_e	References
551	U.N. resolutions 14	Political: voting	Y	82	3,321	1.0000	[302]
552	U.N. resolutions 15	Political: voting	Y	99	4,851	1.0000	[302]
553	U.N. resolutions 16	Political: voting	Y	104	5,356	1.0000	[302]
554	U.N. resolutions 17	Political: voting	Y	110	5,995	1.0000	[302]
555	U.N. resolutions 18	Political: voting	Y	113	6,246	0.9870	[302]
556	U.N. resolutions 20	Political: voting	Y	117	6,672	0.9832	[302]
557	U.N. resolutions 21	Political: voting	Y	122	7,333	0.9935	[302]
558	U.N. resolutions 22	Political: voting	Y	124	7,616	0.9987	[302]
559	U.N. resolutions 23	Political: voting	Y	126	7,855	0.9975	[302]
560	U.N. resolutions 24	Political: voting	Y	126	7,851	0.9970	[302]
561	U.N. resolutions 25	Political: voting	Y	126	7,868	0.9991	[302]
562	U.N. resolutions 26	Political: voting	Y	132	8,641	0.9994	[302]
563	U.N. resolutions 27	Political: voting	Y	132	8,646	1.0000	[302]
564	U.N. resolutions 28	Political: voting	Y	134	8,905	0.9993	[302]
565	U.N. resolutions 29	Political: voting	Y	137	9,202	0.9878	[302]
566	U.N. resolutions 30	Political: voting	Y	143	10,117	0.9965	[302]
567	U.N. resolutions 31	Political: voting	Y	144	10,291	0.9995	[302]
568	U.N. resolutions 32	Political: voting	Y	146	10,585	1.0000	[302]
569	U.N. resolutions 33	Political: voting	Y	148	10,878	1.0000	[302]
570	U.N. resolutions 34	Political: voting	Y	150	11,173	0.9998	[302]
571	U.N. resolutions 35	Political: voting	Y	151	11,287	0.9966	[302]
572	U.N. resolutions 36	Political: voting	Y	155	11,935	1.0000	[302]
573	U.N. resolutions 37	Political: voting	Y	156	12,090	1.0000	[302]
574	U.N. resolutions 38	Political: voting	Y	157	12,243	0.9998	[302]
575	U.N. resolutions 39	Political: voting	Y	158	12,403	1.0000	[302]
576	U.N. resolutions 40	Political: voting	Y	158	12,403	1.0000	[302]
577	U.N. resolutions 41	Political: voting	Y	158	12,403	1.0000	[302]
578	U.N. resolutions 42	Political: voting	Y	158	12,402	0.9999	[302]
579	U.N. resolutions 43	Political: voting	Y	158	12,403	1.0000	[302]
580	U.N. resolutions 44	Political: voting	Y	158	12,403	1.0000	[302]
581	U.N. resolutions 45	Political: voting	Y	154	11,781	1.0000	[302]
582	U.N. resolutions 46	Political: voting	Y	168	13,872	0.9889	[302]
583	U.N. resolutions 47	Political: voting	Y	174	14,944	0.9929	[302]
584	U.N. resolutions 48	Political: voting	Y	178	15,606	0.9907	[302]
585	U.N. resolutions 49	Political: voting	Y	174	14,913	0.9908	[302]

ID	Name	Category	Weighted	N	L	f_e	References
586	U.N. resolutions 50	Political: voting	Y	179	15,826	0.9934	[302]
587	U.N. resolutions 51	Political: voting	Y	180	16,096	0.9991	[302]
588	U.N. resolutions 52	Political: voting	Y	176	15,349	0.9967	[302]
589	U.N. resolutions 53	Political: voting	Y	177	15,500	0.9951	[302]
590	U.N. resolutions 54	Political: voting	Y	174	14,970	0.9946	[302]
591	U.N. resolutions 55	Political: voting	Y	182	16,333	0.9916	[302]
592	U.N. resolutions 56	Political: voting	Y	179	15,812	0.9925	[302]
593	U.N. resolutions 57	Political: voting	Y	187	17,373	0.9990	[302]
594	U.N. resolutions 58	Political: voting	Y	189	17,735	0.9983	[302]
595	U.N. resolutions 59	Political: voting	Y	191	18,140	0.9997	[302]
596	U.N. resolutions 60	Political: voting	Y	191	18,110	0.9981	[302]
597	U.N. resolutions 61	Political: voting	Y	192	18,331	0.9997	[302]
598	U.N. resolutions 62	Political: voting	Y	192	18,331	0.9997	[302]
599	U.N. resolutions 63	Political: voting	Y	192	18,328	0.9996	[302]
600	Biogrid: <i>A. thaliana</i>	Protein interaction	N	406	625	0.0076	[280]
601	Biogrid: <i>C. elegans</i>	Protein interaction	N	3,353	6,449	0.0011	[280]
602	Biogrid: <i>D. melanogaster</i>	Protein interaction	N	7,174	24,897	0.0010	[280]
603	Biogrid: <i>H. sapien</i>	Protein interaction	N	8,205	25,699	0.0008	[280]
604	Biogrid: <i>M. musculus</i>	Protein interaction	N	710	1,003	0.0040	[280]
605	Biogrid: <i>R. norvegicus</i> *	Protein interaction	N	121	135	0.0186	[280]
606	Biogrid: <i>S. cerevisiae</i>	Protein interaction	N	1,753	4,811	0.0031	[280]
607	Biogrid: <i>S. pombe</i>	Protein interaction	N	1,477	11,404	0.0105	[280]
608	DIP: <i>H. pylori</i>	Protein interaction	N	686	1,351	0.0058	[262, 310]
609	DIP: <i>H. sapien</i>	Protein interaction	N	639	982	0.0048	[262, 310]
610	DIP: <i>M. musculus</i>	Protein interaction	N	50	55	0.0449	[262, 310]
611	DIP: <i>C. elegans</i>	Protein interaction	N	2,386	3,825	0.0013	[262, 310]
612	Human: Ccsb	Protein interaction	N	1,307	2,483	0.0029	[261]
613	Human: Ophid	Protein interaction	N	5,464	23,238	0.0016	[57, 58]
614	STRING: <i>C. elegans</i>	Protein interaction	N	1,762	95,227	0.0614	[155]
615	STRING: <i>S. cerevisiae</i>	Protein interaction	N	534	57,672	0.4053	[155]
616	Yeast: Oxford Statistics	Protein interaction	N	2,224	6,609	0.0027	[67]
617	Yeast: DIP	Protein interaction	N	4,906	17,218	0.0014	[4, 262, 310]
618	Yeast: DIP C	Protein interaction	N	2,587	6,094	0.0018	[4, 262, 310]
619	Yeast: FHC	Protein interaction	N	2,233	5,750	0.0023	[4, 43]
620	Yeast: FYI	Protein interaction	N	778	1,798	0.0059	[4, 146]

ID	Name	Category	Weighted	N	L	f_e	References
621	Yeast: PCA	Protein interaction	N	889	2,407	0.0061	[4, 287]
622	Corporate directors in Scotland (1904-1905)*	Social	Y	131	676	0.0794	[77, 267]
623	Corporate ownership (EVA)	Social	N	4,475	4,652	0.0005	[226]
624	Dolphins*	Social	N	62	159	0.0841	[192]
625	Family planning in Korea	Social	N	33	68	0.1288	[259]
626	Unionization in a hi-tech firm*	Social	N	33	91	0.1723	[170]
627	Communication within a sawmill on strike*	Social	N	36	62	0.0984	[208]
628	Leadership course	Social	N	32	80	0.1613	[210]
629	Les Miserables*	Social	Y	77	254	0.0868	[168]
630	Marvel comics	Social	Y	6,449	168,211	0.0081	[8]
631	Mexican political elite	Social	N	35	117	0.1966	[120]
632	Pretty-good-privacy algorithm users	Social	N	10,680	24,316	0.0004	[48]
633	Prisoners	Social	N	67	142	0.0642	[210]
634	Bernard and Killworth fraternity: observed	Social	Y	58	967	0.5850	[39, 40, 260]
635	Bernard and Killworth fraternity: recalled	Social	Y	58	1,653	1.0000	[39, 40, 260]
636	Bernard and Killworth HAM radio: observed	Social	Y	41	153	0.1866	[37, 38, 165]
637	Bernard and Killworth HAM radio: recalled	Social	Y	44	442	0.4672	[37, 38, 165]
638	Bernard and Killworth office: observed	Social	Y	40	238	0.3051	[37, 38, 165]
639	Bernard and Killworth office: recalled	Social	Y	40	779	0.9987	[37, 38, 165]
640	Bernard and Killworth technical: observed	Social	Y	34	175	0.3119	[37, 38, 165]
641	Bernard and Killworth technical: recalled	Social	Y	34	561	1.0000	[37, 38, 165]
642	Kapferer tailor shop: instrumental (t1)	Social	N	35	76	0.1277	[163]
643	Kapferer tailor shop: instrumental (t2)	Social	N	34	93	0.1658	[163]
644	Kapferer tailor shop: associational (t1)	Social	N	39	158	0.2132	[163]
645	Kapferer tailor shop: associational (t2)	Social	N	39	223	0.3009	[163]
646	University Rovira i Virgili (Tarragona) e-mail	Social	N	1,133	5,451	0.0085	[140]
647	Zachary karate club*	Social	N	34	78	0.1390	[315]
648	BA: (100,1)*	Synthetic	N	100	99	0.0200	[26]
649	BA: (100,2)*	Synthetic	N	100	197	0.0398	[26]
650	BA: (1000,1)	Synthetic	N	1,000	999	0.0020	[26]
651	BA: (1000,2)	Synthetic	N	1,000	1,997	0.0040	[26]
652	BA: (500,1)	Synthetic	N	500	499	0.0040	[26]
653	BA: (500,2)	Synthetic	N	500	997	0.0080	[26]
654	ER: (100,25)*	Synthetic	N	100	1,264	0.2554	[86]
655	ER: (100,50)	Synthetic	N	100	2,436	0.4921	[86]

ID	Name	Category	Weighted	N	L	f_e	References
656	ER: (100,75)	Synthetic	N	100	3,697	0.7469	[86]
657	ER: (1000,25)	Synthetic	N	1,000	124,455	0.2492	[86]
658	ER: (1000,50)	Synthetic	N	1,000	249,512	0.4995	[86]
659	ER: (1000,75)	Synthetic	N	1,000	374,846	0.7504	[86]
660	ER: (50,25)	Synthetic	N	50	287	0.2343	[86]
661	ER: (50,50)	Synthetic	N	50	589	0.4808	[86]
662	ER: (50,75)	Synthetic	N	50	936	0.7641	[86]
663	ER: (500,25)	Synthetic	N	500	31,148	0.2497	[86]
664	ER: (500,50)	Synthetic	N	500	62,301	0.4994	[86]
665	ER: (500,75)	Synthetic	N	500	93,780	0.7517	[86]
666	Fractal: (10,2,1)	Synthetic	N	1,024	9,256	0.0177	[279]
667	Fractal: (10,2,2)	Synthetic	N	1,024	16,875	0.0322	[279]
668	Fractal: (10,2,3)	Synthetic	N	1,024	30,344	0.0579	[279]
669	Fractal: (10,2,4)	Synthetic	N	1,024	53,009	0.1012	[279]
670	Fractal: (10,2,5)	Synthetic	N	1,024	89,812	0.1715	[279]
671	Fractal: (10,2,6)	Synthetic	N	1,024	147,784	0.2822	[279]
672	Fractal: (10,2,7)	Synthetic	N	1,024	232,794	0.4445	[279]
673	Fractal: (10,2,8)	Synthetic	N	1,024	343,563	0.6559	[279]
674	H13-4 benchmark	Synthetic	N	256	2,311	0.0708	[16]
675	LF benchmark: (1000,15,50,0.1,2,2)	Synthetic	N	1,000	7,573	0.0152	[180]
676	LF benchmark: (1000,15,50,0.1,3,1)	Synthetic	N	1,000	7,447	0.0149	[180]
677	LFR benchmark: (1000,15,50,0.5,2,2)	Synthetic	N	1,000	7,624	0.0153	[180]
678	LFR benchmark: (1000,15,50,0.5,3,1)	Synthetic	N	1,000	7,177	0.0144	[180]
679	LFR benchmark: (1000,25,50,0.1,2,2)	Synthetic	N	1,000	12,739	0.0255	[180]
680	LFR benchmark: (1000,25,50,0.1,3,1)	Synthetic	N	1,000	12,523	0.0251	[180]
681	LFR benchmark: (1000,25,50,0.5,2,2)	Synthetic	N	1,000	12,744	0.0255	[180]
682	LFR benchmark: (1000,25,50,0.5,3,1)	Synthetic	N	1,000	12,662	0.0253	[180]
683	LF benchmark: (1000,15,50,0.1,0.1,1,2,1)	Synthetic	Y	1,000	7,680	0.0154	[178]
684	LF benchmark: (1000,15,50,0.1,0.1,1,2,2)	Synthetic	Y	1,000	7,791	0.0156	[178]
685	LF benchmark: (1000,15,50,0.5,0.1,1,2,1)	Synthetic	Y	1,000	7,657	0.0153	[178]
686	LF benchmark: (1000,15,50,0.5,0.1,2,2,2)	Synthetic	Y	1,000	7,912	0.0158	[178]
687	LF benchmark: (1000,15,50,0.5,0.5,1,2,1)	Synthetic	Y	1,000	7,693	0.0154	[178]
688	LF benchmark: (1000,15,50,0.5,0.5,1,2,2)	Synthetic	Y	1,000	7,906	0.0158	[178]
689	LF benchmark: (1000,25,50,0.1,0.1,1,2,1)	Synthetic	Y	1,000	12,660	0.0253	[178]
690	LF benchmark: (1000,25,50,0.1,0.1,2,2,2)	Synthetic	Y	1,000	12,641	0.0253	[178]

ID	Name	Category	Weighted	N	L	f_e	References
691	LF benchmark: (1000,25,50,0.5,0.1,1,2,1)	Synthetic	Y	1,000	12,771	0.0256	[178]
692	LF benchmark: (1000,25,50,0.5,0.1,2,2,2)	Synthetic	Y	1,000	12,772	0.0256	[178]
693	LF benchmark: (1000,25,50,0.5,0.5,1,2,1)	Synthetic	Y	1,000	12,962	0.0259	[178]
694	LF benchmark: (1000,25,50,0.5,0.5,2,2,2)	Synthetic	Y	1,000	12,881	0.0258	[178]
695	LF-NG benchmark	Synthetic	Y	128	1,024	0.1260	[178, 224]
696	Random fully-connected: (100)	Synthetic	Y	100	4,950	1.0000	[†]
697	Random fully-connected: (500)	Synthetic	Y	500	124,750	1.0000	[†]
698	WS: (100,1,0.1)	Synthetic	N	100	100	0.0202	[305]
699	WS: (100,1,0.5)	Synthetic	N	73	73	0.0278	[305]
700	WS: (100,4,0.1)	Synthetic	N	100	407	0.0822	[305]
701	WS: (100,4,0.5)	Synthetic	N	100	522	0.1055	[305]
702	WS: (1000,1,0.1)	Synthetic	N	850	850	0.0024	[305]
703	WS: (1000,1,0.5)	Synthetic	N	877	877	0.0023	[305]
704	WS: (1000,4,0.1)	Synthetic	N	1,000	4,053	0.0081	[305]
705	WS: (1000,4,0.5)	Synthetic	N	1,000	5,138	0.0103	[305]
706	KOSKK:(1000,1,10,10,5 × 10 ⁻⁵ ,1 × 10 ⁻³ ,100)	Synthetic	Y	519	2,096	0.0156	[174]
707	KOSKK:(1000,1,10,10,5 × 10 ⁻⁵ ,1 × 10 ⁻³ ,1000)	Synthetic	Y	895	7,682	0.0192	[174]
708	KOSKK:(1000,1,100,10,5 × 10 ⁻⁵ ,1 × 10 ⁻³ ,1000)	Synthetic	Y	870	4,725	0.0125	[174]
709	KOSKK:(1000,1,100,105 × 10 ⁻⁵ ,1 × 10 ⁻³ ,100)	Synthetic	Y	652	2,125	0.0100	[174]
710	KOSKK:(1000,1,50,10,5 × 10 ⁻⁵ ,1 × 10 ⁻³ ,100)	Synthetic	Y	459	1,554	0.0148	[174]
711	KOSKK:(1000,1,50,10,5 × 10 ⁻⁵ ,1 × 10 ⁻³ ,1000)	Synthetic	Y	851	4,960	0.0137	[174]
712	Trade product proximity	Trade	Y	775	283,094	0.9439	[150]
713	World trade in metal (1994): Net	Trade	Y	80	875	0.2769	[77, 275]
714	World trade in metal (1994): Total	Trade	Y	80	875	0.2769	[77, 275]

†See the description at the beginning of this appendix for details of this network.

Appendix D

Hamiltonian and Network Details

In this appendix we provide additional technical details of the Potts Hamiltonian and the networks that we study in Chapter 6.

D.1 Potts Hamiltonian summation

We sum over $i \neq j$ in the Hamiltonian in Eq. 6.1 because of the existence of interactions that become antiferromagnetic at a resolution λ that is orders of magnitude larger than nearly all of the other Λ_{ij} . If we sum over all i and j , the maximum energy of the system is given by

$$\mathcal{H}(\Lambda_{\max}) = \mathcal{H}_{\max} = - \sum_i J_{ii}. \quad (\text{D.1})$$

In some networks Λ_{\max} is several orders of magnitude larger than nearly all of the other Λ_{ij} values and consequently $\mathcal{H}(\Lambda_{\max})$ is several orders of magnitude larger than the energies at most of the other sampled resolutions. For these networks, \mathcal{H}_{eff} is then very small over much of the range of ξ .¹ This effect is demonstrated in Fig. D.1 for the Caltech Facebook network [295].

D.2 Removing self-edges

In all of the networks that we consider, we have removed self-edges. However, the standard null model $P_{ij} = k_i k_j / (2m)$ includes some probability that a self-edge exists (i.e., $P_{ii} = k_i^2 / (2m) \neq 0$). By not including the diagonals in the Hamiltonian, we neglect the possible existence of these self-edges and the equality $\sum_{ij} P_{ij} = 2m$ no longer holds. For most networks, the contributions P_{ii} are typically small if m is

¹See Section 6.3 for the definition of \mathcal{H}_{eff} .

Appendix D

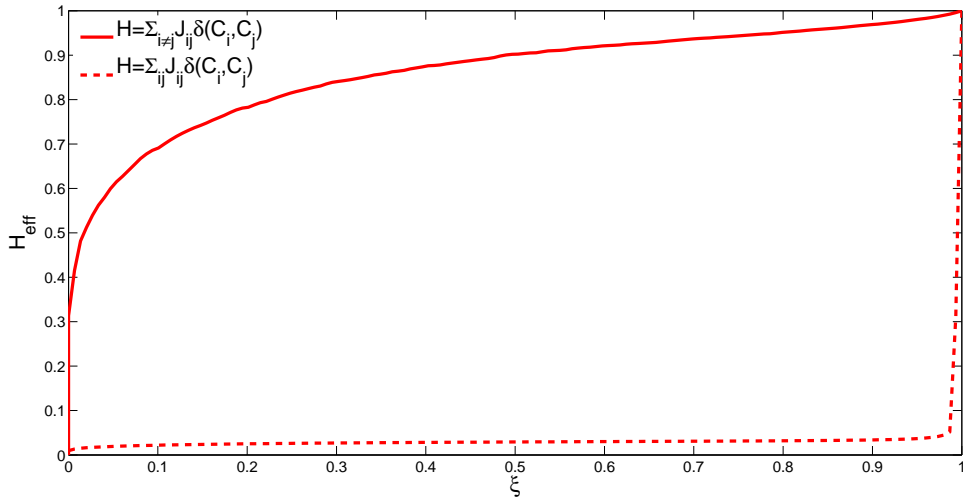


Figure D.1: A comparison of the \mathcal{H}_{eff} curves for the Caltech Facebook network [295] when $\mathcal{H}(\xi)$ is calculated by only summing over all $i \neq j$ (solid line) and summing over all i, j (dashed line).

large², so this is not a significant problem [220]. In addition, as we noted in Section 5.2.2, self-edges always occur within a community, so they will always contribute to the summation in Eq. 6.1 irrespective of exactly how the nodes are partitioned into communities. This implies that self-edges play no role when selecting the community partition that minimizes the interaction energy at a particular resolution.

²For example, self-edges in the Caltech Facebook network account for 0.45% of the total edge weight.

Appendix E

Robustness of MRFs to Network Perturbations

In this appendix we perform tests to check that the distance measures that we define in Section 6.4 are robust to perturbations of the network. Many networks are obtained empirically, so it is expected that there will be links erroneously included in the network that do not exist, and links that do actually exist will be erroneously omitted from the network. For any taxonomies derived using the MRF framework to be meaningful it is essential that the distance measures are robust to such false positive and negative links. We check the robustness of the distance measures by investigating the effect of rewiring some fraction of network links on the distances between the networks.

E.1 Rewiring mechanisms

We consider two rewiring mechanisms. First, we randomly rewire some percentage of the links in the network subject to the constraints that we maintain the degree distribution of the original network as well as the network connectivity (i.e., the rewired network forms a single connected component).¹ Second, we randomly rewire some percentage of the links subject only to the constraint that we maintain the network connectivity.

¹We use the procedure described in Ref. [201] to create randomized networks with the same degree distribution as the original network; but we add the constraint that the randomized networks must form a single connected component.

E.1.1 Partial rewiring

Because we are perturbing the original network, we focus on the distance matrices $\mathbf{D}^{\mathcal{H}}$, \mathbf{D}^S , and \mathbf{D}^{η} , which can be calculated directly for each network. We consider 25 of the original networks of varying sizes and edge densities, which we highlight in bold in Table C.1.² In Fig. E.1, we show the distance matrices for this subset of networks when various numbers of links have been rewired and the strength distribution maintained. The first column shows the matrices for the original networks block-diagonalized using the cost function in Eq. 6.15.³ The subsequent columns show the distance matrices as increasingly larger numbers of edges are rewired. The node ordering in each of these distance matrices is the same as the ordering for the matrix in the first column of the corresponding row. Unsurprisingly, as the number of rewirings is increased, the blocks in the matrices are gradually destroyed. However, the matrices for the first few columns still appear similar to the original distance matrices. This suggests that our distance measures are robust to networks containing false positive and negative links.

In the final column of Fig. E.1, we see that for L rewirings (where L is the number of links in a network), much of the original block structure has been destroyed, although some structure is still visible. The distance matrices in this figure were produced using random rewirings in which the strength distribution and connectivity of the networks were maintained. Randomizations under these constraints only destroy the community structure in the networks, so some of the network properties remain unchanged. The persistence of some block structure even after L rewiring suggests that our technique is able to identify this remaining structure. However, the block-structure in the final column is clearly not as good as in the first column so, as expected, the distances are less effective at clustering networks after their mesoscopic structure is destroyed.

E.1.2 Complete rewiring

To ensure a more complete randomization of the networks, we now perform $10L$ rewirings. If there were an equal probability of rewiring each edge then, on average, every edge would be rewired 10 times. However, because we impose the constraints

²We study only 25 networks because of the computational costs of rewiring a large number of networks multiple times; however, we have performed the same analysis for 5 different subsets of 25 networks and obtained similar results.

³Note that the node orderings for $\mathbf{D}^{\mathcal{H}}$, \mathbf{D}^S , and \mathbf{D}^{η} are not necessarily the same.

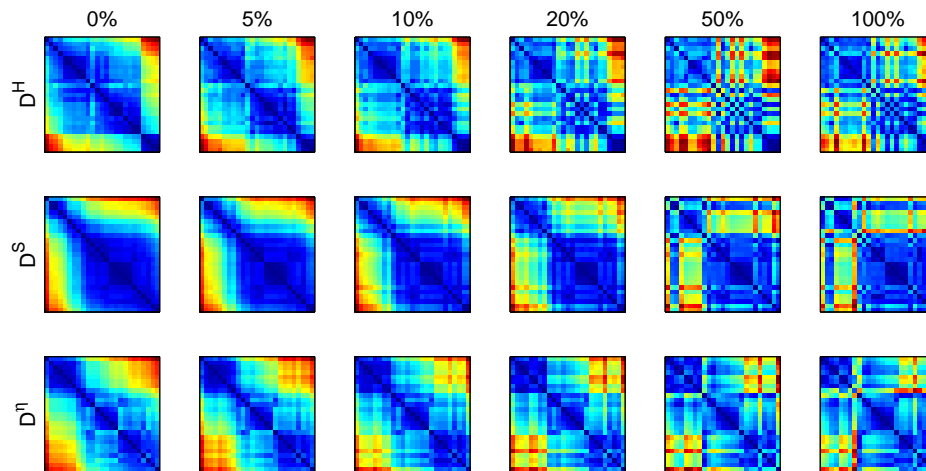


Figure E.1: Block-diagonalized distance matrices \mathbf{D}^H (top row), \mathbf{D}^S (middle row), and \mathbf{D}^r (bottom row) for the 25 networks in bold in Table C.1. The columns show the distance matrices following randomizations of the original network in which some percentage of links are rewired and the degree distribution and connectivity of the networks are maintained; the first column shows the distance matrix for the original networks. The distance matrices for the randomizations are the mean pairwise distances between networks, where the mean is calculated over all possible distances between 10 random realizations of each network. The ordering of the nodes in each of the distance matrices for randomized networks is the same as the ordering in the matrices of the original networks.

Appendix E

that the connectivity and the degree distribution must be maintained, this restricts which edges can be rewired and results in a non-uniform rewiring probability.

To provide some insight into the fraction of edges that get rewired, we perform 1,000 randomizations of $10L$ rewirings for the Zachary Karate Club network [315]. For each simulation, we find the number of different edges that exist at any stage during the rewiring process as a fraction of the total number of possible edges [the number of possible edges is given by $\frac{1}{2}N(N-1)$]. For the case where the only constraint is that the connectivity is maintained, on average 83% of the possible edges exist at some stage of the rewiring process. The minimum fraction of edges that are visited during any of the 1,000 randomizations is 79% and the maximum is 86%. For the case where we add the additional constraint that the degree distribution must be maintained, on average 61% of edges exist at some stage during the rewiring process, with a minimum of 57% and a maximum of 66% during a single simulation.

We also calculate the number of times that edges that exist at any stage of the rewiring process are themselves rewired. In Fig. E.2, we show the distribution of the number of times any edge is rewired. Over 1,000 simulations, when we only maintain network connectivity 96% of edges are rewired and when we also maintain the degree distribution 98% are rewired. In the former case, each edge is rewired on average 1.7 times and in the latter case each edge is rewired on average 2.3 times. The average number of rewirings is higher in the case in which we maintain the degree distribution because there are fewer edges that allow the additional constraint to be satisfied and consequently these edges exist and get rewired more frequently.

Figure E.3 shows the \mathbf{D}^H , \mathbf{D}^S , and \mathbf{D}^n distance matrices for $10L$ rewirings. The first column again shows the distance matrices for the original networks block-diagonalized using the cost function in Eq. 6.15. The second and third columns then show the distance matrices for randomizations in which the degree distribution is preserved and destroyed, respectively. The node orderings of the matrices in the second and third columns are again the same as the orderings for the matrix of the first column of the corresponding row. The second column in Fig. E.3 demonstrates that, when the degree distribution is maintained (even for “completely” randomized networks), some block structure remains in the distance matrices. The third column shows that when the degree distribution is not maintained, much of this structure is destroyed, but that some block structure is still visible. When the networks are “completely” randomized, with the only constraint being that the connectivity is maintained, then one is in effect producing random graphs. These random graphs might, however, have some common properties, such as the number of nodes and the

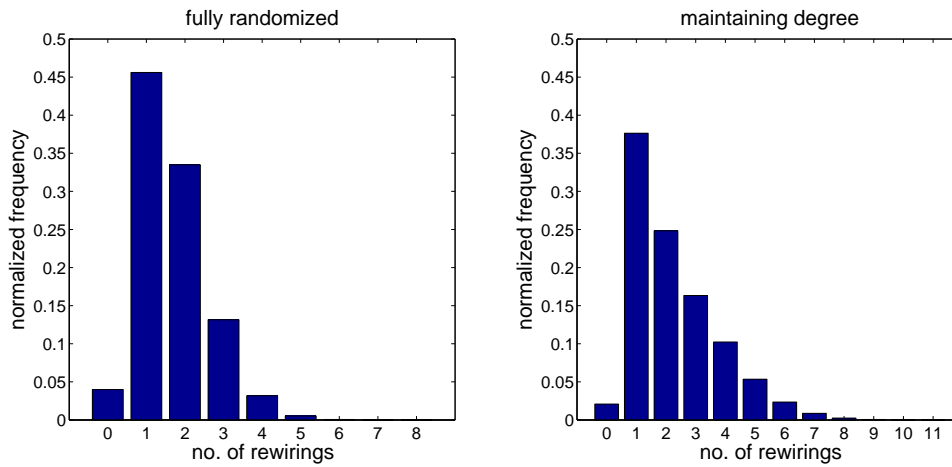


Figure E.2: Distribution of the number of times each edge is rewired when we perform $10L$ rewirings on the Zachary Karate Club network [315]. We show the distribution when (left) only the connectivity is maintained and (right) the connectivity and the degree distribution are maintained. The results are aggregated over 1,000 simulations.

fraction of possible edges present (see Section 6.3.2). The presence of, albeit weak, block structure in the final column of Fig. E.3 suggests that the MRF method is able to identify some of these fundamental network properties.

The block-diagonalized distance matrices in Fig. E.3 suggest that the MRF distance measures we propose are robust and that our approach provides a good method for identifying networks with similar mesoscopic structure across multiple scales. They also suggest that our technique can still identify similar networks even when the community structure has been destroyed, although the block-structure is not as well-defined. The MRF method also seems able to identify similar networks once the strength distribution has been destroyed, although the block-structure in the distance matrices is then poorly defined.

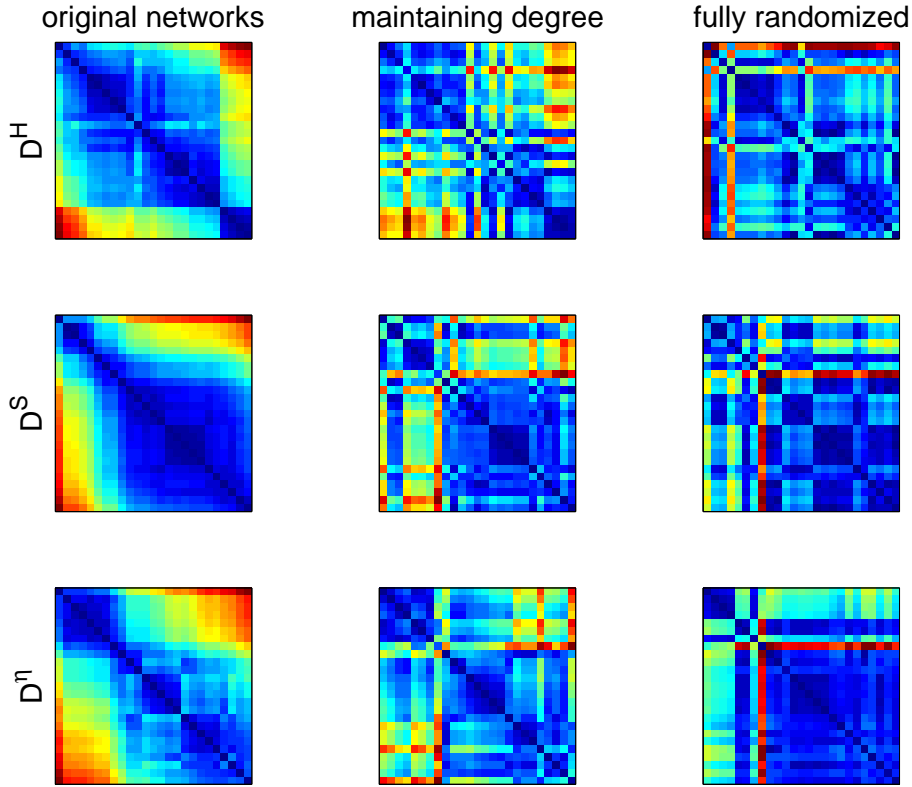


Figure E.3: Block-diagonalized distance matrices \mathbf{D}^H (top row), \mathbf{D}^S (middle row), and \mathbf{D}^n (bottom row) for the 25 networks in bold in Table C.1. The first column shows the distance matrices for the original networks. The second column shows the distance matrices following randomizations of the original network in which 10 times the number of links in the network have been rewired but under the constraints that the degree distribution and connectivity of the networks are maintained. The third column shows the distance matrices following randomizations of the original network in which 10 times the number of links in the network have been rewired but only the connectivity of the networks is maintained (i.e., the degree distribution is destroyed). The distance matrices for the randomizations are composed of the mean pairwise distances between the networks, where the mean is calculated over all possible distances between 10 random realizations of each network. The ordering of the nodes in each of the distance matrices for the randomized networks is the same as the ordering in the matrices of the original networks.

Appendix F

Robustness of MRFs and Taxonomies to Alternative Heuristics

In this section, we check that the MRFs and taxonomies described in Chapter 6 are robust with respect to the choice of computational heuristic used to minimize the Hamiltonian in Eq. 6.1.

F.1 Robustness of MRFs

In Fig. F.1, we show MRFs for three networks calculated using greedy [44], spectral [221] and simulated annealing algorithms [141]. The three algorithms agree very closely on the shapes of the \mathcal{H} , S and η MRFs for all three networks. The MRFs are most similar for the Roll call: U.S. Senate 102 network [203, 241, 306] with the \mathcal{H} MRF almost identical for the three heuristics. In general, the largest differences in the shapes of the MRFs occur for the spectral algorithm, which is unsurprising given the structure of the algorithm described in Section 5.10. However, these differences are still small. Because we know that the spectral algorithm tends to find lower quality partitions (see Fig. B.1), for the remainder of this section we will focus on the greedy and simulated annealing algorithms.¹

¹If the spectral algorithm performed significantly faster than the other algorithms then it would be worth investigating the effect of the lower quality partitions on the MRFs. If the MRFs were similar despite the lower quality of the partitions then the increased speed might justify using the spectral algorithm. In practice, however, the spectral algorithm converges on an optimal partition slightly slower than the greedy algorithm. The greedy algorithm is therefore better both in terms of computational costs and the quality of the partitions that it finds.

Appendix F

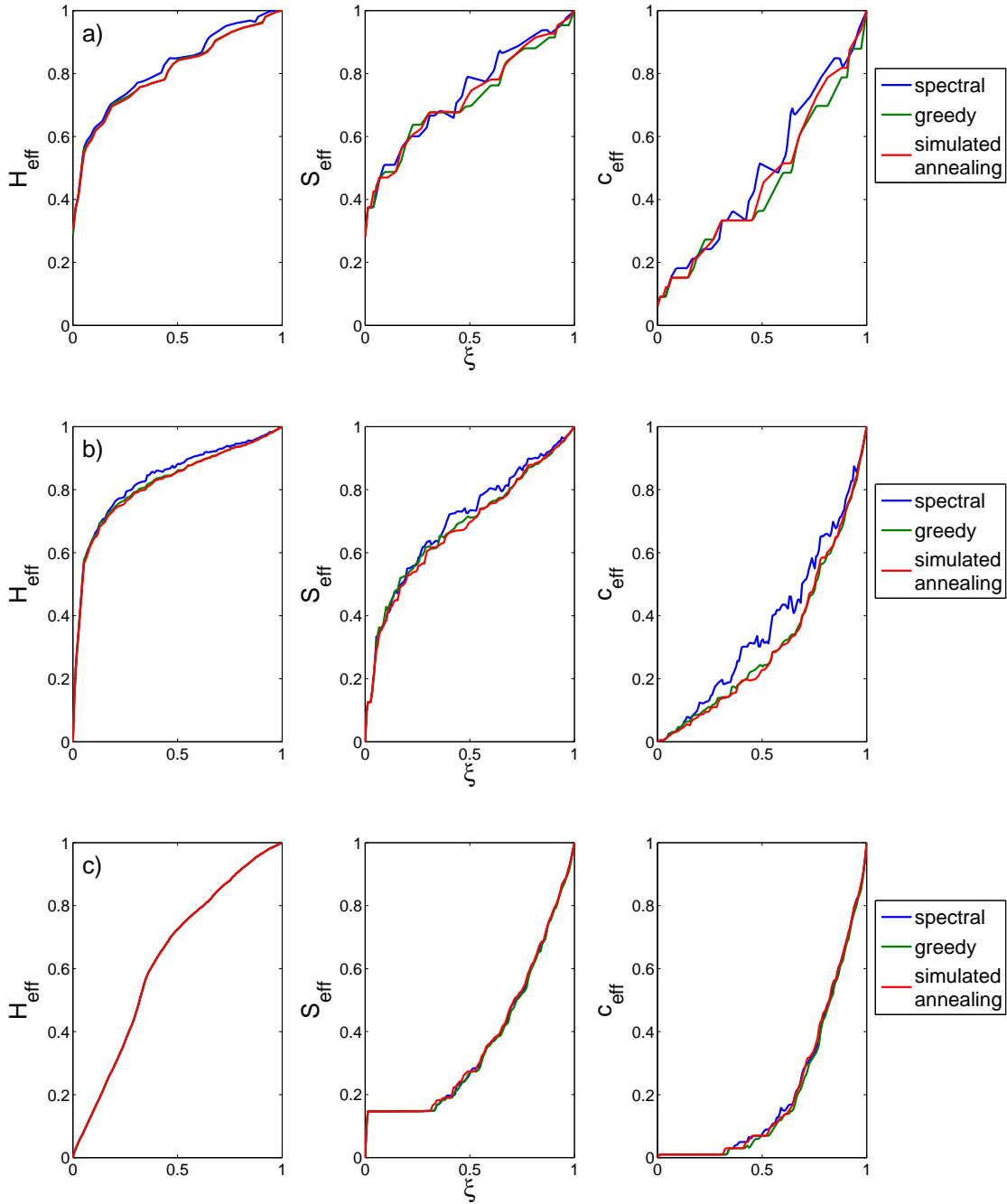


Figure F.1: Comparison of the MRFs produced using greedy, spectral and simulated annealing optimization heuristics. We show the MRFs for the (a) Zachary Karate Club network [315] (b) Garfield: Small-world citations network [119] (c) Roll call: U.S. Senate 102 network [203, 241, 306].

F.2 Robustness of taxonomies

Although Fig. F.1 shows good agreement between the shape of the MRFs for the different algorithms, we check nevertheless that the small differences that do occur do not have a significant effect on the network taxonomy. Because of the computational cost of detecting communities using simulated annealing, we investigate the effect on the taxonomy using a subset of small networks (i.e., networks with up to a few hundred nodes). The MRFs for small networks tend to be much noisier than the MRFs for large networks (see, for example, Fig. F.1(a) showing the MRFs for the Zachary Karate Club network which has only 34 nodes), so any differences between algorithms are likely to be more pronounced for small networks than for larger networks. Therefore, if the taxonomy is robust for a subset of small networks, we can be confident that it will also be robust if we include larger networks.

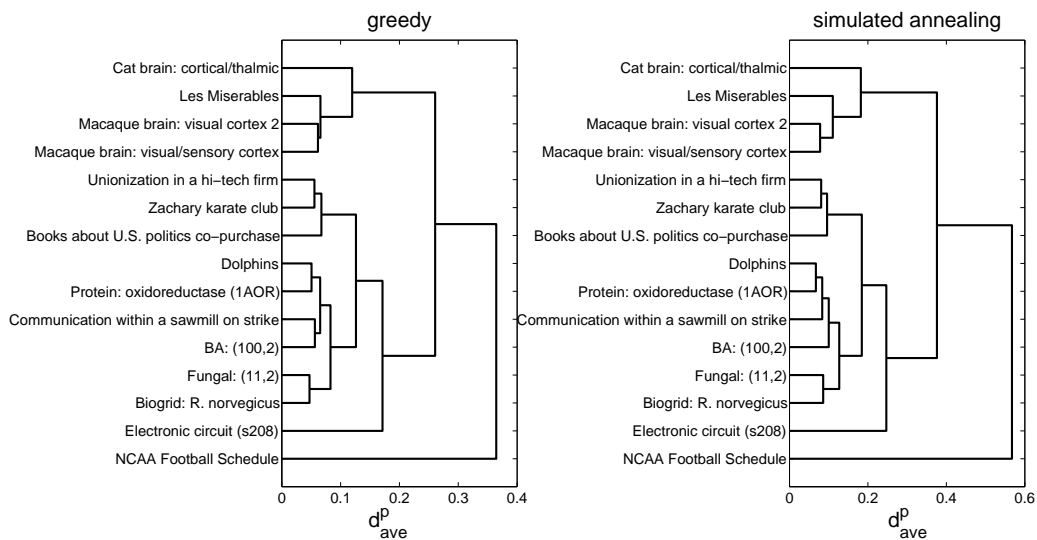


Figure F.2: Comparison of the dendrograms produced using a greedy algorithm and simulated annealing for a subset of 15 networks.

F.2.1 Dendrogram correlations

In Fig. F.2, we show dendrograms for the greedy algorithm and simulated annealing for a subset of 15 networks. On visual inspection the dendrograms appear very similar, with only a few small differences in the heights at which leaves and clusters combine. To quantify the similarity between a pair of dendrograms, we define a dendrogram correlation coefficient φ . Recall from Eq. 6.17 that for a dendrogram

constructed from the PCA-distance matrix \mathbf{D}^p with elements d_{ij}^p using average-linkage clustering, the distance t_{ij} between a node i in cluster \mathcal{C} and a node j in cluster \mathcal{C}' is given by

$$t_{ij} = d_{\text{ave}}(\mathcal{C}, \mathcal{C}') = \frac{1}{|\mathcal{C}||\mathcal{C}'|} \sum_{i \in \mathcal{C}} \sum_{j \in \mathcal{C}'} d_{ij}^p.$$

To compare dendrograms constructed using the greedy algorithm and simulated annealing, with distances t_{ij} and s_{ij} between pairs of networks, respectively, we define a dendrogram correlation coefficient φ as

$$\varphi = \frac{\sum_{i < j} (s_{ij} - \bar{s})(t_{ij} - \bar{t})}{\sqrt{\left[\sum_{i < j} (s_{ij} - \bar{s})^2 \right] \left[\sum_{i < j} (t_{ij} - \bar{t})^2 \right]}}, \quad (\text{F.1})$$

where \bar{s} is the mean of the distances s_{ij} and \bar{t} the mean value of the t_{ij} .² Dendrograms with identical distances between clusters will have a dendrogram correlation $\varphi = 1$. The dendrogram correlation for the example dendrograms shown in Fig. F.2 is 0.997. This is clearly very high, but to judge exactly how high the dendrogram correlation is we compare the observed correlations with those for random dendrograms.

F.2.2 Dendrogram randomizations

We first produce a distribution of dendrogram correlation coefficients for a larger number of dendrograms. To produce the distribution of dendrogram correlations, we calculate the MRFs for a subset of 25 networks using both algorithms.³ We then randomly select 15 networks from this subset 10,000 times and for each selection generate the dendrogram distance matrix with elements t_{ij} for both algorithms and calculate the dendrogram correlation coefficient. Using this procedure, we can compare many different dendrograms, but we limit the computational cost by only calculating the simulated annealing MRFs for 25 networks. However, we note that even this is computationally quite intensive using the simulated annealing algorithm because, to produce the MRF for each network, one still needs to detect communities

²The dendrogram correlation is similar to the cophenetic correlation given in Eq. 6.19. The difference is that the dendrogram correlation compares the distances in two dendrograms whereas the cophenetic correlation compares the distances between objects in a dendrogram with distances in the underlying distance matrix.

³We mark the 25 networks with an asterisk * in Table C.1.

at many different resolutions.⁴ We compare the observed distribution of dendrogram correlation coefficients with the distribution for randomized dendrograms. For each of the 10,000 subsets of networks, we create 100 randomizations of the simulated annealing dendrogram and calculate the dendrogram correlation between each of these randomized dendrograms and the corresponding unrandomized dendrogram produced using the greedy algorithm. To produce random dendrograms, we use the double-permutation procedure described in Refs. [182,183]. The randomization takes place in two steps: First, we randomize the distances at which the different clusters join together. For example, consider an unrandomized dendrogram in which clusters A and B join together at a distance of 0.45 and clusters C and D join at a distance of 0.65. After the randomization, A and B might join at a distance of 0.65 and C and D at a distance of 0.45. Second, we randomize the networks corresponding to each leaf in the dendrogram. This randomization procedure maintains the distances and the shape of the dendrogram.

In Fig. F.3 we compare the distributions of dendrogram correlation coefficients between the greedy algorithm dendrograms and the unrandomized and randomized simulated annealing dendrograms. The dendrogram correlation is clearly significantly higher for the unrandomized case, with only a small overlap in the tails of the two distributions. In fact, the dendrogram correlation between the greedy and simulated annealing dendrograms is greater than 0.99 for 63% of the studied dendrograms.

To summarize this section, Figure F.1 shows that there are small differences in the MRFs generated for the different algorithms, but Fig. F.3 highlights that these differences have very little effect on the resulting dendrograms. The results of this section therefore demonstrate that the taxonomies that we create in Chapter 6 are robust with respect to the choice of optimization heuristic.

⁴We detect communities at 150 resolutions for each network because this seems like a reasonable compromise between the computational cost of detecting communities at a larger number of resolutions and the noisy MRFs that result when we find communities at only a small number of resolutions.

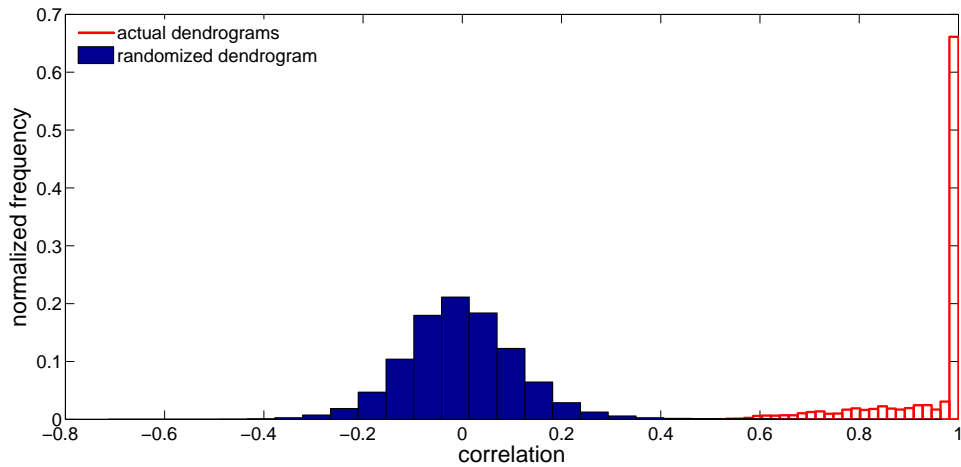


Figure F.3: Distribution of the dendrogram correlation between dendrograms generated using the greedy algorithm and simulated annealing. To produce the distribution of dendrogram correlations, we calculate the MRFs for a subset of 25 networks using both algorithms. We then randomly select 15 networks from this subset 10,000 times and for each selection generate the distance matrix corresponding to the dendrogram for both algorithms and calculate the dendrogram correlation coefficient. We also show the distribution of dendrogram correlation coefficients for randomized data. For each of the 10,000 subsets of 15 networks, we generated 100 randomizations of the simulated annealing dendrogram and calculated the dendrogram correlations between each of these random dendrograms and the corresponding unrandomized dendrogram produced using the greedy algorithm. We describe the dendrogram randomization procedure in more detail in the main text.

References

- [1] Data downloaded on 19th December 2008 from <http://uk.finance.yahoo.com/>.
- [2] B. ADAMCSEK, G. PALLA, I. J. FARKAS, I. DERÉNYI, AND T. VICSEK, *CFinder: locating cliques and overlapping modules in biological networks*, *Bioinformatics*, 22 (2006), pp. 1021–1023.
- [3] L. A. ADAMIC AND N. GLANCE, *The political blogosphere and the 2004 U.S. election: divided they blog*, in *LinkKDD '05: Proceedings of the 3rd international workshop on Link discovery*, 2005, pp. 36–43.
- [4] S. AGARWAL, C. M. DEANE, M. A. PORTER, AND N. S. JONES, *Revisiting Date and Party Hubs: Novel Approaches to Role Assignment in Protein Interaction Networks*, *PLoS Computational Biology*, 6 (2010), p. e1000817.
- [5] Y. Y. AHN, J. P. BAGROW, AND S. LEHMANN, *Communities and hierarchical organization of links in complex networks*, arXiv:0903.3178, (2009).
- [6] ———, *Link communities reveal multiscale complexity in networks*, *Nature*, 466 (2010), pp. 761–764.
- [7] Y. AIBA, N. HATANO, H. TAKAYASU, K. MARUMO, AND T. SHIMIZU, *Triangular arbitrage as an interaction among foreign exchange rates*, *Physica A*, 310 (2002), pp. 467–479.
- [8] R. ALBERICH, J. MIRO-JULIA, AND F. ROSSELLO, *Marvel Universe looks almost like a real social network*, arXiv:cond-mat/0202174, (2002).
- [9] R. ALBERT AND A.-L. BARABÁSI, *Statistical mechanics of complex networks*, *Review of Modern Physics*, 74 (2002), pp. 47–97.
- [10] R. ALBERT, H. JEONG, AND A.-L. BARABÁSI, *Error and attack tolerance of complex networks*, *Nature*, 406 (2000), pp. 378–382.

References

- [11] F. ALLEN AND A. BABUS, *The Network Challenge: Strategy, Profit, and Risk in an Interlinked World*, Wharton School Publishing, Philadelphia, PA, USA, 2009, ch. Networks in Finance, pp. 367–382.
- [12] F. ALLEN AND D. GALE, *Financial contagion*, *Journal of Political Economy*, 108 (2000), pp. 1–33.
- [13] L. A. N. AMARAL AND J. M. OTTINO, *Complex networks*, *European Physical Journal B*, 38 (2004), pp. 147–162.
- [14] P. W. ANDERSON, K. J. ARROW, AND D. PINES, eds., *The Economy as an Evolving Complex System (Santa Fe Institute Studies in the Sciences of Complexity Proceedings)*, Addison-Wesley, Reading, MA, USA, 1988.
- [15] A. ARENAS, A. DÍAZ-GUILERA, J. KURTHS, Y. MORENO, AND C. ZHOU, *Synchronization in complex networks*, *Physics Reports*, 469 (2008), pp. 93–153.
- [16] A. ARENAS, A. DÍAZ-GUILERA, AND C. J. PÉREZ-VICENTE, *Synchronization Reveals Topological Scales in Complex Networks*, *Physical Review Letters*, 96 (2006), p. 114102.
- [17] A. ARENAS, A. FERNANDEZ, AND S. GÓMEZ, *Analysis of the structure of complex networks at different resolution levels*, *New Journal of Physics*, 10 (2008), p. 053039.
- [18] W. B. ARTHUR, *Complexity and the Economy*, *Science*, 284 (1999), pp. 107–109.
- [19] W. B. ARTHUR, S. N. DURLAUF, AND D. A. LANE, eds., *The Economy as an Evolving Complex System II (Santa Fe Institute Studies in the Sciences of Complexity Proceedings)*, Addison-Wesley, Reading, MA, USA, 1997.
- [20] S. ASUR AND S. PARTHASARATHY, *On the use of viewpoint neighborhoods for dynamic graph analysis*, tech. rep., OSU-CISRC-9/08-TR50, 2008.
- [21] ———, *A viewpoint-based approach for interaction graph analysis*, in *KDD '09: Proceedings of the 15th ACM SIGKDD international conference on Knowledge discovery and data mining*, 2009, pp. 79–88.

-
- [22] S. ASUR, S. PARTHASARATHY, AND D. UCAR, *An event-based framework for characterizing the evolutionary behavior of interaction graphs*, in KDD '07: Proceedings of the 13th ACM SIGKDD international conference on Knowledge discovery and data mining, 2007, pp. 913–921.
- [23] L. BACKSTROM, D. HUTTENLOCHER, J. KLEINBERG, AND X. LAN, *Group formation in large social networks: membership, growth, and evolution*, in KDD '06: Proceedings of the 12th ACM SIGKDD international conference on Knowledge discovery and data mining, 2006, pp. 44–54.
- [24] V. K. BALAKRISHNAN, *Schaum's Outline of Graph Theory*, McGraw-Hill, New York, NY, USA, 1997.
- [25] Y. BAR-YAM, *A mathematical theory of strong emergence using multiscale variety*, Complexity, 9 (2004), pp. 15–24.
- [26] A.-L. BARABÁSI AND R. ALBERT, *Emergence of Scaling in Random Networks*, Science, 286 (1999), pp. 509–512.
- [27] N. N. BATADA, T. REGULY, A. BREITKREUTZ, L. BOUCHER, B.-J. BREITKREUTZ, L. HURST, AND M. TYERS, *Stratus Not Altocumulus: A New View of the Yeast Protein Interaction Network*, PLoS Biology, 4 (2006), p. e317.
- [28] V. BATAGELJ, 2003. Data available at <http://vlado.fmf.uni-lj.si/pub/networks/data/2mode/journals.htm>.
- [29] V. BATAGELJ AND A. MRVAR, 2006. Data available at <http://vlado.fmf.uni-lj.si/pub/networks/data/default.htm>.
- [30] V. BATAGELJ, A. MRVAR, AND M. ZAVERŠNIK, *Network analysis of texts*, in Proceedings of the 5th International Multi-Conference Information Society – Language Technologies, T.Erjavec and J. Gros, eds., 2002, pp. 143–148.
- [31] S. BATTISTON, D. DELLI GATTI, M. GALLEGATI, B. C. GREENWALD, AND J. E. STIGLITZ, *Liaisons Dangereuses: Increasing Connectivity, Risk Sharing, and Systemic Risk*, NBER Working Paper Series, w15611 (2009). Available at SSRN: http://papers.ssrn.com/sol3/papers.cfm?abstract_id=1532069#.

References

- [32] J. BAUMES, M. GOLDBERG, AND M. MAGDON-ISMAIL, *Intelligence and Security Informatics*, vol. 3495 of Lecture Notes in Computer Science, Springer, Berlin/Heidelberg, Germany, 2005, ch. Efficient Identification of Overlapping Communities, pp. 27–36.
- [33] D. P. BEBBER, J. HYNES, P. R. DARRAH, L. BODDY, AND M. D. FRICKER, *Biological solutions to transport network design*, Proceedings of the Royal Society B, 274 (2007), pp. 2307–2315.
- [34] N. H. F. BEEBE, 2002. The authors collaboration network in computational geometry was produced from the BibTeX bibliography available at <http://www.math.utah.edu/~beebe/bibliographies.html>. The network data is available at <http://vlado.fmf.uni-lj.si/pub/networks/data/collab/geom.htm>.
- [35] T. Y. BERGER-WOLF, M. LAHIRI, C. TANTIPATHANANANDH, AND D. KEMPE, *Finding Structure in Dynamic Networks*, in Workshop on Information in Networks (WIN-09), 2009.
- [36] T. Y. BERGER-WOLF AND J. SAIA, *A framework for analysis of dynamic social networks*, in KDD '06: Proceedings of the 12th ACM SIGKDD international conference on Knowledge discovery and data mining, 2006, pp. 523–528.
- [37] H. R. BERNARD AND P. D. KILLWORTH, *Informant Accuracy in Social Network Data*, Human Organization, 35 (1976), pp. 269–286.
- [38] ———, *Informant Accuracy in Social Network Data II*, Human Communication Research, 4 (1977), pp. 3–18.
- [39] H. R. BERNARD, P. D. KILLWORTH, AND L. SAILER, *Informant accuracy in social network data IV: a comparison of clique-level structure in behavioral and cognitive network data*, Social Networks, 2 (1979-1980), pp. 191–218.
- [40] ———, *Informant accuracy in social-network data V: An experimental attempt to predict actual communication from recall data*, Social Science Research, 11 (1982), pp. 30–66.
- [41] M. BERNASCHI, L. GRILLI, AND D. VERGNI, *Statistical analysis of fixed income market*, Physica A, 308 (2002), pp. 381–390.
- [42] D. A. BERRY AND B. W. LINDGREN, *Statistics: Theory and Methods*, Brooks/Cole, Pacific Grove, CA, USA, 1990.

-
- [43] N. BERTIN, N. SIMONIS, D. DUPUY, M. E. CUSICK, J. D. J. HAN, H. B. FRASER, F. P. ROTH, AND M. VIDAL, *Confirmation of organized modularity in the yeast interactome*, PLoS Biology, 5 (2007), p. e153.
- [44] V. D. BLONDEL, J. GUILLAUME, R. LAMBIOTTE, AND E. LEFEBVRE, *Fast unfolding of communities in large networks*, Journal of Statistical Mechanics, 2008 (2008), p. P10008.
- [45] L. E. BLUME AND S. N. DURLAUF, eds., *The Economy as an Evolving Complex System III: Current Perspectives and Future Directions*, Oxford University Press, Oxford, UK, 2005.
- [46] S. BOCCALETTI, V. LATORA, Y. MORENO, M. CHAVEZ, AND D.-U. HWANG, *Complex networks: Structure and dynamics*, Physics Reports, 424 (2006), pp. 175–308.
- [47] N. BOCCARA, *Modeling Complex Systems*, Springer-Verlag, New York, NY, USA, 2003.
- [48] M. BOGUÑÁ, R. PASTOR-SATORRAS, A. DÍAZ-GUILERA, AND A. ARENAS, *Models of social networks based on social distance attachment*, Physical Review E, 70 (2004), p. 056122.
- [49] B. BOLLOBÁS, *Modern Graph Theory*, Academic Press, New York, NY, USA, 2001.
- [50] ———, *Random Graphs*, Cambridge University Press, Cambridge, UK, 2nd ed., 2001.
- [51] F. BOSCHETTI, M. PROKOPENKO, I. MACREADIE, AND A.-M. GRISOGONO, *Knowledge-Based Intelligent Information and Engineering Systems*, vol. 3583 of Lecture Notes in Computer Science, Springer, Berlin/Heidelberg, Germany, 2005, ch. Defining and Detecting Emergence in Complex Networks, pp. 573–580.
- [52] M. BOSS, H. ELSINGER, M. SUMMER, AND S. THURNER, *Network topology of the interbank market*, Quantitative Finance, 4 (2004), pp. 677–684.
- [53] J.-P. BOUCHAUD AND M. POTTERS, *Theory of Financial Risk and Derivative Pricing: From Statistical Physics to Risk Management*, Cambridge University Press, Cambridge, UK, 2003.

References

- [54] J. M. BOWER AND D. BEEMAN, *The Book of GENESIS: Exploring Realistic Neural Models with the GEneral NEural SIMulation System*, Telos, Santa Clara, CA, US, 1998.
- [55] U. BRANDES, D. DELLING, M. GAERTLER, R. GÖRKE, M. HOEFER, Z. NIKOLOSKI, AND D. WAGNER, *On modularity clustering*, IEEE Transactions on Knowledge and Data Engineering, 20 (2008), pp. 172–188.
- [56] A. BRODER, R. KUMAR, F. MAGHOUL, P. RAGHAVAN, S. RAJAGOPALAN, R. STATA, A. TOMKINS, AND J. WIENER, *Graph structure in the Web*, Computer Networks, 33 (2000), pp. 309–320.
- [57] K. BROWN AND I. JURISICA, *Unequal evolutionary conservation of human protein interactions in interologous networks*, Genome Biology, 8 (2007), p. R95.
- [58] K. R. BROWN AND I. JURISICA, *Online Predicted Human Interaction Database*, Bioinformatics, 21 (2005), pp. 2076–2082.
- [59] M. K. BRUNNERMEIER, S. NAGEL, AND L. H. PEDERSEN, *Carry Trades and Currency Crashes*, NBER Working Paper Series, 14473 (2008). Available at SSRN: <http://ssrn.com/abstract=1297722>.
- [60] G. CALDARELLI, *Scale-Free Networks*, Oxford University Press, Oxford, UK, 2007.
- [61] T. CALLAGHAN, P. J. MUCHA, AND M. A. PORTER, *Random walker ranking for NCAA division IA football*, American Mathematical Monthly, 114 (2007), pp. 761–777.
- [62] D. S. CALLAWAY, M. E. J. NEWMAN, S. H. STROGATZ, AND D. J. WATTS, *Network Robustness and Fragility: Percolation on Random Graphs*, Physical Review Letters, 85 (2000), pp. 5468–5471.
- [63] J. Y. CAMPBELL, A. W. LO, AND A. C. MACKINLAY, *The Econometrics of Financial Markets*, Princeton University Press, Princeton, NJ, USA, 1997.
- [64] S. ÇUKURA, M. ERYİĞİTA, AND R. ERYİĞİT, *Cross correlations in an emerging market financial data*, Physica A, 376 (2007), pp. 555–564.
- [65] D. CHAKRABARTI, R. KUMAR, AND A. TOMKINS, *Evolutionary clustering*, in KDD '06: Proceedings of the 12th ACM SIGKDD international conference on Knowledge discovery and data mining, 2006, pp. 554–560.

-
- [66] G. CHAMBERLAIN AND M. ROTHSCHILD, *Arbitrage, Factor Structure, and Mean-Variance Analysis on Large Asset Markets*, *Econometrica*, 51 (1983), pp. 1281–1304.
- [67] P. Y. CHEN, C. M. DEANE, AND G. REINERT, *Predicting and validating protein interactions using network structure*, *PLoS Computational Biology*, 4 (2008), p. e1000118.
- [68] Y. CHI, X. SONG, D. ZHOU, K. HINO, AND B. L. TSENG, *Evolutionary spectral clustering by incorporating temporal smoothness*, in *KDD '07: Proceedings of the 13th ACM SIGKDD international conference on Knowledge discovery and data mining*, 2007, pp. 153–162.
- [69] ———, *On evolutionary spectral clustering*, *ACM Transactions on Knowledge Discovery from Data*, 3 (2009), pp. 1–30.
- [70] R. COHEN, K. EREZ, D. BEN AVRAHAM, AND S. HAVLIN, *Resilience of the Internet to Random Breakdowns*, *Physical Review Letters*, 85 (2000), pp. 4626–4628.
- [71] J. J. COLEMAN, *Party Decline in America*, Princeton University Press, Princeton, NJ, USA, 1996.
- [72] G. CONNOR AND R. A. KORAJCZYK, *Performance measurement with the arbitrage pricing theory : A new framework for analysis*, *Journal of Financial Economics*, 15 (1986), pp. 373–394.
- [73] M. M. DACOROGNA, R. GENÇAY, U. A. MÜLLER, R. B. OLSEN, AND O. V. PICTET, *An Introduction to High-Frequency Finance*, Academic Press, San Diego, CA, USA, 2001.
- [74] M. M. DACOROGNA, U. A. MÜLLER, R. J. NAGLER, R. B. OLSEN, AND O. V. PICTET, *A geographical model for the daily and weekly seasonal volatility in the foreign exchange market*, *Journal of International Money and Finance*, 12 (1993), pp. 413–438.
- [75] L. DANON, A. DÍAZ-GUILERA, J. DUCH, AND A. ARENAS, *Comparing community structure identification*, *Journal of Statistical Mechanics*, 2005 (2005), p. P09008.

References

- [76] A. DAVIS, B. B. GARDNER, AND M. R. GARDNER, *Deep South*, University of Chicago Press, Chicago, IL, USA, 1941.
- [77] W. DE NOOY, A. MRVAR, AND V. BATAGELJ, *Exploratory Social Network Analysis with Pajek*, Cambridge University Press, Cambridge, UK, 2004.
- [78] J. DEAN AND M. R. HENZINGER, *Finding related pages in the World Wide Web*, *Computer Networks*, 31 (1999), pp. 1467–1479.
- [79] T. DI MATTEO, T. ASTE, AND R. N. MANTEGNA, *An interest rates cluster analysis*, *Physica A*, 339 (2004), pp. 181–188.
- [80] P. DOMINGOS, *The role of Occam’s razor in knowledge discovery*, *Data Mining and Knowledge Discovery*, 3 (1999), pp. 409–425.
- [81] J. DRIESSON, B. MELENBERG, AND T. NIJMAN, *Common factors in international bond returns*, *Journal of International Money and Finance*, 22 (2003), pp. 629–656.
- [82] S. DROŹDŹ, S. A. Z. GÓRSKI, AND J. KWAPIEŃ, *World currency exchange rate cross-correlations*, *European Physical Journal B*, 58 (2007), pp. 499–502.
- [83] D. DUAN, Y. LI, Y. JIN, AND Z. LU, *Community mining on dynamic weighted directed graphs*, in *CNIKM ’09: Proceeding of the 1st ACM international workshop on Complex networks meet information & knowledge management*, 2009, pp. 11–18.
- [84] R. O. DUDA, P. E. HART, AND D. G. STORK, *Pattern Classification*, Wiley, New York, NY, USA, 2001.
- [85] N. EAGLE AND A. PENTLAND, *Reality mining: sensing complex social systems*, *Personal Ubiquitous Computing*, 10 (2006), pp. 255–268.
- [86] P. ERDŐS AND A. RÉNYI, *On random graphs*, *Publicationes Mathematicae*, 6 (1959), pp. 290–297.
- [87] ———, *On the evolution of random graphs*, *Publications of the Mathematical Institute of the Hungarian Academy of Sciences*, 5 (1960), pp. 17–61.
- [88] ———, *On the strength of connectedness of a random graph*, *Acta Mathematica Scientia Hungary*, 12 (1961), pp. 261–267.

-
- [89] K. ESBENSEN AND P. GELADI, *Principal component analysis*, Chemometrics and Intelligent Laboratory Systems, 2 (1987), pp. 37–52.
- [90] T. S. EVANS AND R. LAMBIOTTE, *Line graphs, link partitions, and overlapping communities*, Physical Review E, 80 (2009), p. 16105.
- [91] T. FALKOWSKI, *Community Dynamics in Natural and Human Networks*, in Proceedings of 2nd European Symposium on Nature-inspired Smart Information, 2006.
- [92] T. FALKOWSKI, J. BARTELHEIMER, AND M. SPILIOPOULOU, *Community Dynamics Mining*, in Proceedings of 14th European Conference on Information Systems (ECIS 2006), 2006.
- [93] —, *Mining and Visualizing the Evolution of Subgroups in Social Networks*, in WI '06: Proceedings of the 2006 IEEE/WIC/ACM International Conference on Web Intelligence, 2006, pp. 52–58.
- [94] T. FALKOWSKI, A. BARTH, AND M. SPILIOPOULOU, *DENGRAPH: A Density-based Community Detection Algorithm*, in WI '07: Proceedings of the IEEE/WIC/ACM International Conference on Web Intelligence, 2007, pp. 112–115.
- [95] —, *Studying Community Dynamics with an Incremental Graph Mining Algorithm*, in Proceedings of the 14th Americas Conference on Information Systems, 2008.
- [96] T. FALKOWSKI AND M. SPILIOPOULOU, *Data Mining for Community Dynamics*, Künstliche Intelligenz, 3 (2007), pp. 23–29.
- [97] —, *Users in Volatile Communities: Studying Active Participation and Community Evolution*, in UM '07: Proceedings of the 11th international conference on User Modeling, 2007, pp. 47–56.
- [98] T. J. FARARO AND M. SUNSHINE, *A Study of a Biased Friendship Network*, Syracuse University Press, Syracuse, NY, USA, 1964.
- [99] I. J. FARKAS, D. ÁBEL, G. PALLA, AND T. VICSEK, *Weighted network modules*, New Journal of Physics, 9 (2007), p. 180.

References

- [100] R. R. FAULKNER, *Music on Demand. Composers and Careers in the Hollywood Film Industry*, Transaction Books, New Brunswick, NJ, USA, 1983.
- [101] G. FEENEY AND D. HESTER, *Stock market indices: A principal component analysis*, Cowles Foundation, Monograph, 19 (1967), pp. 110–138.
- [102] D. J. FELLEMAN AND D. C. VAN ESSEN, *Distributed Hierarchical Processing in the Primate Cerebral Cortex*, *Cerebral Cortex*, 1 (1991), pp. 1–47.
- [103] E. FERGUSON AND T. COX, *Exploratory Factor Analysis: A Users' Guide*, *International Journal of Selection and Assessment*, 1 (1993), pp. 84–94.
- [104] D. FIRTH AND A. SPIRLING, *Divisions of the United Kingdom House of Commons, from 1992 to 2003 and Beyond*, Working paper, (2003). Available at <http://www2.warwick.ac.uk/fac/sci/statistics/staff/academic/firth/software/tapir/firth-spirling.pdf>.
- [105] S. FORTUNATO, *Community detection in graphs*, *Physics Reports*, 486 (2010), pp. 75–174.
- [106] S. FORTUNATO AND M. BARTHÉLEMY, *Resolution limit in community detection*, *Proceedings of the National Academy of Sciences of the U.S.A.*, 104 (2007), pp. 36–41.
- [107] S. FORTUNATO AND C. CASTELLANO, *Encyclopedia of Complexity and System Science*, Springer, Berlin, Germany, 2009, ch. Community Structure in Graphs.
- [108] J. H. FOWLER, *Connecting the Congress: A Study of Cosponsorship Networks*, *Political Analysis*, 14 (2006), pp. 456–487.
- [109] —, *Legislative cosponsorship networks in the US House and Senate*, *Social Networks*, 28 (2006), pp. 454–465.
- [110] L. C. FREEMAN, *A Set of Measures of Centrality Based on Betweenness*, *Sociometry*, 40 (1977), pp. 35–41.
- [111] —, *Some antecedents of social network analysis*, *Connections*, 19 (1996), pp. 39–42.
- [112] —, *Finding social groups: A meta-analysis of the southern women data*, in *Dynamic Social Network Modeling and Analysis: workshop summary and papers*, 2003, pp. 39–97.

-
- [113] M. D. FRICKER, L. BODDY, AND D. P. BEBBER, *The Mycota: Biology of the Fungal Cell*, vol. 3, Springer, Berlin, Germany, 2nd ed., 2007, ch. Network organisation of mycelial fungi, pp. 307–328.
- [114] M. D. FRICKER, L. BODDY, T. NAKAGAKI, AND D. P. BEBBER, *Adaptive Networks: Theory, Models and Applications*, NECSI Studies on Complexity, Springer, Berlin/Heidelberg, Germany, 2009, ch. Adaptive biological networks, pp. 51–70.
- [115] Y. V. FYODOROV AND A. D. MIRLIN, *Analytical Derivation of the Scaling Law for the Inverse Participation Ratio in Quasi-One-Dimensional Disordered Systems*, Physical Review Letters, 69 (1992), pp. 1093–1096.
- [116] P. GAI AND S. KAPADIA, *Contagion in Financial Networks*, Bank of England Working Paper No. 383, (2010). Available at SSRN: http://papers.ssrn.com/sol3/papers.cfm?abstract_id=1577043.
- [117] G. GALATI, S. JEANNEAU, AND R. WIDERA, *Triennial Central Bank Survey: Foreign exchange and derivatives market activity*, tech. rep., Bank for International Settlements, 2001.
- [118] A. GARAS, P. ARGYRAKIS, AND S. HAVLIN, *The structural role of weak and strong links in a financial market network*, European Physical Journal B, 63 (2008), pp. 265–271.
- [119] E. GARFIELD, I. H. SHER, AND R. J. TORPIE, *The Use of Citation Data in Writing the History of Science*, The Institute for Scientific Information, Philadelphia, PA, USA, 1964.
- [120] J. GIL-MENDIETA AND S. SCHMIDT, *The political network in Mexico*, Social Networks, 18 (1996), pp. 355–381.
- [121] M. GIRVAN AND M. E. J. NEWMAN, *Community structure in social and biological networks*, Proceedings of the National Academy of Sciences of the U.S.A., 99 (2002), pp. 7821–7826.
- [122] K. S. GLEDITSCH, *Expanded Trade and GDP Data*, Journal of Conflict Resolution, 46 (2002), pp. 712–724.
- [123] J. P. GLEESON, *Cascades on correlated and modular random networks*, Physical Review E, 77 (2008), p. 46117.

References

- [124] D. F. GLEICH, 2001. Data available at <http://www.cise.ufl.edu/research/sparse/matrices/Gleich/wb-cs-stanford.html>.
- [125] P. GLEISER AND L. DANON, *Community Structure in Jazz*, Advances in Complex Systems, 6 (2003), pp. 565–573.
- [126] M. GOLDBERG, M. MAGDON-ISMAIL, S. KELLEY, K. MERTSALOV, AND W. WALLACE, *Communication dynamics of blog networks*, in Proceedings of SNAKDD 2008: KDD Workshop on Social Network Mining and Analysis, in conjunction with the 14th ACM SIGKDD International Conference on Knowledge Discovery and Data Mining (KDD 2008), 2008.
- [127] A. GOLDENBERG, A. X. ZHENG, S. E. FIENBERG, AND E. M. AIROLDI, *A Survey of Statistical Network Models*, Foundations and Trends in Machine Learning, 2 (2010), pp. 129–233.
- [128] B. H. GOOD, Y. A. DE MONTJOYE, AND A. CLAUSET, *Performance of modularity maximization in practical contexts*, Physical Review E, 81 (2010), p. 46106.
- [129] P. GOOD, *Permutation, Parametric, and Bootstrap Tests of Hypotheses*, Springer-Verlag, New York, NY, USA, 2005.
- [130] C. A. E. GOODHART AND L. FIGLIUOLI, *Every minute counts in financial markets*, Journal of International Money and Finance, 10 (1991), pp. 23–52.
- [131] C. A. E. GOODHART, T. ITO, AND R. G. PAYNE, *One Day in June, 1993: A Study of the Working of Reuters 2000-2 Electronic Foreign Exchange Trading System*, NBER Working Paper Series, (1995). Available at SSRN: <http://ssrn.com/abstract=225089>.
- [132] S. GOPAL, *Societies and Cities in the Age of Instant Access*, Springer, Berlin, Germany, 2007.
- [133] A. Z. GÓRSKI, S. DRÓZDZ, AND J. KWAPIEŃ, *Scale free effects in world currency exchange network*, European Physical Journal B, 66 (2008), pp. 91–96.
- [134] C. W. J. GRANGER AND P. NEWBOLD, *Spurious regressions in econometrics*, Journal of Econometrics, 2 (1974), pp. 111–120.

-
- [135] M. S. GRANOVETTER, *The Strength of Weak Ties*, American Journal of Sociology, 78 (1973), pp. 1360–1380.
- [136] P. D. GRÜNWARD, I. J. MYUNG, AND M. A. PITT, *Advances in Minimum Description Length: Theory and Applications*, MIT Press, Cambridge, MA, USA, 2005.
- [137] T. GUHR, A. MÜLLER-GROELING, AND H. A. WEIDENMÜLLER, *Random-matrix theories in quantum physics: common concepts*, Physics Reports, 299 (1998), pp. 189–425.
- [138] D. M. GUILLAUME, M. M. DACOROGNA, R. R. DAVÉ, U. A. MÜLLER, R. B. OLSEN, AND O. V. PICTET, *From the bird's eye to the microscope: A survey of new stylized facts of the intra-daily foreign exchange markets*, Finance and Stochastics, 1 (1997), pp. 95–129.
- [139] R. GUIMERÀ AND L. A. N. AMARAL, *Functional cartography of complex metabolic networks*, Nature, 433 (2005), pp. 895–900.
- [140] R. GUIMERÀ, L. DANON, A. DÍAZ-GUILERA, F. GIRALT, AND A. ARENAS, *Self-similar community structure in a network of human interactions*, Physical Review E, 68 (2003), p. 065103.
- [141] R. GUIMERÀ, M. SALES, AND L. A. N. AMARAL, *Modularity from fluctuations in random graphs and complex networks*, Physical Review E, 70 (2004), p. 025101.
- [142] R. GUIMERÀ, M. SALES-PARDO, AND L. A. N. AMARAL, *Classes of complex networks defined by role-to-role connectivity profiles*, Nature Physics, 3 (2007), pp. 63–69.
- [143] L. GUTTMAN, *Some necessary conditions for common-factor analysis*, Psychometrika, 19 (1954), pp. 149–161.
- [144] P. HAGMANN, L. CAMMOUN, X. GIGANDET, R. MEULI, C. J. HONEY, V. J. WEDEEN, AND O. SPORNS, *Mapping the Structural Core of Human Cerebral Cortex*, PLoS Biology, 6 (2008), p. e159.
- [145] L. HAKES, J. W. PINNEY, D. L. ROBERTSON, AND S. C. LOVELL, *Protein-protein interaction networks and biology—what's the connection?*, Nature Biotechnology, 26 (2008), pp. 69–72.

References

- [146] J. D. J. HAN, N. BERTIN, T. HAO, D. S. GOLDBERG, G. F. BERRIZ, L. V. ZHANG, D. DUPUY, A. J. WALHOUT, M. E. CUSICK, F. P. ROTH, AND M. VIDAL, *Evidence for dynamically organized modularity in the yeast protein-protein interaction network*, *Nature*, 430 (2004), pp. 88–93.
- [147] A. HEATH, C. UPPER, P. GALLARDO, AND P. MESNY, *Triennial Central Bank Survey: Foreign exchange and derivatives market activity*, tech. rep., Bank for International Settlements, 2007.
- [148] T. HEIMO, J. KUMPULA, K. KASKI, AND J. SARAMÄKI, *Detecting modules in dense weighted networks with the Potts method*, *Journal of Statistical Mechanics*, 2008 (2008), p. P08007.
- [149] M. H. HEYER AND F. P. SCHLOERB, *Application of Principal Component Analysis to Large-scale Spectral Line Imaging Studies of the Interstellar Medium*, *Astrophysical Journal*, 475 (1997), pp. 173–187.
- [150] C. A. HIDALGO, B. KLINGER, A. L. BARABÁSI, AND R. HAUSMANN, *The Product Space Conditions the Development of Nations*, *Science*, 317 (2007), pp. 482–487.
- [151] P. HOLME, B. J. KIM, C. N. YOON, AND S. K. HAN, *Attack vulnerability of complex networks*, *Physical Review E*, 65 (2002), p. 056109.
- [152] J. HOPCROFT, O. KHAN, B. KULLIS, AND B. SELMAN, *Tracking evolving communities in large linked networks*, *Proceedings of the National Academy of Sciences of the U.S.A.*, 101 (2004), pp. 5249–5253.
- [153] D. A. JACKSON, *Stopping Rules in Principal Components Analysis: A Comparison of Heuristical and Statistical Approaches*, *Ecology*, 74 (1993), pp. 2204–2214.
- [154] M. B. JDIDIA, C. ROBARDET, AND E. FLEURY, *Communities detection and analysis of their dynamics in collaborative networks*, in 2nd International Conference on Digital Information Management, 2007, pp. 28–31.
- [155] L. J. JENSEN, M. KUHN, M. STARK, S. CHAFFRON, C. CREEVEY, J. MULLER, T. DOERKS, P. JULIEN, A. ROTH, M. SIMONOVIC, P. BORK, AND C. VON MERING, *STRING 8—a global view on proteins and their functional interactions in 630 organisms*, *Nucleic Acids Research*, 37 (2009), pp. D412–D416.

-
- [156] H. JEONG, B. TOMBOR, R. ALBERT, Z. N. OLTVAI, AND A.-L. BARABÁSI, *The large-scale organization of metabolic networks*, Nature, 407 (2000), pp. 651–654.
- [157] R. JIN, S. MCCALLEN, AND E. ALMAAS, *Trend Motif: A Graph Mining Approach for Analysis of Dynamic Complex Networks*, in ICDM '07: Proceedings of the 2007 Seventh IEEE International Conference on Data Mining, 2007, pp. 541–546.
- [158] J. C. JOHNSON AND L. KREMPEL, *Network Visualization: The “Bush Team” in Reuters News Ticker 9/11-11/15/01*, Journal of Social Structures, 5 (2004).
- [159] I. T. JOLLIFFE, *Principal Component Analysis*, Springer-Verlag, New York, NY, USA, 1986.
- [160] K. G. JÖRESKOG, *Some Contributions to Maximum Likelihood Factor Analysis*, Psychometrika, 32 (1967), pp. 443–482.
- [161] J. KAMBHU, S. WEIDMAN, AND N. KRISHNAN, *New directions for understanding systemic risk*, New York Economic Policy Review, 13 (2007).
- [162] G. KAMPIS, L. GULYAS, Z. SZASZI, AND Z. SZAKOLCZI, *Dynamic Social Networks and the Textrend/CIShell Framework*, in Applications of Social Network Analysis, 2009.
- [163] B. KAPFERER, *Strategy and transaction in an African factory*, Manchester University Press, Manchester, UK, 1972.
- [164] B. KARRER, E. LEVINA, AND M. E. J. NEWMAN, *Robustness of community structure in networks*, Physical Review E, 77 (2008), p. 046119.
- [165] P. D. KILLWORTH AND H. R. BERNARD, *Informant accuracy in social network data III: A comparison of triadic structure in behavioral and cognitive data*, Social Networks, 2 (1979-1980), pp. 19–46.
- [166] D. H. KIM AND H. JEONG, *Systematic analysis of group identification in stock markets*, Physical Review E, 72 (2005), p. 046133.
- [167] M. S. KIM AND J. HAN, *A particle-and-density based evolutionary clustering method for dynamic networks*, Proceedings of the VLDB Endowment, 2 (2009), pp. 622–633.

References

- [168] D. E. KNUTH, *The Stanford GraphBase: A Platform for Combinatorial Computing*, Addison-Wesley, Reading, MA, USA, 1993.
- [169] C. KOLLIAS AND K. METAXAS, *How efficient are FX markets? Empirical evidence of arbitrage opportunities using high-frequency data*, Applied Financial Economics, 11 (2001), pp. 435–444.
- [170] D. KRACKHARDT, *The ties that torture: Simmelian tie analysis in organizations*, Research in the Sociology of Organizations, 16 (1999), pp. 183–210.
- [171] V. KREBS, 2004. Network compiled by Valdis Krebs and not previously published. The data is available at <http://www.orgnet.com/>.
- [172] A. KUBÍK, *Toward a formalization of emergence*, Artificial Life, 9 (2003), pp. 41–65.
- [173] S. KULLBACK AND R. A. LEIBLER, *On Information and Sufficiency*, The Annals of Mathematical Statistics, 22 (1951), pp. 79–86.
- [174] J. M. KUMPULA, J.-P. ONNELA, J. SARAMÄKI, K. KASKI, AND J. KERTÉSZ, *Emergence of Communities in Weighted Networks*, Physical Review Letters, 99 (2007), p. 228701.
- [175] M. LAHIRI AND T. Y. BERGER-WOLF, *Mining Periodic Behavior in Dynamic Social Networks*, in ICDM '08: Proceedings of the 2008 Eighth IEEE International Conference on Data Mining, 2008, pp. 373–382.
- [176] L. LALOUX, P. CIZEAU, J.-P. BOUCHAUD, AND M. POTTERS, *Noise Dressing of Financial Correlation Matrices*, Physical Review Letters, 83 (1999), pp. 1467–1470.
- [177] R. LAMBIOTTE, J. C. DELVENNE, AND M. BARAHONA, *Laplacian dynamics and multiscale modular structure in networks*, arXiv:0812:1770, (2008).
- [178] A. LANCICHINETTI AND S. FORTUNATO, *Benchmarks for testing community detection algorithms on directed and weighted graphs with overlapping communities*, Physical Review E, 80 (2009), p. 016118.
- [179] A. LANCICHINETTI, S. FORTUNATO, AND J. KERTÉSZ, *Detecting the overlapping and hierarchical community structure of complex networks*, New Journal of Physics, 11 (2009), p. 033015.

-
- [180] A. LANCICHINETTI, S. FORTUNATO, AND F. RADICCHI, *Benchmark graphs for testing community detection algorithms*, Physical Review E, 78 (2008), p. 046110.
- [181] A. LANCICHINETTI, M. KIVELA, J. SARAMÄKI, AND S. FORTUNATO, *Characterizing the community structure of complex networks*, PLoS ONE, 5 (2010), p. e11976.
- [182] F.-J. LAPOINTE AND P. LEGENDRE, *A Statistical Framework to Test the Consensus of Two Nested Classifications*, Systematic Zoology, 39 (1990), pp. 1–13.
- [183] ———, *Comparison Tests for Dendrograms: A Comparative Evaluation*, Journal of Classification, 12 (1995), pp. 265–282.
- [184] E. A. LEICHT AND M. E. J. NEWMAN, *Community Structure in Directed Networks*, Physical Review Letters, 100 (2008), p. 118703.
- [185] J. LESKOVEC, J. KLEINBERG, AND C. FALOUTSOS, *Graphs over time: densification laws, shrinking diameters and possible explanations*, in KDD '05: Proceedings of the eleventh ACM SIGKDD international conference on Knowledge discovery in data mining, 2005, pp. 177–187.
- [186] J. LI, W. K. CHEUNG, J. LIU, AND C. H. LI, *On Discovering Community Trends in Social Networks*, in WI-IAT '09: Proceedings of the 2009 IEEE/WIC/ACM International Joint Conference on Web Intelligence and Intelligent Agent Technology, 2009, pp. 230–237.
- [187] T. W. LIAO, *Clustering of time series data – a survey*, Pattern Recognition, 38 (2005), pp. 1857–1874.
- [188] Y.-R. LIN, Y. CHI, S. ZHU, H. SUNDARAM, AND B. L. TSENG, *Facetnet: a framework for analyzing communities and their evolutions in dynamic networks*, in WWW '08: Proceeding of the 17th international conference on World Wide Web, 2008, pp. 685–694.
- [189] ———, *Analyzing communities and their evolutions in dynamic social networks*, ACM Transactions on Knowledge Discovery from Data, 3 (2009), pp. 1–31.
- [190] Y. R. LIN, H. SUNDARAM, Y. CHI, J. TATEMURA, AND B. L. TSENG, *Blog Community Discovery and Evolution Based on Mutual Awareness Expansion*,

References

- in WI '07: Proceedings of the IEEE/WIC/ACM International Conference on Web Intelligence, 2007, pp. 48–56.
- [191] Z. LIU, Y.-C. LAI, AND N. YE, *Propagation and immunization of infection on general networks with both homogeneous and heterogeneous components*, Physical Review E, 67 (2003), p. 031911.
- [192] D. LUSSEAU, K. SCHNEIDER, O. J. BOISSEAU, P. HAASE, E. SLOOTEN, AND S. M. DAWSON, *The Bottleneck Dolphin Community of Doubtful Sound Features a Large Proportion of Long-Lasting Associations: Can Geographic Isolation Explain This Unique Trait?*, Behavioral Ecology and Sociobiology, 54 (2003), pp. 396–405.
- [193] R. K. LYONS, *Tests of microstructural hypotheses in the foreign exchange market*, Journal of Financial Economics, 39 (1995), pp. 321–351.
- [194] K. MACON, P. J. MUCHA, AND M. A. PORTER, *Community Structure in the United Nations General Assembly*, arXiv:1010.3757, (2010).
- [195] L. MAHADEVA, K. SVIRYDENSKA, AND R. GARRATT, *Tracking Systemic Risk in the International Banking Network*, Working paper, (2010).
- [196] S. MANGAN AND U. ALON, *Structure and function of the feed-forward loop network motif*, Proceedings of the National Academy of Sciences of the U.S.A., 100 (2003), pp. 11980–11985.
- [197] R. N. MANTEGNA, *Hierarchical structure in financial markets*, European Physical Journal B, 11 (1999), pp. 193–197.
- [198] R. N. MANTEGNA AND H. E. STANLEY, *An Introduction to Econophysics*, Cambridge University Press, Cambridge, UK, 2000.
- [199] H. MARKOWITZ, *Portfolio selection*, Journal of Finance, 7 (1952), pp. 77–91.
- [200] M. MARTENS AND P. KOFFMAN, *The inefficiency of Reuters foreign exchange quotes*, Journal of Banking and Finance, 22 (1998), pp. 347–366.
- [201] S. MASLOV AND K. SNEPPEN, *Specificity and Stability in Topology of Protein Networks*, Science, 296 (2002), pp. 910–913.
- [202] R. M. MAY, S. A. LEVIN, AND G. SUGIHARA, *Ecology for bankers*, Nature, 451 (2008), pp. 893–895.

-
- [203] N. M. McCARTY, K. T. POOLE, AND H. ROSENTHAL, *Polarized America: The Dance of Ideology and Unequal Riches*, MIT Press, Cambridge, MA, USA, 2007.
- [204] M. McDONALD, O. SULEMAN, S. WILLIAMS, S. HOWISON, AND N. F. JOHNSON, *Detecting a currency's dominance or dependence using foreign exchange network trees*, *Physical Review E*, 72 (2005), p. 46106.
- [205] ———, *Impact of unexpected events, shocking news, and rumors on foreign exchange market dynamics*, *Physical Review E*, 77 (2008), p. 46110.
- [206] M. L. MEHTA, *Random Matrices*, Elsevier, San Diego, CA, USA, 2004.
- [207] M. MEILÄ, *Comparing clusterings – an information based distance*, *Journal of Multivariate Analysis*, 98 (2007), pp. 873–895.
- [208] J. H. MICHAEL AND J. G. MASSEY, *Modeling the communication network in a sawmill*, *Forest Products Journal*, 47 (1997), pp. 25–30.
- [209] S. MILGRAM, *The small world problem*, *Psychology Today*, 1 (1967), pp. 60–67.
- [210] R. MILO, S. ITZKOVITZ, N. KASHTAN, R. L. S. SHEN-ORR, I. AYZENSHTAT, M. SHEFFER, AND U. ALON, *Superfamilies of Evolved and Designed Networks*, *Science*, 303 (2004), pp. 1538–1542.
- [211] R. MILO, S. SHEN-ORR, S. ITZKOVITZ, N. KASHTAN, D. CHKLOVSKII, AND U. ALON, *Network Motifs: Simple Building Blocks of Complex Networks*, *Science*, 298 (2002), pp. 824–827.
- [212] M. MOLLOY AND B. REED, *A critical point for random graphs with a given degree sequence*, *Random Structures and Algorithms*, 6 (1995), pp. 161–180.
- [213] Y. MORENO, M. NEKOVEE, AND A. F. PACHECO, *Dynamics of rumor spreading in complex networks*, *Physical Review E*, 69 (2004), p. 066130.
- [214] P. J. MUCHA, T. RICHARDSON, K. MACON, M. A. PORTER, AND J.-P. ONNELA, *Community Structure in Time-Dependent, Multiscale, and Multiplex Networks*, *Science*, 328 (2010), pp. 876–878.
- [215] T. NEPUSZ, A. PETRÓCZI, L. NÉGYESSY, AND F. BAZSÓ, *Fuzzy communities and the concept of bridgeness in complex networks*, *Physical Review E*, 77 (2008), p. 016107.

References

- [216] M. E. J. NEWMAN, *The structure of scientific collaboration networks*, Proceedings of the National Academy of Sciences of the U.S.A., 98 (2001), pp. 404–409.
- [217] ———, *The Structure and Function of Complex Networks*, SIAM Review, 45 (2003), pp. 167–256.
- [218] ———, *Fast algorithm for detecting community structure in networks*, Physical Review E, 69 (2004), p. 066133.
- [219] ———, 2006. Network compiled by Mark Newman and not previously published. The data is available at <http://www-personal.umich.edu/~mejn/netdata/>.
- [220] ———, *Finding community structure in networks using the eigenvectors of matrices*, Physical Review E, 74 (2006), p. 036104.
- [221] ———, *Modularity and community structure in networks*, Proceedings of the National Academy of Sciences of the U.S.A., 103 (2006), pp. 8577–8582.
- [222] ———, *The physics of networks*, Physics Today, 61 (2008), pp. 33–38.
- [223] ———, *Networks: An Introduction*, Oxford University Press, Oxford, UK, 2010.
- [224] M. E. J. NEWMAN AND M. GIRVAN, *Finding and evaluating community structure in networks*, Physical Review E, 69 (2004), p. 026113.
- [225] M. E. J. NEWMAN, D. J. WATTS, AND A.-L. BARABÁSI, eds., *The Structure and Dynamics of Networks*, Princeton University Press, Princeton, NJ, USA, 2006.
- [226] K. NORLEN, G. LUCAS, M. GEBBIE, AND J. CHUANG, *EVA: Extraction, Visualization and Analysis of the Telecommunications and Media Ownership Network*, in Proceedings of International Telecommunications Society 14th Biennial Conference (ITS2002), 2002.
- [227] J.-P. ONNELA, *Taxonomy of Financial Assets*, Master’s thesis, Helsinki University of Technology, Finland, 2002.
- [228] ———, *Complex Networks in the Study of Financial and Social Systems*, Master’s thesis, Helsinki University of Technology, 2006.
- [229] J.-P. ONNELA, A. CHAKRABORTI, K. K, J. KERTÉSZ, AND A. KANTO, *Dynamics of market correlations: Taxonomy and portfolio analysis*, Physical Review E, 68 (2003), p. 056110.

-
- [230] J.-P. ONNELA, A. CHAKRABORTI, K. KASKI, AND J. KERTÉSZ, *Dynamic asset trees and portfolio analysis*, European Physical Journal B, 30 (2002), pp. 285–288.
- [231] J.-P. ONNELA, K. KASKI, AND J. KERTÉSZ, *Clustering and information in correlation based financial networks*, European Physical Journal B, 38 (2004), pp. 353–362.
- [232] J.-P. ONNELA, J. SARAMÄKI, J. HYVÖNEN, G. SZABÓ, D. LAZER, K. KASKI, J. KERTÉSZ, AND A.-L. BARABÁSI, *Structure and Tie Strengths in Mobile Communication Networks*, Proceedings of the National Academy of Sciences of the U.S.A., 104 (2007), pp. 7332–7336.
- [233] G. PALLA, A.-L. BARABÁSI, AND T. VICSEK, *Quantifying social group evolution*, Nature, 446 (2007), pp. 664–667.
- [234] G. PALLA, I. DERÉNYI, I. J. FARKAS, AND T. VICSEK, *Uncovering the overlapping community structure of complex networks in nature and society*, Nature, 435 (2005), pp. 814–818.
- [235] R. K. PAN AND S. SINHA, *Collective behavior of stock price movements in an emerging market*, Physical Review E, 76 (2007), p. 046116.
- [236] R. PASTOR-SATORRAS AND A. VESPIGNANI, *Epidemic Spreading in Scale-Free Networks*, Physical Review Letters, 86 (2001), pp. 3200–3203.
- [237] C. PÉRIGNON, D. R. SMITH, AND C. VILLA, *Why common factors in international bond returns are not so common*, Journal of International Money and Finance, 26 (2007), pp. 284–304.
- [238] V. PLEROU, P. GOPIKRISHNAN, B. ROSENOW, L. A. N. AMARAL, T. GUHR, AND H. E. STANLEY, *Random matrix approach to cross correlations in financial data*, Physical Review E, 65 (2002), p. 066126.
- [239] V. PLEROU, P. GOPIKRISHNAN, B. ROSENOW, L. A. N. AMARAL, AND H. E. STANLEY, *Universal and Nonuniversal Properties of Cross Correlations in Financial Time Series*, Physical Review Letters, 83 (1999), pp. 1471–1474.
- [240] P. PONS AND M. LATAPY, *Computer and Information Sciences - ISCIS 2005*, vol. 3733 of Lecture Notes in Computer Science, Springer, Berlin/Heidelberg,

References

- Germany, 2005, ch. Computing Communities in Large Networks Using Random Walks, pp. 284–293.
- [241] K. T. POOLE AND H. ROSENTHAL, *Congress: A Political-Economic History of Roll Call Voting*, Oxford University Press, Oxford, UK, 1997.
- [242] M. A. PORTER, P. J. MUCHA, M. E. J. NEWMAN, AND A. J. FRIEND, *Community structure in the United States House of Representatives*, *Physica A*, 386 (2007), pp. 414–438.
- [243] M. A. PORTER, P. J. MUCHA, M. E. J. NEWMAN, AND C. M. WARMBRAND, *A network analysis of committees in the U.S. House of Representatives*, *Proceedings of the National Academy of Sciences of the U.S.A.*, 102 (2005), pp. 7057–7062.
- [244] M. A. PORTER, J.-P. ONNELA, AND P. J. MUCHA, *Communities in Networks*, *Notices of the American Mathematical Society*, 56 (2009), pp. 1082–1097, 1164–1166.
- [245] A. L. PRICE, N. J. PATTERSON, R. M. PLENGE, M. E. WEINBLATT, N. A. SHADICK, AND D. REICH, *Principal components analysis corrects for stratification in genome-wide association studies*, *Nature Genetics*, 38 (2006), pp. 904–909.
- [246] D. J. DE S. PRICE, *A general theory of bibliometric and other cumulative advantage processes*, *Journal of the American Society for Information Science*, 27 (1976), pp. 292–306.
- [247] F. RADICCHI, C. CASTELLANO, F. CECCONI, V. LORETO, AND D. PARISI, *Defining and identifying communities in networks*, *Proceedings of the National Academy of Sciences of the U.S.A.*, 101 (2004), pp. 2658–2663.
- [248] A. RANALDO AND P. SÖDERLIND, *Safe Haven Currencies*, to appear in *Review of Finance*, (2010). Available at SSRN: <http://ssrn.com/abstract=1097593>.
- [249] A. RAPOPORT, *Contribution to the theory of random and biased nets*, *Bulletin of Mathematical Biophysics*, 19 (1957), pp. 257–277.
- [250] ———, *Cycle distribution in random nets*, *Bulletin of Mathematical Biophysics*, 10 (1968), pp. 145–157.

-
- [251] A. RAPOPORT AND W. J. HORVATH, *A study of a large sociogram*, Behavioral Science, 6 (1961), pp. 279–291.
- [252] R. RASKIN AND H. TERRY, *A principal-components analysis of the Narcissistic Personality Inventory and further evidence of its construct validity*, Journal of Personality and Social Psychology, 54 (1988), pp. 890–902.
- [253] P. K. REDDY, M. KITSUREGAWA, P. SREEKANTH, AND S. S. RAO, *A Graph Based Approach to Extract a Neighborhood Customer Community for Collaborative Filtering*, in DNIS '02: Proceedings of the Second International Workshop on Databases in Networked Information Systems, 2002, pp. 188–200.
- [254] J. REICHARDT AND S. BORNHOLDT, *Statistical mechanics of community detection*, Physical Review E, 74 (2006), p. 016110.
- [255] J. M. REITZ, 2000. ODLIS is maintained by Joan Reitz and was converted into the network used here by A. Mrvar and V. Batagelj. The data is available at <http://vlado.fmf.uni-lj.si/pub/networks/data/dic/odlis/Odlis.htm>.
- [256] J. G. RESTREPO, E. OTT, AND B. R. HUNT, *Characterizing the Dynamical Importance of Network Nodes and Links*, Physical Review Letters, 97 (2006), p. 94102.
- [257] J. RISSANEN, *Modeling by shortest data description*, Automatica, 14 (1978), pp. 465–471.
- [258] F. J. ROETHLISBERGER AND W. J. DICKSON, *Management and the Worker*, Harvard University Press, Cambridge, MA, USA, 1939.
- [259] E. M. ROGERS AND D. L. KINCAID, *Communication Networks. Toward a New Paradigm for Research*, The Free Press, New York, NY, USA, 1981.
- [260] A. K. ROMNEY AND S. C. WELLER, *Predicting informant accuracy from patterns of recall among individuals*, Social Networks, 6 (1984), pp. 59–77.
- [261] J. F. RUAL, K. VENKATESAN, T. HAO, T. HIROZANE-KISHIKAWA, A. DRICOT, N. LI, G. F. BERRIZ, F. D. GIBBONS, M. DREZE, N. AYIVI-GUEDEHOUSOU, ET AL., *Towards a proteome-scale map of the human protein-protein interaction network*, Nature, 437 (2005), pp. 1173–1178.

References

- [262] L. SALWINSKI, C. S. MILLER, A. J. SMITH, F. K. PETTIT, J. U. BOWIE, AND D. EISENBERG, *The database of interacting proteins: 2004 update*, *Nucleic Acids Research*, 32 (2004), pp. D449–D451.
- [263] A. SARR AND T. LYBEK, *Measuring Liquidity in Financial Markets*, IMF Working Paper, (2002). Available at SSRN: <http://ssrn.com/abstract=880932>.
- [264] J. W. SCANNELL, G. A. P. C. BURNS, C. C. HILGETAG, M. A. O’NEIL, AND M. P. YOUNG, *The Connectional Organization of the Cortico-thalamic System of the Cat*, *Cerebral Cortex*, 9 (1999), pp. 277–299.
- [265] B. SCHELTER, M. WINTERHALDER, AND J. TIMMER, eds., *Handbook of Time Series Analysis*, Wiley-VCH, Weinheim, Germany, 2006.
- [266] S. SCHIAVO, J. REYES, AND G. FAGIOLO, *International trade and financial integration: a weighted network analysis*, *Quantitative Finance*, 10 (2010), pp. 389–399.
- [267] J. SCOTT AND M. HUGHES, *The anatomy of Scottish capital: Scottish companies and Scottish capital, 1900-1979*, Croom Helm, London, UK, 1980.
- [268] A. I. SELVERTSON AND M. MOULINS, eds., *The Crustacean Stomatogastric System: A Model for the Study of Central Nervous Systems*, Springer-Verlag, Berlin, Germany, 1987.
- [269] A. M. SENGUPTA AND P. P. MITRA, *Distributions of singular values for some random matrices*, *Physical Review E*, 60 (1999), pp. 3389–3392.
- [270] C. R. SHALIZI, *Complex Systems Science in Biomedicine*, Topics in Biomedical Engineering, Springer, Berlin/Heidelberg, Germany, 2005, ch. Methods and Techniques of Complex Systems Science: An Overview, pp. 33–114.
- [271] C. R. SHALIZI, M. F. CAMPERI, AND K. L. KLINKNER, *Discovering functional communities in dynamical networks*, in *Statistical Network Analysis: Models, Issues, and New Directions*, E. M. Airoldi, D. M. Blei, S. E. Feinberg, A. Goldenberg, E. P. Xing, and A. X. Zheng, eds., Springer-Verlag, New York, NY, USA, 2007, pp. 140–157.
- [272] P. SIECZKA AND J. A. HOLYST, *Correlations in commodity markets*, *Physica A*, 388 (2009), pp. 1621–1630.

-
- [273] H. A. SIMON, *On a Class of Skew Distribution Functions*, *Biometrika*, 42 (1955), pp. 425–440.
- [274] ———, *The architecture of complexity*, *Proceedings of the American Philosophical Society*, (1962), pp. 467–482.
- [275] D. A. SMITH AND D. R. WHITE, *Structure and Dynamics of the Global Economy Network Analysis of International Trade 1965–1980*, *Social Forces*, 70 (1992), pp. 857–893.
- [276] R. R. SOKAL AND F. J. ROHLF, *The comparison of dendrograms by objective methods*, *Taxon*, 11 (1962), pp. 33–40.
- [277] R. SOLOMONOFF AND A. RAPOPORT, *Connectivity of random nets*, *Bulletin of Mathematical Biophysics*, 13 (1951), pp. 107–117.
- [278] P. T. SPELLMAN, G. SHERLOCK, M. Q. ZHANG, V. R. IYER, K. ANDERS, M. B. EISEN, P. O. BROWN, D. BOTSTEIN, AND B. FUTCHER, *Comprehensive Identification of Cell Cycle-regulated Genes of the Yeast *Saccharomyces cerevisiae* by Microarray Hybridization*, *Molecular Biology of the Cell*, 9 (1998), pp. 3273–3297.
- [279] O. SPORNS, *Small-world connectivity, motif composition, and complexity of fractal neuronal connections*, *BioSystems*, 85 (2006), pp. 55–64.
- [280] C. STARK, B. J. BREITKREUTZ, T. REGULY, L. BOUCHER, A. BREITKREUTZ, AND M. TYERS, *BioGRID: a general repository for interaction datasets*, *Nucleic Acids Research*, 34 (2006), pp. D535–D539.
- [281] S. H. STROGATZ, *Nonlinear Dynamics and Chaos*, Addison-Wesley, Reading, MA, USA, 1994.
- [282] J. SUN, C. FALOUTSOS, S. PAPADIMITRIOU, AND P. S. YU, *GraphScope: parameter-free mining of large time-evolving graphs*, in *KDD '07: Proceedings of the 13th ACM SIGKDD international conference on Knowledge discovery and data mining*, 2007, pp. 687–696.
- [283] S. R. SUNDARESAN, I. R. FISCHHOFF, J. DUSHOFF, AND D. I. RUBENSTEIN, *Network metrics reveal differences in social organization between two fission-fusion species, *Grevys zebra* and *onager**, *Oecologia*, 151 (2007), pp. 140–149.

References

- [284] L. TANG, H. LIU, J. ZHANG, AND Z. NAZERI, *Community evolution in dynamic multi-mode networks*, in KDD '08: Proceeding of the 14th ACM SIGKDD international conference on Knowledge discovery and data mining, 2008, pp. 677–685.
- [285] C. TANTIPATHANANANDH AND T. BERGER-WOLF, *Constant-factor approximation algorithms for identifying dynamic communities*, in KDD '09: Proceedings of the 15th ACM SIGKDD international conference on Knowledge discovery and data mining, 2009, pp. 827–836.
- [286] C. TANTIPATHANANANDH, T. BERGER-WOLF, AND D. KEMPE, *A framework for community identification in dynamic social networks*, in KDD '07: Proceedings of the 13th ACM SIGKDD international conference on Knowledge discovery and data mining, 2007, pp. 717–726.
- [287] K. TARASSOV, V. MESSIER, C. R. LANDRY, S. RADINOVIC, M. M. S. MOLINA, I. SHAMES, Y. MALITSKAYA, J. VOGEL, H. BUSSEY, AND S. W. MICHNICK, *An in Vivo Map of the Yeast Protein Interactome*, *Science*, 320 (2008), pp. 1465–1470.
- [288] A. TERO, S. TAKAGI, T. SAIGUSA, K. ITO, D. P. BEBBER, M. D. FRICKER, K. YUMIKI, R. KOBAYASHI, AND T. NAKAGAKI, *Rules for Biologically Inspired Adaptive Network Design*, *Science*, 327 (2010), pp. 439–442.
- [289] G. TIBELY, M. KARSAI, L. KOVANEN, K. KASKI, J. KERTÉSZ, AND J. SARAMÄKI, *Communities and beyond: mesoscopic analysis of a large social network with complementary methods*, arXiv:1006.0418, (2010).
- [290] M. TOYODA AND M. KITSUREGAWA, *Creating a Web community chart for navigating related communities*, in HYPERTEXT '01: Proceedings of the 12th ACM conference on Hypertext and Hypermedia, 2001, pp. 103–112.
- [291] —, *Extracting evolution of web communities from a series of web archives*, in HYPERTEXT '03: Proceedings of the fourteenth ACM conference on Hypertext and hypermedia, 2003, pp. 28–37.
- [292] —, *Web Community Chart: A Tool for Navigating the Web and Observing Its Evolution*, IEICE TRANSACTIONS on Information and Systems, E86-D (2003), pp. 1024–1031.

-
- [293] ———, *A system for visualizing and analyzing the evolution of the web with a time series of graphs*, in HYPertext '05: Proceedings of the sixteenth ACM conference on Hypertext and hypermedia, 2005, pp. 151–160.
- [294] V. A. TRAAG AND J. BRUGGEMAN, *Community detection in networks with positive and negative links*, Physical Review E, 80 (2009), p. 036115.
- [295] A. L. TRAUD, E. D. KELSIC, P. J. MUCHA, AND M. A. PORTER, *Community Structure in Online Collegiate Social Networks*, arXiv:0809.0960, (2009).
- [296] R. S. TSAY, *Analysis of Financial Time Series*, Wiley-Interscience, Hoboken, NJ, USA, 2005.
- [297] L. R. TUCKER AND R. C. MACCALLUM, *Exploratory Factor Analysis*, Working paper, (1997). Available at <http://www.unc.edu/~rcm/book/factornew.htm>.
- [298] J. UTANS, W. T. HOLT, AND A. N. REFENES, *Principal components analysis for modeling multi-currency portfolios*, in Proceedings of the Fourth International Conference on Neural Networks in the Capital Markets, 1997, pp. 359–368.
- [299] T. W. VALENTE, K. CORONGES, C. LAKON, AND E. COSTENBADER, *How Correlated are Network Centrality Measures?*, Connections, 28 (2008), pp. 16–26.
- [300] S. VAN DONGEN, *A New Cluster Algorithm for Graphs*, tech. rep., National Research Institute for Mathematics and Computer Science in the Netherlands, 1998.
- [301] W. F. VELICER AND D. N. JACKSON, *Component Analysis versus Common Factor Analysis: Some Issues in Selecting an Appropriate Procedure*, Multivariate Behavioral Research, 25 (1990), pp. 1–28.
- [302] E. VOETEN, *Clashes in the Assembly*, International Organization, 54 (2000), pp. 185–215.
- [303] Y. WANG, B. WU, AND N. DU, *Community Evolution of Social Networks: Feature, Algorithm and Model*, arXiv:0804.4356, (2008).

References

- [304] S. WASSERMAN AND K. FAUST, *Social Network Analysis: Methods and Applications*, Cambridge University Press, Cambridge, UK, 1994.
- [305] D. J. WATTS AND S. H. STROGATZ, *Collective dynamics of “small-world” networks*, *Nature*, 393 (1998), pp. 440–442.
- [306] A. S. WAUGH, L. PEI, J. H. FOWLER, P. J. MUCHA, AND M. A. PORTER, *Party Polarization in Congress: A Network Science Approach*, arXiv:0907.3509, (2010).
- [307] K. F. WIDAMAN, *Common Factor Analysis Versus Principal Component Analysis: Differential Bias in Representing Model Parameters?*, *Multivariate Behavioral Research*, 28 (1993), pp. 263–311.
- [308] E. P. WIGNER, *On a Class of Analytic Functions From the Quantum Theory of Collisions*, *Annals of Mathematics*, 53 (1951), pp. 36–67.
- [309] D. WILCOX AND T. GEBBIE, *An analysis of cross-correlations in an emerging market*, *Physica A*, 375 (2007), pp. 584–598.
- [310] I. XENARIOS, L. SALWINSKI, X. J. DUAN, P. HIGNEY, S. M. KIM, AND D. EISENBERG, *DIP, the Database of Interacting Proteins: a research tool for studying cellular networks of protein interactions*, *Nucleic Acids Research*, 30 (2002), pp. 303–305.
- [311] E. YONEKI, D. GREENFIELD, AND J. CROWCROFT, *Dynamics of Inter-Meeting Time in Human Contact Networks*, in *ASONAM '09: Proceedings of the 2009 International Conference on Advances in Social Network Analysis and Mining*, 2009, pp. 356–361.
- [312] M. P. YOUNG, *The Organization of Neural Systems in the Primate Cerebral Cortex*, *Proceedings: Biological Sciences*, 252 (1993), pp. 13–18.
- [313] H. YU, P. BRAUN, M. A. YILDIRIM, I. LEMMENS, K. VENKATESAN, J. SAHALIE, T. HIROZANE-KISHIKAWA, F. GEBREAB, N. LI, N. SIMONIS, ET AL., *High-Quality Binary Protein Interaction Map of the Yeast Interactome Network*, *Science*, 322 (2008), pp. 104–110.
- [314] G. U. YULE, *A Mathematical Theory of Evolution, Based on the Conclusions of Dr. J. C. Willis, F.R.S.*, *Philosophical Transactions of the Royal Society*

- of London. Series B, Containing Papers of a Biological Character, 213 (1925), pp. 21–87.
- [315] W. W. ZACHARY, *An Information Flow Model for Conflict and Fission in Small Groups*, *Journal of Anthropological Research*, 33 (1977), pp. 452–473.
- [316] D. H. ZANETTE, *Critical behavior of propagation on small-world networks*, *Physical Review E*, 64 (2001), p. 050901.
- [317] S. ZHANG, R.-S. WANG, AND X.-S. ZHANG, *Identification of overlapping community structure in complex networks using fuzzy c-means clustering*, *Physica A*, 374 (2007), pp. 483–490.
- [318] Y. ZHAO, E. LEVINA, AND J. ZHU, *Community extraction for social networks*, arXiv:1005.3265, (2010).
- [319] D. ZHOU, I. COUNCILL, H. ZHA, AND C. L. GILES, *Discovering Temporal Communities from Social Network Documents*, in *ICDM '07: Proceedings of the 2007 Seventh IEEE International Conference on Data Mining, 2007*, pp. 745–750.